2008-07-15

Effects of Moisture on Combustion of Live Wildland Forest Fuels

Brent M. Pickett
Brigham Young University - Provo

EFFECTS OF MOISTURE ON COMBUSTION OF LIVE WILDLAND FOREST FUELS

by

Brent M. Pickett

A dissertation submitted to the faculty of

Brigham Young University

in partial fulfillment of the requirements for the degree of

Doctor of Philosophy

Department of Chemical Engineering

Brigham Young University

August 2008

BRIGHAM YOUNG UNIVERSITY

GRADUATE COMMITTEE APPROVAL

of a dissertation submitted by

Brent M. Pickett

This dissertation has been read by each member of the following graduate committee and by a majority vote has been found satisfactory.

Date	Thomas H. Fletcher, Chair
Date	David R. Weise
Date	Larry L. Baxter
Date	W. Vincent Wilding
Date	Kenneth A. Solen

BRIGHAM YOUNG UNIVERSITY

As chair of the candidate's graduate committee, I have read the dissertation of Brent M. Pickett in its final form and have found that (1) its format, citations, and bibliographical style are consistent and acceptable and fulfill university and department style requirements; (2) its illustrative materials including figures, tables, and charts are in place; and (3) the final manuscript is satisfactory to the graduate committee and is ready for submission to the university library.

Date

Thomas H. Fletcher
Chair, Graduate Committee

Accepted for the Department

Larry L. Baxter
Graduate Coordinator

Accepted for the College

Alan R. Parkinson
Dean, Ira A. Fulton College of Engineering and Technology

ABSTRACT

EFFECTS OF MOISTURE ON COMBUSTION OF LIVE WILDLAND FOREST FUELS

Brent M. Pickett

Department of Chemical Engineering

Doctor of Philosophy

Current operational wildland fire models are based on numerous correlations from experiments performed on dry (dead) fuel beds. However, experience has shown distinct differences in burning behaviors between dry and moist (live) fuels. To better understand these fundamental differences, an experiment was designed to use a flat-flame burner to simulate a moving fire front which heated and ignited a stationary, individual fuel sample. Samples included various U.S. species from the California chaparral, the intermountain west, and the southeastern regions. Temperature, mass, and video images were recorded throughout each experimental run from which numerous data values were obtained such as time to ignition, ignition temperature, flame height, time of flame duration, and mass release rates.

Qualitative results showed various phenomena such as color change, bubbling, bursting, brand formation, and bending; these phenomena were species-dependent.

Quantitative results showed differences in the ignition values (time, temperature, and mass) among species. It was observed that all moisture did not leave the interior of the sample at the time of ignition. Also, from the temperature history profiles, no plateau was observed at 100°C, but instead at 200-300°C. This indicates a need to treat evaporation differently than the classical combustion model. Samples were treated with solvents in attempt to extract the cuticle from the surface. These treated samples were compared to non-treated samples, though no significant combustion characteristics were observed. The time of color change for the treated samples varied significantly, indicating that the cuticle was indeed removed from the surface.

Two-leaf configurations were developed and compared to determine combustion interactions between leaves. A second leaf was placed directly above the original leaf. Results showed that the time of flame duration of the upper leaf was significantly affected by the presence of the lower leaf. Causes for the prolonged flame were found to be the consumption of O_2 by the lower leaf and the obstruction provided by the lower leaf, creating a wake effect which displaced hot gases from the flat-flame burner as well as entrained surrounding room temperature gas.

A semi-physical model based on fluid dynamics and heat and mass transfer was developed that included the observed plateau at 200-300°C, rather than at 100°C; this was done for both the single- and two-leaf configurations. Another model using a statistical approach was produced which described the combustion of a bush that incorporated data obtained from the experimental results. Overall burning times and percentage of fuel consumption were obtained for various fuel loadings using this statistical model.

ACKNOWLEDGEMENTS

I wish to give my thanks to all the people who have helped me in completing this project. First, I would like to thank my advisor, Tom Fletcher, for all his help and guidance as well as other members of my committee: David Weise, Larry Baxter, Vince Wilding, and Ken Solen for their input and insight. Others that played an instrumental part are Bret Butler for his insight into the project, Joey Chong and Kenneth Outcalt for collecting and shipping fuel samples, and all the great undergraduate students for the long hours that they spent on the project: Becky (Wunder) Miller, Carl Isackson, Sarah Christensen, Jenna Fletcher, Liz Haack, Megan Woodhouse, Wesley Cole, Marcus Arthur, and Tien Do. Great appreciation goes to the financial support from the USDA Forest Service both from the Pacific Southwest Research Station and from the Rocky Mountain Research Station. Also, thanks to Brigham Young University for allowing me to continue my eduation and for the support that they have given me.

Special thanks to my parents, Matt and Becky Pickett, and in-laws Charles and Kay Olson, for their support and prayers on my behalf. To my kids, Olivia and Matthew, for the joy and sanity they give me. Most especially to my sweet, beautiful wife Janae for her constant love and support. Thank you Janae. Eternal thanks to my Heavenly Father and to His Son, Jesus Christ, for helping me understand Their plan for me and my family.

TABLE OF CONTENTS

LIST OF TABLES

LIST OF FIGURES

NOMENCLATURE

Symbol	
A_s	surface area of leaf including both sides and thickness [cm^2]
Bi	Biot number defined as hL_c/k [-]
C_i	species-specific constants to fit Equation 2.1
FH	maximum flame height [cm]
FL	fuel loading [leaves/cm^2]
H_i	combined term at boundary *i* defined as h_i/k [m^{-1}]
ID	inner diameter [mm]
IZ	ignition zone height above leaf [cm]
$J_i(r)$	Bessel function of order *i* [-]
$K_n(x)$	kernel function from finite Fourier transform – Equation 6.9
L	length of sample [cm]
L_c	characteristic length defined as V/A_s [cm]
MC	moisture content of sample on a dry-basis [%]
MR	mass release rate [g/s]
OD	outer diameter [mm]
P	perimeter of leaf [cm], pressure [atm]
Pr	Prandtl number [-]
Q(t)	combined terms function from transformation – Equation 6.8
Q_c	heat release of fuel [kW]
R	leaf radius [cm]
Re	Reynold's number – $\rho_a \cdot v \cdot d/\mu_a$ [-]
SA	surface area of leaf of one side [cm^2]
T	temperature [ºC]
UBF	fraction of unburned fuel (final whole leaves/initial whole leaves)
V	volume of leaf [cm^3]
W	width of sample [cm]
a_i	pre-exponential factor for reaction *i* [various]
b_i	time-dependent exponential factor for reaction *i* [s^{-1}]
c_p	heat capacity [J/kg-K]
d	diameter of leaf [cm]
$f_i(t)$	heterogeneous condition function at boundary *i* [W/m^2]
g(t)	source term function [W/m^3]
h_i	heat transfer coefficient at boundary *i* [W/m^2-K]
k	thermal conductivity [W/m-K], constant for power-law fit [-], kinetic energy for turbulence model [m^2/s^2]
l_p	pixel length [cm]
m	sample mass [g]
n	number of pixels [-]

q	energy transfer [W]
r	radial direction of leaf [mm]
t	time during experimental run [s]
u	normalized temperature defined as T-T_0 [ºC]
$\overline{\overline{u}}_{n,m}$	transformed temperature
v	gas velocity from flat-flame burner [m/s]
w_p	pixel width [cm]
x	axial direction of leaf [cm], axial distance along lead [m]
y_i	mass fraction of species i [-]
z_i	mole fraction of species i [-]

Greek

Δr	radial distance from bead surface in the leaf [m]
Δx	leaf thickness [mm]
$\Phi(t)$	Heaviside function [-]
α	slope for linear regression [various], thermal diffusivity $k/\rho c_p$ [m^2/s]
β	intercept for linear regression [various]
χ	first listed reactant of reaction in Equation 6.13 [-]
δ	second listed reactant of reaction in Equation 6.13 [-]
ε	sample emittance, emissivity [-], dissipation for turbulence model [m^2/s^3]
ϕ	power-law coefficient [-]
η	heat source or sink value [W/m^3]
κ	moisture time factor for analytical model [-]
λ_n	eigenvalues for axial direction [m^{-1}]
σ	Stefan-Boltzmann constant [$5.67 \cdot 10^{-8}$ W/m^2-K^4]
μ	combined term for lumped capacitance model – Equation 6.3 [s^{-1}]
$\nu_{r,i}$	coefficient of reactant i [-]
ρ	density [kg/m^3]
τ	time variable for integration [s]
ω_m	eigenvalues for radial direction [m^{-1}]

Subscript

0	initial value of sample (T, m), at boundary position $x = 0$ (h_i, H_i, $f_i(t)$, T, x)
∞	value of bulk gas (T)
Brn	value at burnout (flaming) (T, m)
FH	value at maximum flame height (MR, T, m, t)
Fuel	value of combined heats of pyrolysis and combustion (η)
H2O	value of water in sample (MR, m, η)
R	at boundary position $r = R$ (h_i, H_i, $f_i(t)$)
VM	volatile matter (m)
X	at boundary position $x = \Delta x$ (h_i, H_i, $f_i(t)$)
a	air or flat-flame burner gases (k, ρ, μ)
b	bead or connection with leaf (q, T, x, d)
cc	color change (t)
dry	value of oven-dried sample (m)

fd	flame duration (*t*)
fd_t	overall flame duration of bush (*t*)
gas	gas from apparatus (*T*)
h	horizontal (*n*)
id	ignition delay (*t*)
ig	value at ignition (*MR*, *T*, *m*, *t*)
l	leaf (*k*, *T*, *q*)
o	overall (*n*)
p,i	product of reaction *i* (*MR*)
r,i	reactant of reaction *i* (*MR*)
surr	surrounding (*T*)
v	vertical (*n*)
w	wire or lead (*k*, *d*)

Superscript

A	value of leaf at position A – 4.0 cm above FFB (*MR*, *T*, *m*, *t*)
B	value of leaf at position B – 6.5 cm above FFB (*MR*, *T*, *m*, *t*)

1. Introduction

Before the 19th century, forest fires were mainly low-intensity fires that burned only undergrowth. In recent decades, fire suppression has caused undergrowth to accumulate, which has caused fires to transition to burn the tree canopy (high-intensity crown fires). Also, fire suppression has allowed for shrub species to produce ideal fuel arrangements for high-intensity surface fires. This fire suppression and droughts have caused many areas in the United States and throughout the world to experience these high-intensity fires, which cause damage to both the ecology and property. These fires have caused millions of dollars of damage to homes and other structures, particularly in the western United States.

To reduce the large amount of fuel in the forest floors, the Forest Service has attempted to thin the forest by prescribed burns and tree mastication. Prescribed burns are intentional fires started under favorable conditions (combination of wind, fuel, moisture content, temperature, etc.) designed to reduce fuel accumulation. The conditions of the prescribed burn, however, do not always guarantee that a fire will be confined to the desired area or that it will not burn out of control or that it will burn at all. Wildfire models have been used to better predict the path the fire takes under specified conditions.

Weber (1991) describes three types of models that have been developed for wildfire prediction: statistical, empirical, and physical. Statistical models make no attempt to include physical phenomena in the model, but are entirely statistical

descriptions of how fire burns through a fuel bed. Empirical models (also known as semi-physical or semi-empirical models) use statistical correlations from test fires, but do not distinguish between modes of heat transfer (conduction, convection, and radiation). Physical models do distinguish between modes of heat transfer, and are, therefore, a more fundamental approach to predict fire behavior. Studies performed at the Fire Science Laboratory in Missoula, MT suggest that fire spread occurs mainly by convective flames, while radiation mostly preheats the fuel bed (Cohen et al., 2006).

Rothermel (1972) developed an empirical model which is based on a theoretical model by Frandsen (1971). Rothermel (1972) uses correlations derived from laboratory experiments performed mostly on dead (low-moisture) samples (Byram, 1959; Fosberg and Deeming, 1971; Rothermel, 1972; Van Wagner, 1973; Albini, 1976); Rothermel's model was later adapted by Albini (1975). His model was originally made to predict fire spread from dead fuels in a contiguous (homogeneous) bed, such as litter or grass, and has been implemented in the United States (Andrews, 1986). Rothermel's model, however, is over-sensitive to vegetation height and has difficulty predicting fire behavior in high-moisture (live) fuels (Catchpole et al., 2002) and through heterogeneous fuel beds.

Physical models are inherently more robust because of the physical parameters included in the modes of heat transfer. However, the physical models that have been produced have not been thoroughly validated; therefore, they have not been included in the operational field models BEHAVE (Andrews, 1986) and FARSITE (Finney, 1998). A thorough understanding of the physical phenomena in wildland fires is required in physical models. A single model using all forms of physical phenomena would be

computationally intensive, and therefore, not feasible to incorporate in the field, but would aid the overall understanding of wildland fires. More sophisticated models (Clark et al., 1996a, b; Linn, 1997; Dupuy and Larini, 1999; Reisner et al., 2000; Linn et al., 2002; Linn et al., 2005) have been created that incorporate the complete fluid dynamics of the system and show the interaction of wind and fire, but these sophisticated models need better combustion-phase modeling. Since the current Rothermel model that is used in the United States does not sufficiently predict fire behavior in live fuels, and since most correlations are derived from tests on dead fuels, there is a need to study the effects of moisture in the combustion of live fuels.

2. Literature Review

Fire spread rate has been modeled as a series of successive ignitions that is controlled by the time and temperature that are required for ignition to occur and the distance between fuel particles. Most wildland fire models contain a critical temperature from which ignition is determined. The fuel (or cell for cellular formulation) where the temperature surpasses the critical or ignition temperature is considered to be burning fuel. Therefore, this temperature must be known for the fuel that is being modeled. The time it takes for ignition to occur is also an important parameter which can be useful in fire spread models. These two parameters (ignition temperature and time to ignition) are addressed below in Section 2.1. Ignition Characteristics. Another important parameter for fire spread is the amount of fuel that is being consumed (mass release rate), which can be related to the heat release rate and also to the flame height. These issues are addressed below in Section 2.2. Mass Release. Moisture content is defined in this dissertation on a dry-weight basis (Babrauskas, 2003).

2.1 Ignition Characteristics

2.1.1 Ignition of Wood Fuels

Ignition temperature (T_{ig}) values have been determined for a variety of wood fuels for more than a century. Babrauskas (2001) reviewed and tabulated (also by Smith (2005)) many of these ignition values; he found a large variation in the T_{ig} from various

studies performed on low-moisture, solid wood. These studies were performed under a variety of conditions which can alter the T_{ig} dramatically. Babrauskas (2001) gave reasons for the variation in T_{ig} as follows: (1) the definition of ignition that is used, (2) piloted vs. autoignition conditions, (3) the design of the test apparatus and its operating conditions, (4) specimen conditions (e.g., size, moisture, orientations), and (5) species of wood; the last two reasons (4 and 5) are genuine variations for T_{ig} which are most important for modeling. Heat flux has been seen to quantitatively alter the ignition temperature. There is a minimum heat flux from which ignition can occur; Babrauskas (2001) gave T_{ig} at the minimum heat flux (5-10 kW/m^2) to be 250ºC for both piloted and autoignition, and also indicates that T_{ig} should increase with increasing heat flux (Table 2.1). The minimum heat flux temperature may not be as useful for wildland fires since the heating rates (100 K/s) (Butler et al., 2004a) and subsequent heat fluxes are much higher than the minimum heat flux.

Table 2.1. Summary of ignition temperature results.

	Flux		
	Minimum (5-10 kW/m^2)	Low (10-30 kW/m^2)	Medium (30-75 kW/m^2)
Ignition type	Glowing or glowing/flaming		Flaming
T_{ig} (ºC), piloted	250	350 - 400 peak, lower for fluxes close to minimum	300 - 310 hardwoods 350 - 365 softwoods
T_{ig} (ºC), autoignition	250	No data	380 - 500 ??
Data adapted from Babrauskas (2001)			

The result that T_{ig} increases with increasing heat flux is misleading when looking at certain individual experiments reviewed by Babrauskas (2001). Li and Drysdale (1992) performed ignition experiments on four types of wood species (Western red cedar, obeche, white pine, and mahogany) while varying heat flux from 15-32 kW/m^2. The

measured T_{ig} clearly decreases as heat flux increases (Figure 2.1). As much as 150ºC difference in T_{ig} can be seen (in obeche samples) over the 17 kW/m^2 range. It is also interesting to note that the change in T_{ig} with heat flux is not the same for each species; white pine showed a slower decrease in T_{ig} with increasing heat flux compared to the other species. A similar decrease in T_{ig} with heat flux is shown by Moghtaderi and coworkers (1997) in Figure 2.2, though the trend is not as dramatic.

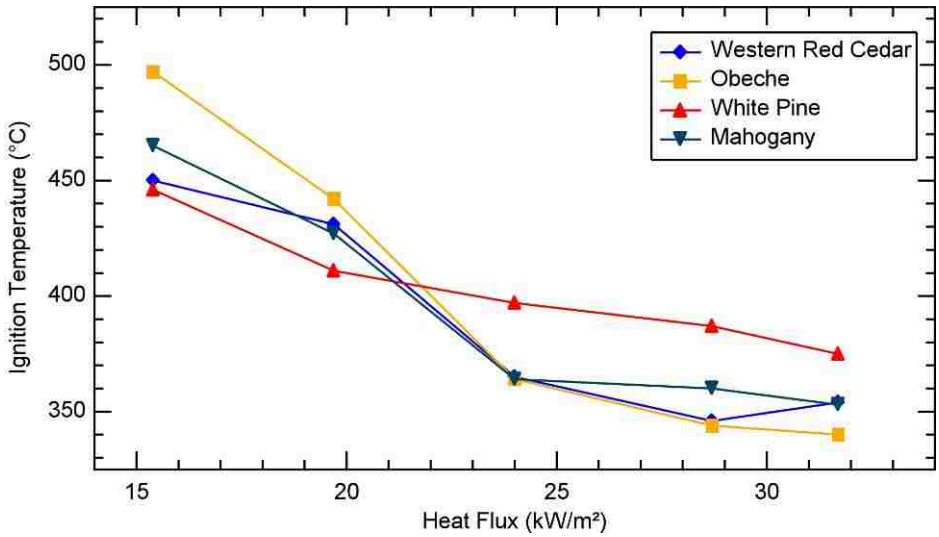

Figure 2.1. Piloted ignition temperature variation with heat flux for 4 wood species. Data from Li and Drysdale (1992).

Time to ignition (t_{ig}) is defined as the time difference between when the fuel sample is immersed in the experimental apparatus to the time when it ignites (piloted or autoignition). Li and Drysdale (1992) measured values of t_{ig} as a function of heat flux (Figure 2.3). An inverse relationship was observed between t_{ig} and heat flux. The results of Li and Drysdale (1992) make sense physically; at lower heat fluxes the wood heats up more slowly, which requires more time (and temperature) for ignition to occur. Also,

since T_{ig} is lower at a higher heat fluxes, this would take even less time for the sample to obtain the required T_{ig}.

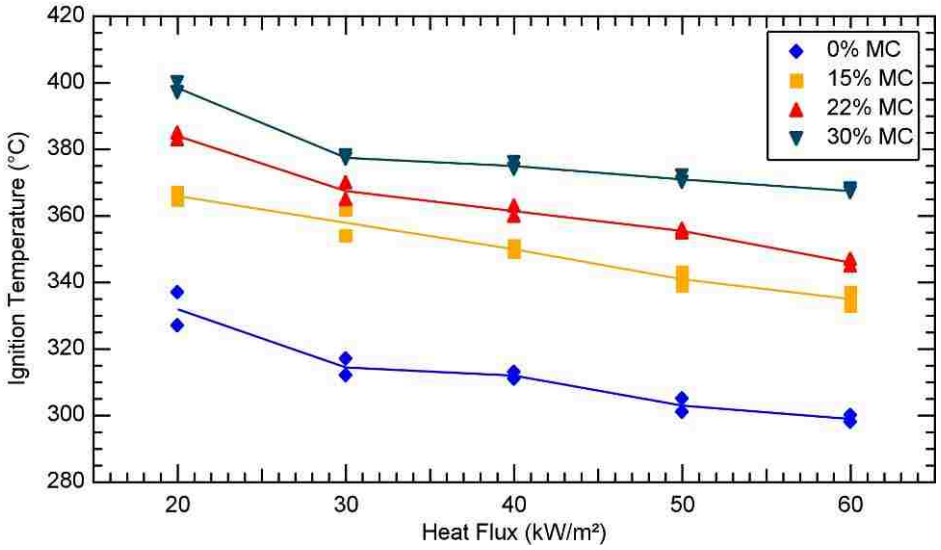

Figure 2.2. Piloted igntion temperature variation with heat flux as moisture content (dry-weight basis) changes for Radiata pine. Data from Moghtaderi (1997).

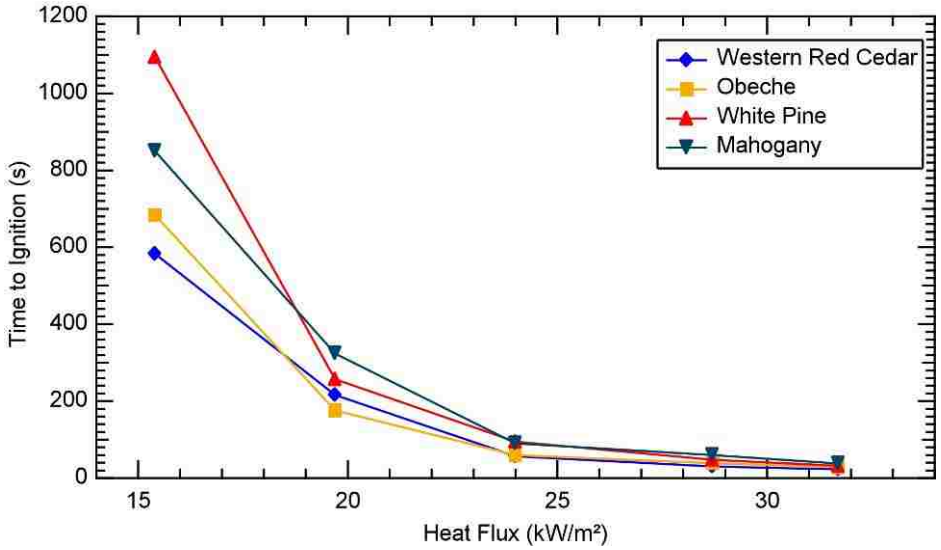

Figure 2.3. Variation of time to piloted ignition with heat flux for 4 wood species. Data from Li and Drysdale (1992).

Most experiments reviewed by Babrauskas (2001) were performed on dry wood with the exception of Moghtaderi (1997). Data from Moghtaderi (1997) (Figure 2.2) show an increase of T_{ig} as moisture content (*MC*) increases. Similar results are shown by Mardini and Lavine (1995) (Table 2.2) where the higher *MC* is shown on the first row of Table 2.2 for each individual species. It can be seen that the higher *MC* yields the higher t_{ig} for each species. In addition, for three of the species (underlined), the subsurface (below the surface 1.1 mm deep) T_{ig} increased with higher *MC*, while for the other three species, T_{ig} remained the same as *MC* increased. It appears from the data that moisture has a greater effect on t_{ig} than T_{ig}.

Table 2.2. Autoignition temperature and time to ignition for six types of wood as moisture varies.

Species	*MC* (%)	T_{ig} (ºC)	t_{ig} (s)	Species	*MC* (%)	T_{ig} (ºC)	t_{ig} (s)
Chamise	62	277	825	Pine	130	277	1650
	53	277	710		112	267	1400
White Fir	89	287	1350	Cedar	136	277	1450
	68	287	850		97	277	950
Mahogany	78	325	1417	Peeled Mahogany	59	297	1200
	77	307	1190		36	277	610

The underlined species indicate an increase in ignition temperature with increasing moisture content.
Data taken from Mardini and Lavine (1995).

2.1.2 Ignition of Foliage Fuels

The rate of fire spread in wildland fires is not usually associated with wood, but rather from the finer fuels (grasses, duff, shrubs, leaves, etc.), since these burn much more rapidly. Babrauskas (2003) also reviewed experiments performed on foliage fuels; this study was similar to his review of wood fuels (Babrauskas, 2001). Smith (2005) tabulated much of the information from Babrauskas (2003) and reported an average autoignition temperature of 314ºC and an average piloted ignition temperature of 308ºC, which are much higher than the minimum wood T_{ig} of 250ºC. In addition, Smith

performed experiments on 6 species of moist leaves over a flat-flame burner (FFB) (Engstrom et al., 2004; Smith, 2005); the average T_{ig} and t_{ig} data are tabulated in Table 2.3 and vary with species. However, large standard deviations in the values of T_{ig} and t_{ig} were observed for each species. Leaf-to-leaf variations were attributed to changes in the surface area-to-volume ratio (thickness), leaf geometry (surface area, perimeter), and moisture content; species-to-species variations were attributed to the chemistry differences between foliage samples, and also to the amount of essential oils (extractives) inside the foliage sample. These effects must be quantified and are discussed below.

Table 2.3. Average autoignition data (ignition temperature and time to ignition) for six live species.

Species	T_{ig} (°C)	t_{ig} (s)	Species	T_{ig} (°C)	t_{ig} (s)
Manzanita	409	2.83	Gambel oak	231	0.69
Scrub oak	317	1.12	Canyon maple	277	0.53
Ceanothus	473	4.93	Big sagebrush	386	1.50
Data taken from Smith (2005).					

2.1.2.1 Moisture Effects

Montgomery and Cheo (1969) determined t_{ig} values for 6 plant species in a muffle furnace as a function of variations in *MC* (rainy season, dry season, and oven-dry). Fresh samples were harvested in the dry season and saturated in water to obtain an approximate rainy season *MC*. Results of t_{ig} versus *MC* are shown in Figure 2.4. It is clear that the t_{ig} increases linearly with *MC*. However, the slope appears to differ for some species (e.g. slope is higher for Gum Rock Rose than for Black Sage). In addition, the higher moisture content samples were saturated in water (not a natural *MC*); this could have altered the true behavior of moisture in live (fresh) leaves.

Xanthopoulos and Wakimoto (1993) performed experiments on live branches of 3 conifer species in a hot-air convective column. They determined a relationship (shown in Equation 2.1) for t_{ig}, the gas temperature of the apparatus, and the *MC* of the branch.

$$t_{ig} = C_1 \cdot \exp\left(-C_2 \cdot T_{gas} + C_3 \cdot MC\right) \tag{2.1}$$

where C_1, C_2, and C_3 are species-specific constants to fit the data and T_{gas} is the apparatus gas temperature (ºC). Their conclusion indicates that t_{ig} increases exponentially with increasing *MC* and decreasing T_{gas}. It should also be noted that the coefficients varied greatly for each species as shown in Figure 2.5, which suggests that ignition parameters (T_{ig} and t_{ig}) are species-dependent.

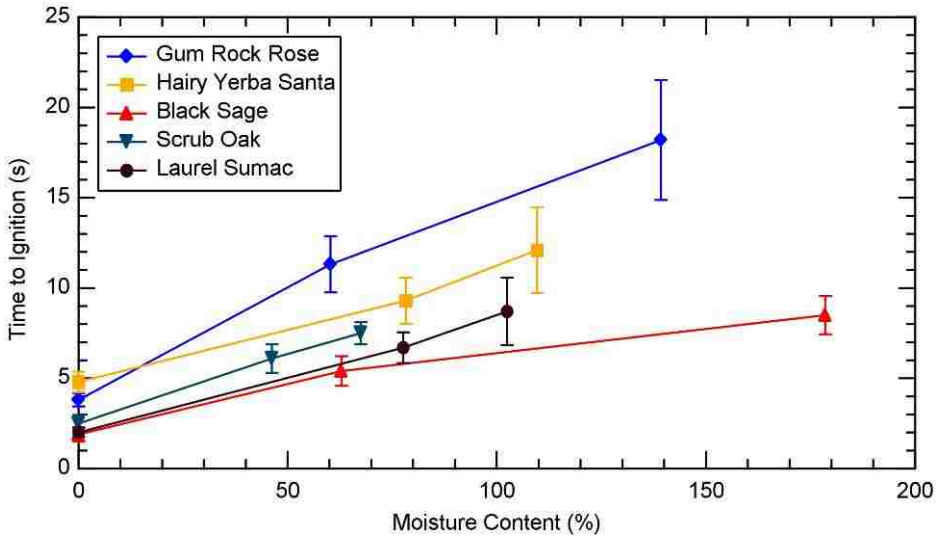

Figure 2.4. Average time to ignition versus moisture content for 5 species. Data taken from Montgomery and Cheo (1969). Error bars represent one standard deviation.

Dimitrakopoulos and Papaioannou (2001) performed t_{ig} experiments on 24 fresh species of Mediterranean forest fuels in a radiator cone apparatus and determined the flammability for each species. Their results show a linear increase (see Equation 2.2) of t_{ig} with *MC* that is species-dependent.

$$t_{ig} = \alpha \cdot MC + \beta \tag{2.2}$$

where α and β are species-dependent constants that fit the data for a linear regression. The 24 species from Dimitrakopoulos and Papaioannaou (2001) were separated into 4 categories depending on the slope (α) of the regression (higher slope means less flammable); these categories are shown in Figure 2.6. The extremely flammable species (*Laurus nobilis* and *Eucalyptus camaldulensis*) with lower slopes contain high amounts of essential oils or extractives that are more volatile at lower temperatures (early pyrolysis region). These extractives can cause ignition even in higher moisture fuels. Extractives are discussed in Section 2.1.2.3. Chemistry Effects.

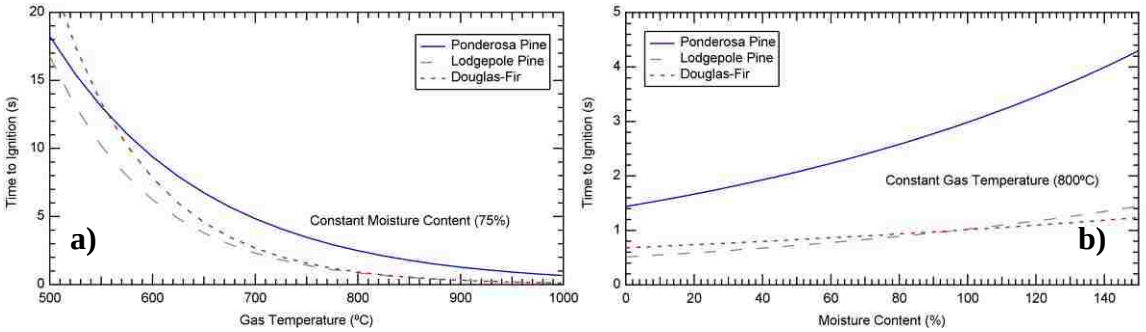

Figure 2.5. Predicted time to ignition for 3 different conifer species from Xanthopoulos and Wakimoto (1993) as a function of (a) gas temperature with moisture content held constant at 75% and (b) moisture content with gas temperature held constant at 800ºC (see Equation 2.1).

Weise and coworkers (2005b) also performed t_{ig} experiments on ornamental vegetation of southern California in a cone calorimeter. They determined a linear relationship with t_{ig} and the amount of moisture in green fuel samples. The linear relationships from Dimitrakopoulos and Papaioannaou (2001) and Weise et al. (2005b) show that *MC* and the amount of water can possibly be interchanged in correlating t_{ig}.

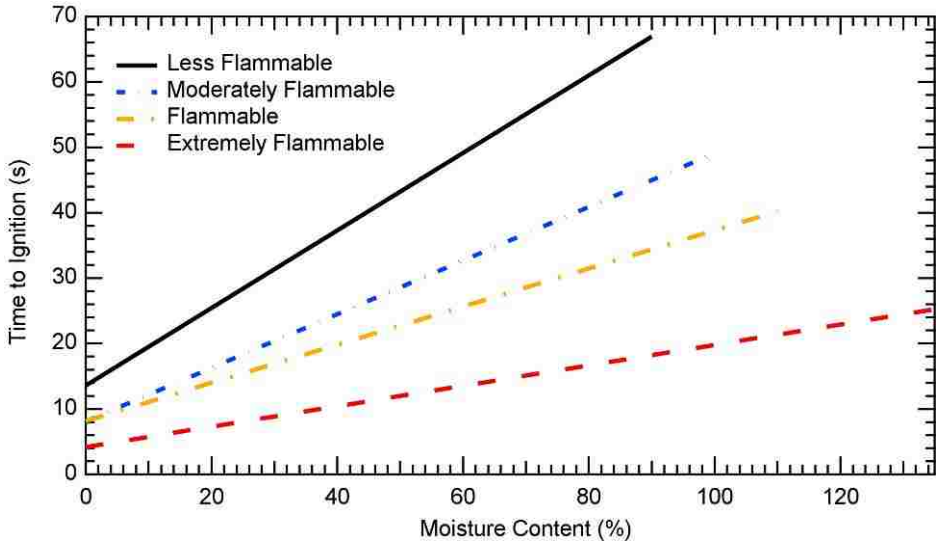

Figure 2.6. Predicted time to ignition versus moisture content of 24 Mediterranean live species grouped into flammability categories. Regressions from Dimitrakopoulos and Papaioannou (2001).

Smith (2005) performed experiments on fresh samples of 8 species from California and Utah. He attempted to relate the T_{ig} and t_{ig} to the amount of moisture (m_{H2O}) in the sample (determined from the initial mass and the *MC*). Because of the large amount of scatter in the natural fuel data, the linear correlations (T_{ig} or $t_{ig} = \alpha \cdot m_{H2O} + \beta$) for both T_{ig} and t_{ig} versus m_{H2O} were not conclusive for all species. The 95% confidence intervals for the slope (α) had a higher magnitude than the slope itself for most species. Smith (2005) gave other relations for T_{ig} and t_{ig} by correlating both moisture and thickness.

Catchpole et al. (2002) gave a plausible reason for increasing T_{ig} (and hence, t_{ig}) with increasing *MC*. Since water molecules are the first driven off in the heating-up of live fuels, most of the water will have left the sample at lower heating rates before ignitable gases (from pyrolysis) are driven off. At higher heating rates or in larger particles, the sample still loses water vapor from the deeper layers, while the surface is

giving off ignitable gases. The water vapor dilutes the ignitable gases, which requires a higher temperature (and longer delay time) to ignite them. The ignitable gases must be within the flammability limits before ignition can occur.

Other studies have been performed on fuel with high moisture contents, (Weise et al., 2005c; Zhou et al., 2005; Sun et al., 2006) but were performed on fuel beds or in baskets, not on an individual sample basis. These studies are also very important to better understand the overall combustion process in high-moisture fuels, but are not discussed at length here.

2.1.2.2 Thickness Effects

For flaming ignition to occur, the concentration of ignitable gases from pyrolysis must be within the flammability limits. Forest fuels vary in surface area-to-volume ratio (similar to thickness), which may cause differences in ignition. The ignitable gases must be released from the interior of the sample to obtain an acceptable concentration for ignition. Mass transfer resistance of these gases from thicker samples may delay ignition (and also require a higher temperature) because the required flammable concentration is more difficult to attain.

Montgomery and Cheo (1971) performed t_{ig} experiments on 32 leaf species in a muffle furnace. All leaves were cut into 3.0 × 1.0 cm rectangular samples and air-dried. Time to ignition was found to correlate linearly with thickness (Δx) as shown in Figure 2.7. Babrauskas (2003) explained that a linear relationship with Δx indicates that the leaves behave as thermally-thin material, meaning that the thermal gradient through the leaf is minimal.

Smith (2005) also showed that thickness had an effect on the ignitability (T_{ig} and t_{ig}) for 3 California chaparral species. He showed that there is a general trend for T_{ig} and t_{ig} to increase with increasing thickness, but it was not significant for all species, as can be seen in the scatter in the data. The trends, however, appeared to be species-specific (i.e. the slope was different for each species). Because neither moisture nor thickness alone had significant effects, Smith (2005) used a combined correlation to further reduce data scatter.

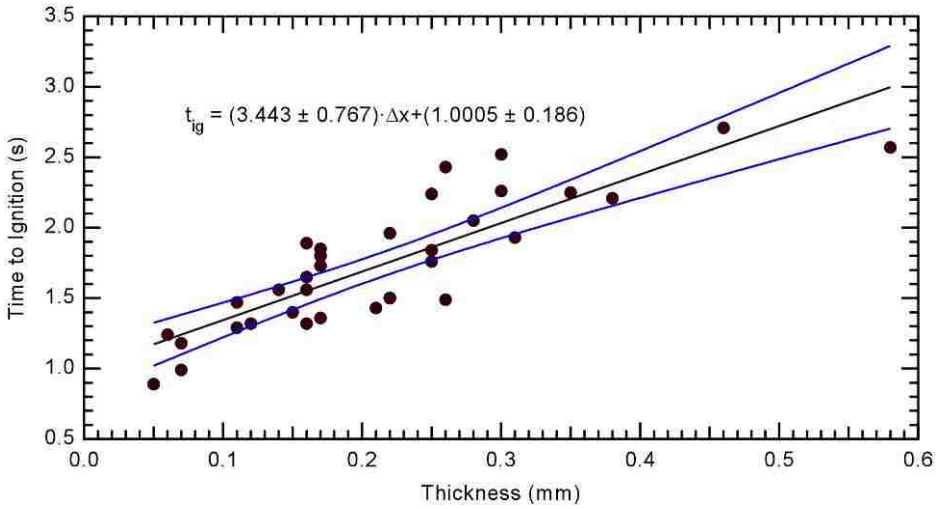

Figure 2.7. Time to ignition versus thickness for 32 plant species. Data taken from Montgomery and Cheo (1971). Linear regression equation is shown with '±' as the 95% confidence interval.

2.1.2.3 Chemistry Effects

Since fire spread is dependent on the fuel type, the effects of the chemical components of the fuel must be examined. Susott (1980) divided forest fuels into five groups that can have an effect on fire behavior: (1) moisture, (2) inorganic material (ash), (3) cellulosic material (cellulose and hemicellulose), (4) lignin, and (5) extractives. Moisture is expected to decrease fire flammability as explained in Section 2.1.2.1.

Moisture Effects; inorganic material is also expected to decrease flammability (Philpot, 1970; Susott, 1980). Cellulosic material is broken down to produce mainly pyrolysis gases (Shafizadeh, 1968) (volatiles), while lignin is responsible for most of the char that is formed (Shafizadeh and McGinnis, 1971). Extractives are compounds that are more volatile and have a higher heat content than other pyrolysis products (Philpot and Mutch, 1971), which can affect the T_{ig} and the rate at which the fire spreads. The model of Rothermel (1972) was developed from correlations from dry, dead fuels; his model has been adapted to treat live fuels like dead fuels that have a high *MC*. Dead fuels which were used for the experimental correlations are high in cellulosic material and lignin, but are lacking in not only moisture but also extractives (Susott, 1980). Ether extractives are a complicated mixture of oils, waxes, fats, and terpenes (Philpot and Mutch, 1971). Volatiles from these extractives can be more accessible to an oxidizer than other pyrolysis gases from the bulk of the leaf material (cellulose and hemicellulose) not only because of their greater volatility, but also because of their location in the fuel (Philpot, 1969) (i.e. on the outer surface). Also, terpenes have an extremely low flammability limit (Weast and Astle, 1982), which can increase the rate of fire spread. The effect of extractives must also be included in fire spread models.

Susott (1980) performed thermal analysis experiments on 3 types of conifer needles to study the impact of extractives in fire behavior. Freeze-dried and ground samples underwent 3 extraction techniques to obtain extractives, which then underwent thermal analysis by separately heating the original sample and the 3 extracted samples at 20ºC/min from room temperature to 500ºC. The volatilized gases were then consumed by combustion, and the required oxygen was measured. Susott (1980) found that the

extractive material accounted for about 80% of the volatiles below 300ºC. Shafizadeh and coworkers (1977) examined the effects of extractives on 6 species of forest fuels using techniques similar to those used by Susott (1980). They estimated that the heat from extractives accounted for 60% of the total heat released for temperatures between 100-500ºC; this is due mainly to ether extractives. Benzene-ethanol extractives were released at a lower temperature (below 300ºC) which would play a greater role at ignition. Both Susott (1980) and Shafizadeh et al. (1977) ground their samples before performing experiments in order to reduce the effects of heat and mass transfer of the extractives. Also, these heating rates (0.33 K/s) are much lower than those experienced in wildland fires (100 K/s) (Butler et al., 2004a).

Philpot and Mutch (1971) analyzed the trends of *MC*, ether extractives, and heat content for ponderosa pine and Douglas-fir needles over two fire seasons in western Montana. From June to September, *MC* increased for 1 and 2 year old needles from about 80 to 120%, while it decreased for new needles from about 220 to 130%. Ether extractive percentage (dry-weight basis) peaked at the height of the fire season (August for western Montana) at 9-10%. Total energy content increased slightly for Douglas-fir from about 21 to 22 MJ/kg, and reached a low for pine needles at about 21.5 MJ/kg in mid-July. The major finding from their research appears to be the increase in the amount of extractives present at the height of the fire season (a 100% increase for fir, smaller for pine).

Trujillo (1976) investigated the changes in the amount of ether extractives by heating 2 chaparral species. Samples were placed under an infrared lamp (imitating preheating) at 195-220ºC for 5 minutes to determine crude fat (ether extractives) content. Ether extractive percentage decreased from 9.6 to 7.7% (nearly a 20% change) for

pointleaf manzanita, and also decreased from 5.6 to 4.6% (nearly an 18% change) for shrub live oak. The release of these extractives before the flame reaches the fuel where the extractive originated may increase the rate of fire spread in fuel beds. The total amount of these volatiles is small, and accounts for little of the total energy content from the fuel sample (Pompe and Vines, 1966). However, they are important during ignition and the early stages of combustion because of their high volatility and low flammability limit. Brown and coworkers (2003) found that leaves, needles, and bark contained a higher fraction of extractives, and pyrolyzed differently between hardwood and softwood samples. They also suggest that bulk pyrolysis chemistry can be estimated from the extractives content of the fuel and can be implemented easily in wildland fire spread models.

Susott (1982) performed thermal analyses on 43 forest fuels (22 species of foliage, wood, stems, and bark). Collected samples were frozen upon harvest, freeze-dried to below 10% *MC*, and ground-up to pass through a 20 mesh screen (< 1.041 mm). Calorimetry experiments (for fuel, volatiles, and char) and evolved gas analyses (EGA – similar to thermal analysis experiments by Susott (1980)) were performed on all 43 samples. The heats of combustion ranged from 17.4 to 24.0 MJ/kg with the average being 21.4 ± 1.4 MJ/kg (standard deviation); these data show little variation in the heats of combustion among all the samples studied (foliage, wood, stems, and bark). The EGA analyses show that the samples differ by how volatiles are released at different temperature ranges: 200-300ºC is characteristic for extractives (Susott, 1980), 300-400ºC is characteristic for cellulose and hemicellulose (Philpot, 1971), 400ºC+ is characteristic of stable compounds (e.g. lignin (Tang, 1967)). Susott (1982) divided these samples into

three groups based on heats of combustion and EGA results: (1) wood – low heat of combustion, low char yield, and relatively high amounts of combustible volatiles, (2) foliage – wide range of heat of combustion and volatile yield, and intermediate char yield, and (3) bark or lignin – high heat of combustion, high char yield, and wide range of combustible volatiles. Large variation occurred among the three groups, but was fairly similar within individual groups (i.e. different foliage species behaved similarly). This similar behavior among species is not observed in wildland fires (i.e. species burn differently in the field). The samples in Sussott's experiments had been ground, thus reducing the effects of heat and mass transfer, which may be the reason for similarities in combustion behavior within groups.

Rogers and coworkers (1986) further analyzed 2 foliage species (gallberry and ponderosa pine) that exhibited unexpected behavior from Susott (1982). They found that both foliage species contained cutin, which was responsible for volatiles produced above 400ºC during pyrolysis. Cutin (the main component of the cuticle of a plant) is a complex polymer with C_{16} and C_{18} aliphatic chains with various carboxylic acid groups attached; ether, ester, or peroxide groups link the polymer together (Martin and Juniper, 1970). The cuticle of a plant may be important in characterizing the flammability of a plant, and thus its importance in wildland fires.

2.2 Mass Release

Fire spread rate can also be related to the amount of heat released from the fuel bed. This heat release can ignite fuel further down the fuel bed, causing the flames to propagate. Heat release in wildland fuels can be linearly related to the mass release if the fuel beds are similar (moisture content, composition, packing ratio). The EGA work

performed by Susott (1982) indicated that foliage is chemically similar, so the mass release rate should be important in fire spread models since it is related to the heat release rate. Mass release has also been correlated to the flame height (Byram, 1959; Fons et al., 1963; Thomas, 1963; Putnam, 1965; Nelson, 1980; Albini, 1981; Weise et al., 2005a).

Burrows (2001) performed experiments on eucalypt forest fuels by burning leaves and twigs of varying diameters. Flame duration of both flaming and char combustion were determined as well as the mass release rate. It was found that dry leaves burned at a rate equivalent to that of a 4 mm diameter twig, with small twigs (1-3 mm) being the most flammable component of a normal fuel array in eucalypt fuel beds. The mass release rate was also correlated to the diameter of round wood with a nearly inverse equation ($d^{-0.910}$); this equation is good only for wood cylinders ranging from 2-65 mm (twigs and branches). This equation cannot be applied to broadleaf species, since they do not have a true diameter. Leaf thickness (0.1-1.0 mm) cannot replace diameter, since extrapolation of the diameter (thickness) would yield extremely high predictions for mass release rate (45-500 g/s).

Flame height has been related to the heat release of steady-state natural fuels in what is known as the two-fifths power law (Putnam, 1965; Drysdale, 1999) as shown in Equation 2.3.

$$\frac{FH}{d} \propto \left(\frac{Q_c}{d^{5/2}} \right)^{2/5} \propto \frac{Q_c^{2/5}}{d} \Rightarrow FH = k \cdot Q_c^{2/5} \tag{2.3}$$

where FH is the flame height, d is the diameter of the fuel, Q_c is the heat release (kW), and k is a constant specific to the data. Dupuy and coworkers (2003) performed combustion experiments on oven-dried samples of pine needles and excelsior. Samples were placed in baskets of 3 varying sizes (20, 28, and 40 cm) and ignited, while an array

of thermocouples recorded temperatures in and above the fuel basket. They correlated the maximum flame height and the maximum heat release rate to fit a non-steady state correlation that was slightly different from Equation 2.3, where the two-fifths power varied. However, their new correlation was not significantly different from Equation 2.3 when *k* was equal to 0.2.

Sun and coworkers (2006) also performed similar basket experiments to those of Dupuy and coworkers (2003), although they compared live and dead chaparral species and used an IR camera instead of thermocouples. They found a time delay (defined as the difference between the maximum mass release time and the maximum flame height time) which was linearly related to moisture content. It was also found that the two-fifths power law was adequate for dry fuels, but not for high-moisture (live) fuels. When the *MC* is high, the heat release rate in the power law expression should be calculated at the time when the maximum flame height is obtained, not at the time of the maximum mass release rate.

Weise and coworkers (2005a) combined mass release results from high-moisture (live) fuel experiments on a single-leaf basis (Engstrom et al., 2004; Smith, 2005), in baskets (Sun et al., 2006), and in a fuel bed (Zhou et al., 2005) relating flame height and mass release rate to fit the relation shown in Equation 2.4.

$$FH = 0.417 \cdot \sqrt{MR} \tag{2.4}$$

where *MR* is the mass release rate (g/s) and *FH* is the flame height (m). From these data it may be possible to correlate mass release and flame height for live fuels across a range of scales, which could be useful in modeling fire spread in live fuels.

2.3 Previous Work at Brigham Young University

Two journal articles (Engstrom et al., 2004; Fletcher et al., 2007) and one thesis (Smith, 2005) have been produced at Brigham Young University using the individual sample experimental apparatus (flat-flame burner). This section describes what work was performed by each investigator and how it differed from the current work with the experimental apparatus.

Engstrom and coworkers (2004) developed the original experiment and recorded preliminary data on dry chaparral species (manzanita, ceanothus, scrub oak, chamise – decribed in Section 4.3.1. California Chaparral Species). Smith (2005) performed experiments on live chaparral and also increased the number of species studied to include some intermountain west species (Gambel oak, canyon maple, big sagebrush, and Utah juniper – described in Section 4.3.2 Intermountain West Species). Smith expanded the number of total experiments performed to nearly 1000. Smith obtained initial mass data, but he did not include any mass data or mass correlations, and the data were included in a journal article (Fletcher et al., 2007).

Both qualitative and quantitative data were presented in previous publications. Some of these data from previous investigators, as well as new data obtained after these publications, are presented in this dissertation. For example, new information about bursting was observed and is included (see Section 5.1.1.4. Bursting). Experiments were performed on more species (foliage from Douglas-fir, white fir, fetterbush, gallberry, wax myrtle, saw palmetto, and excelsior (aspen wood shaving) – described in Section 4.3. Experimental Fuels), and the total number of experiments exceeded 2300. Correlations that were performed in this dissertation include data from previous investigators, since the data are still applicable to better understand the combustion of live forest fuels.

2.4 Literature Summary

Dry, dead fuels have been used extensively in obtaining correlations used in current fire spread models. However, it has been observed in wildland fires that live fuels behave quite differently from dead fuels. Ignition temperature and time to ignition may be altered not only because of the moisture in the leaf, but also because of the thickness of the leaf. Chemistry effects have been studied with shredded foliage, eliminating heat and mass transfer effects, showing little species-dependent behavior for foliage. Therefore, experiments that include heat and mass transfer effects are necessary to quantify species-dependent combustion behavior. The presence of extractives may alter ignition and subsequent burning behavior. Since these extractives are found in the cuticle, understanding the effects of the cuticle during combustion is necessary. Mass release studies have been correlated to the flame height in various studies, but have not been correlated on live, individual samples. These data and correlations are necessary to improve current wildland fire models.

3. Objectives and Approach

3.1 Objectives

The overall objective of this project was to study the combustion of live wildland fuels, particularly the effects of moisture during combustion. Specific tasks for this project include:

1) Study and determine qualititative combustion characteristics of live wildland fuels;
2) Develop ignition, flame height, mass release, and burnout correlations that can be applied to current fire spread models;
3) Determine combustion interactions between multiple experimental samples;
4) Determine the effects of the cuticle during combustion;
5) Develop mathematical models that describe live fuel combustion for individual samples and also for multiple samples (two-leaf and bush models).

3.2 Approach

Individual and two-leaf experiments were performed over a flat-flame burner which ignited the fuel samples. Fourteen individual live species were used in experiments as well as a dead fuel (excelsior) for comparison. Each task listed above was realized by using the following approaches (corresponding to task number above):

1) Video images were obtained for each run from which physical phenomena were observed. These phenomena were typically species-dependent. More information is discussed in Section 5.1.1. Qualitative Results.

2) Values of time to ignition, ignition temperature, mass released at ignition, maximum flame height, time to maximum flame height, mass release rates, and flame durations were determined after analysis of the experimental run. Correlations between these dependent variables and independent variables of initial amount of moisture, thickness, surface area, and perimeter were determined by using linear fits to the data. More information is discussed in Section 5.1.2. Quantitative Results.

3) Experimental configurations for two-leaf combustion were developed and used to determine various differences in combustion such as flame duration and time to ignition. More information is discussed in Section 5.2. Two-Leaf Experiments.

4) The cuticle was removed from broadleaf samples. These samples were burned over the flat-flame burner and results were analyzed. Results from these cuticle-removed experiments were compared to experiments without the cuticle being removed. More information is discussed in Section 5.2. Two-Leaf Experiments.

5) Single-leaf and two-leaf models were developed to describe heat and mass transfer to and from a two-dimensional axisymmetric leaf. Two models that describe only heat transfer use analytical approaches. Two models that describe both heat and mass transfer use numerical approaches; one

was modified from Lu (2006), the other was developed using Fluent®. A statistical bush model was also developed that describes ignition interactions between leaf samples. More information is discussed in Section 6. Leaf Modeling.

4. Description of Experiments

4.1 Experimental Apparatus

The experimental apparatus is designed to simulate an oncoming flame front which heats up and ignites an individual fuel sample. Measurements of temperature, mass, and video images were all recorded simultaneously throughout the entire burning process (water evaporation, ignition, devolatilization, and flaming extinction; char combustion not included). The experiment mimics temperatures and heating rates in wildland fires, which are thought to be about 1200 K (Butler et al., 2004b) and 100 K/s (Butler et al., 2004a), respectively.

4.1.1 Flat-Flame Burner

The heat source for the fuel sample is provided by a flat-flame burner (FFB). Fuel gases (CH_4 and H_2) and an inert gas (N_2) are introduced to the bottom of the apparatus, which then flow through small tubes (ID 0.7 mm, OD 1.0 mm). Oxidizer (air) enters the middle section of the apparatus and flows around the tubes (Figure 4.1b). The top of the FFB (3 × 7.5 cm) forms a honeycomb pattern (shown in Figure 4.1c) allowing the fuel and air to combine into tiny diffusion flames (1-3 mm). The fuel sample does not touch the flame from the burner; it is only enveloped by the resulting post-combustion gases which are laminar, stable, and repeatable. Post-flame conditions at 5 cm above the FFB had a temperature of 987 ± 12ºC (± indicates the standard deviation) and 10 mol% O_2

(Engstrom et al., 2004). Heat fluxes were reported to be 80-140 kW/m^2 for the various species studied (Fletcher et al., 2007).

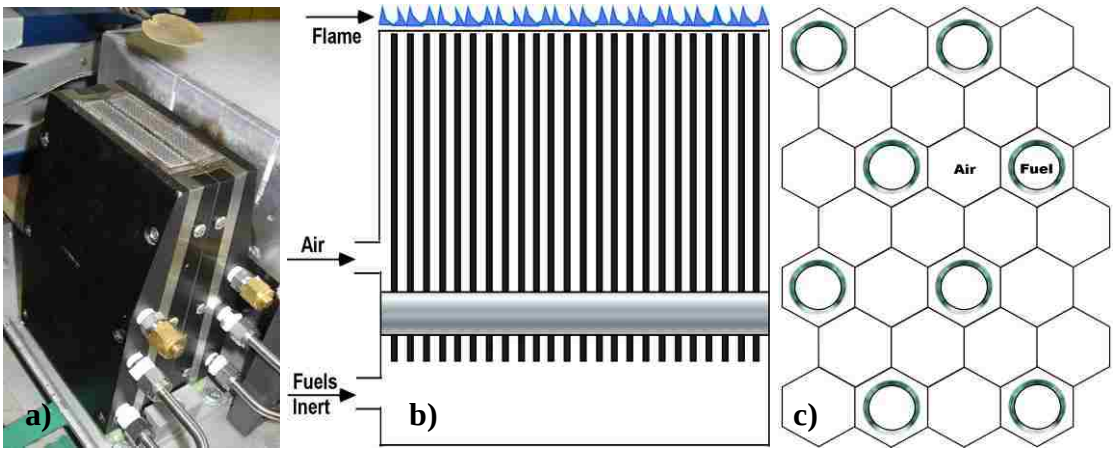

Figure 4.1. (a) Flat-flame burner (FFB) with a schematic of (b) a vertical cross section and (c) the top view.

The FFB was positioned on a moveable platform which was then pulled at a constant velocity (0.13 m/s) by a 0.5 hp motor. The FFB stopped directly under the fuel sample providing a constant heat source to heat up and ignite the sample. A radiant panel was also included in the original design (Engstrom et al., 2004; Smith, 2005), but was not used extensively in the experimental process.

4.1.2 Temperature Measurements

The leaf temperature was measured in two ways: (1) by a thermocouple embedded in the leaf and (2) by an infrared camera. Each temperature measurement is discussed below.

4.1.2.1 Thermocouple

A 127 μm type-K (chromel-alumel) thermocouple was used to measure the leaf temperature during the experimental run. A pinhole was made in the leaf into which the thermocouple was embedded. The location of the pinhole was normally selected to be near the main tip of the leaf, assuming ignition occurs near the perimeter. Due to excessive movement during the burning process in the non-broadleaf species, the thermocouple was not used when burning these species. When measuring the gas temperature (T_{gas}) with the thermocouple, the temperature correction due to radiation was found to be minimal (17ºC) (Engstrom et al., 2004) because of the small bead diameter. The rate of data acquisition for the thermocouple was 18-19 Hz.

The video images (see Section 4.1.3. Video Images) showed that the thermocouple leads above the FFB glowed, indicating that these wires were at a high temperature, and that conduction through these wires to the thermocouple bead may be significant (i.e. a temperature difference between the leaf and the bead may be observed). A preliminary model describing this temperature correction is described in Appendix C. 'A. Thermocouple Conduction through Leads'.

4.1.2.2 Infrared Camera

A FLIR thermal imaging (IR) camera (model A20M) was used to measure the surface temperature of the fuel sample throughout the experimental run. Since the sample moved during the run, it was impossible to specify one particular location to measure the surface temperature. Using the FLIR software, a specified area was outlined that enclosed the leaf surface throughout the entire experimental run. Assuming that ignition would

occur at the highest temperature on the leaf, the maximum temperature within the specified area was used as the overall measured temperature. A constant emittance (ε) was assumed throughout the entire burn period. The surface temperature from the IR camera and thermocouple temperature appeared to correlate well (Smith, 2005; Fletcher et al., 2007) using an emittance of 0.70-0.85, with the best fit (by a least squares method) having an emittance of 0.75. The rate of data acquisition for the IR camera was 30 Hz. Differences in these time steps (18-19 Hz vs. 30 Hz) were corrected by normalizing the profiles to the time when the FFB stopped moving (observed in both the IR camera and video images); a Visual Basic Applications macro performing this normalization and other data analyses is shown in Appendix A. 'A. Analysis Macros for BYU Forest Fire Research'.

4.1.3 Video Images

An analog Sony Handycam (CCD-TRV138 Video Hi8) camcorder recorded the experimental run; the images were imported to a computer by a National Instruments PCI-1411 IMAQ device where the image was subsequently digitized. The rate of acquisition was 18-19 Hz. From these digital images, ignition, maximum flame height, and burnout (and other qualitative information) were obtained. The procedure to obtain these values is discussed in Section 4.2. Leaf History.

4.1.4 Mass Measurements

The fuel sample of interest was attached by an alligator clip to a stationary, horizontal rod positioned on a Mettler Toledo cantilever mass balance (XS204) with an accuracy of 0.1 mg. A counter weight stabilized the rod and fuel sample. The mass was

measured throughout the experimental run at a rate of 18-19 Hz. The mass data, thermocouple temperature data (Section 4.1.2.1. Thermocouple), and video images (Section 4.1.3. Video Images) were time-stamped using a National Instruments LabView 7.1 program; these data (and others) were then used for analysis. Helpful mass data analyses are explained in the sections below.

4.1.4.1 Buoyancy Correction

Because the hot convective gases from the FFB created a buoyancy force on the leaf, the raw mass history data showed a large discontinuity when the FFB passed under the leaf sample (see Figure 4.2). This discontinuity yielded negative mass values at the end of the experiment. To correct this unrealistic mass history curve, a constant buoyant force was assumed throughout the run, allowing the mass to shift to a final realistic value (positive mass). Originally, the mass was assumed constant through the time of the discontinuity (i.e. time when buoyancy was first observed in the raw history data to when it leveled off). Because mass was released during this short discontinuity time interval, this constant mass assumption was not accurate. To improve this assumption, a linear regression was determined from the data approximately 1 s (20 time-steps) directly after the discontinuity time interval (data in parallelogram of Figure 4.2), yielding a mass release rate. This rate was then extrapolated through the discontinuity time interval, which yielded realistic mass values (i.e. no longer constant) during the time of discontinuity.

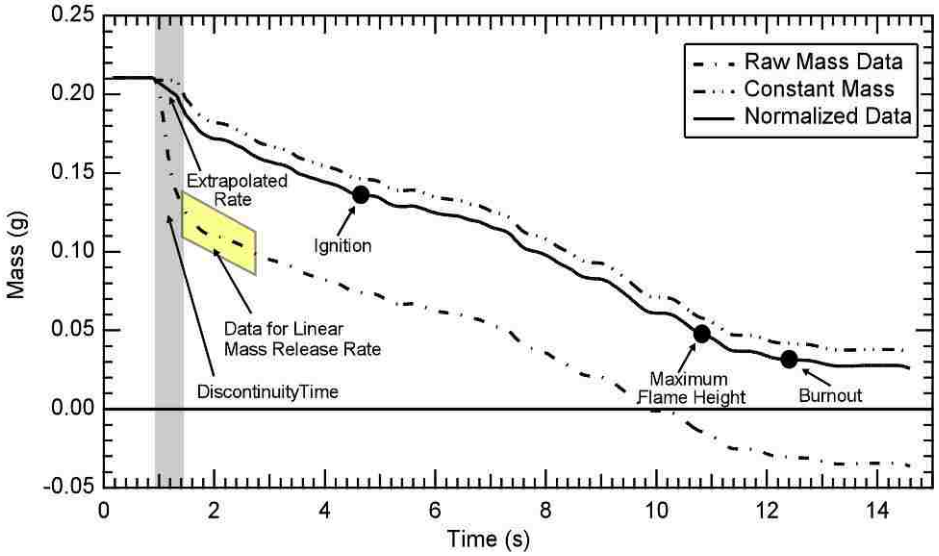

Figure 4.2. Raw mass history data for a canyon maple leaf compared to (a) constant mass through the discontinuity time (dotted line) and (b) extrapolated mass release rate through the discontinuity time (normalized data, solid line).

One test of the applicability of the buoyancy correction is to check the final mass measured at the end of flaming combustion. Using this buoyancy correction, values of the final mass after combustion were 5-20% of the original wet mass, depending on the moisture content of the original sample. These fuels had a volatile matter content of about 80% on a dry basis (Fletcher et al., 2007), leaving a combined ash and char content of about 20% on a dry basis. This was consistent with the observed upper bound for final mass. When moisture was present in the original sample, the overall remaining mass percentage decreased (e.g. with a moisture content of 100%, the final mass (ash and char) should be 10% of the original mass). Because of the agreement between the measured final mass (after buoyancy correction) and the theoretical final mass (remaining ash and char), the constant buoyant force assumption was deemed acceptable. From this corrected mass history profile, specific times for ignition, maximum flame height, and burnout were determined from video images (see Figure 4.2).

4.1.4.2 Mass Release Rate

To determine the mass release rate at any point during the experimental run, the derivative of the normalized mass history data was taken by the point-to-point derivative of the tabulated data. However, this derivative method yielded large amounts of scatter in the mass release rate curve (MR (dm/dt) vs. t as shown in Figure 4.3) due to the small acquisition frequency (18-19 Hz), the sensitivity of the mass balance, and the overall noise of the data. Because of this scatter, values of mass release rate at times of interest (ignition, flame height, burnout) obtained by the point-to-point method were not considered reliable.

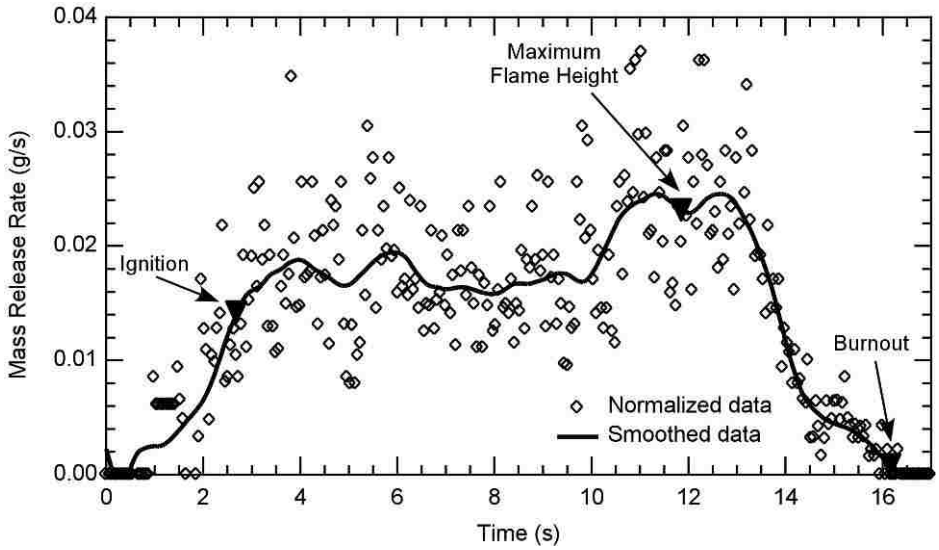

Figure 4.3. Mass release rate data for a manzanita leaf. The normalized data were obtained by a finite difference method while the smoothed data were obtained by a piecewise-cubic regression.

To smooth the scatter, the normalized data were fit in a piecewise-manner to a cubic polynomial regression, since a single regression did not account for the large number of observed discontinuities. The piecewise regression consisted of fitting the

desired data point and a predetermined number of time-steps (25) in each direction to a cubic polynomial. A regression was performed for each data point, and the derivative was taken at each time step using the regressed cubic coefficients to obtain the smoothed overall mass release rate (code for regression shown in Appendix A. 'B. Cubic Function and Gauss Elimination Technique'). The number of regression time-steps was determined arbitrarily; more time-steps smooth the data until no discontinuities are observed (single cubic regression to all the data), while fewer time-steps augment the number and magnitude of the discontinuities (cubic spline function that fits each data point exactly). These smoothed data gave more reliable mass release rates at times of interest than did the point-to-point difference method; they can also help identify regions of evaporation and/or pyrolysis.

4.1.5 Moisture Content Measurements

Moisture content (*MC*) was determined on each day of experiments by a CompuTrac moisture analyzer, which heated approximately 2 g of foliage to 98ºC and maintained that temperature until the mass ceased to change. Moisture content is defined as the mass of moisture divided by the mass of the dry sample (m_{H2O}/m_{dry} or $(m_0-m_{dry})/m_{dry}$), which definition is typically used in the forest products industry. Each *MC* analysis took about 10-20 min depending on the species and *MC*. Two to four replicates of *MC* were taken and averaged for that particular experimental period, which took about an hour to burn 10-15 individual samples. The average value of *MC* was assigned to those samples burned during that experimental period. Freshly-cut samples were burned within 2 days of arrival (bags remained sealed until experiment), since *MC* decreased as the

sample sat in the laboratory. Moisture contents of live samples ranged from 25% to 200%.

4.1.6 Leaf Geometric Measurements

The following sections describe the procedure to determine various leaf parameters. These measurements were performed prior to the experimental run, though some techniques (surface area and perimeter) were analyzed after the experiment.

4.1.6.1 Length, Width, Thickness, Mass

The leaf length (L), width (W), and thickness (Δx) were determined before the experiment by a Chicago Brand digital caliper with an accuracy of 0.01 mm. Length and width were defined as the longest distance from top-to-bottom and side-to-side, respectively (see Figure 4.4a,b). Leaf thickness was measured at multiple locations on the flat leaf (see Figure 4.4c) (excluding leaf veins), and the mean thickness was determined and used as a constant value. Initial mass (m_0) as also measured by a Mettler Todelo mass balance (AB104) and recorded; this balance and the combustion balance showed similar results (± 1 mg).

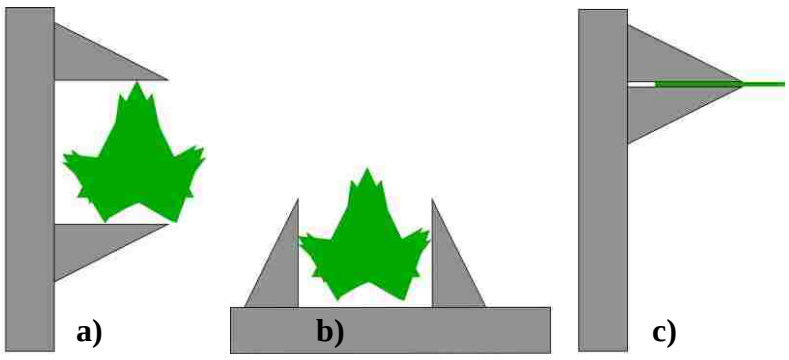

Figure 4.4. Caliper measurement schematic of (a) length, (b) width, and (c) thickness.

4.1.6.2 Surface Area and Perimeter

Prior to the experimental run, digital photographs were taken of each individual sample on a white background. These pictures enabled a measurement to be taken of the surface area (*SA*) and perimeter (*P*) of the leaf, which are not easily measured by hand. The raw image was first converted to a black-and-white image (BW) (see Figure 4.5a). To determine the *SA*, a Matlab code (Appendix A. 'C. Surface Area and Perimeter Code') read the digital BW image as a matrix of intensity numbers ranging from 0-255 in each pixel, black being 0, white being 255. The image was cropped to fit the length and width of the leaf (both measurements were known as discussed in the previous section). If a pixel value was lower than a specified threshold (typically about 100-120), the code reassigned that pixel to a value of 0 (black); otherwise the pixel was reassigned to 255 (white) (see Figure 4.5b). The fraction of black pixels over total pixels was determined; this fraction was then multiplied by the known length and width of the leaf to determine the overall surface area (fraction $\times L \times W = SA$).

The perimeter was calculated using a Matlab function to determine the edge of a visual image by using a variety of methods (e.g. Sobel, Prewitt, Roberts, etc.) (Gonzalez et al., 2004). The result of the edge function using the Sobel method is shown in Figure 4.5c; there are also options for only horizontal or vertical edges of the image which emphasize the edge in its respective direction. The line shown in Figure 4.5c can represent the perimeter of the leaf; this line however is a one-dimensional value (length) on a two-dimensional image (length × width), which must be interpreted.

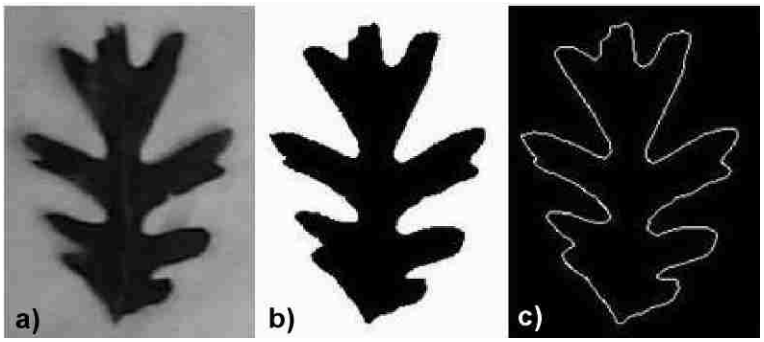

Figure 4.5. Image analysis of a gambel oak broadleaf to determine the surface area and perimeter: (a) Uncropped black-and-white image, (b) surface area image from code, (c) perimeter code image using the Sobel method of the edge function.

To validate a perimeter code using the Matlab edge function, actual perimeters were first determined for 14 randomly selected broadleaf samples. The perimeters were measured by tracing the perimeter of each sample on paper. A string or dental floss was used to outline the entire perimeter of the traced leaf, which was then measured to obtain the actual perimeter of the leaf. The accuracy of this measurement was assumed to be within 3-6%.

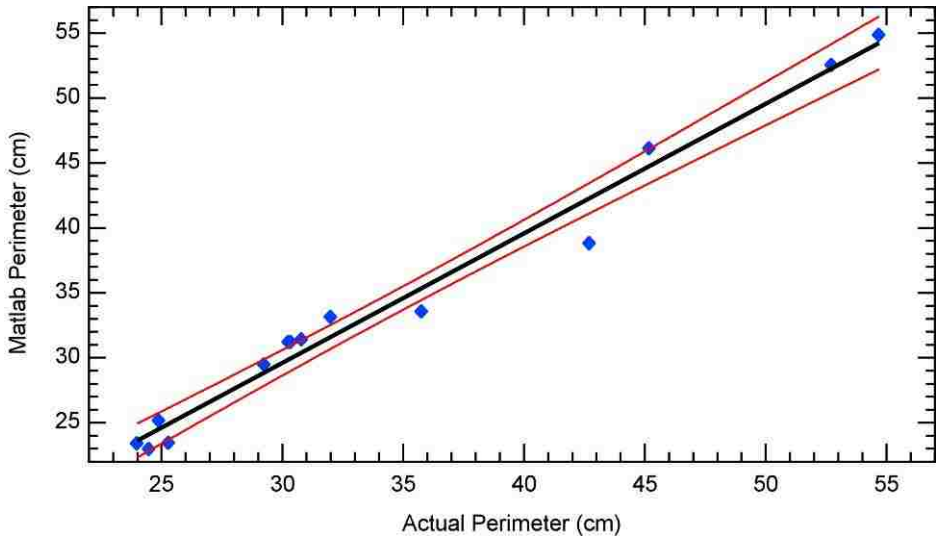

Figure 4.6. Parity plot showing the Matlab-calculated perimeter versus the actual measured perimeter with 95% confidence bands.

The horizontal and vertical distances between pixels (w_p and l_p where $w_p \approx l_p$) were estimated from the known width and length divided by the number of pixels in each direction. The number of edge pixels (from the Matlab function) was determined for each of the edge function options (overall = n_o, horizontal = n_h, vertical = n_v). The first method to determine P was to average the horizontal and vertical distance multiplied by the total number of overall edge pixels ($P = 0.5 \cdot n_o \cdot [w_p + l_p]$) which overestimated the actual or measured P. The second method to determine P was to add the products of the pixel distance and the number of horizontal and vertical edge pixels ($P = w_p \cdot n_h + l_p \cdot n_v$) which underestimated the actual P. Since the first and second methods were over- and underestimates, respectively, an average between the two methods was taken to obtain P.

The actual perimeter and the Matlab-calculated perimeter are compared in the parity plot shown in Figure 4.6. The average error between the Matlab and actual perimeter is 3.4% with the largest error (of the 14) being 9.2%. The linear fit of the parity plot gives a slope and intercept of 0.998 ± 0.09 and -0.310 ± 3.24, respectively, with an r^2 of 0.98 (± indicates 95% confidence interval). This shows that the Matlab-calculated perimeter was an acceptable value.

4.1.7 Fuel Sample Placement

The fuel sample was attached by an alligator clip connected to a stationary, horizontal rod; this rod was placed on the combustion mass balance (stabilized by a counter-weight). The thermocouple was also attached to the horizontal rod to minimize noise to the mass balance. The thermocouple bead was embedded in the tip of the broadleaf samples (displayed in Figure 4.7). For normal experimental runs (configuration

1), the alligator clip and fuel sample were located 4 cm above the FFB; this height above the FFB was also defined as position A.

Table 4.1. Leaf and/or equipment positions for the various experimental configurations used with the FFB.

Configuration	Position A	Between A & B	Position B
1	Leaf with Embedded Thermocouple	-	-
2	Leaf	-	Thermocouple (T_{gas}), Leaf
3	-	-	Thermocouple (T_{gas}), Leaf
4	Metal Disk	-	Thermocouple (T_{gas}), Leaf
5	-	-	Thermocouple (T_{gas})
6	Leaf	O_2 Analyzer	Leaf
7	-	O_2 Analyzer	Leaf

Other configurations used in multi-leaf experiments were also devised (see Table 4.1 and Figure 4.8). Leaf samples and other equipment were also placed at 4 cm above the FFB (position A) and at 6.5 cm above the FFB (defined as position B). Differences in configurations were designed to isolate particular differences between variables (e.g. t_{ig}, T_{ig}) at both positions. Since only one mass balance was programmed for data collection into LabView, the mass history of the multi-leaf configurations (i.e. configurations 2 and 6) was recorded on leaf samples at position B.

For configurations with a thermocouple and leaf sample at position B (configurations 2, 3, and 4), the thermocouple was placed just below the leaf surface, recording the T_{gas} that the leaf experienced during the experiment (leaf surface temperature was measured with the IR camera). The non-combustible metal disk (configuration 4) was used to compare the effects of fluid dynamics on the leaf at position B. The O_2 analyzer is discussed in the following section.

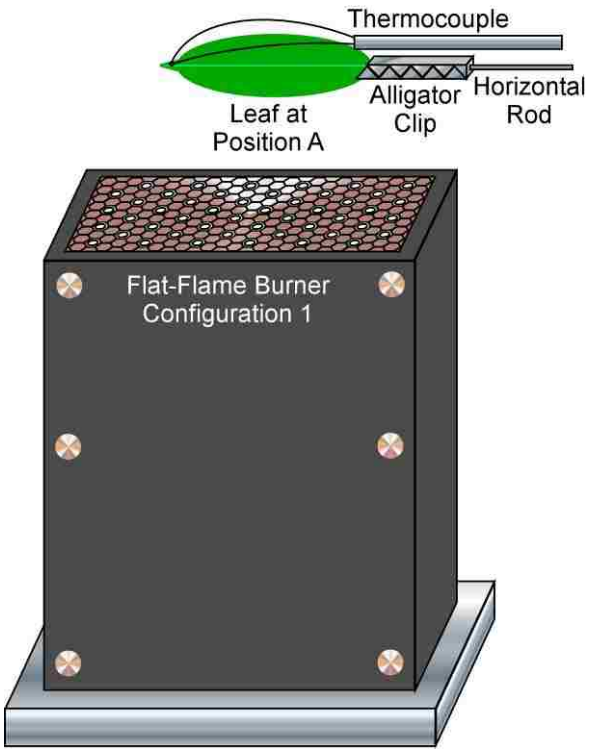

Figure 4.7. Schematic of a single-leaf at position A with embedded thermocouple (configuration 1).

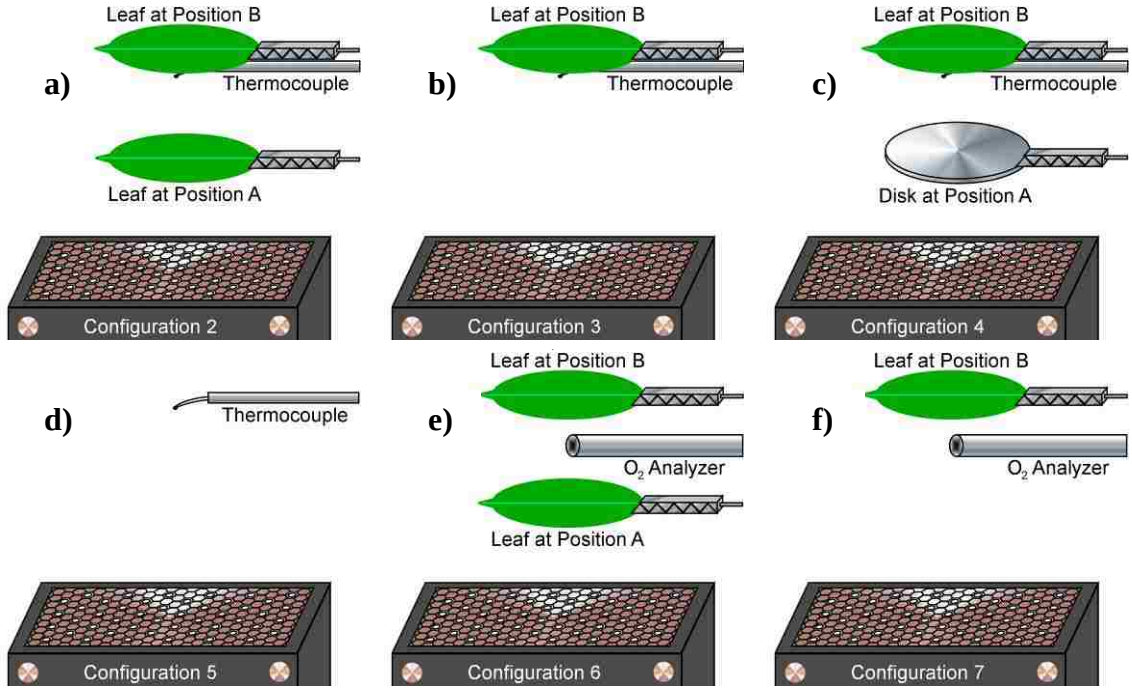

Figure 4.8. Schematic of various experimental configurations of leaf samples and equipment at positions A and B and in between. (a) configuration 2, (b) configuration 3, (c) configuration 4, (d) configuration 5, (e) configuration 6, and (f) configuration 7. Further details for each configuration are found in Table 4.1.

4.1.8 O_2 Content Analysis

An Alpha-Omega Instruments (Series 2000) O_2 analyzer was used to determine the concentration (mol%) of O_2 in the FFB post-flame gases. A metal tube was placed in the convective gases that extracted a low flow rate of gases so as to avoid affecting the overall flow dynamics of the FFB. The hot gases were then pumped through a heat exchanger to cool the gases and then fed through the analyzer. A delay of 3-5 seconds was observed. A steady-state O_2 concentration was determined by placing the metal tube at a desired height above the FFB and periodically recording the O_2 content over an extended period of time (~5 min); the average of these recorded values was determined to be the steady-state O_2 concentration. For a non-steady-state process (during an experimental run of 30 s – i.e. configurations 6 & 7), the minimum O_2 content value was recorded as the O_2 concentration.

4.1.9 Cuticle Extraction

The cuticle is a waxy layer found on the surface of a leaf designed to protect the leaf from dehydration, damaging UV light, and various chemical and mechanical dangers; the cuticle also gives the leaf some structural support (Martin and Juniper, 1970). Understanding the effects of the cuticle on combustion was desirable; therefore, the cuticle was removed from certain leaf species, and results were compared to experiments performed on regular (untreated) samples. Campbell and McInnes (1999) describe various ways to remove the cuticle from the leaf surface by chemical and mechanical means. For the combustion experiments, organic solvents (dichloromethane – CH_2Cl_2, chloroform – $CHCl_3$, n-hexane – C_6H_{14}, xylene – C_8H_{10}) were used for chemical cuticle removal, while abrasion techniques (600 grit sandpaper) were used for mechanical

removal. The goal was to sufficiently remove the cuticle without destroying the remaining leaf material.

4.1.9.1 Chemical Removal

Broadleaf samples were initially soaked in the organic solvent for 10-20 s, removed and dried with a paper towel. This method proved ineffective due to the solvent absorbing into the leaf material, thus altering the inherent combustion of the leaf sample. In the next method, solvents were applied to leaf surface (lying flat) with a small (1 in) paint brush by brushing the leaf approximately 50 times and drying the leaf with a paper towel, thus allowing less contact of the solvent to the leaf material (less solvent absorption into leaf). Since C_6H_{14} and C_8H_{10} have a lower vapor pressure (i.e. lower volatility) than CH_2Cl_2 and $CHCl_3$, C_6H_{14} and C_8H_{10} were not as effective in removing the cuticle. These solvents (C_6H_{14} and C_8H_{10}) remained on the leaf surface and sometimes absorbed into the leaf surface.

To determine if the cuticle was removed from the leaf surface due to solvent extraction, leaf samples were divided in half and held at room temperature, one half treated with solvent, the other half not treated. The mass of the halved samples were recorded at periodic intervals (~10 min). It was found that more mass evolved from the treated leaf halves; Figure 4.9a shows the mass evolution normalized by the initial mass before solvent application. Also, the treated samples experienced discoloration and shriveling (Figure 4.9b). Assuming that mass evolving from the leaf halves was water (which the cuticle is suppose to retain), more mass release of treated samples shows at least some removal of the cuticle. Moreover, experiments on treated samples were completed within 15-25 min of solvent application so that leaf properties (e.g. initial *MC*,

structure) did not change significantly. This time period (15-25 min) allowed for adequate solvent evaporation from the leaf surface. Solvent experiments using whole leaf samples were subjected to the same treatment as described above, and the results were compared to untreated samples (see Section 5.3. Cuticle Extraction Experiments).

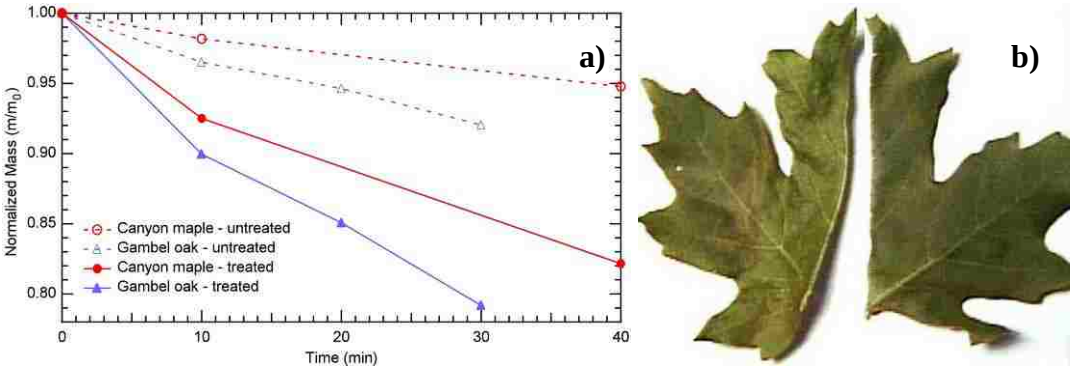

Figure 4.9. (a) Normalized mass history of treated compared to non-treated samples for gambel oak and canyon maple species. (b) Image of canyon maple species after ~1 hr.

4.1.9.2 Mechanical Removal

Abrasion of the leaf by sandpaper (done by hand) was also explored as a technique for cuticle removal. After some abrasion, a gray waxy coat (presumably the cuticle) appeared on the leaf surface, which was eventually removed. Abrasion made the leaf much more pliable, thereby altering the overall structure of the leaf, possibly even destroying cell tissue and plugging normal moisture escape locations. It was not determined if only the cuticle was removed during this process. It is possible that much more that the cuticle was removed. Applying water to the surface before abrasion eased the process, but had the potential of altering the overall moisture content of the leaf. Mechanical removal appeared to be effective for thicker leaves (> 0.4 mm), but destroyed

thinner leaves. This technique was not used extensively due to the various problems just enumerated.

4.2 Leaf History

The following are definitions used to describe various times during the experimental run. These times correspond to other measurements such as m, T, MR, etc. which are helpful in analyzing data and obtaining trends.

4.2.1 Initial Time

The initial time is the start time or the time when the leaf started to heat-up during the experimental run. This times was defined in two ways: for experiments run with a thermocouple embedded in the leaf (1) the first time step (from LabView) which exceeded 30ºC, and for experiments without a thermocouple (2) the value of 2 time steps (~ 0.11 s) that preceded the stopping point of the FFB. This value of 2 time steps (definition 2) is consistent when using a thermocouple (definition 1).

4.2.2 Ignition Time

The ignition time was defined as the time when the first sustainable flame was observed (frame-by-frame) from the LabView video images (Smith, 2005). Sometimes sparks or non-sustainable flames were observed from the leaf sample, but were not defined as ignition. Time to ignition (t_{ig}) was defined as the difference between the ignition time and the initial time.

4.2.3 Maximum Flame Height Time

Initial attempts to measure the maximum flame height time for each experimental run proved to be very subjective; this time was initially determined by frame-by-frame inspection. A new approach was developed to analyze the digital image taken from LabView in a way that is not subjective (nor quite as tedious). The approach is similar to the method used to determine the surface area of the leaf (see Section 4.1.6.2. Surface Area and Perimeter). Each LabView image for the experimental run was converted to a black-and-white (BW) image, and a threshold was specified. A flame area Matlab code (Appendix A. 'D. Flame Height Time Code') determined the area of the flame (observed as white pixels) for each LabView image (see Figure 4.10). The image in the experimental run with the highest white pixel count (i.e. largest area) was defined as the image with the maximum flame height; the corresponding time of the images was the maximum flame height time. The time to maximum flame height (t_{fh}) was defined as the difference between the maximum flame height time and the ignition time. Once the flame height time was obtained, flame heights were estimated (± 0.5 cm accuracy) from the original images using the thickness and/or length of the alligator clip as a reference.

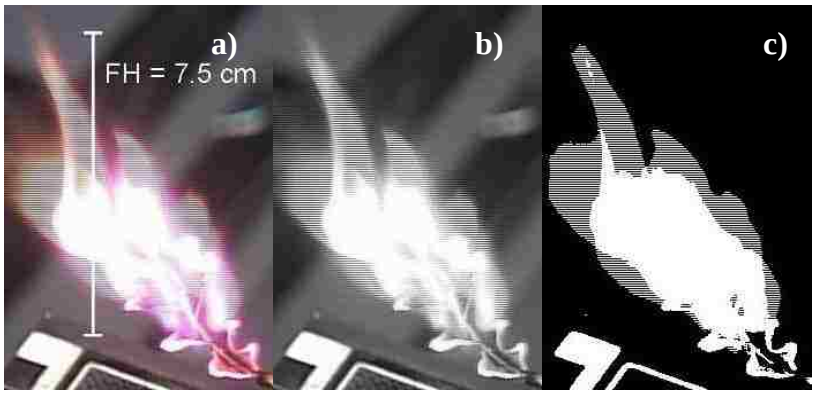

Figure 4.10. Experimental run showing the maximum flame height time for a gambel oak leaf. (a) Original LabView image with cropped alligator clip. (b) Converted black-and-white image. (c) Matlab flame area image.

4.2.4 Burnout Time

The burnout time was defined as the time when the last flame was observed (frame-by-frame) from the LabView video images. This definition limits combustion to devolatilization (excludes char combustion) and assumes that fire spread occurs mostly due to volatiles combustion. The time of flame duration (t_{fd}) was defined as the difference between the burnout time and the ignition time.

4.3 Experimental Fuels

Over 2100 different experiments were performed on 3 groups of species in the United States: (1) southwest Mediterranean (California chaparral), (2) dry interior west (intermountain west), and (3) humid southern (southeastern U.S.). Most experiments were performed on live (moist) samples. Approximately 1.5 lbs of each species was harvested (small branches including leaf foliage), placed in plastic bags, sealed, and shipped (overnight) for testing to the laboratory at Brigham Young University (BYU). Once the samples arrived at BYU, samples were kept sealed and cool until testing (usually 0-2 days after arrival in order to minimize drying in the laboratory). Individual broadleaf samples were selected and detached from the branches at random. Non-broadleaf samples were similarly detached at random; sample sizes were selected to fit within the domain of the FFB. Excelsior was also tested and is discussed below. Most species information discussed below was obtained from a number of sources (Petrides, 1998; Miller and Miller, 1999; Fralish and Franklin, 2002; Ornduff, 2003; Stubbendieck et al., 2003).

4.3.1 California Chaparral Species

California chaparral species are found in a Mediterranean climate with wet, mild winters and hot, dry summers (15-25 inches of rain per year). Individual leaves are typically stiff, thick, heavily cutinized (i.e. thick cuticles), and generally evergreen. Species were collected at the North Mountain Experimental Area adjacent to the San Bernardino National Forest. Four species were tested and are discussed below. Important characteristics of chaparral species are shown in Table 4.2 (also published in (Fletcher et al., 2007)); the American Society for Testing Materials (ASTM) standards were used for determining ash content, volatile matter, and elemental content (Karr, 1978). Images for each species are shown in Figure 4.11. For all species (if shown in tables) ash content and volatile matter testing was performed at BYU while elemental tests were performed at Huffman Laboratories in Golden, Colorado. Variability of values in tables was 0.3%.

Table 4.2. Characteristics of California chaparral species from measured data.

Species	Ash Content* (%)	Volatile Matter Content* (%)	Moisture Content* (%)	Ultimate Analysis† (%)		Leaf Thickness (mm)	Leaf Length (cm)	Leaf Width (cm)
Manzanita	2.2	76.9	25-105	C	52.77	0.15-1.0	2.0-4.0	1.3-2.6
				H	6.32			
				N	0.78			
				O	40.13			
Ceanothus	3.2	75.8	35-105	C	52.94	0.1-0.9	1.0-2.4	0.8-1.6
				H	6.30			
				N	1.08			
				O	39.67			
Scrub Oak	5.1	74.5	40-100	C	51.47	0.015-0.8	2.0-4.4	1.0-2.8
				H	6.50			
				N	1.99			
				O	40.03			
Chamise	2.8	76.9	50-90	C	51.48	0.5-0.6 (needle diameter)	4.0-6.5 (sprig length)	0.4-0.6 (needle length)
				H	6.61			
				N	1.31			
				O	40.60			

*Wt%, Dry basis; †Wt%, Dry ash free basis

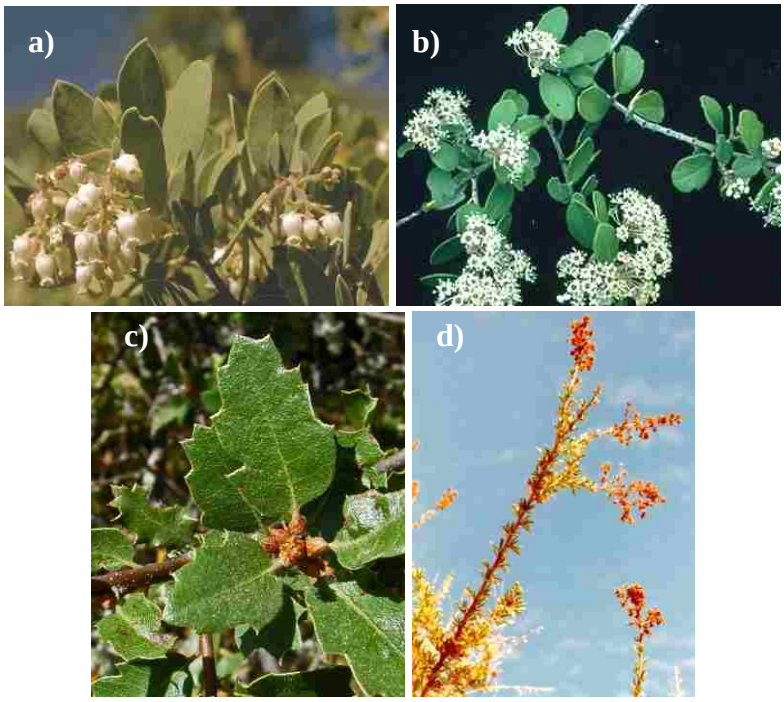

Figure 4.11. Images of California chaparral species: (a) manzanita – Beatrice F. Howitt © California Academy of Sciences (Howitt, 2008), (b) ceanothus – © Br. Alfred Brousseau, Saint Mary's College (Brousseau, 2008), (c) scrub oak – photo by Neal Kramer (Kramer, 2008), and (d) chamise – copyright © Lee Dittmann; used with permission (Dittmann, 2008).

4.3.1.1 Manzanita

Eastwood's manzanita (*Arctostaphylos glandulosa*)[1] is a broadleaf species with leaves that are typically elliptical in shape, though a single point may appear at the end of the leaf. It is larger than other chaparral species (*L* and *W*) and can be quite thick. The species name *glandulosa* means "with glands"; these glands can secret substantial amount of waxes. Manzanita typically has a thick cuticle on the leaf surface compared to other species studied. Manzanita provides the most uniform shape of all species studied, and thus numerous experimental runs were performed on this species. Also, because of

[1] Source for common and scientific plant names – USDA Plants database: http://plants.usda.gov

its near disk-like shape, properties of manzanita were used to model the combustion of a cylindrical disk (see Section 6. Leaf Modeling).

4.3.1.2 Ceanothus

Hoaryleaf ceanothus (*Ceanothus crassifolius*) is also a broadleaf species with leaves that are elliptical in shape, though not as elongated as manzanita (*L*/*W* is closer to unity). Ceanothus is the smallest chaparral leaf species studied, though its leaves are much thicker than scrub oak and are comparable to manzanita (*crassifolius* meaning "thick-leaved"). The perimeter is also sometimes surrounded by tiny teeth-like projections (*Ceanothus* meaning "spiny shrub").

4.3.1.3 Scrub Oak

Scrub oak (*Quercus berberidifolia*) is also a broadleaf species with leaves that are elliptical in shape. Leaf size is larger than ceanothus, though somewhat smaller than manzanita. The upper surface of the leaf is shiny and smooth, while the lower surface typically is covered with short, soft hair. The perimeter commonly has 7-20 spines that are longer and more distinct than the teeth of ceanothus.

4.3.1.4 Chamise

Chamise (*Adenostoma fasciculatum Hook. & Am*) is a non-broadleaf species where needles (or small pointy leaves) form in small bundles (fascicles) or clusters around the stem; typically 3-10 needles per bunch. Needles are typically smooth and have grooves up the middle. Stems branch substantially and loosely (diffuse). Sprig lengths of

chamise were arbitrarily chosen by clipping terminal stems at random that would fit within the domain of the FFB.

4.3.2 Intermountain West Species

Intermountain west species are found in climates with hot, dry summers and can have either mild or harsh winters, depending on the location and elevation of the individual sample. Provo, UT and the surrounding areas typically have cold, harsh, wet winters. These species were collected in the forests and deserts surrounding BYU in Provo (within 1-1.5 hr driving distance). Each harvest location is discussed in each individual species section. Six species were tested and are discussed below. Important characteristics of these species are shown in Table 4.3 (adapted from Fletcher (2007)). Images for each species are shown in Figure 4.12.

4.3.2.1 Gambel Oak

Gambel oak (*Quercus gambelii* Nutt.) is a deciduous, broadleaf species with deeply lobed fingers which can sometimes reach near the center vein of the leaf. Gambel oak typically has 6-12 lobes on each leaf. The upper surface of the leaf is shiny and smooth, while the lower surface typically is covered with dense, short, soft hair. This broadleaf is significantly thinner than chaparral broadleaf species. This species was typically harvested on mountain slopes and in canyons at an elevation from 1200-1600 m (3900-5200 ft). Samples were selected with sizes to fit within (or near to) the domain of the FFB.

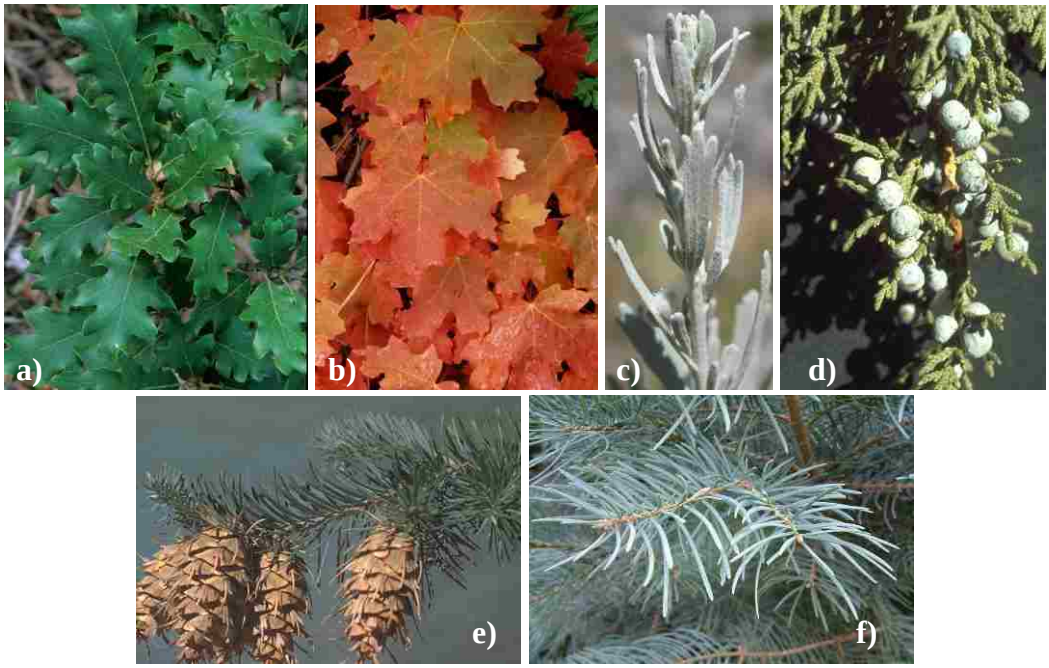

Figure 4.12. Images of intermountain west species: (a) gambel oak (Sivinski, 2008), (b) canyon maple (Sivinski, 2008), (c) big sagebrush (Willand, 2008), (d) Utah juniper – J.E. (Jed) and Bonnie McClellan © California Academy of Sciences (McClellan and McClellan, 2008), (e) Douglas-fir – Charles Webber © California Academy of Sciences (Webber, 2008), and (f) white fir (Landry, 2008).

4.3.2.2 Canyon Maple

Canyon maple (*Acer grandidentatum* Nutt.) is a deciduous, broadleaf species with blunt fingers. The leaf typically has 5 primary veins with 3-5 primary lobes or teeth (*dentatum* meaning "teeth"); the teeth are not as deeply cut as the lobes of the gambel oak species. The surface (both upper and lower) can be covered either with hair or a waxy coating. This species is also significantly thinner than the chaparral broadleaf species. This species was typically harvested on mountain slopes and in canyons at an elevation from 1200-1600 m (3900-5200 ft). Samples were selected with sizes to fit within (or near to) the domain of the FFB.

4.3.2.3 Big Sagebrush

Big sagebrush (*Artemisia tridentata* Nutt.) is a deciduous, broadleaf species with leaves that are triangular in shape with three blunt teeth at the tip of the leaf (*tri* meaning "three", *dentata* meaning "teeth"), the tip being the short edge of an isosceles triangle. This species has much higher moisture content than other species, though is much smaller (by mass and thickness). This species was typically harvested on desert plains and occasionally in canyons at an elevation from 1100-1500 m (3600-4900 ft).

4.3.2.4 Utah Juniper

Utah juniper (*Juniperus osteosperma* (Torr.) Little) is an evergreen, multi-stemmed, non-broadleaf (conifer) species with scale-like needles. These needles lack a resin gland but are typically covered with a white, waxy coating. This species was typically harvested on the desert plains at an elevation from 1100-1500 m (3600-4900 ft). Sprig lengths of juniper where arbitrarily chosen by clipping terminal stems at random that would fit within the domain of the FFB.

4.3.2.5 Douglas-Fir

Douglas-fir (*Pseudotsuga menziesii* (Mirbel) Franco) is an evergreen, non-broadleaf (conifer) species with thin, flat needles surrounding the stem. These needles contain a stomata band on the lower surface of the needle and are somewhat aromatic. This species was typically harvested at a higher elevation than the aforementioned intermountain west species at an elevation from 1400-1800 m (4600-5900 ft). Sprig

lengths of Douglas-fir where arbitrarily chosen by clipping terminal stems at random that would fit within the domain of the FFB.

Table 4.3. Characteristics of intermountain west species from measured data.

Species	Ash Content* (%)	Volatile Matter Content* (%)	Moisture Content* (%)	Ultimate Analysis† (%)		Leaf Thickness (mm)	Leaf Length (cm)	Leaf Width (cm)
Gambel Oak	2.9	83.5	50-125	C	49.15	0.1-0.4	3.0-11.0	1.5-9.0
				H	6.23			
				N	2.52			
				O	42.10			
Canyon Maple	3.5	83.9	55-160	C	45.93	0.1-0.5	2.0-6.0	3.0-8.0
				H	6.14			
				N	2.11			
				O	45.82			
Big Sagebrush	3.9	85.2	100-195	C	48.52	0.1-0.5	2.0-5.0	0.6-1.2
				H	6.46			
				N	2.25			
				O	42.77			
Utah Juniper	4.0	84.8	40-100	C	49.92	1.0-1.5 (needle diameter)	3.5-8.0 (sprig length)	0.4-1.0 (needle length)
				H	6.88			
				N	1.33			
				O	41.87			
Douglas-Fir	NA	NA	80-145	NA		0.3-0.7 (needle diameter)	2.3-7.5 (sprig length)	NA
White Fir	NA	NA	80-100	NA		0.4-0.9 (needle diameter)	2.2-6.3 (sprig length)	NA

*Wt%, Dry basis; †Wt%, Dry ash free basis

4.3.2.6 White Fir

White fir (*Abies concolor* (Gord. & Glend.) Lindl. ex Hildebr.) is an evergreen, non-broadleaf species with two rows of needles each side of the stem that occasionally curl upward from the stem. These needles are longer than Douglas-fir needles and have 4-7 rows of stomata on the lower surface. White fir is strongly aromatic. This species was harvested at an elevation similar to Douglas-fir at an elevation from 1400-1800 m (4600-

5900 ft). Sprig lengths of white fir where arbitrarily chosen by clipping terminal stems at random that would fit within the domain of the FFB.

4.3.3 Southeastern Species

Southeastern species are found in a humid, subtropical climate with hot, humid summers and chilly to mild winters with significant amounts of precipitation. Large amounts of fuel are produced in this climate where fires can burn through these dense shrub species. Southeastern species were collected on the Eglin Air Force Base 10 miles south of Crestview, Florida. Four species were tested and are discussed below. Important characteristics of these species are shown in Table 4.4. Images for each species are shown in Figure 4.13. ASTM tests (ash, volatile, elemental) were not performed on southeastern species because limited samples and time were available.

Table 4.4. Characteristics of southeastern species from measured data.

Species	Moisture Content* (%)	Leaf Thickness (mm)	Leaf Length (cm)	Leaf Width (cm)
Fetterbush	80	0.2-0.6	3.4-6.2	1.6-3.1
Gallberry	95	0.3-0.4	3.0-4.2	1.1-1.9
Wax Myrtle	105	0.3-0.5	5.1-8.3	1.4-2.3
Saw Palmetto	70	0.1-0.3	5.7-9.9	0.7-1.9
*Wt%, Dry basis				

4.3.3.1 Fetterbush

Fetterbush Lyonia (*Lyonia lucida* (Lam.) K. Koch) is an evergreen species with elliptical leaves that taper to a point. The leaves are a dark, shiny green on the upper surface, while lighter on the lower surface. Fetterbush is thinner than chaparral broadleaf species though similar in size to manzanita.

4.3.3.2 Gallberry

Gallberry (*Ilex glabra* (L.) Gray) is an evergreen species with elliptical leaves that have a tapering base and an obtuse tip with a few very blunt teeth. Leaves are generally tough, leathery, and thick, but are thinner than other chaparral species though similar in size to manzanita.

Figure 4.13. Images of southeastern species – courtesy of the University of South Carolina Herbarium, photos by Linda Lee (Lee, 2008): (a) fetterbush, (b) gallberry, (c) wax myrtle, and (d) saw palmetto.

4.3.3.3 Wax Myrtle

Wax myrtle (*Myrica cerifera*) is an evergreen species with elliptical leaves with a long, tapering base. The leaves are fairly narrow and generally curl in various directions (e.g. do not lay flat). Wax myrtle is strongly aromatic and is thinner than other chaparral broadleaf species.

4.3.3.4 Saw Palmetto

Saw palmetto (*Serenoa repens* (Bartr.) Small) is spike-shaped leaf that spiral around a common stem forming a palm- or fan-shaped plant. Lengths of these palms can be up to 1 m long with the individual leaves being 3-5 cm wide. Palms are fibrous and tough. Leaves taper to a point that generally have two tips which typically consist of dead plant material. Lengths of saw palmetto were arbitrarily determined by clipping terminal leaves at random that would fit within the domain of the FFB.

4.3.4 Excelsior

Excelsior consists of the aspen wood shavings (*Populus tremuloides Michx.*) and is commonly used as packing for shipping. It appears as bands or strings of wood (see Figure 4.14a) that are cylindrical in shape but fairly thin (d = 0.4-1.5 mm). Lengths of the experimental samples were arbitrarily chosen by clipping pieces of excelsior (see Figure 4.14b) that would fit within the domain of the FFB; these lengths ranged from 3.5-7.5 cm.

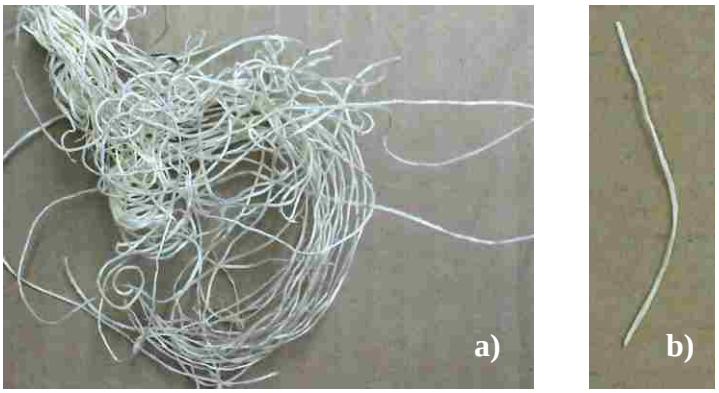

Figure 4.14. Excelsior samples as (a) grouped bands or strings and as (b) arbitrary length used for experimental run.

Moisture content of dry excelsior (e.g. samples sitting in the laboratory) corresponded to (was affected by) the humidity of the atmosphere (equilibrium *MC*). Moisture content of wet excelsior (e.g. treated with water) was altered by placing samples over warm water in a sealed environment for 3-4 hr. This raised the *MC* values close to the wood fiber saturation point (Simpson and TenWolde, 1999). *MC* for these excelsior experiments ranged from 3-31% on a dry-mass basis.

5. Experimental Results and Discussion

Experiments were performed on over 2300 individual fuel samples, both for single-sample and two-leaf configurations. Over 160 cuticle extraction experiments were also performed to determine the effects of the cuticle on leaf combustion. Results and correlations are shown here.

5.1 Single-Sample Experiments

Over 1800 experiments were performed on single-samples (configuration 1). Both qualitative and quantitative data were obtained from these experiments.

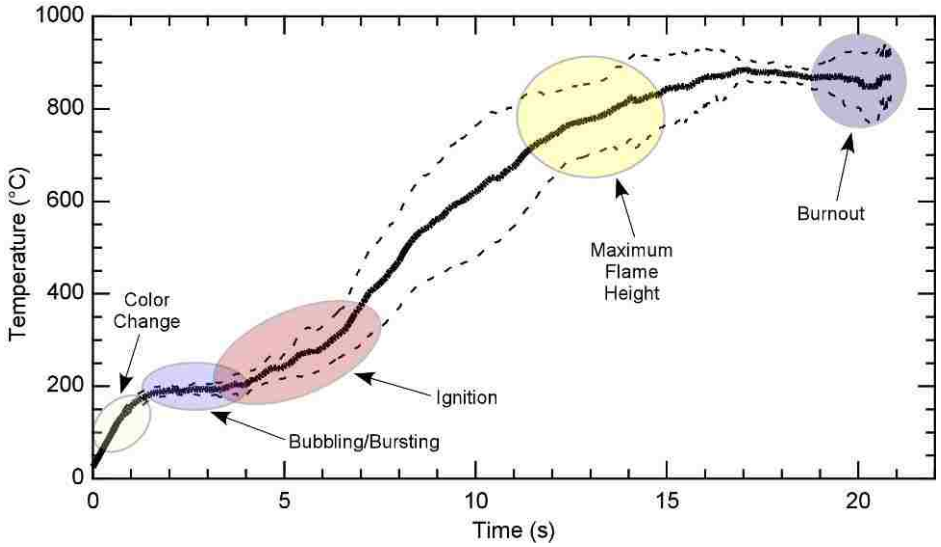

Figure 5.1. Representative temperature profile (manzanita) showing possible times and temperatures of color change, bubbling/bursting, ignition, maximum flame height, and burnout.

5.1.1 Qualitative Results

The following sections describe the overall burning characteristics of the various leaf species that were studied. Significant observations obtained from the video and IR images are discussed. Some of these qualitative observations for particular species are described by Smith (2005) and Fletcher et al. (2007). A temperature profile showing the general time and temperature of some of these observations is shown in Figure 5.1.

5.1.1.1 Overall Burning Characteristics

Ignition varied among the species presented. If tips were present on horizontal broadleaf samples, ignition normally occurred at these the tips (local ignition) of the leaves (e.g. scrub oak, sagebrush). Saw palmetto was an extreme species where local ignition occurred quickly on the two tips of the leaf. Occasionally the flames from the saw palmetto tip could not be sustained to ignite the remaining leaf body. If no significant tips were present on the leaf (e.g. manzanita, ceanothus), the leaf ignited uniformly around the perimeter (uniform ignition). Once ignited, the flame propagated towards the center of the leaf. The flames from the perimeter coalesced into one flame and subsequently burned to a maximum flame height; this height usually occurred slightly over half-way through the flaming period; the average for all samples was 56.73 ± 0.10% ('±' indicates 95% confidence interval). The flame then diminished and extinguished.

For non-broadleaf samples, ignitions normally occurred in multiple locations (multiple needles) on the samples. Some species (e.g. Douglas-fir, juniper) regularly experienced jetting which occurs when the sample ignites quickly, but due to the high mass transfer rate of gases from the sample, local ignition cannot be sustained; this often

occurred multiple times in one experiment from various needles on the non-broadleaf sample, causing somewhat violent burning (see Figure 5.2). These jets were observed to blow into the FFB. After the local ignitions were sustained, the flames from these various ignitions coalesced into one flame, usually engulfing the entire sample in flame. Because these non-broadleaf samples have more multiple tip locations and typically ignite more quickly than the broadleaf species, the surface area and perimeter exposed to the heat source seems to significantly affect the ignition behavior of the sample.

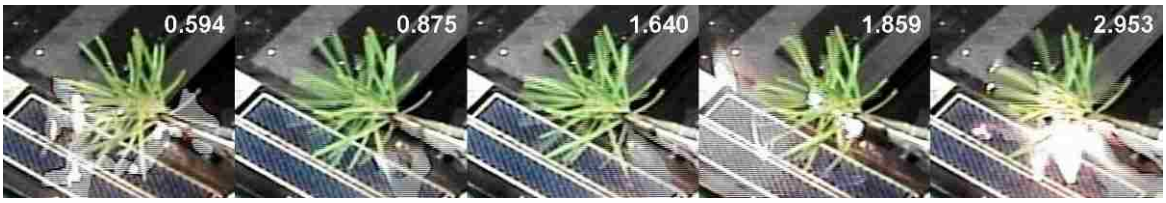

Figure 5.2. Jetting sequence for a Douglas-fir sample. Numbers indicate the time difference (s) from the initial time of the experimental run. Video in Appendix D.

5.1.1.2 Color Change

Most broadleaf samples experienced a color change after the initial time but before ignition. Samples turn from a dusty green to a wet or shiny green during this color change process. It is believed that this color change is due to melting waxes (e.g. cuticle) on the surface of the leaf. Quantitative results of this color change is further discussed in Section 5.3 Cuticle Extraction Experiments.

5.1.1.3 Bubbling

Bubble formation is characterized by small amounts of either (1) liquid accumulating on the top leaf surface (liquid bubbling) or (2) gas pockets forming within the leaf material (interior bubbling). Each type of bubbling is discussed here.

Liquid bubbling was observed solely in manzanita samples. Liquid was observed before ignition and collected around the perimeter of the leaf, which then propagated towards the center of the leaf. The pooled liquid then began to move around the leaf surface (similar to water droplets evaporating on a hot skillet) (Figure 5.4). This liquid evaporated from the leaf surface then the leaf ignited soon thereafter. This behavior normally occurred at a moderate *MC* (~75%).

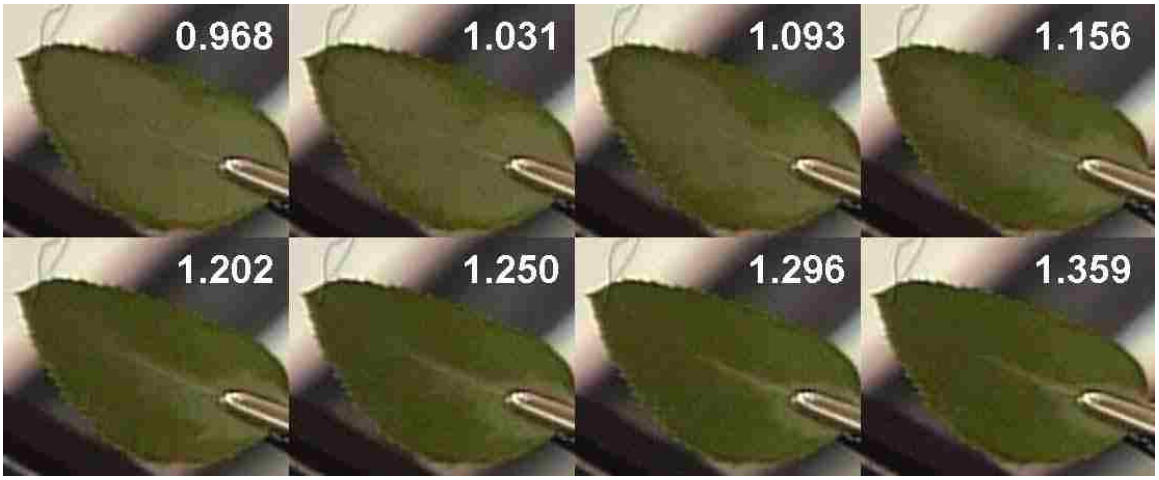

Figure 5.3. Color change sequence for a manzanita leaf. Numbers indicate the time difference (s) from the initial time of the experimental run. Video in Appendix D.

To determine the nature of this liquid, individual samples were subjected to the convective gases of the FFB and, when observed to bubble, were quickly removed from the FFB. The liquid was observed to solidify (or resolidify) once removed from the FFB (Figure 5.5). This indicates that the liquid is primarily a wax and most likely the cuticle of the manzanita surface. This resolidified wax was scraped off the surface of the leaf, but the sample was lost before analysis could be performed. Scraping off the wax will need to be repeated; the analysis can be performed by gas chromatography, mass spectrometry, or other methods for better characterization.

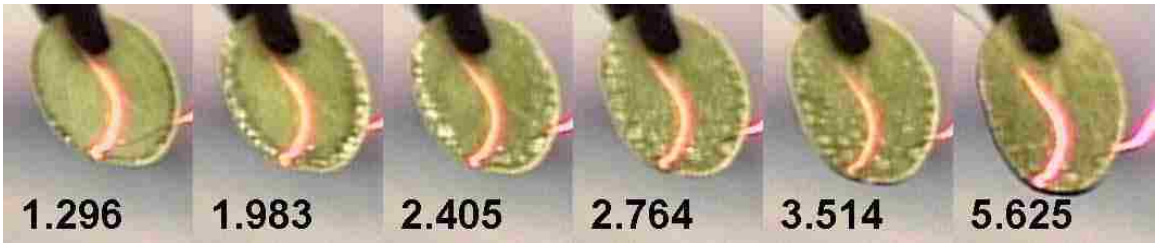

Figure 5.4. Liquid bubbling sequence for a manzanita leaf. Numbers indicate the time difference (s) from the initial time of the experimental run. Video in Appendix D.

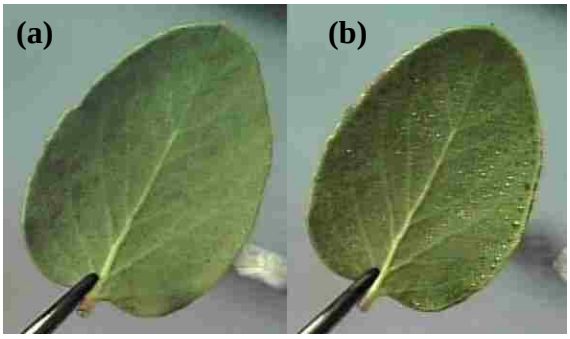

Figure 5.5. (a) Manzanita leaf prior to subjection to FFB. (b) Leaf after FFB which shows resolidified wax on the leaf surface.

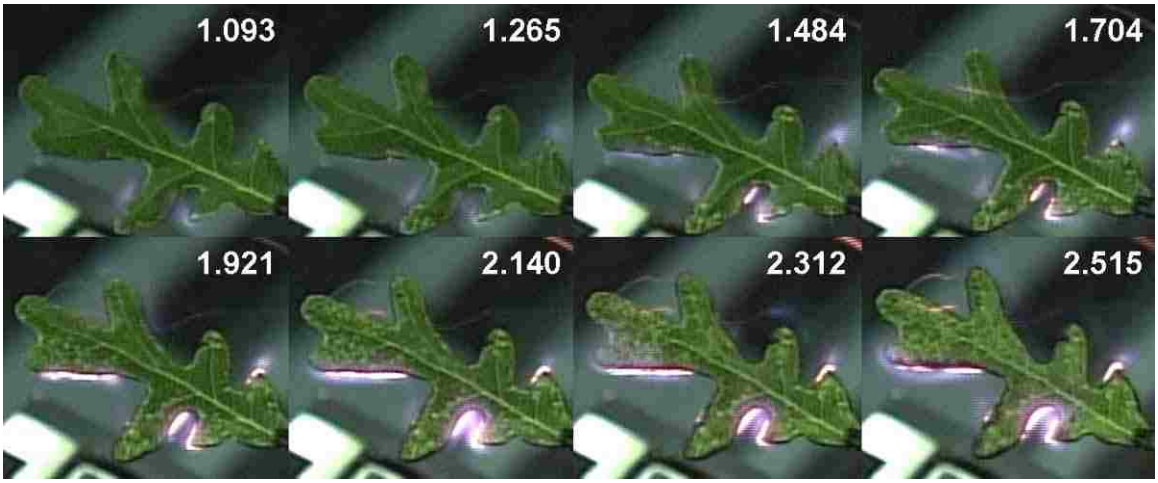

Figure 5.6. Interior bubbling sequence for a gambel oak leaf. Numbers indicate the time difference (s) from the initial time of the experimental run. Video in Appendix D.

Interior bubbling was observed in all broadleaf species except sagebrush and the southeastern species, and occurred primarily at moderate *MC* (~60-90%, varied by

species). This phenomenon was observed as visible spots or bubbles that appeared to originate in the intercellular spaces of the leaf and did not move about the surface as observed in liquid bubbling. Mild audible crackling was also observed. Interior bubbling is most likely caused as small gas pockets of water vapor escape the surface of the leaf. Pressure builds inside these small gas pockets as the temperature rises. The pockets of evaporated moisture try to escape from the interior of the leaf, and the mass transfer of this moisture is limited by pore diffusion and/or the waxy layer on the surface.

5.1.1.4 Bursting

Bursting was observed in all chaparral broadleaf species at high *MC* (~90-130%, varied by species), and was characterized by small explosions within the leaf surface and possibly by the ejection of small leaf material from the main leaf body. It was often accompanied by violent crackling sounds and by craters or pockmarks on the leaf surface. This phenomenon is thought to be similar in nature to interior bubbling (i.e. the evaporation of water on the inside of the leaf causes a pressure increase). Whether a leaf bubbles or bursts depends on the thickness of the leaf as well as other physiological variables (e.g. *MC*, stomata).

Figure 5.7. (a) Bursting manzanita during reaction in FFB. Video in Appendix D. (b) Upper surface of burst manzanita leaf. Sample was removed from FFB after bursting occurred. Number indicates the time difference (s) from the initial time of the experimental run.

Bursting was observed in the chaparral broadleaf species (manzanita, ceanothus, scrub oak) but not in the other broadleaf species studied, particularly intermountain species (canyon maple, gambel oak, sagebrush). Craters resulting from the burst leaf were approximately 6 mm in diameter for manzanita leaves (Figure 5.7), which is fairly large compared to the dimensions of the leaves. Figure 5.8 shows the video camera image and the IR image of a manzanita leaf at two different times during the experimental run. Analysis of the IR images shows a surface temperature drop of about 40°C at the burst location over a period of 0.10 s. It is believed that this local temperature drop is due to evaporated water escaping from the hot pocket inside the leaf surface following the burst.

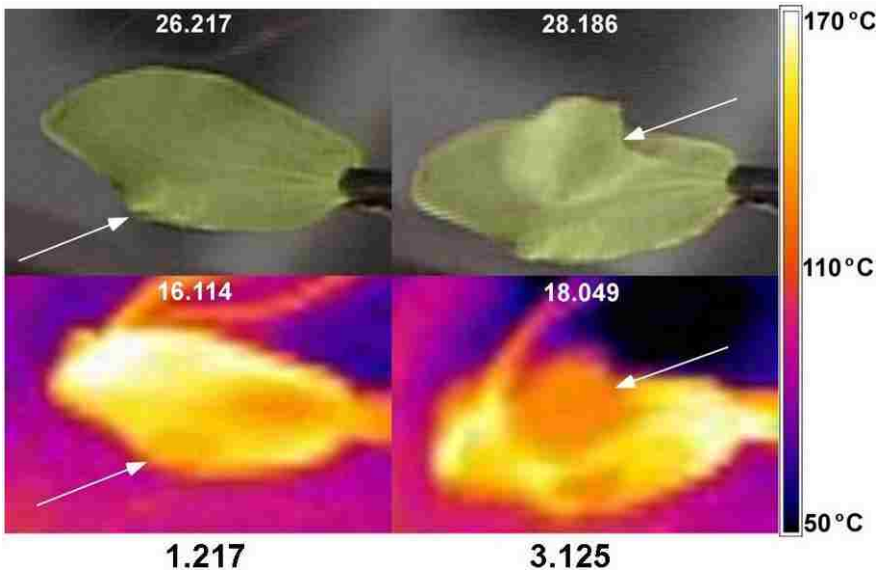

Figure 5.8. Video camera images (top) and corresponding IR camera images (bottom) of a bursting manzanita leaf. The duller yellow spots indicate a lower temperature in the bursting region. White numbers indicate the original recorded time (s) for the respective video and IR images. Black numbers indicate the time difference (s) from the initial time of the experimental run. Two videos in Appendix D.

There are two main routes for evaporated moisture to escape from the leaf interior: (1) through the stomata (small pores that monitor the transfer of CO_2 and H_2O

into and out of the leaf (Sadava et al., 2008)) or (2) through the epidermal layers (see Figure 5.9). The path of least resistance is for the moisture to evaporate into the void spaces surrounding the spongy mesophyll cells on the lower interior part of the leaf. From there, the vaporized moisture can either escape through the stomata (usually more numerous or even exclusively on the lower side of the leaf (Willmer and Fricker, 1996)) or bubble/burst through the lower epidermis. Stomata tend to close in the absence of light (Sadava et al., 2008) which would most likely occur when being shipped. Even if the stomata were closed, the guard cells would most likely be the path of least resistance for moisture to escape.

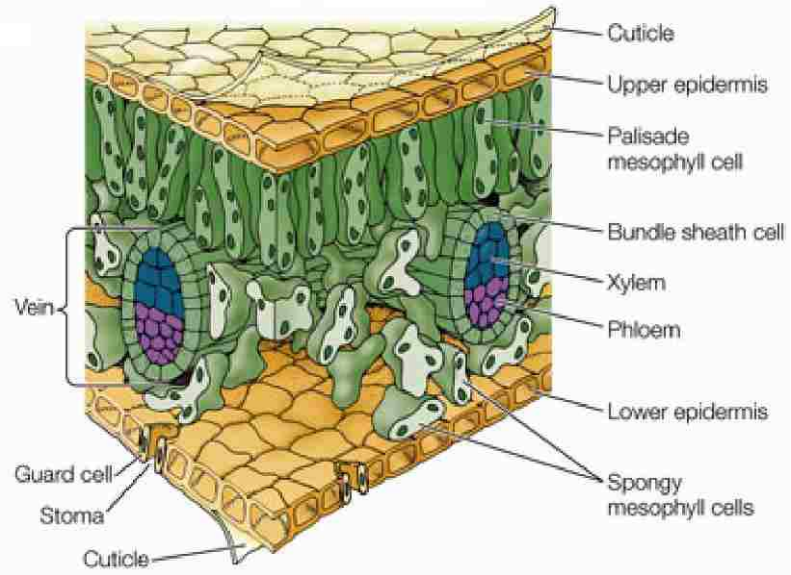

Figure 5.9. Three-dimensional diagram showing the general structure of a leaf. Image provided by Sadava et al. Figure 34.23A (2008); used with permission.

If the leaf heats up faster than the moisture can diffuse through the epidermal layer or out the stomata, then the pressure builds inside the leaf until it exceeds the surface tension of the leaf, which causes moisture to be released by interior bubbling or

bursting. Experiments on ceanothus and scrub oak have shown bursting on the lower side of the leaf, while the upper side remains intact. However, evidence of the burst was visible on the upper side (Figure 5.10). The upper side of the leaf contains columns of organized cells (palisade mesophyll cells) which can protect the upper side from bursting. However, manzanita exhibited upper-side bursting, suggesting that the layer of palisade cells in the manzanita leaves is not as organized as in the ceanothus and scrub oak leaves.

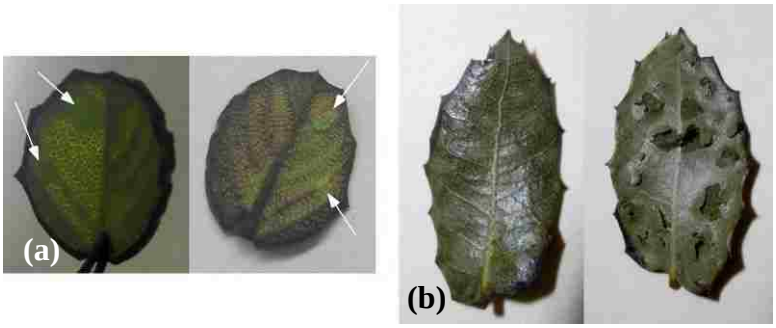

Figure 5.10. Upper (left) and lower (right) images of (a) ceanothus and (b) scrub oak leaves following subjection to the FFB that were quickly removed after bursting. These images display lower-side bursting with evidence of the burst on the upper side.

On one particular day of experiments, a hissing noise was observed when scrub oak leaves were burned right-side-up, suggesting that the vapor inside the leaf could not exit the stoma quickly enough. However, when the leaves were burned up-side-down, little or no hissing was observed, indicating that the vapor was exiting through the more numerous stomata located on the underside of the leaf (i.e. the top of an up-side-down leaf).

No intermountain broadleaf species experienced bursting, although some experienced interior bubbling. This may be due to thickness of the intermountain species, which is about 0.15 mm thinner on average than the chaparral species, or due to structural

differences or compositions between different species of leaves. The thicker species (chaparral) may have the necessary mass transfer resistance inside the leaf to create sufficient pressure for full-scale bursting, which the thinner species do not have. Bursting may be a form of interior bubbling on a larger scale; hence, violent crackling is observed in bursting while only mild crackling is observed in interior bubbling.

Bursting does not occur in every sample with high *MC* (as does bubbling with moderate *MC*). One shipment of samples was filled with two different manzanita types: (1) a rounder, paler, smoother-to-the-touch leaf with a *MC* of 78%, and (2) a straighter, slightly greener, and rougher-to-the-touch leaf with a *MC* of 68% (Figure 5.11). The higher *MC* leaves (1) did not experience bursting while the lower *MC* leaves (2) did. The higher *MC* leaves appeared to be earlier in growth (i.e. younger) than the lower *MC* leaves (indicated by the black stems in Figure 5.11b). It is possible that bursting behavior relates to the stage of growth the leaf is experiencing.

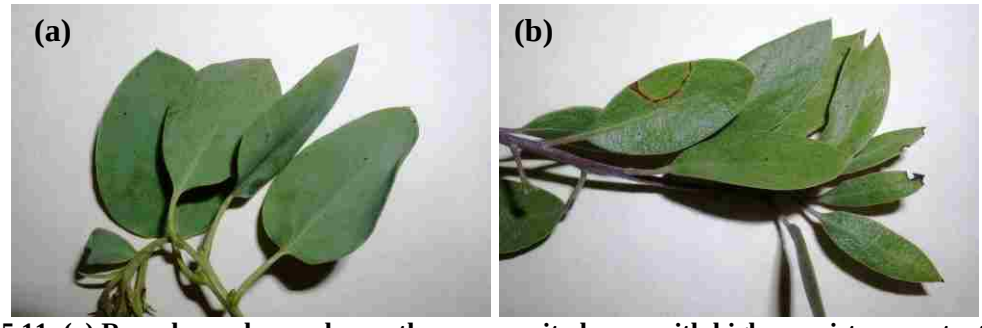

Figure 5.11. (a) Rounder, paler, and smoother manzanita leaves with higher moisture content (78%). (b) Straighter, greener, and rougher manzanita leaves with lower moisture content (68%).

5.1.1.5 Brand Formation

Brand formation occurs when pieces either of ignited or potentially ignitable material are separated from the leaf or stem, causing them to be lofted to another area,

which could start new fires. The formation of brands was observed in many of the species studied, but in a variety of ways. The most common type of brand formation was the ejection of leaf material as a result of bursting. The small particles (< 1 mg) were not observed to ignite, but had the possibility of igniting while entrained in the down-wind flames of the wildland fire. Scrub oak leaves sometimes had protruding spines around the perimeter of the leaf. If the scrub oak leaf had a high *MC* and a high heat flux, these spines explosively separated from the main body of the leaf (typically just before ignition). These spines were ejected from the main leaf body, forming small brands; this is similar to bursting, but the only the spines were ejected. Since these bursting-type events (dealing with small materials) would have a low probability of igniting fuel down-wind due to their small mass (< 1 mg), their behavior was not made a large focus of study.

Figure 5.12. Brand formation sequence of sagebrush leaf showing tip and stem ignition as well as leaf brand. Numbers indicate the time difference (s) from the initial time of the experimental run. Video in Appendix D.

Sagebrush also experienced brand formation in a unique manner. Ignition for sagebrush usually occurred first on one or more of the three lobes on the tip of the leaf. Not long after the ignition of the tip, the stem of the leaf would ignite (Figure 5.12). If this stem ignition occurred early in the experimental run, the stem would burn well before the rest of the leaf, detaching the leaf from the alligator clip; the whole leaf would be

considered a brand (~25 mg). When harvesting the sagebrush samples, it was observed that the leaves tended to fall off the branch very easily. Since the sagebrush stems are prone to ignite early and are fairly weak, the possibility of brand formation is much higher (as compared to bursting-type events).

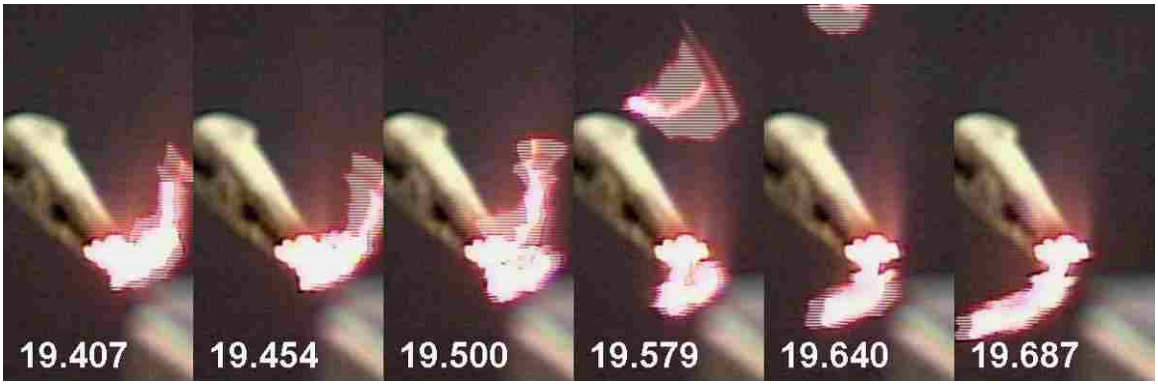

Figure 5.13. Brand formation sequence of a chamise sample. Numbers indicate the time difference (s) from the initial time of the experimental run. Video in Appendix D.

The non-broadleaf species (particularly chamise and juniper) were observed to form sizeable brands after ignition. Ignition normally started on the individual needles then propagated to the stem. However, brands were commonly formed when the stems burned before the bulk of the upper section (before all the needles burned). This weakened the stem and did not support the weight of the upper section of the sample (Figure 5.13). Brands were also observed to form from the ignited berries of the juniper samples. These berries burned significantly longer than the rest of the sample, which caused the berries to fall from the sample onto the FFB (Figure 5.14). Another form of brand formation in non-broadleaf samples was in Douglas-fir and white fir. These species experienced jetting (discussed above in Section 5.1.1.1. Overall Burning Characteristics)

which ejected whole, flaming needles from the main sample. Brand formation from these non-broadleaf samples would yield significant (yet still small) brands.

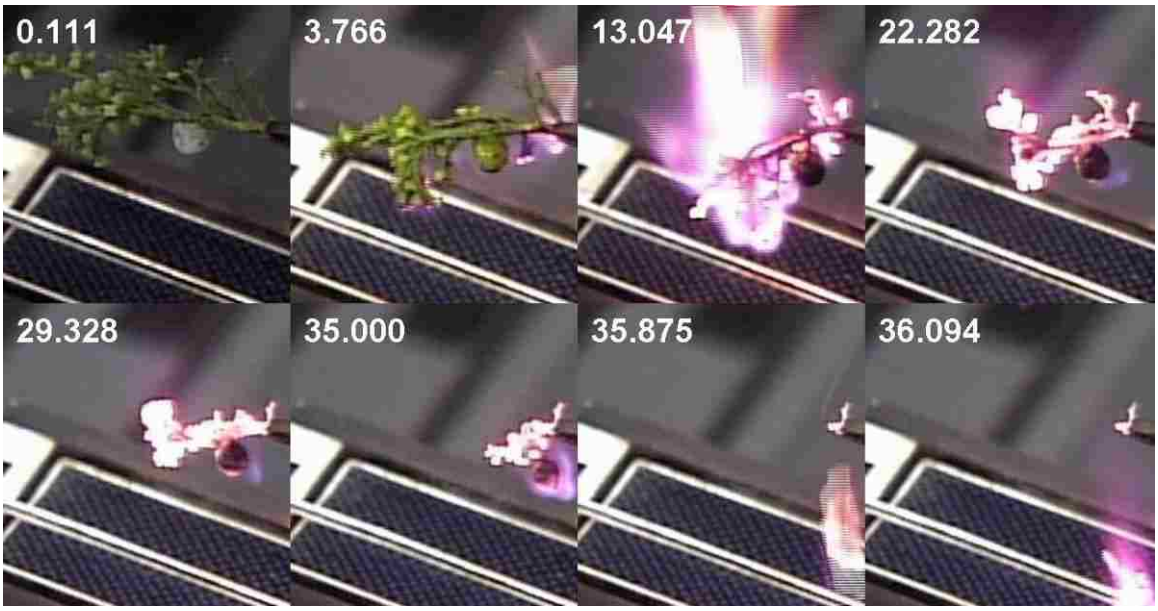

Figure 5.14. Brand formation sequence for a berry on a juniper sample. Numbers indicate the time difference (s) from the initial time of the experimental run. Video in Appendix D.

5.1.1.6 Bending

When the leaf is exposed to the hot convective gases of the FFB, the leaf experiences bending which opposes the direction of the convective gases. Bending can occur before and after ignition. All species experienced this phenomenon to some degree. The amount of bending appears to correlate with the thickness of the leaf (i.e. thinner leaf allows for more bending). It is believed that bending is caused by the pyrolysis of the leaf material or by moisture evaporation from the bottom surface. The lower epidermis and spongy mesophyll cells are being destroyed while the leaf droops and bends towards the FFB surface (Figure 5.15). As more of the leaf mass is released through pyrolysis, the

influence of the momentum of the convective gases begins to take effect, causing the leaf to bend upward.

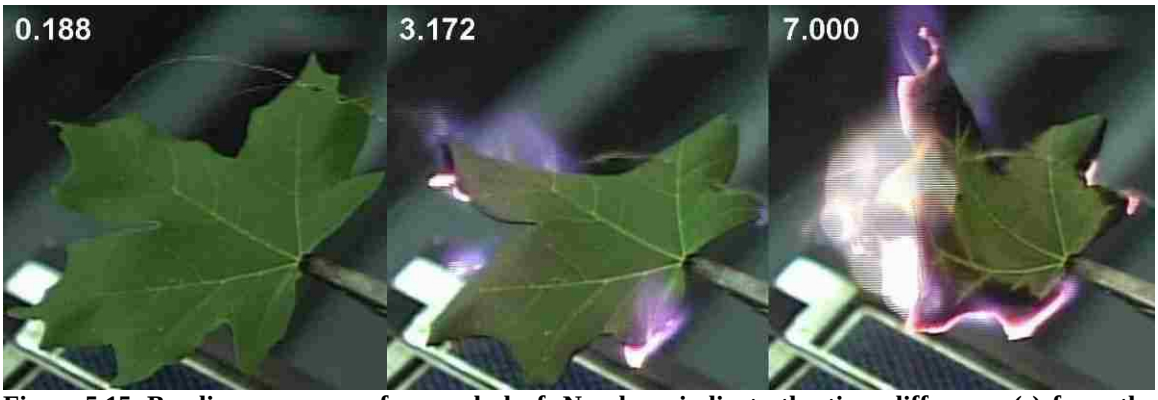

Figure 5.15. Bending sequence of a maple leaf. Numbers indicate the time difference (s) from the initial time of the experimental run. Video in Appendix D.

5.1.2 Quantitative Results

Quantitative values such as time (t), temperature (T), mass (m), and mass release rate (MR) were obtained from the experimental runs at various times (e.g. ignition, maximum flame height, and at burnout). These results and correlations for single-leaf experiments are discussed below. These correlations were developed for a laminar heat source with no wind or slope; verification of applicability will need to be determined for real fire situations.

5.1.2.1 Ignition

Ignition data for the FFB apparatus were presented by Smith (2005) and Fletcher et al. (2007), including time and temperature data (t_{ig} and T_{ig}), but not mass ignition data. Average ignition values (including a normalized mass released at ignition (m_{ig}/m_0)) are shown in Table 5.1; these values are given regardless of moisture or geometric

parameters. These data in Table 5.1 include all experiments performed at BYU (i.e. data from Smith (2005) as well as data obtained after Smith). These natural fuels with numerous initial variables (Δx, MC, m_{H2O}, SA, P) showed a large degree of scatter in all ignition parameters as reflected in the large values of the standard deviation. Other recorded data with averages and 95% confidence intervals are shown in Appendix B. 'A. Average Values with Seasonal Variation'.

Table 5.1. Average values of time to ignition, ignition temperature, and normalized mass released at ignition along with confidence intervals (95%) and standard deviations (σ) for each species.

Species	Time to Ignition (t_{ig} [s])			Ignition Temperature (T_{ig} [°C])			Normalized Mass at Ignition (m_{ig}/m_0)		
	Avg	CI (95%)	σ	Avg	CI (95%)	σ	Avg	CI (95%)	σ
Manzanita	2.953	0.215	2.118	359.40	11.77	111.80	0.123	0.014	0.099
Ceanothus	5.135	0.330	2.215	408.26	19.69	126.51	0.328	0.033	0.142
Scrub Oak	1.238	0.249	1.972	312.23	17.85	133.73	0.181	0.034	0.162
Chamise	1.143	0.196	0.661	265.75	19.94	61.51	0.109	0.045	0.114
Gambel Oak	0.708	0.066	0.422	239.71	15.82	93.98	0.144	0.029	0.106
Canyon Maple	0.645	0.098	0.557	251.65	17.21	95.63	0.210	0.033	0.124
Big Sagebrush	1.575	0.134	0.821	331.20	23.12	136.85	0.279	0.086	0.199
Utah Juniper	1.449	0.238	1.158	274.21	23.30	80.24	0.114	0.026	0.111
Douglas-Fir	0.299	0.155	0.484	189.11	21.76	61.38	0.043	0.039	0.110
White Fir	0.684	0.379	1.088	190.41	16.49	46.51	0.058	0.038	0.101
Fetterbush	2.502	0.374	0.798	261.54	29.37	62.76	0.280	0.110	0.198
Gallberry	2.785	0.568	1.025	323.13	46.29	83.58	0.312	-	-
Wax Myrtle	0.900	0.555	0.874	270.36	41.68	65.60	0.075	0.045	0.054
Saw Palmetto	0.903	0.618	1.070	273.52	43.02	74.50	0.076	0.055	0.091
Excelsior	0.288	0.049	0.194	261.63	14.48	51.48	0.076	0.031	0.107
All	1.977	0.106	2.130	312.94	6.56	124.62	0.155	0.011	0.146

These averaged data show significant variation in ignition parameters for most species. Time to ignition values for live species ranged from 5.135 s for ceanothus to 0.299 s for Douglas-fir; excelsior had an even lower average value of 0.288 s. Ignition temperatures ranged from 408°C for ceanothus to 189°C for Douglas-fir; excelsior was lower than most live species at 262°C. Normalized mass values ranged from 0.328

(meaning 32% of the original mass had been released at ignition) for ceanothus to 0.043 for Douglas-fir; excelsior was again lower than most species at 0.076.

Table 5.2. Linear regressions of the ignition temperature versus time to ignition for all species. α and β are the slope and intercept coefficients, respectively. ± indicates the 95% confidence interval.

Species	T_{ig} (°C) vs. t_{ig} (s)			
	α	β	r^2	Significant?
Manzanita	14.890 ± 5.191	314.977 ± 19.162	0.0840	+
Ceanothus	10.508 ± 8.866	353.201 ± 49.947	0.0337	+
Scrub Oak	11.395 ± 8.724	290.087 ± 21.962	0.0316	+
Chamise	3.012 ± 32.251	262.041 ± 44.612	0.0010	
Gambel Oak	100.258 ± 35.448	162.749 ± 30.749	0.1870	+
Canyon Maple	43.170 ± 29.754	222.946 ± 25.899	0.0649	+
Big Sagebrush	40.586 ± 26.991	268.144 ± 47.580	0.0615	+
Utah Juniper	39.196 ± 17.430	209.107 ± 34.963	0.3082	+
Douglas-Fir	289.427 ± 303.857	156.671 ± 48.293	0.1239	
White Fir	23.030 ± 12.947	174.404 ± 16.688	0.2980	+
Fetterbush	13.181 ± 38.375	228.556 ± 100.563	0.0281	
Gallberry	29.165 ± 45.637	241.894 ± 134.909	0.1279	
Wax Myrtle	28.281 ± 49.003	244.915 ± 60.202	0.1419	
Saw Palmetto	32.744 ± 38.660	243.954 ± 52.982	0.2210	
Excelsior	197.825 ± 50.331	205.564 ± 17.646	0.5709	+
All	24.772 ± 2.738	260.617 ± 8.222	0.1870	+

Table 5.3. Linear regressions of the normalized mass released at ignition versus time to ignition for all species. α and β are the slope and intercept coefficients, respectively. ± indicates the 95% confidence interval.

Species	m_{ig}/m_0 vs. t_{ig} (s)			
	α	β	r^2	Significant?
Manzanita	0.038 ± 0.004	0.001 ± 0.014	0.7110	+
Ceanothus	0.029 ± 0.013	0.186 ± 0.072	0.2119	+
Scrub Oak	0.079 ± 0.018	0.082 ± 0.038	0.4867	+
Chamise	0.074 ± 0.073	0.041 ± 0.092	0.1680	+
Gambel Oak	0.109 ± 0.064	0.060 ± 0.056	0.1803	+
Canyon Maple	0.089 ± 0.037	0.138 ± 0.041	0.3014	+
Big Sagebrush	0.034 ± 0.207	0.242 ± 0.240	0.0054	
Utah Juniper	0.044 ± 0.020	0.042 ± 0.041	0.2231	+
Douglas-Fir	0.109 ± 0.100	-0.009 ± 0.019	0.2255	+
White Fir	0.072 ± 0.020	0.009 ± 0.027	0.6766	+
Fetterbush	0.010 ± 0.144	0.255 ± 0.381	0.0017	
Gallberry	-	-	-	
Wax Myrtle	0.039 ± 0.044	0.045 ± 0.051	0.4340	
Saw Palmetto	0.077 ± 0.022	0.005 ± 0.034	0.8756	+
Excelsior	0.373 ± 0.132	-0.041 ± 0.056	0.5018	+
All	0.036 ± 0.004	0.089 ± 0.013	0.2646	+

Fletcher et al. (2007) noted that the average t_{ig} value follows the decreasing trend of T_{ig} for most of the broadleaf species except for canyon maple; this trend is verified in the data of Table 5.1 for the broadleaf chaparral and intermountain species. The southeastern species of fetterbush and gallberry showed relatively higher t_{ig} values than most other species, especially wax myrtle and saw palmetto (the other southeastern species). However, this did not necessarily correspond to a higher T_{ig}. Linear regressions were performed to determine relationships between t_{ig}, T_{ig}, and m_{ig}/m_0 and are shown in Table 5.2 and Table 5.3.

Most species showed a positive correlation (positive α) relating T_{ig} and m_{ig}/m_0 to t_{ig}. The T_{ig} vs. t_{ig} correlations were nearly all significant (confidence interval lower than α) except for chamise, Douglas-fir, and the southeastern species. Non-broadleaf species displayed large amounts of scatter with nearly constant T_{ig}. A limited number of runs (12-18) were performed on southeastern species, yielding larger confidence intervals, and hence not significantly positive correlations. The m_{ig}/m_0 vs. t_{ig} correlations were nearly all significant except for sagebrush, fetterbush, and wax myrtle. Sagebrush samples had an initial mass of ~30 mg which is much closer to the accuracy of the mass balance than that of other species. Mass noise appears to increase as the initial mass decreases. Because of experimental scatter with the mass balance for gallberry, only one mass data point was obtained; no correlation could be derived.

The large amount of scatter in the data made it difficult to give definitive correlations for these ignition parameters by using known parameters. Smith (2005) provided possible linear correlations using Δx and m_{H2O} (determined from m_0 and MC) as known parameters to determine both t_{ig} and T_{ig} for each species. These correlations had

large amounts of uncertainty (again due to the large scatter of the data), particularly the T_{ig} correlations. Fletcher et al. (2007) suggested that the average T_{ig} could be used in place of the correlation, yielding small variation from the correlation.

Table 5.4. Linear regressions of the time of ignition versus leaf thickness for all broadleaf species. α and β are the slope and intercept coefficients, respectively. ± indicates the 95% confidence interval.

Species	t_{ig} (s) vs. Δx (mm)			
	α	β	r^2	Significant?
Manzanita	6.654 ± 1.677	-0.355 ± 0.860	0.1461	+
Ceanothus	7.712 ± 2.143	1.011 ± 1.182	0.2248	+
Scrub Oak	2.894 ± 1.923	0.200 ± 0.696	0.0370	+
Gambel Oak	0.750 ± 1.199	0.558 ± 0.255	0.0097	
Canyon Maple	0.990 ± 1.124	0.437 ± 0.261	0.0237	
Big Sagebrush	3.938 ± 1.625	0.551 ± 0.440	0.1366	+
Fetterbush	2.992 ± 3.498	1.306 ± 1.444	0.1521	
Gallberry	9.504 ± 21.605	-0.459 ± 7.397	0.0650	
Wax Myrtle	8.196 ± 7.938	-2.187 ± 3.028	0.3461	+
Saw Palmetto	-11.038 ± 10.134	3.773 ± 2.689	0.3194	-
All	8.171 ± 0.584	-0.846 ± 0.239	0.3753	+

The old data from Smith (2005) as well as new data were reanalyzed with the hope of better understanding the effects of moisture and geometric parameters. Numerous linear correlations for t_{ig} (s), T_{ig} (°C), and m_{ig}/m_0 (dependent variables) by varying Δx (mm), MC (%), m_{H2O} (g), SA (cm^2), and P (cm) (independent variables) for each species (3 dependent × 5 independent × 16 species). Correlations involving non-broadleaf species geometric parameters (Δx, SA, P) could not be obtained. The best single-independent-variable-term correlations obtained were for t_{ig} vs. Δx (Table 5.4) and t_{ig} vs. m_{H2O} (Table 5.5) as could be predicted from Smith (2005) and Fletcher et al. (2007). Clearly, not all species had significantly positive correlations, but these (t_{ig} vs. Δx and t_{ig} vs. m_{H2O}) were the most consistent. Additional correlations not presented in this section are included in Appendix B. 'B. Linear Correlations'.

Table 5.5. Linear regressions of the time of ignition versus mass of moisture for all species. α and β are the slope and intercept coefficients, respectively. ± indicates the 95% confidence interval.

Species	t_{ig} (s) vs. m_{H2O} (g)			
	α	β	r^2	Significant?
Manzanita	17.882 ± 3.943	1.564 ± 0.363	0.1762	+
Ceanothus	65.222 ± 13.273	2.976 ± 0.514	0.3509	+
Scrub Oak	-2.355 ± 4.158	1.418 ± 0.378	0.0052	
Chamise	-0.148 ± 1.763	1.157 ± 0.259	0.0006	
Gambel Oak	3.124 ± 1.132	0.457 ± 0.101	0.1655	+
Canyon Maple	1.101 ± 2.266	0.559 ± 0.211	0.0073	
Big Sagebrush	39.343 ± 13.973	0.900 ± 0.269	0.1760	+
Utah Juniper	0.166 ± 0.738	1.395 ± 0.340	0.0022	
Douglas-Fir	0.033 ± 0.139	0.131 ± 0.059	0.0082	
White Fir	1.373 ± 3.585	0.281 ± 1.119	0.0187	
Fetterbush	7.260 ± 8.671	1.666 ± 1.061	0.1467	
Gallberry	41.658 ± 37.552	0.394 ± 2.211	0.3064	+
Wax Myrtle	22.541 ± 9.880	-0.602 ± 0.728	0.7210	+
Saw Palmetto	-7.339 ± 36.655	1.359 ± 2.369	0.0156	
Excelsior	38.750 ± 24.369	0.194 ± 0.096	0.1724	+
All	-1.124 ± 0.821	2.107 ± 0.130	0.0047	-

Table 5.6. Linear regressions for various correlations of lumped broadleaf species involving surface area and perimeter. α and β are the slope and intercept coefficients, respectively. ± indicates the 95% confidence interval.

Correlation	α	β	r^2	Significant?
t_{ig} (s) vs. SA (cm^2)	-0.114 ± 0.030	2.899 ± 0.241	0.0749	-
t_{ig} (s) vs. P (cm)	-0.101 ± 0.017	3.541 ± 0.269	0.1658	-
T_{ig} (°C) vs. SA (cm^2)	-5.537 ± 1.582	315.809 ± 11.409	0.0660	-
T_{ig} (°C) vs. P (cm)	-3.933 ± 0.797	334.721 ± 12.275	0.1234	-
m_{ig}/m_0 vs. SA (cm^2)	-0.006 ± 0.003	0.222 ± 0.022	0.0277	-
m_{ig}/m_0 vs. P (cm)	-0.002 ± 0.002	0.211 ± 0.023	0.0108	-

It should be noted that saw palmetto had a significantly negative correlation for t_{ig} vs. Δx. This could be due to local (non-uniform) ignition at the dry tips of the leaf sample and to the limited number of samples. It is also interesting to note that the t_{ig} vs. m_{H2O} correlation is positive for a number of species (e.g. manzanita, gambel oak, sagebrush), but it is significantly negative when all species are lumped together. This shows a difference among species. These two correlations (Table 5.4 and Table 5.5) can be used

for many species, both broadleaf and non-broadleaf, to determine the t_{ig}. Once t_{ig} is determined, Table 5.2 and Table 5.3 could be used to determine either T_{ig} or m_{ig}/m_0.

Other correlations for t_{ig}, T_{ig}, and m_{ig}/m_0 proved that a limited number of species (< 4) had significant relationships (positive or negative), particularly independent variables *SA* and *P*. However, correlations using *SA* and *P* were significantly negative when all broadleaf species were lumped together (Table 5.6).

One of the main purposes of this research is to characterize the effects of moisture on live fuels during combustion. It is therefore expedient that evaporation of moisture during combustion of these individual samples be studied. The classical combustion model assumes that all moisture first evolves from the sample at a temperature near the boiling point of water. The classical model of ignition, which occurs when a combustible mixture of pyrolysis gases is obtained, should follow shortly after moisture evaporation.

To better analyze the effects of evaporation of moisture from the fuel sample, the mass released at ignition (m_{ig}) was compared to the original mass of moisture (m_{H2O}) for a number of fuel samples, as shown in Figure 5.16. Assuming a classical model, if ignition occurred at the moment evaporation ended, the data points should lie on (or close to) the parity line. The majority of the data fell below the parity line, indicating that ignition did not occur at the end of global evaporation, but possibly at the end of evaporation locally. Regardless, a significant amount of moisture (30-60%) remained in the sample at the time ignition occurred.

One reason moisture remained in the sample could be due to local ignition. Ignition could occur on a tip or needle while the bulk of the moisture remained in the inner layers of the sample. Another reason for moisture remaining could be due to the

physical nature of the live sample. Moisture could not escape the outer boundaries of the sample, thus the structure of the sample (e.g. exterior cell walls such as the epidermis) must first be pyrolyzed before the moisture can escape. Thus, even 'free' moisture (Simpson and TenWolde, 1999) can require some pyrolysis of the fuel material before interior moisture escapes from the sample. This pyrolysis requires a higher temperature than required for evaporation alone. Qualitative phenomena such as interior bubbling and bursting (Sections 5.1.1.3. Bubbling and 5.1.1.4. Bursting, respectively) are examples of moisture escaping before the structure can completely devolatilize.

A linear regression of the data shown in Figure 5.16 was performed for all species. The slope (α or dm_{ig}/dm_{H2O}) for each regression is shown in Table 5.7 along with a confidence level of 95%. The intercept was set to zero, assuming that ignition would occur immediately if no moisture were in the sample. A classical model would show data having a slope of 1 (on the parity line); however, each species has a slope significantly lower than 1.

The magnitude of the slopes may be inversely related to flammability (i.e., propensity to ignite) for a given species. The species with lower slopes (i.e. juniper, chamise, Douglas-fir, etc.) are more flammable than those with higher slopes (i.e. ceanothus and manzanita). Dimitrakopoulos and Papaioannaou (2001) performed flammability analyses on live Mediterranean fuels, and found a linear relationship between MC and time to ignition (t_{ig}), with species having lower slopes (dt_{ig}/dMC) being more flammable. The data shown in Figure 5.16 are consistent with the findings of Dimitrakopoulos and Papaioannaou (Figure 2.6), although these data from the FFB experiments are on a mass basis (m_{ig} vs. m_{H2O}) instead of time (t_{ig} vs. MC).

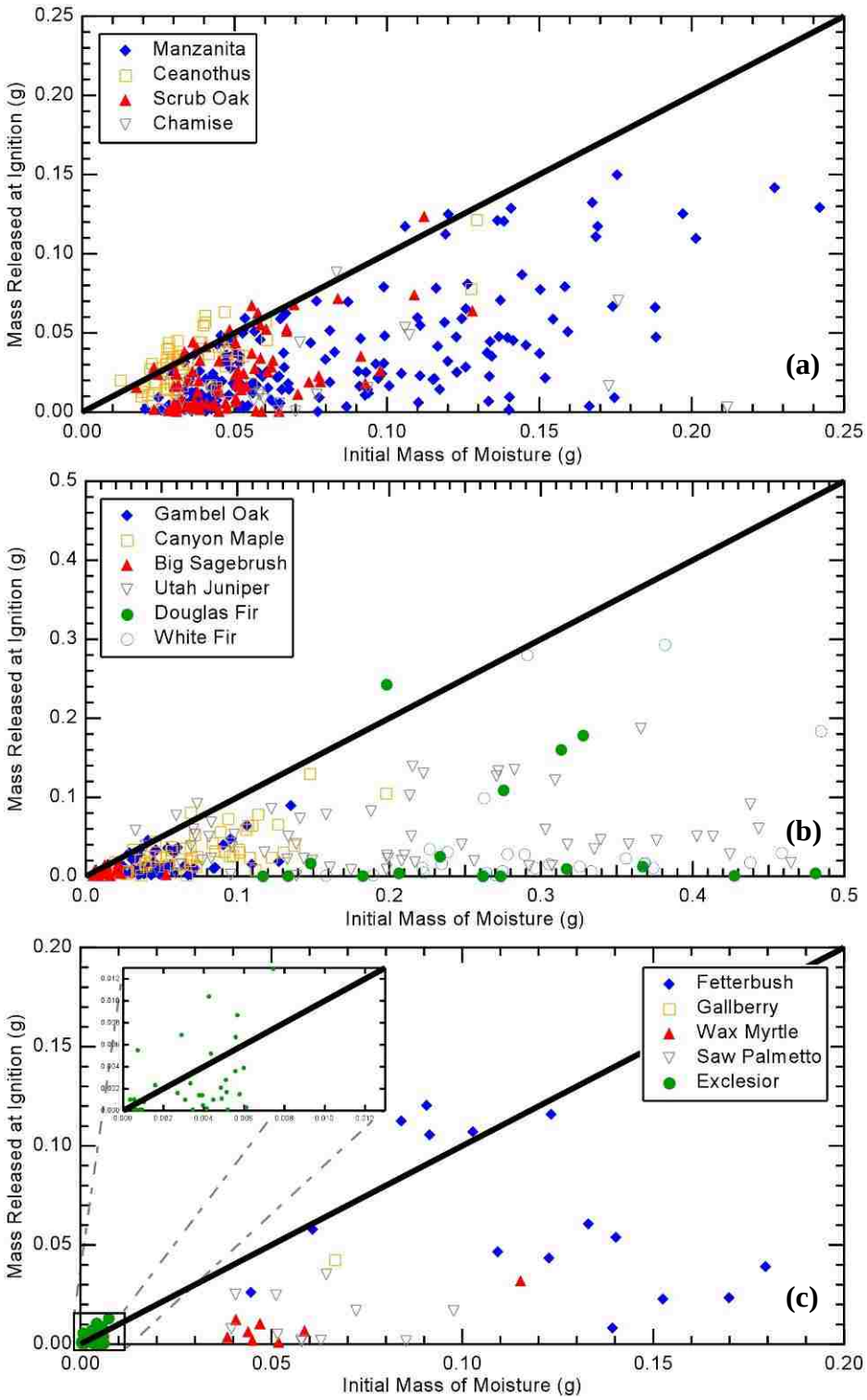

Figure 5.16. Data of the mass released at ignition versus the initial mass of moisture for (a) California chaparral species, (b) intermountain west species, and (c) southeastern species and excelsior.

Table 5.7. Slope (α) of linear regressions of mass released at ignition versus mass of moisture data shown in Figure 5.16. ± indicates the 95% confidence interval.

Species	m_{ig} (g) vs. m_{H2O} (g)		
	α	r^2	Significant?
Manzanita	0.408 ± 0.039	0.7033	+
Ceanothus	0.794 ± 0.075	0.8622	+
Scrub Oak	0.491 ± 0.076	0.6819	+
Chamise	0.128 ± 0.057	0.4807	+
Gambel Oak	0.326 ± 0.072	0.6288	+
Canyon Maple	0.443 ± 0.062	0.7866	+
Big Sagebrush	0.296 ± 0.152	0.4246	+
Utah Juniper	0.115 ± 0.027	0.5022	+
Douglas-Fir	0.042 ± 0.060	0.0743	
White Fir	0.146 ± 0.090	0.2899	+
Fetterbush	0.453 ± 0.224	0.5737	+
Gallberry	NA	NA	
Wax Myrtle	0.192 ± 0.089	0.7871	+
Saw Palmetto	0.180 ± 0.131	0.4854	+
Excelsior	0.729 ± 0.248	0.5201	+
All	0.139 ± 0.015	0.3245	+

Individual excelsior samples are distinctly different from live species. First, single excelsior samples are long, thin, and cylindrical (single needle) while non-broadleaf species (i.e. juniper, chamise, etc.) have multiple needles at various orientations. Secondly, moisture was introduced to the excelsior samples by diffusion and not by an active biological process. The fiber saturation point, which is typically about 30% *MC* for wood (Simpson and TenWolde, 1999), was possibly achieved from this diffusive process but not exceeded. Therefore, all moisture within the excelsior samples was 'bound' to the wood-like material. Since the water treatment process was relatively short (3-4 hr) as compared to live fuels, the 'bound' moisture in excelsior may not have as strong of physical and/or chemical bonds with the wood fiber (Simpson and TenWolde, 1999) as do live fuels. In addition, the cellular structure of a live leaf differs from that of dead wood. The slope of m_{ig} vs. m_{H2O} (Table 5.7) for excelsior is 0.729 ± 0.248, which was higher than that of most other live species (all except ceanothus), meaning that it behaved

more like the classical combustion model (moisture is driven off before ignition occurs) than the live species. This may be due to the lack of mass transfer resistance in the thin, cylindrical sample, thus allowing the moisture to release easily from the sample. This lack of mass transfer resistance may also be due to diffusion. Moreover, due to the low *MC* (< 30%) and lower initial mass (m_0 ~ 0.02 g), the mass of moisture in the sample (m_{H2O}) is low compared to all other species (excelsior shown in insert of Figure 5.16c).

5.1.2.2 Temperature History

Classical combustion modeling assumes that evaporation occurs at a constant temperature of 100°C (Rothermel, 1972; Albini, 1980). Temperature profiles from both thermocouple and IR measurements show no plateau at 100°C, but rather at 200-300°C for most broadleaf species, as shown in Figure 5.17a. This plateau at higher temperatures is more prominent in thicker leaves (i.e. ceanothus, manzanita, gallberry).

This plateau at higher temperatures is thought to be a delayed moisture evaporation due to moisture transfer resistance in the leaf. In the absence of light (e.g. during shipment), stoma on the leaf tend to close (Sadava et al., 2008), thus limiting moisture passage out of the leaf. Also, cell walls may first need to be broken down (devolatilized at these higher temperatures) before moisture within that cell can be released. Because of the two-dimensional nature of leaf combustion and the complicated mass and heat transfer involved inside and around the leaf, no plateau is observed at 100°C.

Temperature histories for excelsior showed no plateau at either 100 or 200-300ºC, but a slight plateau (if any) at 350-425ºC (Figure 5.17b). This plateau was normally observed well after ignition and was usually observed near the time of the maximum

flame height. The plateau may be due to the heat of pyrolysis for the excelsior at 350-425ºC; this plateau was not observed in live species.

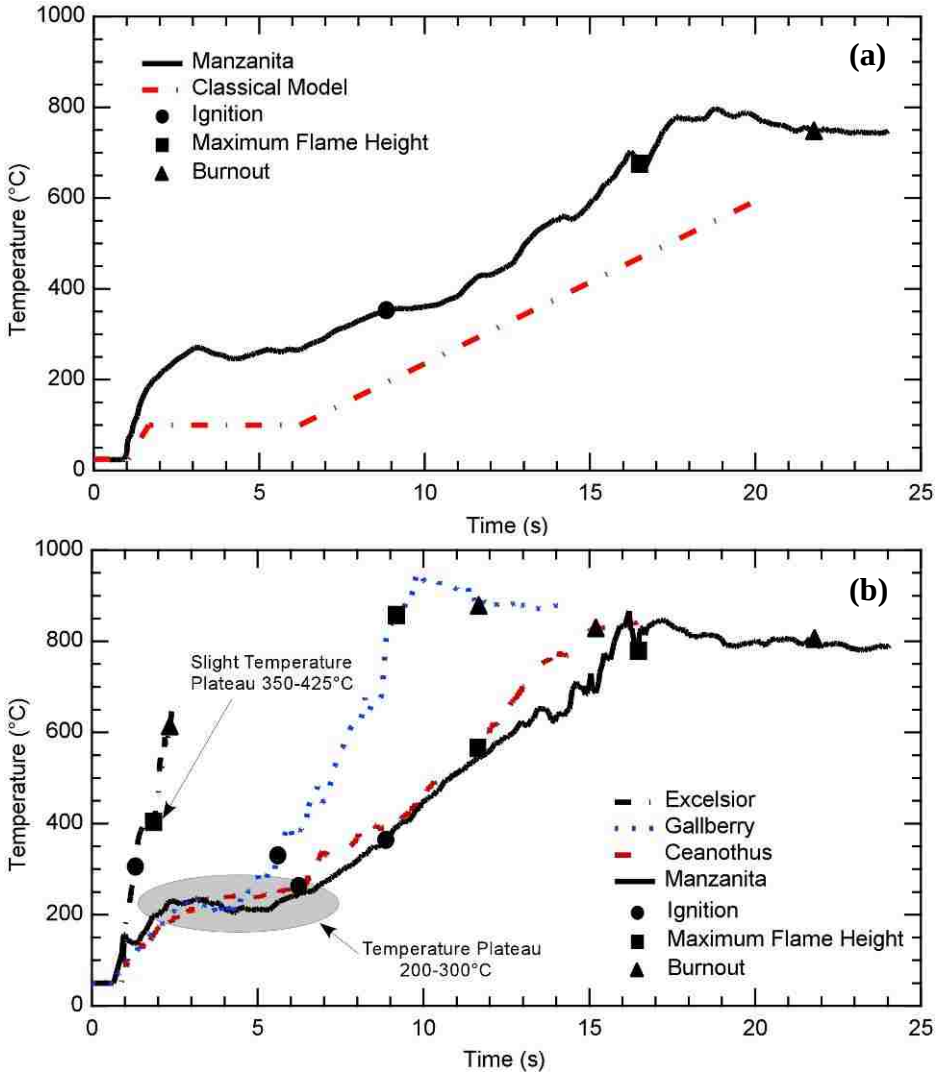

Figure 5.17. (a) Comparison of a thermocouple temperature history of a manzanita leaf with the classical combustion model, (e.g. Rothermel (1972)). (b) Representative IR temperature histories for a variety of samples. A temperature plateau was observed at 200-300ºC for live species. A slight temperature plateau was observed at 350-425ºC for excelsior.

The IR profile was determined from an area drawn near the location of the thermocouple (near the perimeter of the leaf), and the maximum temperature within that area was reported. It was of interest to determine the temperature in a location away from

the original area, such as in the middle of the leaf away from the perimeter. To do this another area was drawn that remained within the leaf boundaries, away from the perimeter. It was observed that the center or middle temperature was significantly lower than the original or perimeter temperature; Figure 5.18 shows the average values of perimeter and middle temperature for multiple manzanita runs. This center temperature profile showed a plateau at 140°C, lower than the 200-300°C plateau from the perimeter profile, but still higher than evaporation. The center profile had a much longer plateau than the perimeter profile. Temperature variations across the leaf were sometimes up to 350°C, which was observed for most broadleaf species.

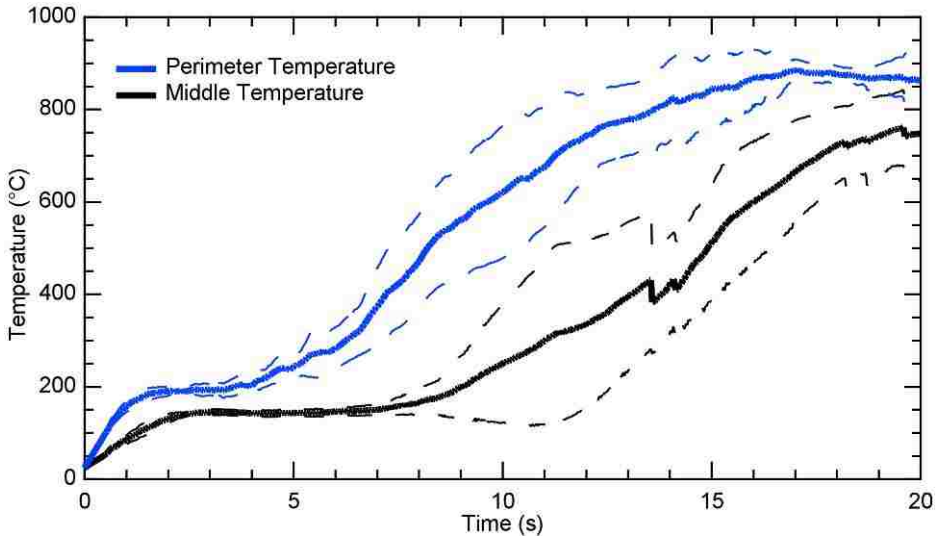

Figure 5.18. Comparison of IR temperature profiles determined at the perimeter and middle of manzanita leaves.

This lower temperature plateau (140°C) and the large temperature variation across the leaf, as well as the understanding that a significant amount of moisture remains in the leaf, indicate that both evaporation and combustion occur concurrently. The perimeter ignites and burns while the center or interior is still evaporating. The actual temperature

(140°C), may be higher than 100°C because the moisture would be a mixture of water an carbohydrates or other volatile organic compounds (VOC), which would increase the boiling temperature. Also, the surface tension of the moisture inside the leaf (e.g. capillary action) could prohibit the water boiling at the normal 100°C.

5.1.2.3 Mass Release Rates

Mass release rates are important because they can be directly related to the heat release rate during wildland fires. The average mass release rates (with confidence intervals of 95%) at ignition (MR_{ig}) and at maximum flame height (MR_{FH}) are shown in Figure 5.19. It appears that for some broadleaf species with nearly elliptical shape (i.e. ceanothus, scrub oak, wax myrtle) similar mass release rates were observed at ignition and at maximum flame height ($MR_{ig} \approx MR_{FH}$ for that species). Other species (i.e. manzanita, fetterbush, gallberry) exhibited significantly different mass release rates at these two conditions (i.e. ratio of MR_{ig}/MR_{FH} was different than unity). Since moisture remains in the leaf prior to ignition as discussed in the previous section, mass release at ignition is assumed to be primarily due to moisture release. This assumption indicates that manzanita (where $MR_{ig} < MR_{FH}$) has the ability to retain moisture (even while igniting) better than fetterbush and gallberry (where $MR_{ig} > MR_{FH}$). Broadleaf species with non-elliptical shape, where ignition generally occurs locally (i.e. gambel oak, canyon maple, big sagebrush, saw palmetto), exhibited different mass release rates at ignition than at maximum flame height. Ignition occurred on the dry/dead tips of the saw palmetto leaf, then nearly extinguished before igniting the bulk of the leaf. This local tip

ignition of saw palmetto may have more impact on moisture retention than on the other non-elliptical species.

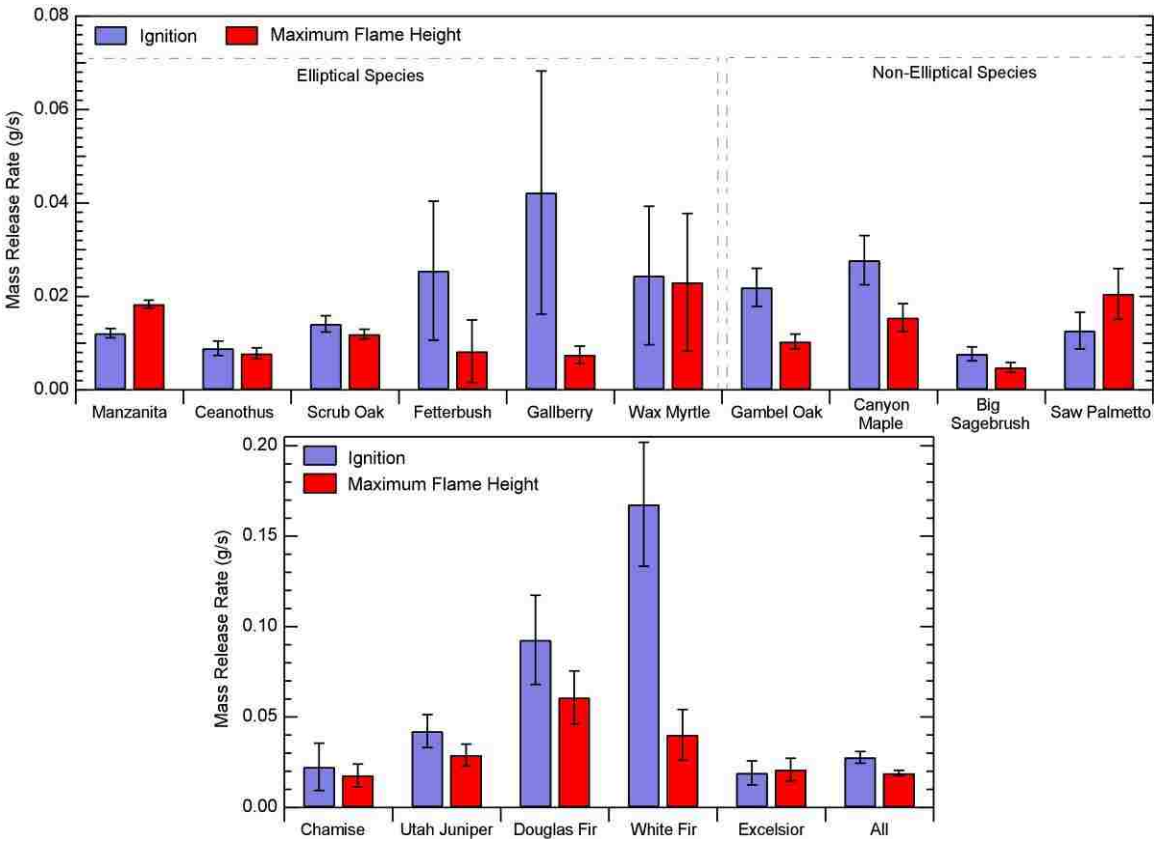

Figure 5.19. Average mass release rates for each species at ignition and maximum flame height for (a) broadleaf species (both elliptical and non-elliptical) and (b) non-broadleaf species, excelsior, and all species lumped together. Note the scale difference between the two figures. Error bars indicate the 95% confidence intervals.

Non-broadleaf species (i.e. chamise, juniper, Douglas-fir, white fir) exhibited much higher mass release rates (both at ignition and at maximum flame height) than most broadleaf species (note scale difference), which is consistent with the high surface-to-volume ratio in the non-broadleaf species. There was also a large difference observed within the same species between MR_{ig} an MR_{FH}, which can be attributed to jetting (high mass transfer away from the sample) that occurred in the non-broadleaf samples.

Excelsior, being small and cylindrical in shape, showed similar rates at ignition and at maximum flame height, and the magnitude of the rates was higher than in other smaller broadleaf species such as ceanothus, scrub oak, and sagebrush. However, when normalized to the original mass (MR/m_0), smaller samples (e.g. sagebrush and excelsior) had significantly higher values than most other species in their respective categories (i.e. sagebrush compared to other broadleaf species, excelsior compared to other non-broadleaf species). Excelsior had normalized mass release rates at ignition (MR_{ig}/m_0) approximately 2.5 times higher than white fir; this species had the highest non-normalized mass release rate.

Table 5.8. Linear regressions of the mass release rate at ignition versus mass of moisture for all species. α and β are the slope and intercept coefficients, respectively. ± indicates the 95% confidence interval.

Species	MR_{ig} (g/s) vs. m_{H2O} (g)			
	α	β	r^2	Significant?
Manzanita	0.0796 ± 0.0162	0.0054 ± 0.0016	0.3445	+
Ceanothus	0.0401 ± 0.0794	0.0074 ± 0.0033	0.0147	
Scrub Oak	0.1201 ± 0.0828	0.0085 ± 0.0042	0.0730	+
Chamise	0.1495 ± 0.0474	0.0065 ± 0.0090	0.6961	+
Gambel Oak	0.2225 ± 0.1505	0.0108 ± 0.0091	0.1585	+
Canyon Maple	0.2660 ± 0.1221	0.0089 ± 0.0098	0.2574	+
Big Sagebrush	-0.2278 ± 0.1566	0.0114 ± 0.0029	0.1513	-
Utah Juniper	0.1627 ± 0.0560	0.0113 ± 0.0128	0.3905	+
Douglas-Fir	-0.2394 ± 0.0951	0.1830 ± 0.0407	0.4131	-
White Fir	0.1308 ± 0.3646	0.1289 ± 0.1133	0.0182	
Fetterbush	-0.1650 ± 0.3638	0.0439 ± 0.0433	0.0587	
Gallberry	-1.1433 ± 1.9110	0.1092 ± 0.1148	0.1922	
Wax Myrtle	0.5010 ± 0.3000	-0.0092 ± 0.0224	0.6132	+
Saw Palmetto	0.0543 ± 0.2337	0.0093 ± 0.0151	0.0209	
Excelsior	-3.5780 ± 3.6541	0.0326 ± 0.0142	0.0718	
All	0.1867 ± 0.0247	0.0106 ± 0.0037	0.2249	+

Linear regressions were performed to determine the effects of moisture (MC, m_{H2O}) and geometric (Δx, SA, P) parameters on the mass release rate (both at ignition and at maximum flame height). Although some species exhibited a significant positive

correlation (positive slope for α) for a particular dependent variable, no variable proved significant for all species. However, the most significant independent variables (i.e. most number of significant species) for both MR_{ig} and MR_{FH} were m_{H2O} and P. These regressions are found in Table 5.8, Table 5.9, Table 5.10, and Table 5.11.

Table 5.9. Linear regressions of the mass release rate at maximum flame height versus mass of moisture for all species. α and β are the slope and intercept coefficients, respectively. ± indicates the 95% confidence interval.

Species	MR_{FH} (g/s) vs. m_{H2O} (g)			
	α	β	r^2	Significant?
Manzanita	0.0540 ± 0.0157	0.0139 ± 0.0015	0.1993	+
Ceanothus	0.0729 ± 0.0623	0.0051 ± 0.0026	0.0684	+
Scrub Oak	0.1329 ± 0.0477	0.0057 ± 0.0024	0.2154	+
Chamise	0.1347 ± 0.0308	0.0047 ± 0.0047	0.6670	+
Gambel Oak	0.0359 ± 0.0570	0.0079 ± 0.0035	0.0362	
Canyon Maple	0.0517 ± 0.0748	0.0118 ± 0.0061	0.0394	
Big Sagebrush	0.0549 ± 0.1408	0.0039 ± 0.0025	0.0182	
Utah Juniper	0.1532 ± 0.0254	0.0010 ± 0.0056	0.7378	+
Douglas-Fir	0.0791 ± 0.0693	0.0305 ± 0.0300	0.1294	+
White Fir	0.1739 ± 0.1074	-0.0105 ± 0.0335	0.2822	+
Fetterbush	0.1835 ± 0.1213	-0.0107 ± 0.0131	0.7515	+
Gallberry	0.0223 ± 0.1450	0.0062 ± 0.0086	0.0093	
Wax Myrtle	0.2283 ± 0.3774	0.0053 ± 0.0325	0.3260	
Saw Palmetto	-0.1097 ± 0.3165	0.0274 ± 0.0204	0.0454	
Excelsior	-5.0211 ± 3.3186	0.0393 ± 0.0130	0.1587	-
All	0.1176 ± 0.0111	0.0082 ± 0.0016	0.3608	+

Table 5.10. Linear regressions of the mass release rate at ignition versus perimeter for all species. α and β are the slope and intercept coefficients, respectively. ± indicates the 95% confidence interval.

Species	MR_{ig} (g/s) vs. P (cm)			
	α	β	r^2	Significant?
Manzanita	0.0024 ± 0.0006	-0.0096 ± 0.0056	0.2502	+
Ceanothus	0.0010 ± 0.0017	0.0040 ± 0.0080	0.0221	
Scrub Oak	0.0017 ± 0.0009	-0.0010 ± 0.0080	0.1207	+
Gambel Oak	0.0015 ± 0.0012	-0.0065 ± 0.0235	0.1040	+
Canyon Maple	0.0019 ± 0.0006	-0.0314 ± 0.0181	0.4500	+
Big Sagebrush	-0.0012 ± 0.0011	0.0159 ± 0.0076	0.0935	-
Fetterbush	-0.0006 ± 0.0063	0.0325 ± 0.0708	0.0031	
Gallberry	-0.0218 ± 0.0324	0.2011 ± 0.2381	0.2303	
Wax Myrtle	0.0034 ± 0.0092	-0.0220 ± 0.1268	0.0718	
Saw Palmetto	0.0015 ± 0.0013	-0.0104 ± 0.0200	0.3525	+
All	0.0008 ± 0.0001	0.0057 ± 0.0019	0.2124	+

Table 5.11. Linear regressions of the mass release rate at maximum flame height versus perimeter for all species. α and β are the slope and intercept coefficients, respectively. ± indicates the 95% confidence interval.

Species	MR_{FH} (g/s) vs. P (cm)			
	α	β	r^2	Significant?
Manzanita	0.0029 ± 0.0005	-0.0073 ± 0.0043	0.4383	+
Ceanothus	0.0021 ± 0.0012	-0.0020 ± 0.0060	0.1285	+
Scrub Oak	0.0014 ± 0.0005	-0.0004 ± 0.0047	0.2007	+
Gambel Oak	0.0005 ± 0.0005	0.0013 ± 0.0092	0.0780	+
Canyon Maple	0.0005 ± 0.0004	0.0019 ± 0.0125	0.0973	+
Big Sagebrush	0.0009 ± 0.0008	-0.0013 ± 0.0056	0.1273	+
Fetterbush	0.0042 ± 0.0029	-0.0359 ± 0.0303	0.7401	+
Gallberry	0.0005 ± 0.0024	0.0037 ± 0.0176	0.0186	
Wax Myrtle	0.0026 ± 0.0081	-0.0126 ± 0.1103	0.1238	
Saw Palmetto	0.0016 ± 0.0020	-0.0035 ± 0.0304	0.2032	
All	0.0002 ± 0.0001	0.0116 ± 0.0019	0.0142	+

5.1.2.4 Flame Height

It was expected that the flame height would correlate with the amount of fuel available (e.g. mass of volatiles (m_{VM})) which was shown by Fletcher et al. (2007) by an increasing linear relationship. These linear relationships are now tabulated in Table 5.12. It was also expected for the flame height to correlate to the rate of reaction of the sample (i.e. mass release rate (MR)). These data for all species (lumped together) were fit to a power-law expression ($FH = k \cdot MR_{FH}^{\phi}$) as is shown in Figure 5.20. Power-law expressions were also performed for all individual species, but they did not have significant results as did all the grouped data.

As mentioned previously, flame height has been related to the heat release in what is known as the two-fifths power law (Drysdale, 1999); heat release can be related to mass release rate if the heats of combustion are similar. Sun and coworkers (2006) indicated that the power-law was not adequate for live fuels. They also indicated that the power-law expression should be calculated at the time when the maximum flame height is obtained, not at the time of the maximum mass release rate. The regressed data showed

that these small, live fuels did not follow the two-fifths power law, but were significantly lower (0.17815 ± 0.026), which was consistent with the findings of Sun and coworkers (2006).

Table 5.12. Linear regressions of the flame height versus mass of volatiles for all species. α and β are the slope and intercept coefficients, respectively. ± indicates the 95% confidence interval.

Species	*FH* (cm) vs. m_{VM}(g)			
	α	β	r^2	Significant?
Manzanita	-1.615 ± 4.126	7.726 ± 0.586	0.0022	
Ceanothus	48.233 ± 14.235	3.483 ± 0.627	0.2414	+
Scrub Oak	5.544 ± 3.743	5.974 ± 0.358	0.0448	+
Chamise	11.431 ± 5.814	4.159 ± 0.892	0.2777	+
Gambel Oak	12.876 ± 4.834	5.537 ± 0.584	0.2415	+
Canyon Maple	12.34 ± 7.034	4.427 ± 0.577	0.1122	+
Big Sagebrush	40.763 ± 153.002	3.754 ± 1.534	0.0059	
Utah Juniper	5.556 ± 2.119	6.557 ± 0.692	0.3385	+
Douglas-Fir	1.243 ± 8.007	10.357 ± 2.112	0.0026	
White Fir	2.76 ± 8.402	7.81 ± 2.286	0.0134	
Fetterbush	13.059 ± 20.786	9.595 ± 2.551	0.0883	
Gallberry	80.016 ± 61.679	4.62 ± 3.016	0.3766	+
Wax Myrtle	-33.625 ± 69.454	9.234 ± 3.963	0.1042	
Saw Palmetto	-15.408 ± 54.748	12.765 ± 4.011	0.0304	
Excelsior	204.347 ± 105.766	3.602 ± 1.611	0.2278	+
All	10.345 ± 1.297	5.78 ± 0.183	0.1783	+

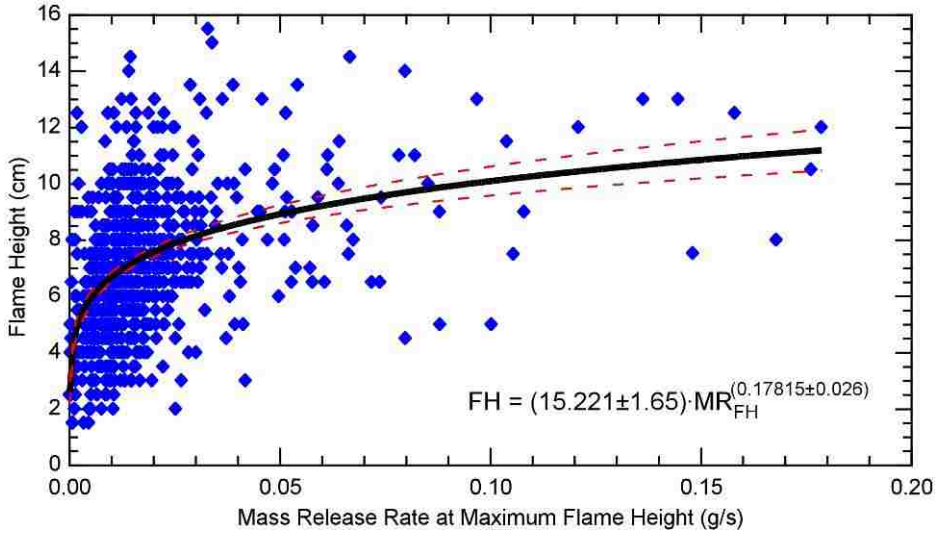

Figure 5.20. Raw data and power-law regression of the flame height versus the mass release rate at maximum flame height for all species. ± indicates the 95% confidence interval.

Table 5.13. Linear regressions of the flame duration versus mass of volatiles for all species. α and β are the slope and intercept coefficients, respectively. ± indicates the 95% confidence interval.

Species	t_{fd} (s) vs. m_{VM}(g)			
	α	β	r^2	Significant?
Manzanita	46.095 ± 5.842	6.071 ± 0.829	0.4566	+
Ceanothus	50.273 ± 19.944	7.692 ± 0.808	0.1265	+
Scrub Oak	43.259 ± 6.625	5.062 ± 0.679	0.4756	+
Chamise	29.789 ± 9.449	8.162 ± 1.424	0.4846	+
Gambel Oak	15.737 ± 3.510	4.698 ± 0.418	0.3420	+
Canyon Maple	30.444 ± 4.543	3.524 ± 0.378	0.5886	+
Big Sagebrush	127.125 ± 32.446	2.214 ± 0.354	0.2970	+
Utah Juniper	17.354 ± 3.266	14.201 ± 1.807	0.5677	+
Douglas-Fir	61.736 ± 14.556	1.945 ± 3.839	0.6598	+
White Fir	24.622 ± 27.631	12.144 ± 7.518	0.0906	
Fetterbush	26.115 ± 13.222	6.842 ± 1.623	0.4889	+
Gallberry	50.872 ± 42.824	4.066 ± 2.094	0.3363	+
Wax Myrtle	-23.161 ± 80.757	9.363 ± 4.608	0.0392	
Saw Palmetto	66.572 ± 59.355	2.445 ± 4.348	0.3323	+
Excelsior	79.270 ± 21.565	0.783 ± 0.328	0.5164	+
All	31.612 ± 1.491	6.110 ± 0.267	0.5547	+

5.1.2.5 Burnout

The time of flame duration (t_{fd}) was expected to correlate with the amount of fuel available, and is roughly related to reaction rate if the mass of the charred leaf is small. Figure 5.21 shows t_{fd} vs. m_{VM} for all species, and linear regressions are shown in Table 5.13. Chaparral broadleaf species were found to have a similar t_{fd} at a given amount of volatile material (i.e. similar slope α). However, chamise had a faster t_{fd} with higher m_{VM} (smaller α) as compared to the other chaparral species. Big sagebrush had the highest slope but also had a short average t_{fd}; the high moisture content and small leaf contributed to the short t_{fd}. The burning period for Utah juniper was approximately 10 s longer than the other intermountain broadleaf species (similar α but higher β). Douglas-fir had a longer t_{fd} at a higher m_{VM} (similar to juniper). However, at a lower m_{VM} Douglas-fir had a much shorter t_{fd}, acting more like the broadleaf intermountain species.

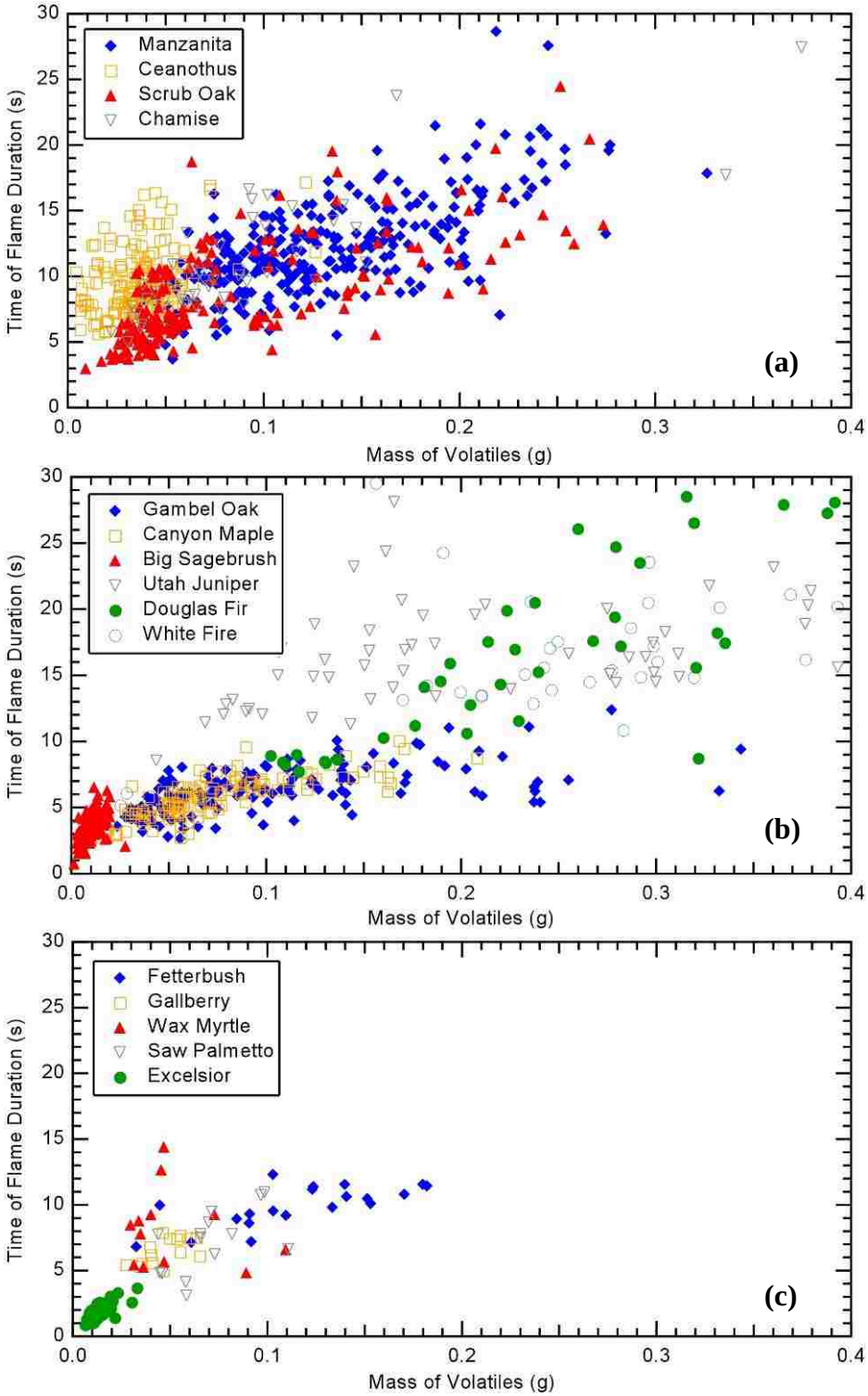

Figure 5.21. Time of flame duration versus the mass of volatiles for (a) California chaparral species, (b) intermountain west species, and (c) southeastern species and excelsior.

In general, the value of t_{fd} of the three broadleaf intermountain species (gambel oak, canyon maple, big sagebrush) appeared to be less than the southeastern species (fetterbush, gallberry, wax myrtle, saw palmetto). Generally, these southeastern species had a lower t_{fd} value than the chaparral broadleaf species (manzanita, ceanothus, scrub oak).

5.1.2.6 Seasonal Variation

The seasons in which the samples were examined could have an effect on the burning characteristics for each species. Leaf characteristics obtained prior to each experiment (MC, m_0, Δx, SA, P) were examined for seasonal variation, as were combustion characteristics (t_{ig}, t_{FH}, t_{fd}, FH, T_{ig}, T_{FH}, T_{fd}, m_{ig}/m_0, m_{FH}/m_0, m_{Brn}/m_0, MR_{ig}, MR_{FH}). Seasons were divided into months rather than actual dates: spring (Sp) (March – May), summer (Su) (June – August), fall (F) (September – November), and winter (W) (December – February). Each individual species was sorted according to season, and averages and confidence intervals (95%) were determined for the sorted seasons. Each live species did not always have recorded data for each season (e.g. southeastern species were harvested only in the spring), or had only a limited number (1) of batches for each season.

The sections below discuss the variations in leaf and combustion characteristics for the individual species among the 4 seasons. If a variable listed above is not discussed or tabulated for a particular species, it can be assumed that either there were no recorded data for that seasonal comparison (e.g. spring vs. fall) or that the comparison was not significantly different between seasons. Significantly different is defined here as when

the averages plus or minus the confidence intervals (95%) for two seasons do not overlap. Actual values for averages and confidence intervals are included in Appendix B. 'A. Average Values with Seasonal Variation'.

5.1.2.6.1 California Chaparral Species

Significant differences in average values for each season for California chaparral species are shown in Table 5.14. Variation could be due to the specific year and/or month in which the samples for that species were harvested, particularly for initial variables. For example, a drought with strong Santa Ana winds in southern California during the fall of 2007 could have brought the fall average for moisture content significantly lower than other seasons for manzanita and scrub oak. Samples were not consistently harvested throughout the year. Variations for each species are discussed below.

Table 5.14. Significant differences of leaf and combustion characteristics among seasons for California chaparral species.

		Manzanita	Ceanothus	Scrub Oak	Chamise
Leaf Characteristics	MC	Su, W > Sp > F	-	Su > F	Sp > Su
	m_0	W > Sp, Su, F	Sp > W	Sp > W, Su F, W > Su	F > W, Su
	Δx	W > Sp, Su, F Su > F	Su, F > W, Sp	Su > Sp, W	-
	SA	W > Su, F	-	Su > W	-
	P	W > Su	-	Su > W	-
Combustion Characteristics	t_{ig}	W > Su, Sp, F	Su, Sp > W	W, F, Su > Sp	-
	t_{FH}	W > Su, F, Sp	Sp, Su > W	Sp > Su > W	-
	t_{fd}	W > Su, Sp, F	Sp, Su > W	Sp > Su, W	Sp > W, Su
	FH	Su > F, W > Sp	Su, W > Sp	-	W > Su
	T_{ig}	W, F, Sp > Su	F, Sp > Su	W > Su, Sp	-
	T_{FH}	W > Su, F	W > Su	-	-
	T_{Brn}	-	W > Su	-	W > Su
	m_{ig}/m_0	-	-	W > Su	Su > W
	m_{FH}/m_0	W > Su > F	-	-	-
	m_{Brn}/m_0	W > Su > F	-	-	-
	MR_{ig}	W > Su, F	-	-	-
	MR_{FH}	F, W > Su	-	-	-

5.1.2.6.1.1 Manzanita

Manzanita showed the most seasonal variation compared to other species in these experiments. Leaf characteristics (*MC*, m_0, Δx, *SA*, *P*) for manzanita had that the highest values in winter while the lowest values typically were in the fall. A slightly higher value for *MC* was observed in summer compared to winter, but this difference was not significant. Combustion characteristics (all others in Table 5.14) also had higher values in winter (except *FH*) than other seasons.

5.1.2.6.1.2 Ceanothus

Ceanothus had higher m_0 values for spring than for winter, while values of Δx in summer and fall were higher than in winter and spring. Time variables (t_{ig}, t_{FH}, t_{fd}) were higher during spring and summer than in winter, while the lowest values of temperature variables (T_{ig}, T_{FH}, T_{Brn}) occurred in in the summer. Values of *FH* for ceanothus and manzanita in the summer and winter were significantly higher than in the spring.

5.1.2.6.1.3 Scrub Oak

Leaf characteristics for scrub oak were typically higher during the summer than other seasons (excluding m_0). Values of ignition variables (t_{ig}, T_{ig}, m_{ig}/m_0) were significantly higher in the winters than those from other seasons. Values of other variables (T_{FH}, T_{Brn}) were higher in the spring than in the summer and winter.

5.1.2.6.1.4 Chamise

Values of *MC* for chamise were higher in the spring than in the summer, while values of m_0 were higher in the fall than in the winter and summer. Values of burnout variables (t_{fd}, T_{Brn}) varied among seasons, with t_{fd} higher in the spring and T_{Brn} higher in the winter. *FH* values were higher in the winter than in the summer; this was opposite from the broadleaf chaparral species (manzanita and ceanothus).

5.1.2.6.2 Intermountain West Species

Significant differences in average values of leaf and combustion characteristics for each season for intermountain west species are shown in Table 5.15. Winter values were obviously not available for broadleaf (deciduous) species. Variations for each species are discussed below.

5.1.2.6.2.1 Gambel Oak

The most seasonal variation was observed for Gambel oak when compared to other intermountain west species. The highest values of leaf characteristics were observed in the summer (excluding Δx). Higher values of mass variables (m_{ig}/m_0, m_{FH}/m_0, m_{Brn}/m_0, MR_{ig}) were observed during the summer than during other seasons, with the lowest values observed in the fall. Values of other combustion characteristics (*FH*, T_{Brn}) were higher in the fall and lower in the spring; the lower spring value for *FH* was consistent with the trend observed for chaparral broadleaf species (manzanita and ceanothus).

5.1.2.6.2.2 Canyon Maple

Leaf characteristics for canyon maple showed significant differences for m_0 and Δx, where m_0 was higher in the summer than in the spring, while Δx was higher in the spring than in the summer. Most combustion characterisitics showed higher values in the summer than in the spring spring except for MR_{ig}.

Table 5.15. Significant differences of leaf and combustion characteristics among seasons for intermountain west species.

		Gambel Oak	Canyon Maple	Big Sagebrush	Utah Juniper	Douglas-Fir
Leaf Characteristics	MC	-	-	-	Su > W	-
	m_0	Su > Sp, F	Su > Sp	-	Su > Sp	-
	Δx	F > Su, Sp	Sp > Su	Sp > Su	-	-
	SA	Su > Sp, F	-	-	-	-
	P	Su > Sp	-	Sp > Su	-	-
Combustion Characteristics	t_{ig}	-	-	-	Su > W > Sp	F > Sp
	t_{fd}	-	Su > Sp	-	-	-
	FH	F, Su > Sp	-	-	-	F > Sp
	T_{ig}	-	Su > Sp	Su > Sp	Su, W > Sp	Sp > F
	T_{Brn}	F > Sp, Su	-	-	-	Sp > F
	m_{ig}/m_0	Su, Sp > F	Su > Sp	-	W, Su > Sp	W > F > Sp
	m_{FH}/m_0	Su, Sp > F	Su > Sp	-	-	-
	m_{Brn}/m_0	Su > F	Su > Sp	-	-	-
	MR_{ig}	Sp, Su > F	Sp > Su	-	W > Su	-

5.1.2.6.2.3 Big Sagebrush

Leaf characteristics for big sagebrush of Δx and P had higher values in the spring than in the summer. However, T_{ig} values were higher in the summer than in the spring.

5.1.2.6.2.4 Utah Juniper

Utah Juniper had significant differences in the leaf characteristics of MC and m_0 where values in the summer were higher than in other seasons. Combustion

characteristics of ignition values (t_{ig}, T_{ig}, m_{ig}/m_0) were typically higher in the summer (and sometimes winter) and lower in the spring. However, the MR_{ig} values were higher in the winter than in the summer.

5.1.2.6.2.5 Douglas-Fir

No significant differences in leaf characteristics were determined for Douglas-fir. Temperature values (T_{ig}, T_{Brn}) were higher in the spring than in the fall. However other ignition values (t_{ig}, m_{ig}/m_0) were lower during spring and typically higher for fall and sometimes winter.

5.1.2.6.2.6 White Fir

No significant differences in seasonal variation were determined for white fir samples.

5.1.2.6.3 Seasonal Flammability

Certain leaf and combustion characteristics can influence on how well a particular species burns during a season. For example a low Δx and MC indicate that the species can burn easily. Also, a low t_{ig} or high T_{ig} could mean the species is more flammable. From the data just presented on each species, this list could indicate which species would be more flammable during a particular season. This list is by no means conclusive and is strictly from the data.

- Spring: canyon maple, Utah juniper, Douglas-fir
- Summer: chamise, big sagebrush

- Fall: manzanita, gambel oak
- Winter: ceanothus, scrub oak

5.2 Two-Leaf Experiments

Generally, fire spreads by the rate of ignition of individual foliage samples. The ignited foliage subsequently burns and ignites other nearby foliage samples. A study was performed to determine the interactions between two leaf samples, including evaporation, combustion, and heating rates. Knowledge of these two-leaf interactions will improve the understanding of the overall combustion process, particularly in ignition and flame propagation through a bush. Various configurations were used to determine differences in combustion behavior between the two leaves. These configurations and their descriptions were discussed in detail in Section 4.1.7. Fuel Sample Placement, Table 4.1, and Figure 4.8.

Table 5.16. Matrix of two-leaf experiments.

Species	Symbol	Moisture Content* (%)	Date (2007)	Configurations (# of runs)
Ceanothus	C1	56.8	June 1	2 (10), 3 (10)
Manzanita	M1	53.3	June 1	2 (10), 3 (5)
Manzanita	M2	42.4	June 20	2 (10), 3 (10)
Manzanita	M3	38.4	August 8	2 (10), 3 (8)
Manzanita	M4	22.7	October 24	2 (10), 3 (10), 4 (10)
Gambel Oak	G1	92.0	June 8	2 (10), 3 (10)
Gambel Oak	G2	84.1	July 2	2 (10), 3 (10)
Gambel Oak	G3	86.1	July 9	2 (10), 3 (10)
Gambel Oak	G4	88.2	July 25	2 (10), 3 (10)
Gambel Oak	G5	83.4	July 30	2 (10), 3 (10)
Gambel Oak	Gd1	7.9	July 12	2 (7), 3 (7)
Gambel Oak	Go1	~80	July 3	6 (8), 7 (4)
Gambel Oak	Go2	~80	July 27	6 (10), 7 (5)

* Wt%, Dry-weight basis

5.2.1 Experimental Sets

Species used in the different configurations were manzanita, ceanothus, and gambel oak. Similarly-sized pairs of leaves for each species were selected so as to minimize the effects of mass and/or surface area. These leaves were selected at random locations from various branches of different plants. Approximately 10 runs (actual numbers of runs are shown in Table 5.16) were performed for each configuration (e.g., 10 runs for configuration 2 vs. 10 runs for configuration 3, etc.) for each day of experiments. Days of experimental runs with corresponding symbols, configurations, and moisture contents are shown in Table 5.16.

Table 5.17. List of measured quantities in the two-leaf configuration experiments.

Measured Quantity	Definition	Experimental Method
Time to ignition (t_{ig})	Difference in time from start of particle heating until first visible flame on or near the leaf surface (either leaf A or B)	Frame-by-frame inspection of video images for presence of sustained, initial flame
Ignition temperature (T_{ig})	Particle temperature at which first visible flame is observed on or near the leaf surface (either leaf A or B)	IR camera, time-synched with the video and focused on the appropriate leaf tip
Gas temperature (T_{qas})	Gas temperature	Thermocouple, corrected for radiation
Flame duration (t_{fd})	Time difference between burnout and ignition	Frame-by-frame inspection of video for presence of flame
Ignition delay time (t_{id})	Time difference between the ignitions of leaves B and A	Frame-by-frame inspection of video for presence of flame

5.2.2 Results and Discussion

A total of 550 experimental runs were performed on the three species indicated, scattered between the different configurations (Table 5.16). Time-dependent mass and temperature data were obtained at either location (A or B). The quantities determined from each experiment are listed in Table 5.17.

Table 5.18. Average time and temperature data from various experimental sets of the two-leaf configurations. ± indicates the 95% confidence interval.

Set	Config	t_{ig} (s)		t_{id} (s)	t_{fd} (s)		T_{ig} (°C)		T_{gas} (°C)
		A	**B**		**A**	**B**	**A**	**B**	**B**
C1	2	6.21 ± 1.36	6.26 ± 0.74	0.05 ± 1.53	10.1 ± 1.59	13.62 ± 1.08	319 ± 50	293 ± 48	NA
	3	-	6.35 ± 1.31	-	-	9.85 ± 1.64	-	269 ± 36	NA
M1	2	2.97 ± 0.83	6.23 ± 2.52	3.26 ± 2.55	14.43 ± 1.65	16.83 ± 4.72	307 ± 46	352 ± 80	NA
	3	-	4.72 ± 2.26	-	-	12.04 ± 4.06	-	245 ± 65	NA
M2	2	2.71 ± 1.23	4.13 ± 0.75	1.42 ± 1.31	12.73 ± 2.03	14.4 ± 1.89	252 ± 42	314 ± 55	372 ± 52
	3	-	2.97 ± 2.48	-	-	10.76 ± 2.14	-	242 ± 94	433 ± 52
M3	2	1.38 ± 0.24	1.59 ± 0.43	0.21 ± 0.51	12 ± 0.49	13.12 ± 1.82	248 ± 28	279 ± 20	704 ± 72
	3	-	1.46 ± 0.26	-	-	10.84 ± 0.7	-	241 ± 32	776 ± 114
M4	2	3.36 ± 1.17	3.49 ± 0.49	0.12 ± 0.96	9.84 ± 1.3	17.36 ± 1.91	362 ± 45	349 ± 85	549 ± 137
	3	-	3.53 ± 1.62	-	-	15.05 ± 1.83	-	256 ± 54	761 ± 132
	4	-	2.69 ± 1.44	-	-	22.97 ± 3.43	-	294 ± 99	522 ± 124
G1	2	0.75 ± 0.17	1.31 ± 0.25	0.56 ± 0.28	6.48 ± 0.76	7.74 ± 0.54	215 ± 30	250 ± 40	422 ± 198
	3	-	1.13 ± 0.26	-	-	5.74 ± 0.36	-	239 ± 35	498 ± 39
G2	2	0.58 ± 0.11	1.07 ± 0.31	0.49 ± 0.39	6.98 ± 0.45	8.02 ± 0.94	286 ± 52	384 ± 105	NA
	3	-	1.15 ± 0.32	-	-	6.27 ± 0.62	-	267 ± 52	NA
G3	2	0.58 ± 0.16	1.17 ± 0.27	0.59 ± 0.26	5.23 ± 0.92	5.87 ± 0.97	278 ± 73	269 ± 114	NA
	3	-	1.03 ± 0.5	-	-	5.54 ± 0.68	-	258 ± 23	NA
G4	2	0.91 ± 0.13	1.51 ± 0.36	0.6 ± 0.37	5.84 ± 0.37	7.91 ± 0.77	308 ± 41	224 ± 34	NA
	3	-	1.26 ± 0.17	-	-	5.11 ± 0.69	-	212 ± 22	NA
G5	2	0.53 ± 0.19	0.95 ± 0.21	0.42 ± 0.25	5.46 ± 0.34	6.97 ± 1.03	237 ± 32	225 ± 29	411 ± 161
	3	-	0.94 ± 0.12	-	-	4.96 ± 0.36	-	244 ± 27	578 ± 159
Gd1	2	0.19 ± 0.05	0.7 ± 0.21	0.51 ± 0.19	3.69 ± 0.9	4.22 ± 0.95	NA	NA	194 ± 106
	3	-	0.41 ± 0.04	-	-	3.11 ± 0.33	-	NA	192 ± 94

5.2.2.1 Comparison of Configurations 2 and 3

The rate of fire spread is thought to be dependent upon the ignition of fine fuels (i.e. samples with high surface-to-volume ratio). Ignition times for leaves at positions A and B ($t_{ig}^{A}\, t_{ig}^{B}$) for configuration 2 (leaf/leaf), and t_{ig}^{B} for configuration 3 (no leaf/leaf) were determined. Figure 5.22 shows a comparison of t_{ig}^{B} for the two configurations. Confidence intervals (95%) were determined using a standard t-test. The t_{ig}^{B} data for a given species in either configuration were the same, as shown in Figure 5.22. The only significantly different experimental set of configurations was for dry gambel oak (Gd1) with a moisture content of 8% (dry-weight basis). For this particular experiment set, t_{ig}^{B} for configuration 2 had 42% higher values than for the configuration 3. This means that for the Gd1 experiment, ignition of leaf B was delayed when leaf A was present.

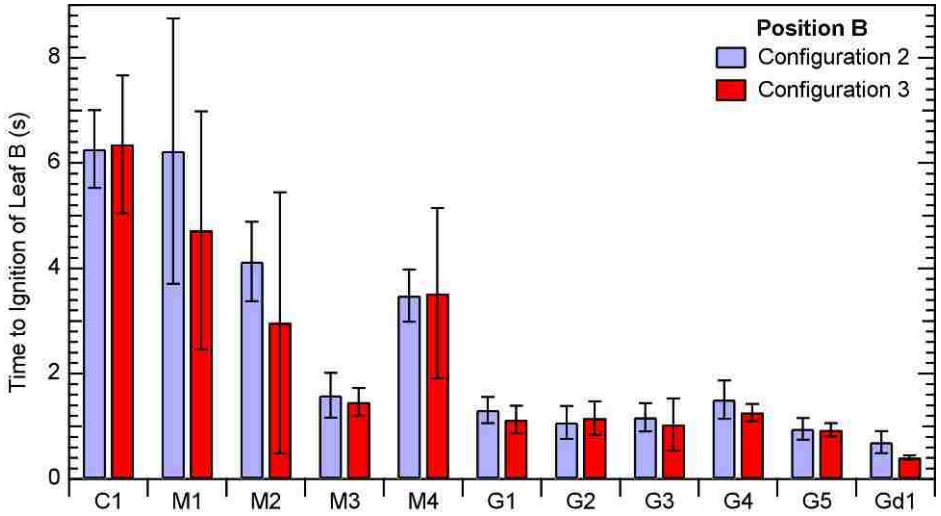

Figure 5.22. Average time to ignition values for leaf B with 95% confidence intervals.

This ignition delay of leaf B seemed to be caused by the lack of leaf moisture content, since all experimental sets with live fuels (and hence higher moisture contents)

did not exhibit similar behavior. The ignition times for the Gd1 experiment were quite small in both cases, but well within the resolution of the video camera (18-19 Hz). The flow dynamics would be nearly the same for both dead (Gd1) and live fuels (all other experimental sets in Figure 5.22), and hence should not cause a difference in t_{ig}^{B} between dead and live fuels.

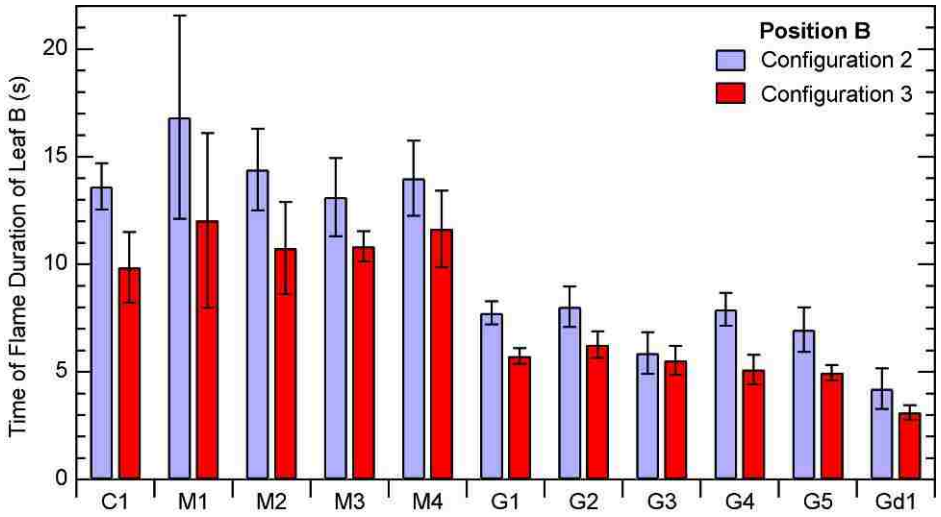

Figure 5.23. Average flame duration values for leaf B with 95% confidence intervals.

The largest difference between configurations 2 and 3 was observed in the flame duration of leaf B (t_{fd}^{B}), as shown by the data in Figure 5.23. Many experiments had significantly different values of t_{fd}^{B} for configuration 2 compared to configuration 3, always showing a higher t_{fd}^{B} for configuration 2 indicating that leaf B burned longer with leaf A present. It should be noted that if the confidence intervals were relaxed slightly (perhaps to a 90% confidence interval), even more experimental sets would be statistically different (i.e. manzanita species). Possible causes for this difference in t_{fd}^{B} may be that the obstruction (leaf A) alters the flow dynamics, or that the combustion of

leaf A alters the local amount of O_2 available to leaf B, or a combination of these two phenomena. These two phenomena are explored later in this dissertation.

Another possibly significant variable that can be determined is the ignition delay time (t_{id}) between the leaf at position A and the leaf and position B (defined as $t_{ig}^{B} - t_{ig}^{A}$). This was only applicable to configuration 2. Figure 5.24 shows the values of t_{ig} of leaves at positions A and B. Values of t_{ig}^{B} for leaf B are significantly higher than t_{ig}^{A} for all gambel oak runs and nearly (again assuming relaxed confidence intervals) significant for the manzanita runs. This ignition delay may be due to the size of leaf A which alters the downstream conditions for leaf B. This would explain why no ignition delay was observed for the ceanothus experiments, since ceanothus leaves are smaller than manzanita or gamble oak leaves.

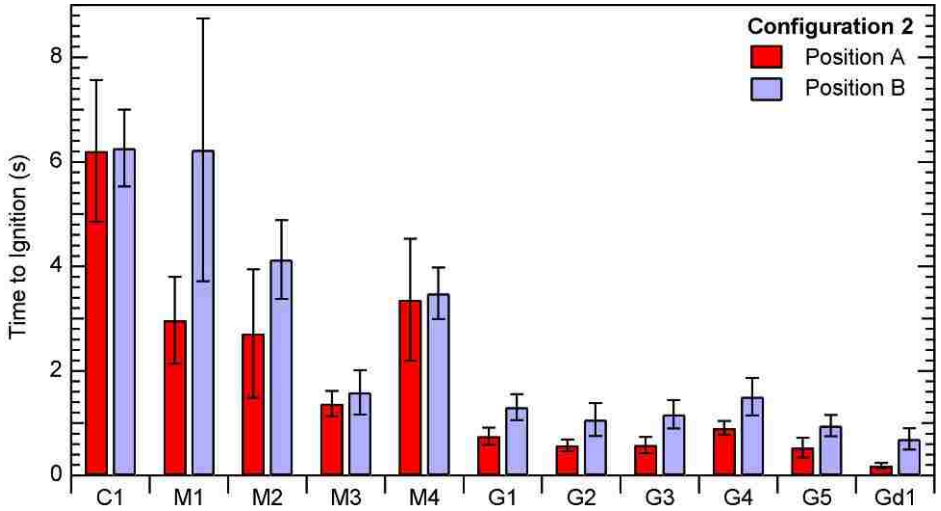

Figure 5.24. Average time to ignition values for leaves A and B for configuration 2 with 95% confidence intervals.

Most other measured variables proved not to be significantly different at either ignition or burnout between configurations 2 and 3, such as normalized mass, surface

temperature from the IR camera, or mass release rate; time and temperature data are tabulated in Table 5.18. However, the gas temperature (measured by the thermocouple) and normalized mass were significantly different at other points in during the experiment, particularly prior to ignition. This is discussed in the following section.

5.2.2.2 Comparison with Configuration 4

To better determine the effects of how the presence of leaf A altered the flow dynamics for leaf B, a thin metal disk instead of a leaf was placed at position A (i.e., configuration 4 as seen in Figure 4.8c). Data from this configuration were compared to data from configurations 2 and 3. Rather than just focusing on ignition and burnout, the entire gas temperature (T_{gas}) and normalized mass (m/m_0) histories were averaged and plotted (along with 95% confidence intervals), as shown in Figure 5.25 for manzanita samples. The average times for ignition and burnout are displayed with a diamond symbol for each configuration, and the confidence intervals for the times of ignition and burnout are displayed as individual data points (appears to be a thicker line).

The temperature plot (Figure 5.25a) shows that local gas temperatures in the initial time region (before ignition, 0-1 s) are significantly higher in configuration 3 (no leaf/leaf) than in configurations 2 (leaf/leaf) and 4 (disk/leaf). This behavior was observed for all species, except for dried gambel oak (Gd1) with a moisture content of 8%. Moisture acts as a heat sink, which yields lower temperatures initially. The gas temperature at position B (with no leaf present at either position) normally has a profile as shown in configuration 5 (i.e., direct convective gases from FFB). A constant gas temperature of about 950°C was observed after the initial heat-up region. A dip in the gas temperature occurred in configuration 3 after initially approaching the maximum

temperature (~950°C). Leaf B in configuration 3 influenced the temperature recorded by the thermocouple directly beneath it. This dip in temperature was likely caused by moisture and/or volatiles leaving leaf B, which was not observed in other configurations due to the obstruction of leaf A for configuration 2 and the metal disk for configuration 4.

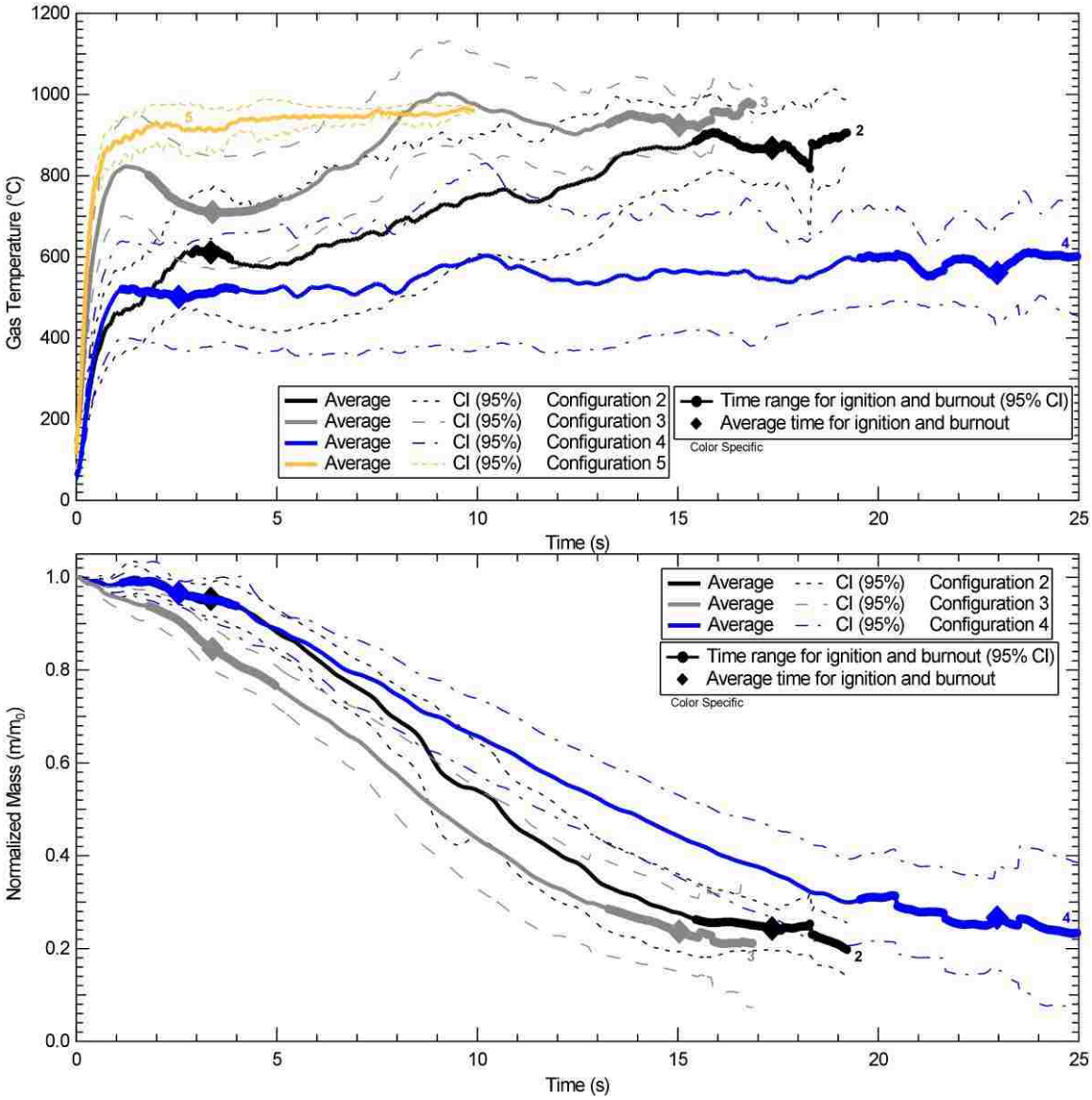

Figure 5.25. (a) Gas temperature (from thermocouple) at position B with 95% confidence intervals (configurations 2-5). (b) Normalized mass of leaf B with 95% confidence intervals (configurations 2-4). These experiments were performed with manzanita samples (M4).

The gas temperature underneath leaf B in configuration 4 leveled out at about 500°C which was significantly lower than configurations 2 and 3 near burnout. The other configurations eventually reached the maximum temperature around 950°C, although not necessarily at the same rate. This lower temperature and lower heating rate observed initially for configuration 4 would prolong the overall combustion process (rate), which was quantifiably observed (see time sequence for configuration 4 in Figure 5.26). Due to the obstruction from the metal disk, the laminar gases (Re ≈ 340 around disk) from the FFB transitioned to turbulent, mainly from recirculation of gases from the upper leaf. This was observed qualitatively as the flame from leaf B moved downward to the surface of the metal disk (see Figure 5.26). This turbulence could entrain some surrounding air (at room temperature) which cools the gases to the observed temperature of 500°C. Other possible reasons for this lower gas temperature would be radiation from the metal disk (causing heat loss from the surface of the disk), and a lack of the combustion process (upstream event) which occurs in configuration 2 but not in configuration 4, particularly when the flame height of leaf A is at a maximum.

This observed turbulence did not increase the rate of combustion as would be expected. The prolonged flame duration may instead be due to a wake effect (displacement of heat and gases necessary for combustion) of the obstruction. If the leaf at position B were placed at a longer distance from the obstruction, the wake effect may not be quite as significant. The flow dynamics (particularly the wake effect) were altered by both the leaf at position A (configuration 2) and the metal disk (configuration 3). However, leaf A moved up and down as well as disintegrated due to combustion, which

allowed leaf B to experience less wake effect through the experimental run than with the metal disk at position A.

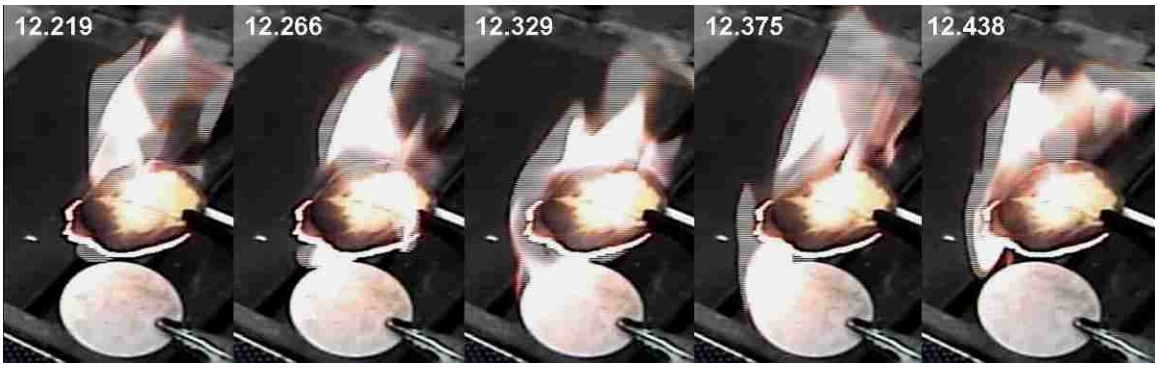

Figure 5.26. Sequence showing flame from leaf B moving downward to the surface of the metal disk. Numbers indicate the time difference (s) from the initial time of the experimental run. Video in Appendix D.

Figure 5.25b shows how the normalized mass changes during the experimental run for configurations 2, 3, and 4. The same mass history was observed at early times for configurations 2 and 4 (configurations with obstructions), with significantly lower mass values at the same times in configuration 3. The difference in mass between configuration 3 and the other two configurations was most observable at ignition and 2-3 s following ignition. After this early time period, mass values from configuration 2 (leaf/leaf) started decreasing more rapidly than in configuration 4 (disk/leaf), and started to behave similarly to configuration 3 (no obstruction). A final value of the normalized mass of approximately 0.2 was observed in all configurations. Since the ash content was approximately 5 wt% (Fletcher et al., 2007) on a dry basis, this means that ~15% of the dry mass did not burn. This ~20% remaining mass is the remaining char and ash left after devolatilation and is consistent with the findings of Fletcher and coworkers. Leaf samples

in configuration 3 took longer to burn, which is consistent with the lower gas temperature for this configuration.

From the data in Figure 5.25, it can be seen that a leaf at position A does affect the combustion of leaf B, particularly around pre-ignition and ignition. This difference early in the experiment can be attributed to the change in flow dynamics. O_2 is not needed for evaporation and initial pyrolysis, and hence local O_2 concentration should not affect the overall combustion behavior of leaf B early during the experiment. The obstructions (configurations 2 and 4) used in these experiments cause a wake effect which displace heat required to burn leaf B, eventually prolonging the combustion process (i.e. a longer flame duration results).

5.2.2.3 Comparison of Configurations 6 and 7

The O_2 concentration (mol%) of the gas stream was measured at a position between A and B, as shown in Figure 4.8e and Figure 4.8f. O_2 analyzer measurements were recorded as the minimum value during the experimental run; the analyzer had a delay of 3-5 s after ignition before a minimum value was obtained, which unfortunately was comparable to the burning times. O_2 data from configurations 6 (leaf/O_2/leaf) and 7 (no leaf/O_2/leaf) are compared in Figure 5.27.

The O_2 content is lower (approximately 20%) for the configuration with leaf A present (configuration 6) than with no leaf at position A (configuration 7). It should first be noted that the difference in O_2 between the two configurations for the Go1 experiment is only significant at the 85% confidence interval. The leaf at position A consumes O_2, which limits the amount of O_2 available to leaf B. This may also prolong the flame duration of leaf B, particularly after ignition occurs on leaf A.

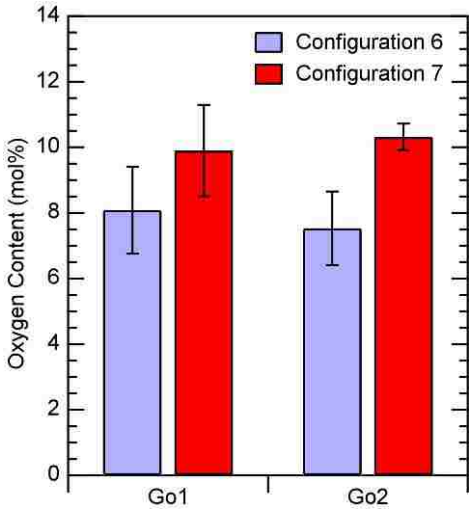

Figure 5.27. Comparison of the average value of O_2 content (mol%) in configurations 6 and 7 with 95% confidence intervals.

These interactions between samples, such as the wake effects and the O_2 consumption, can dramatically affect the way in which modeling is performed. They are significant issues for model development and design. It may not be so easy to approximate by simply adding single-leaf results together. More studies must be performed to quantitatively determine interactions between samples, along with methods of incorporating the interactions into a wildfire model.

5.3 Cuticle Extraction Experiments

Since the cuticle has a higher volatility and higher heat content than the cellulose that comprises much of the leaf material, and also since the cuticle is on the outside of the leaf surface (i.e. closest to oxidizer), it can influence burning rate and fire spread. Thus understanding the behavior of this cuticle during combustion is important in determining its effect on fire behavior and spread. This section discusses the effect of the cuticle on combustion.

Table 5.19. Matrix of cuticle extraction experiments.

Species	Symbol	Moisture Content* (%)	Solvent	Date	Number of Runs (treated, untreated)
Ceanothus	C1	89.19%	$CHCl_3$	June 28, 2006	5, 5
Manzanita	M1	42.42%	CH_2Cl_2	June 20, 2007	10, 10
Manzanita	M2	32.80%	CH_2Cl_2	June 21, 2007	10, 10
Manzanita	M3	39.20%	CH_2Cl_2	August 8, 2007	15, 15
Manzanita	M4	30.16%	CH_2Cl_2	August 10, 2007	10, 10
Manzanita	M5	25.17%	CH_2Cl_2	October 24, 2007	10, 10
Manzanita	M6	54.83%	$CHCl_3$	January 17, 2008	10, 10
Scrub Oak	S1	63.25%	CH_2Cl_2	June 22, 2007	10, 10
Scrub Oak	S2	63.67%	CH_2Cl_2	August 9, 2007	10, 10
* Wt%, Dry-weight basis					

5.3.1 Experimental Sets

A set consisted of two groups of broadleaf samples that were burned during the same experimental period (within 1-1.5 hr): (1) treated samples with the cuticle removed by solvent extraction (see Section 4.1.9.1. Chemical Removal for details about extraction) and (2) untreated samples. Similarly-sized pairs of leaves for each species were selected so as to minimize the effects of mass and/or surface area. Species used for each set include manzanita, ceanothus, and scrub oak. The number of runs of treated and untreated samples, moisture content, and when the experiments were performed are shown in Table 5.19. Burning characteristics of these sets were analyzed and compared and are discussed below.

5.3.2 Results and Discussion

A total of 180 cuticle extraction experiments were performed on the three species indicated. Time-dependent mass and temperature data were obtained for both treated and untreated groups. Analyses were performed primarily on ignition data (t_{ig}, T_{ig}, m_{ig}/m_0, MR_{ig}) since the cuticle most likely affects the ignition of wildland fuels. Another parameter that was observed to be significant for the cuticle extraction experiments was

the time of color change (t_{cc}), which is defined as the time difference between when color change (see Section 5.1.1.2. Color Change for details) was observed to stop and start. This variable was determined from frame-by-frame analysis.

5.3.2.1 Ignition

Average ignition parameters (t_{ig}, T_{ig}, m_{ig}/m_0, MR_{ig}) as well as confidence intervals (95%) were determined for each group in each set of Table 5.19. It was determined that no significant difference was found between treated and untreated leaves for any ignition parameter. For example, t_{ig} data are shown in Figure 5.28 where no set has a clear difference between treated and untreated leaves. Some experimental sets are nearly significant (if a lower confidence intervals were used) such as for sets M2 and M3. However, treated leaves would have a higher average than untreated leaves for set M2, whereas untreated leaves would have a higher average than treated leaves for set M3. Average data for T_{ig}, m_{ig}/m_0, and MR_{ig} for the experimental sets were also determined, but they showed similar behavior to the t_{ig} data. As found in normal single-sample experiments (see Section 5.1.2.1. Ignition), t_{ig} values for either treated or untreated samples could be correlated with T_{ig} and m_{ig}/m_0 values.

Reasons for having a longer t_{ig} for treated leaves could be due to moisture escaping the leaf (from the lack of cuticle) which dilutes the gaseous mixture surrounding the leaf which delays ignition of the volatiles. Also, since the cuticle material (from untreated leaves) has a lower flammability limit than the rest of the leaf, volatiles from the cuticle may enhance ignition. A reason for having a shorter t_{ig} for treated leaves could be due to faster moisture evaporation which requires less heat. This heat could therefore pyrolyze the leaf material causing ignition. This hypothesis assumes that the moisture

does not sufficiently dilute the gases surrounding the leaf; a flammable mixture is still obtained. Most of these experimental sets (particularly manzanita) had a lower moisture content than normal; experiments were performed during a time of drought in southern California. Moisture content may be a substantial factor which could alter these ignition results shown here. If these experiments were repeated at a higher moisture content, a significant trend versus ignition behavior might be obtained.

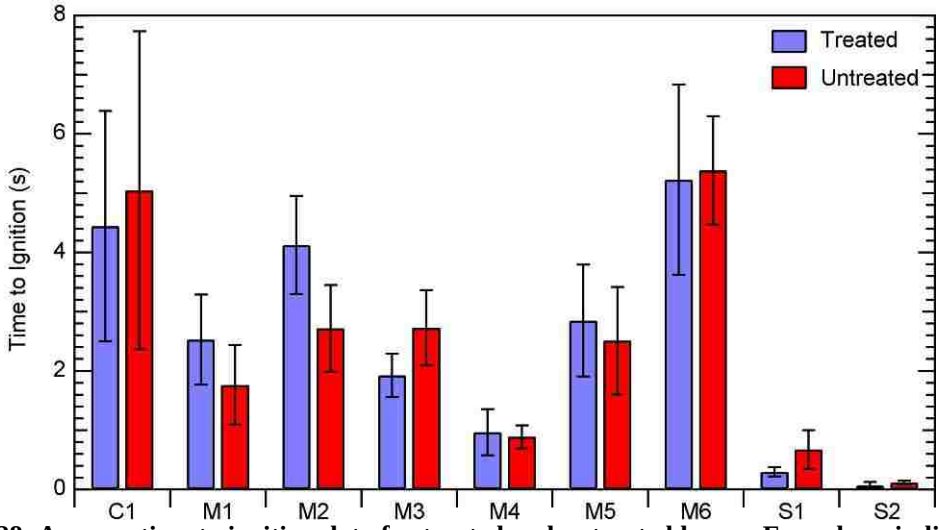

Figure 5.28. Average time to ignition data for treated and untreated leaves. Error bars indicate 95% confidence intervals.

5.3.2.2 Time of Color Change

A color change was observed in nearly every experimental run both for treated and untreated samples. However, the time observed for the color change differed; t_{cc} was 30-70% lower for treated samples depending on the moisture content and species. Since the t_{cc} is higher for untreated samples, this color change was thought to be the melting of the cuticle layer on the surface of the leaf. Liquid bubbling, where waxes pool or congregate on the leaf surface, can be considered a similar phenomenom to color change,

a melting of the waxy layer; waxes melt in greater quantities to accumulate on the surface of the leaf with liquid bubbling. The shorter duration of t_{cc} for treated leaves indicate that less of the cuticle remains on the leaf after solvent application. Some cuticle likely remains because some color change was observed for most samples (treated and untreated). The average t_{cc} (with 95% confidence intervals) for treated and untreated samples for each experimental set is shown in Figure 5.29.

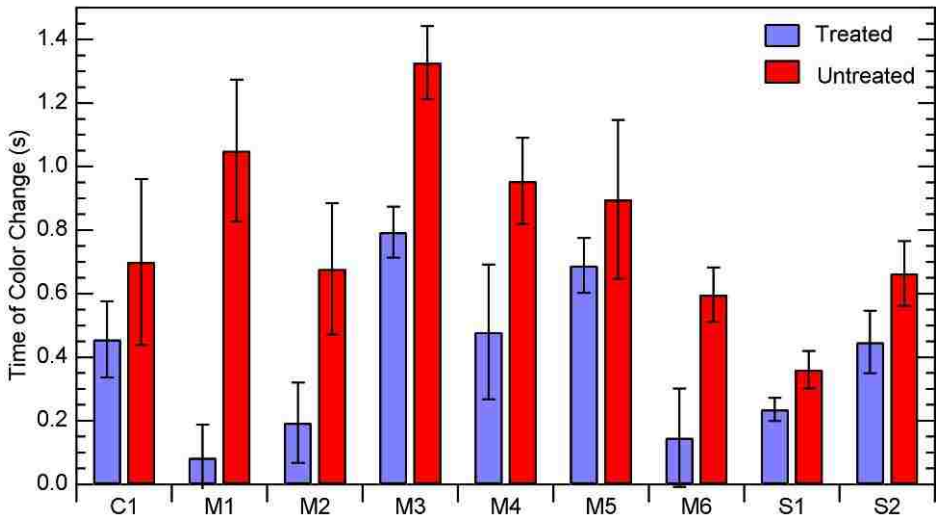

Figure 5.29. Average time of color change data for treated and untreated leaves. Error bars indicate 95% confidence intervals.

Color changes for both treated and untreated samples typically ended at the start of or slightly after the delayed moisture plateau at 200-300°C (see Section 5.1.2.2. Temperature History or Figure 5.1). Since water is not soluble in the solvents used, moisture would have remained in the leaf prior to running the experiment, given that the experiment was performed within a reasonable amount of time after solvent application (15-25 min). Therefore, the bulk of moisture evaporation (though at a higher temperature than normal for 'free' water) was assumed to take place after the cuticle was removed

from the sample. Color change also was observed to end at approximately the same time for both treated and untreated samples. Since the t_{cc} was longer for untreated samples, the time of the first observed color change occurred later (at a higher temperature) for treated samples.

5.4 Summary of Experimental Work

Numerous experiments were performed on live fuel samples over a FFB. Qualitative and quantitative results were determined after analysis of the data. Qualitative data included various phenomena that were observed from video images of the experiments. These phenomena occurred at different leaf conditions such as species, level of *MC*, heating rate, thickness, and the amount of cuticle on the leaf surface. These qualitative phenomena include:

- Jetting – high mass transfer rates from the leaf surface at various angles and directions in the forms of moisture and volatiles. Non-broadleaf species typically experienced this phenomenon.
- Color change – a melting of the waxy layer, most likely the cuticle on the outer leaf surface. The original dusty green color changed to a wet green color as the FFB was first brought under the sample. This was observed in nearly all broadleaf species.
- Bubbling (occurred in two forms):
    - Liquid bubbling – a melting of the waxy layer, though the waxes pooled or congregated on the surface to form liquid bubbles; this was indicative of large amounts of cuticle. The waxes resolidified

on removal from the FFB. This was observed in manzanita samples.

  - Interior bubbling – moisture escaping from the leaf interior through the outer epidermal walls in the form of tiny bubbles that were observed on the leaf surface. This typically occurred in on broadleaf samples at moderate *MC*.

- Bursting – moisture escaping from the sample which typically left craters or pockmarks on the surface. This typically occurred in thicker broadleaf samples at high *MC* and high heat flux.
- Brand formation – the ejection of some or the entire sample that was detached from the main body or stem of the sample. The main type (though numerous forms existed) occurred when the stem prematurely burned and could not sustain the weight of the sample.
- Bending – the breaking down or swelling of the lower epidermal layer causing the broadleaf to bend or curl toward the convective gases of the FFB. This was observed in all broadleaf species, though more prominent in thinner leaves with large surface area.

Quantitative results obtained from the experiments showed ignition values (time to ignition, ignition temperature, normalized mass at ignition) varied significantly by species. Linear correlations were determined between these ignition values (e.g. time to ignition correlated with ignition temperature, time to ignition correlated with normalized mass at ignition). Other linear correlations were determined to relate leaf characteristics (such as thickness, moisture content, initial mass of moisture, surface area, perimeter) to

recorded combustion characteristics of ignition (time to ignition, ignition temperature, normalized mass at ignition).

A significant amount of moisture remained within the leaf sample at the time of ignition for all species studied. This is not consistent with the classical model of evaporation in combustion where all evaporation occurs first before devolatilization. It was also observed that the temperature history profile for a leaf typically showed a plateau at 200-300°C, not at the generally accepted 100°C. This plateau was due to delayed moisture evaporation.

Mass release rates at ignition and maximum flame height also varied with species, though non-broadleaf species typically had higher mass release rates at both ignition and maximum flame height. Excelsior had normalized mass release rates that were significantly higher than live species. The flame height and flame duration were found to have a linear relationship with the amount of fuel available (volatile matter) from the sample. Also, these live individual samples did not follow the generally accepted two-fifths power-law, but followed a power-law correlation that was significantly lower. Both leaf and combustion characteristics were studied for samples burned at different seasons of the year to study variations by seasons. Though some species showed differences by season, no overriding parameter was found to show significantly seasonal variations for all species.

Experiments were performed in two-leaf configurations to determine combustion interactions between leaves. A second leaf was placed directly above the normally tested leaf. The main difference found during combustion was that the flame duration of the upper leaf was significantly longer when the lower leaf was present. This prolonged

burning could be due to the flow dynamics that divert the energy from the FFB away from the upper leaf and/or the consumption of O_2 from the lower leaf which is needed to burn the upper leaf. This may have serious implication for use of single-sample results alone in fire modeling.

The cuticle was removed from some broadleaf species by a solvent (i.e. treated samples), burned over the FFB, and compared to results of experiments performed on untreated samples. No significant differences in combustion parameters were found between the treated and untreated leaves. However, the time of color change was observed to be significantly longer for untreated leaves. This helped show validation that at least some of the cuticle was removed from the leaf surface by solvent treatment.

6. Leaf Modeling

Many wildland fire models have been developed that describe fire spread through a fuel bed, but none has been developed using a fundamental approach on individual samples. Lu (2006) developed a physical model for single samples that was intended for industrial use, not for wildland fires. This chapter focuses primarily on models developed to describe physical phenomena (fluid dynamics and heat and mass transfer) on a single-leaf system. Scale-up to larger systems (two-leaf and bush) is also modeled and discussed.

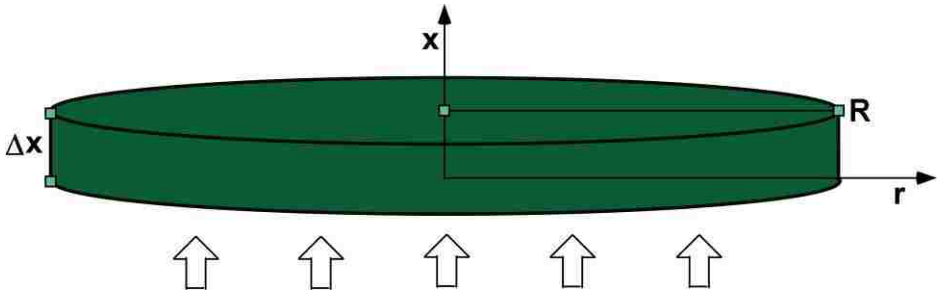

Figure 6.1. Schematic of thin, cylindrical disk used for single-leaf models.

6.1 Single-Leaf Models

Nearly-elliptical leaves (e.g. manzanita) were approximated to be a thin, cylindrical disk with constant radius (see Figure 6.1). This approximation allowed the system to be 2-dimensional (axisymmetric) in spatial coordinates, depending on the type of model used. Convective gases from the FFB heat the bottom, top, and edge of the leaf. The volume of the leaf was assumed to remain constant throughout the transient process.

Leaf properties for the various single-leaf models are shown in Table 6.1. Some properties varied with temperature as indicated in the table; these temperature-dependent properties were used in the single particle combustion and Fluent models. Other physical models used only the constant values from the table.

Table 6.1. Value of leaf properties used in single-leaf models.

Variable	Value	Units	Variable	Value	Units
m_0	0.2275	g	T_0	300	K
R	1.368	cm	T_∞	1285	K
d	2.736	cm	k	0.142	W/m-K
Δx	0.5	mm	$\rho^\dagger$	424.4	kg/m^3
V	0.294	cm^3	$c_p{}^\dagger$	3600	J/kg-K
A_s	12.18	cm^2	MC^*	93.3	%
†Temperature dependent properties; *Wt%, Dry basis					

6.1.1 Heat Transfer Only

Two heat transfer models were developed which help characterize the transient process of live leaf combustion: a lumped capacitance model and an analytical (2D) model, which are discussed in detail below.

6.1.1.1 Lumped Capacitance Model

The lumped capacitance model assumes that the temperature within the solid surface (leaf) is constant throughout the volume of the sample. This is achievable when the thermal resistance of the surrounding fluid is larger than the thermal resistance of the solid (Incropera and DeWitt, 2002). The non-dimensional Biot number relates these two resistances in the following way:

$$Bi = \frac{hL_c}{k} \tag{6.1}$$

where h is the convective heat transfer coefficient, k is the thermal conductivity of the solid, and L_c is a characteristic length, typically defined as the ratio of the volume to surface area of the solid. Systems that have Biot numbers smaller than 0.1 typically have insignificant temperature gradients through the solid (i.e. no spatial dependence on temperature). Since the leaf is thin, the solid thermal resistance (hL_c) is smaller than expected, giving a Biot number between 0.05 – 0.25, depending on the h and k used. Since the Biot number is close to 0.1, the lumped capacitance could be applicable and is investigated here.

A transient model is derived by an energy balance around the system (leaf). This yields two terms from the energy balance (assuming constant physical properties): a transient term and a convective term as shown in Equation 6.2. This is a simple first order ordinary differential equation (ODE) which can be solved with an initial condition ($T(0) = T_0$). Equation 6.3 shows the solution for this ODE.

$$mc_p \frac{dT}{dt} = -hA_s\left(T - T_\infty\right) \tag{6.2}$$

$$T(t) = \left(T_0 - T_\infty\right)\cdot e^{-\mu\cdot t} + T_\infty \qquad \mu = \frac{hA_s}{mc_p} \tag{6.3}$$

Of course, the physical properties (m, c_p, etc.) are not constant throughout the transient process, but a basis is helpful to compare to other models. A temperature profile for the lumped capacitance model is shown in Figure 6.2 as well as a profile for a representative experimental manzanita run. The heat transfer coefficient was altered to follow the trend of the experimental run (h = 46.6 W/m^2-K, Bi = 0.08). This model does not (and was not expected to) predict the delayed moisture evaporation plateau at 200-

300°C. Other models will be presented in an attempt to better characterize this moisture evaporation from the live fuel.

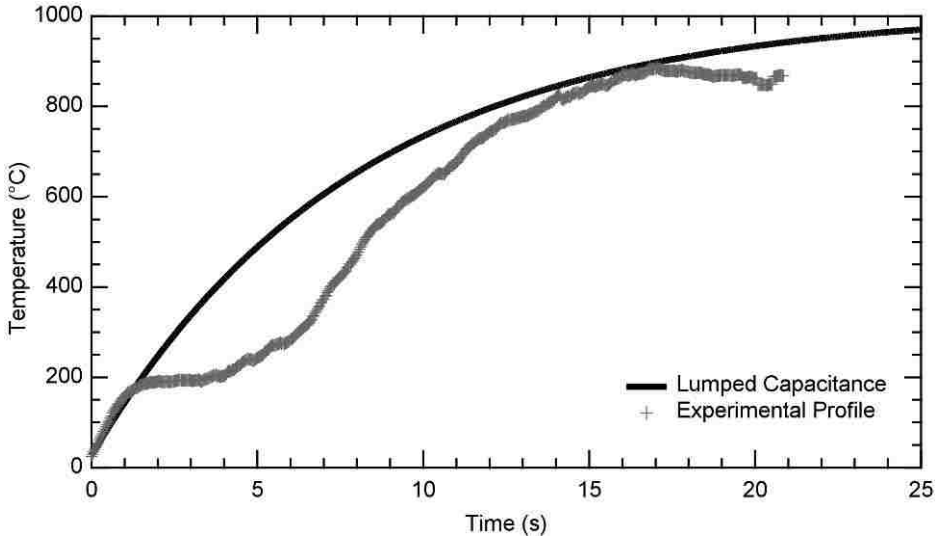

Figure 6.2. Temperature profiles for the lumped capacitance model and a representative experimental run.

6.1.1.2 Analytical Model (2D)

A 2D analytical heat transfer model was developed to enhance the capabilities of the lumped capacitance model. The analytical model allows for source/sink terms in the energy balance as well as non-constant boundary conditions. However, these source/sink terms and boundary conditions need to be time-dependent (not temperature-dependent) for deriving a proper analytical solution. The axisymmetric, transient energy equation is shown in Equation 6.4 with defined boundary and initial conditions (see Figure 6.1 for schematic). All boundary conditions ($x = 0$, $x = \Delta x$, $r = R$) were assessed as Robin conditions.

$$\text{Energy Eq.} \quad \frac{1}{r}\frac{\partial}{\partial r}\left(r\frac{\partial T}{\partial r}\right)+\frac{\partial^2 T}{\partial x^2}+\frac{g(t)}{k}=\frac{1}{\alpha}\frac{\partial T}{\partial t} \qquad T=T(r,x,t)=u+T_0 \tag{6.4a}$$

Norm. Eq. $$\frac{1}{r}\frac{\partial}{\partial r}\left(r\frac{\partial u}{dr}\right)+\frac{\partial^2 u}{\partial x^2}+\frac{g(t)}{k}=\frac{1}{\alpha}\frac{\partial u}{\partial t} \qquad u=u(r,x,t) \tag{6.4b}$$

BC: $x=0$ $$x:\left[-k\frac{\partial T}{\partial x}+h_0 T\right]_{x=0}=f_0(t)\Rightarrow\left[-k\frac{\partial u}{\partial x}+h_0 u\right]_{x=0}=f_0(t)-h_0 T_0 \tag{6.4c}$$

BC: $x=\Delta x$ $$x:\left[k\frac{\partial T}{\partial x}+h_X T\right]_{x=\Delta x}=f_X(t)\Rightarrow\left[k\frac{\partial u}{\partial x}+h_X u\right]_{x=\Delta x}=f_X(t)-h_X T_0 \tag{6.4d}$$

BC: $r=R$ $$r:\left[k\frac{\partial T}{dr}+h_R T\right]_{r=R}=f_R(t)\Rightarrow\left[k\frac{\partial u}{\partial r}+h_R u\right]_{r=R}=f_R(t)-h_R T_0 \tag{6.4e}$$

BC: $r=0$ $$r:T\big|_{r=0}<\infty\Rightarrow u\big|_{r=0}<\infty \tag{6.4f}$$

IC: $t=0$ $$t:T(r,x,0)=T_0\Rightarrow u(r,x,0)=0 \tag{6.4g}$$

where T is the temperature of the leaf as a function of direction (r, x) and time (t), u is the normalized temperature (T-T_0), α is the thermal diffusivity, h_i is the heat transfer coefficient, k is the thermal conductivity, $g(t)$ is a source term function, and $f_i(t)$ is a heterogeneous forcing function used for each Robin boundary condition.

Since the surface temperature of the leaf increases, the heat flux to the leaf decreases over time. To account for this change in heat flux, the heterogeneous condition $f_i(t)$ was assumed to exponentially decrease over time. This allowed for a temperature profile that was comparable to experimental results. Since convective gases were applied directly to the bottom of the leaf, the convective coefficient for the top of the leaf ($x = \Delta x$) was assumed to be approximately ¼ of the value of the bottom of the leaf. This was assumed because of the wake effect (with possible air entrainment) that occurs would give a lower effective heat transfer coefficient on the downstream (top) side than the upstream (bottom) side. The temperature applied to the boundary is the gas temperature

from the FFB; this lower effective heat transfer coefficient can account for some of the observed temperature difference.

Because moisture remains within the leaf surface after ignition, the source/sink term, $g(t)$, was treated to be a combination Heaviside function, $\Phi(t)$, to account for the heat of vaporization (sink), heat of pyrolysis (sink), and heat of combustion (source); this Heaviside function is a simplified way of describing energy sources/sinks. Variables for these source/sink terms are η_{H2O} (evaporation) and η_{Fuel} (pyrolysis and combustion combined). The evaporation of water was assumed to begin immediately and last until some arbitrary time after ignition occurs ($\kappa \cdot t_{ig}$). The ignition time (t_{ig}) and burnout time (t_{Brn}) were determined experimentally. The source/sink term was assumed to be constant throughout the volume of the solid and is shown in Equation 6.5.

$$g(t) = \eta_{H_2O}\left\{\Phi(t) - \Phi\left(t - \kappa \cdot t_{ig}\right)\right\} + \eta_{Fuel}\left\{\Phi\left(t - t_{ig}\right) - \Phi\left(t - t_{Brn}\right)\right\} \tag{6.5}$$

The differential equation in 6.4b is not possible to solve without integral transformations in the r and x directions (Debnath, 1995; Wylie and Barrett, 1995; Solovjov, 2007). The operational properties from a finite Hankel transform (for radial direction) and a finite Fourier transform (for axial direction) are independent of each other for each term in Equation 6.4b, meaning that the order in which the transforms are performed is inconsequential. Both transformations were performed to each term of Equation 6.4b and yield an ODE that is dependent upon time only (Equation 6.6). λ_n and ω_m are eigenvalues obtained from the positive roots of Equations 6.7a and 6.7b, respectively (Solovjov, 2007). A detailed derivation as well as figures showing $f_i(t)$ and $g(t)$ are found in Appendix C. 'B. Analytical Heat Transfer Model Derivation'.

$$\frac{\partial \overline{\overline{u}}_{n,m}}{\partial t} + \alpha\left(\lambda_n^2 + \omega_m^2\right)\overline{\overline{u}}_{n,m} = \frac{\alpha}{k}Q(t) \tag{6.6}$$

$$\left(H_0 H_X - \lambda_n^2\right)\sin\left(\lambda_n \cdot \Delta x\right) + \left(H_0 + H_X\right)\lambda_n \cos\left(\lambda_n \cdot \Delta x\right) = 0 \tag{6.7a}$$

$$-\omega_m J_1\left(\omega_m \cdot R\right) + H_R J_0\left(\omega_m \cdot R\right) = 0 \tag{6.7b}$$

where H_i is combined boundary term (h_i/k), $J_i(r)$ is the Bessel function of order i in the r direction, and $\overline{\overline{u}}_{n,m}$ is the transformed temperature after the Hankel and Fourier transformations. $Q(t)$ (Equation 6.8) is equal to the combined terms from the operations properties after the Hankel and Fourier transforms .

$$\begin{aligned} Q(t) = {} & RJ_0\left(\omega_m R\right)\left[f_R(t) - h_R T_0\right]\int_0^{\Delta x} K_n(x)dx + \left[f_0(t) - h_0 T_0\right]K_n(0)\int_0^R J_0\left(\omega_m r\right)r dr \\ & + \left[f_X(t) - h_X T_0\right]K_n(\Delta x)\int_0^R J_0\left(\omega_m r\right)r dr + g(t)\int_0^{\Delta x} K_n(x)dx\int_0^R J_0\left(\omega_m r\right)r dr \end{aligned} \tag{6.8}$$

The $K_n(t)$ term (Equation 6.9) is the kernel for the Robin-Robin boundary conditions in the axial direction (Solovjov, 2007).

$$K_n(x) = \frac{\lambda_n \cos\left(\lambda_n x\right) + H_0 \sin\left(\lambda_n x\right)}{\sqrt{\frac{\lambda_n^2 + H_0^2}{2}\left(\Delta x + \frac{H_X}{\lambda_n^2 + H_X^2}\right) + \frac{H_0}{2}}} \tag{6.9}$$

The ODE in Equation 6.6 is solved by variation of parameters (Haberman, 2004) with a transformed initial condition $\overline{\overline{u}}_{n,m}(0) = 0$ (see Equation 6.4g). The formal solution of the transformed temperature $\overline{\overline{u}}_{n,m}(t)$ is shown in Equation 6.10. The normalized temperature $u(r,x,t)$ is obtained by the Hankel and Fourier inverse transforms (Equation 6.11) (Debnath, 1995; Solovjov, 2007).

$$\overline{\overline{u}}_{n,m}(t) = \alpha \cdot e^{-\alpha\cdot\left(\lambda_n^2 + \omega_m^2\right)t}\int_0^t Q(t)e^{\alpha\cdot\left(\lambda_n^2 + \omega_m^2\right)\tau}d\tau \tag{6.10}$$

$$u(r,x,t)=\sum_{n=1}^{\infty}\sum_{m=1}^{\infty}\overline{\overline{u}}_{n,m}(t)K_n(x)\frac{J_0(\omega_m r)}{\int_0^R[J_0(\omega_m r)r]^2\,dr} \tag{6.11}$$

This solution is then shifted to obtain the overall temperature *T(r,x,t)* (Equation 6.12).

$$T(r,x,t)=u(r,x,t)+T_0 \tag{6.12}$$

The resulting solution *T(r,x,t)* is the predicted temperature distribution in the leaf, given the stated assumptions and boundary conditions. Summations were truncated to 10 (not infinity) eigenvalues for *n* and *m*.

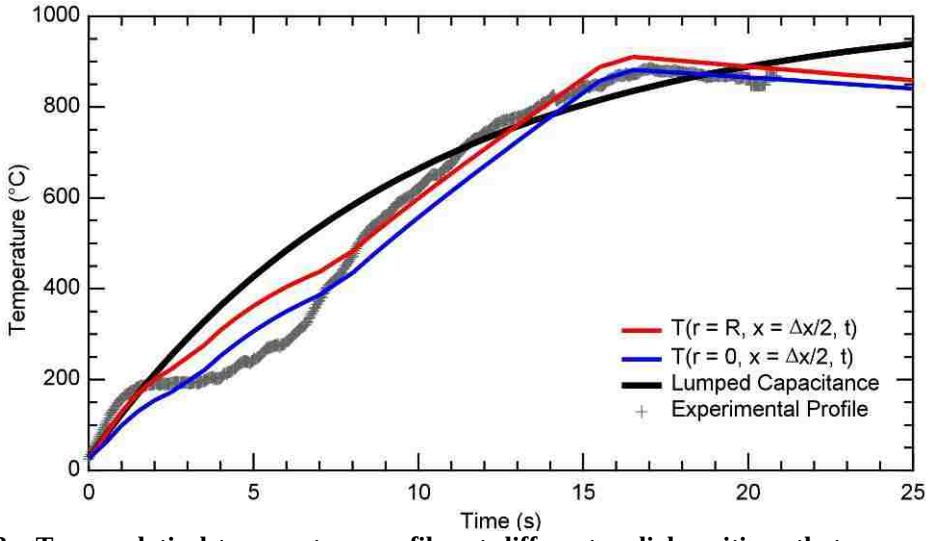

Figure 6.3. Two analytical temperature profiles at different radial positions that are compared to the lumped capacitance and experimental profiles.

Two temperature profiles at two radial locations and the axial center (*T(r = 0, x = Δx/2, t)* and *T(r = R, x = Δx/2, t)*) from the analytical model as well as the lumped capacitance profile and an experimental profile are compared in Figure 6.3. The analytical profiles show acceptable agreement with the experimental results. The temperatures differ between the analytical profiles at the center of the leaf (*r* = 0) and at

the perimeter ($r = R$) by 40-60°C initially, then differ by 10-15°C near the end of the run. This temperature difference is consistent with observed ignition at the perimeter which then propagates toward the center of the leaf. Improvement can be made in the evaporation region (the region with the plateau at 200°C for the experimental profile). The analytical profiles show a slight or no plateau in this region. A more accurate source/sink function, $g(t)$, or an improved boundary condition function, $f_i(t)$, may better represent the experimental temperature profile.

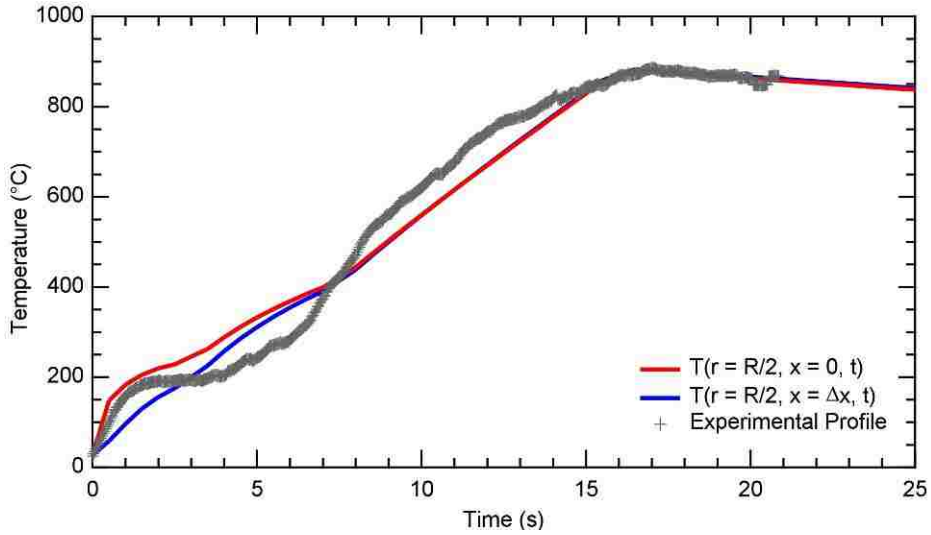

Figure 6.4. Two analytical temperature profiles at different axial positions that are compared to an experimental profile.

Additional temperature profiles were created to investigate the dependence upon axial variations in the leaf sample. Figure 6.4 exhibits the difference in temperature, as a function of time, between the bottom ($x = 0$) and top ($x = \Delta x$) surfaces of the leaf at a fixed radial position ($r = R/2$). Since different convective coefficients were used for the bottom and top boundary conditions, the bottom surface of the leaf increases in temperature much more rapidly than the top. This results in a significant temperature

gradient through the leaf (30-90°C) during the first few seconds of heat-up. This is shown in Figure 6.5, which shows the temperature through the solid volume at various times during combustion (T vs. $x/\Delta x$). This implies that assuming a thermally-thin sample may not be acceptable during the beginning stages of heat-up (i.e. evaporation and ignition).

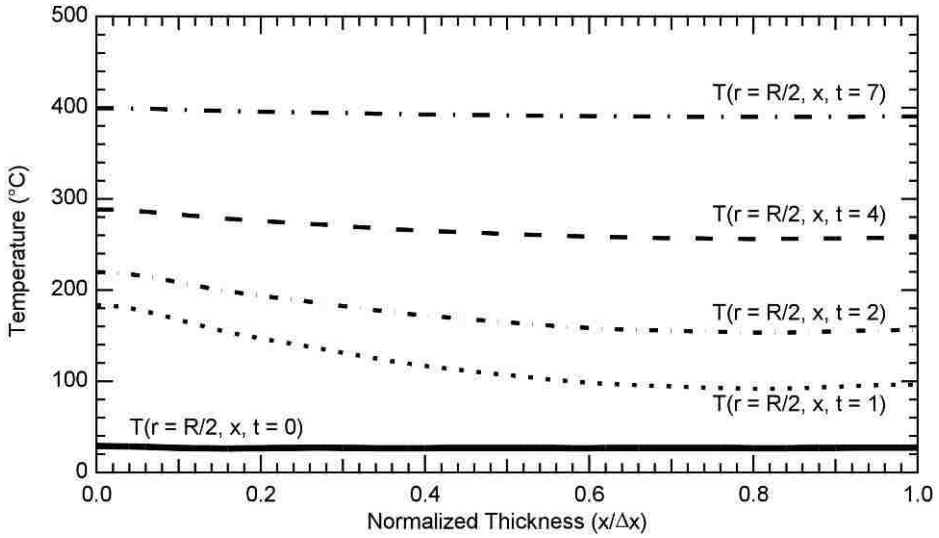

Figure 6.5. Analytical results of temperature compared to normalized thickness at various times.

It is important to note that the analytical model described here is subject to limitations in both capability and accuracy. The model was created for a leaf of uniform thickness and radius and subject to a uniform heat source. Few leaf samples are completely symmetrical (uniform thickness and radius), but this approximation helps increase the understanding of the heat transfer through the leaf. Mass transfer has not been included in this model but is important in better characterizing the overall physics of the combustion process. Assuming constant properties throughout combustion likely represents the greatest limitations to the model. Thermal conductivity, density, and heat

capacity values in the leaf are difficult to obtain and typically change during the experimental run.

6.1.2 Heat and Mass Transfer

The heat only models do not account for mass transfer from the leaf during combustion. Mass transfer can be quite significant during evaporation and pyrolysis. For this reason, physical models including mass and heat transfer were investigated and developed for live leaf combustion.

6.1.2.1 Single Particle Combustion Model

A model including heat and mass transfer was developed by Lu (2006) for various shapes and biomass particles. This model describes a biomass particle that undergoes evaporation, devolatilization, combustion of volatiles, and char oxidation and gasification using balances of mass, momentum, and energy. This model was validated for biomass particle combustion in a single-particle reactor. Assumptions for this model include: (1) all properties are assumed to be transient and one dimensional (1D) in space; (2) local thermal equilibrium exists between solid and gas phase (internal temperature gradients are the same for solid and gas); (3) ideal gas behavior exists; (4) particle aspect ratios and shapes do not change, though size does; and (5) particle boundaries for heat and mass transfer increase relative to that of a sphere by the ratio of the particle surface to that of a volume-equivalent sphere. More information about this model is found in Lu (2006).

Attempts to use this model were made with the same dimensions as found in Table 6.1. However, convergence of this model was not obtained. This model has been demonstrated in other situations to predict the temperatures at both the surface and the

leaf center. Mass release is also predicted. This model may be helpful in understanding the fundamental combustion physics that take place a single particle of various shapes and sizes.

6.1.2.2 Fluent Model (2D)

Another heat and mass transfer model was developed that also takes into account the fluid dynamics of the convective gases from the FFB. The leaf and surrounding fluid domain were assumed to be axisymmetric with the leaf at a sufficient distance from the boundaries to eliminate wall and/or entrance effects on the leaf (see Figure 6.6). Mass, energy, and momentum equations were solved using a transient, axisymmetric Fluent solver.

Figure 6.6. Schematic of 2D Fluent leaf model.

The inlet boundary conditions included a specified velocity (v = 2 m/s), a temperature (T_∞ = 1285 K), and species mass fractions of the inlet gas (y_{O2} = 0.08, y_{H2O} = 0.12, y_{CO2} = 0.04, y_{N2} = 0.76). Velocity was estimated from the inlet gases to the FFB, while temperature was experimentally measured at the leaf position. Species

compositions were determined by assuming equilibrium at the measured temperature and inlet flow rates of fuel, oxidizer, and inert gases. Side boundary conditions were assumed to be adiabatic (zero heat and mass flux from the surface). The outlet boundary was specified as a vent condition (ambient temperature and pressure). The axis boundary was defined to be symmetric (axisymmetric).

Mass transfer from the leaf surface occurs by evaporation of the moisture within the leaf and also by devolatilization of combustibles. Instead of incorporating the classical combustion approach to model evaporation and devolatilization, a comparison to experimental data was used (empirical approach). The elemental composition, the amount of volatiles, char, and ash of the leaf were known (Table 4.2 for manzanita), as well as the initial mass and moisture content. Solid species (C, H, N, O) were assumed to combine to form combustible gases that were injected from the leaf surface into the gas phase. Gases formed from solid species are listed in the reactions below in Equation 6.13. Atomic carbon was assumed to combine with oxygen until no oxygen remained. Any remaining carbon combined with hydrogen, while any residual atomic hydrogen or nitrogen then formed its diatomic counterpart.

$$\begin{aligned}
&(1) \qquad C + O \Rightarrow CO \\
&(2) \qquad C + 4H \Rightarrow CH_4 \\
&(3) \qquad H + H \Rightarrow H_2 \\
&(4) \qquad N + N \Rightarrow N_2 \\
&(5) \qquad H_2O_{<l>} \Rightarrow H_2O_{<g>}
\end{aligned} \tag{6.13}$$

$$MR_{p,i} = \Phi\left(t - t_{ig}\right) \cdot a_i \cdot e^{-b_i \cdot t} \cdot y_{r,\chi}^{\nu_{r,\chi}} \cdot y_{r,\delta}^{\nu_{r,\delta}} \tag{6.14}$$

Mass flow rates for each flammable species (CO, CH_4, H_2, N_2) were determined by global, first-order reactions rates defined in Equation 6.14. The Heaviside function,

$\Phi(t)$, of Equation 6.14 indicates that mass release does not occur until after a defined t_{ig} (3 s). The rate parameters (a_i and b_i) were defined to be time-dependent instead of temperature-dependent (Arrhenius-like parameters); this way ignition could be defined from experimental results (t_{ig} = 3 s). The flow rate of moisture (reaction 5) was separated into two time periods, before and after ignition. Rate parameters for moisture were determined for each time period.

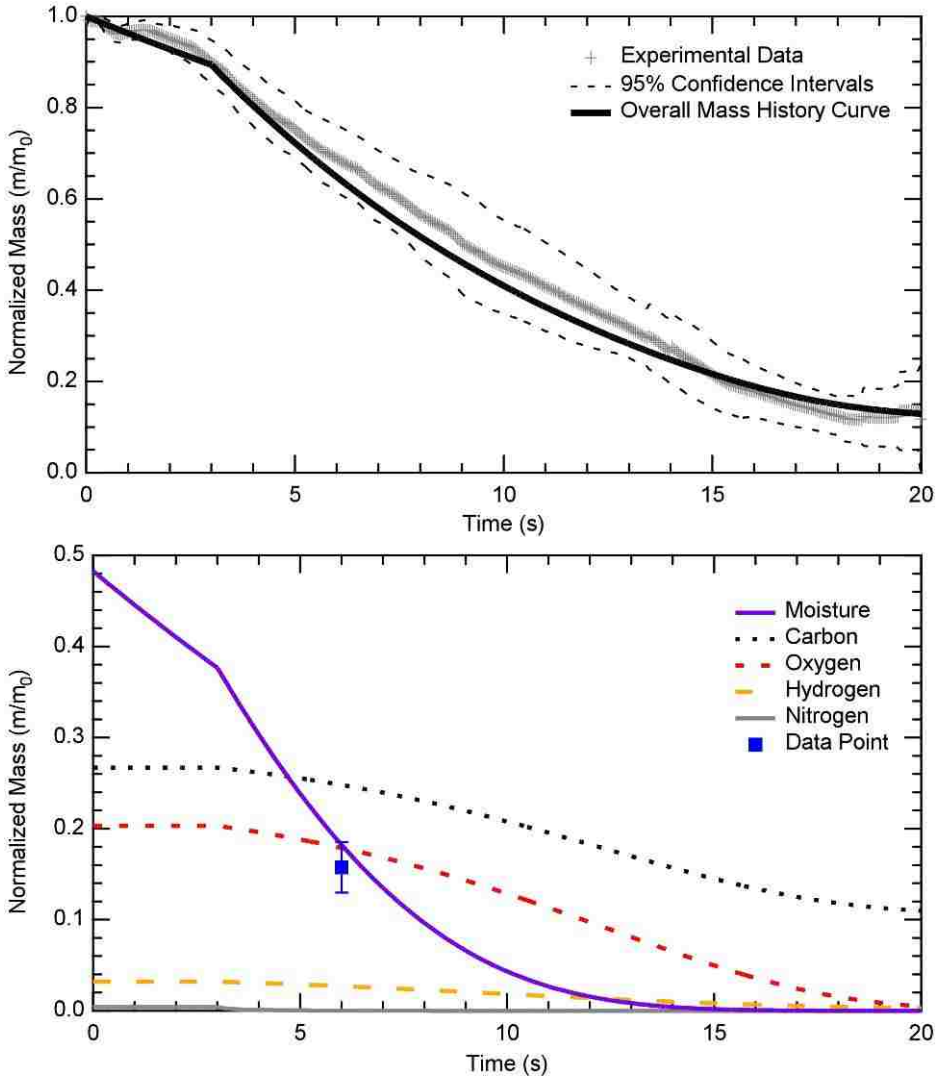

Figure 6.7. (a) Normalized mass profile comparing experimental results to the overall mass history curve determined from the global reactions (Equations 6.13-6.14). (b) Mass profiles for solid species. Notice moisture fits within data point at 6 s.

From the Arrhenius-like parameters, mass profiles were generated for each solid species; the sum of these species was the overall mass history curve. To determine rate parameters (and thus mass flow rates) for the 4 flammable species and for the 2 moisture time periods, the rate parameters were regressed so the overall mass history curve fit to an average value of multiple experimental mass profiles (see Figure 6.7a). The overall mass curve determined from the solid reactions was shown to fit within the error (95% confidence intervals) of the experimental mass profiles throughout most of the run. Mass remaining at the end of combustion was assumed to be char (atomic carbon), thus rate coefficients were altered to allow for carbon content to decrease to the amount of residual char (approximately 11% of original mass) while other solid species were depleted (see Figure 6.7b).

To determine the flow rate of moisture from the leaf more accurately, live manzanita samples (10) were quenched (extinguished) at 6 s after the FFB came under the sample. Mass of the sample (before experiment and after quenching) was recorded, then the samples were placed in a furnace at 100°C where they remained for 4 hr, evaporating the remaining moisture. The final mass was again recorded. This experiment allowed for an estimate of the remaining moisture in the leaf at 6 s after the initial time. By changing the rate parameters for moisture at both time periods, the moisture curve from the solid was allowed to fit within the error bars (average ± 95% confidence intervals) of the data point at 6 s (see Figure 6.7b).

The time-dependent parameter (b_i) was determined to be insignificant when fitting the experimental results for each reaction, thus a constant rate coefficient (a_i) was

used to determine the flow rate of the combustible gases and moisture from the leaf. This reduced the total number of variables to 6 rate constants, 4 for flammable species and 2 for moisture. These rate coefficients for each reaction of Equation 6.13 are shown in Table 6.2.

Table 6.2. Time-dependent rate parameters obtained for reaction mechanism in Equation 6.13.

Reaction	a_i	b_i
1	0.164702	0
2	500	0
3	1	0
4	500	0
5a*	0.078048	0
5b*	0.182951	0
*a – before ignition, b – after ignition		

The leaf boundary condition was defined to be coupled in heat transfer between the solid and gas phases. Mass transfer was specified as a user-defined function (UDF) that allowed for mass to evolve from the leaf surface at a rate which was discussed above. Physical properties of the leaf could be changed by using temperature-specified functions. A temperature-dependent heat capacity for wood was used (Dunlap, 1912) and is shown in Equation 6.15. Since volume was assumed to be constant in the model, density would decrease as mass decreased. Experimental temperature and density (derived from mass) were correlated to determine a linear temperature-dependent density; this is shown in Equation 6.16.

$$c_p\left[J/kg/K\right] = -217.509 + 4.86 \cdot T\left[K\right] \tag{6.15}$$

$$\rho\left[kg/m^3\right] = 996.98 - 0.74356 \cdot T\left[K\right] \tag{6.16}$$

Volumetric heat sinks were also used in the leaf volume to account for the heat required to evaporate the water and to pyrolyze the combustible gases from the solid

phase. The sink term for evaporation was defined as the flow rate of moisture from the sample (defined above) multiplied by the heat of evaporation of water (temperature-dependent correlation obtained from DIPPR (2008)) divided by the volume of the leaf to give consistent units of W/m^3. A volumetric heat source heated up the leaf from the flame created from the volatiles; this was assumed to be the 1/15 of the heat of combustion (22,250 kJ/kg – obtained from manzanita in a bomb calorimeter (ASTM D2015-00)).

An unsteady 1st order implicit, axisymmetric Fluent solver was used to solve the heat and mass transfer equations. A standard k-ε turbulence model was used with default Fluent values. Energy and species equations were also used to solve transport of heat and mass. Species used were O_2, H_2O, CO_2, CO, CH_4, H_2, and N_2 with global, gas-phase combustion reactions of CO, H_2, and CH_4 (oxidation with O_2) were used with default Arrhenius parameters from Fluent. The pressure-velocity coupling used was the SIMPLE method, and the discretization technique used on the unstructured grid points was first-order upwind (Patankar, 1980). Initial conditions for the solver were as follows: P = 1 atm, k = 1 m^2/s^2, ε = 1 m^2/s^3, z_{N2} = 1, and T = 300 K. The grid consisted of solid and gas phases with refinement in the solid leaf. A grid refinement study showed that at least 385 cells within the leaf surface and a time step of 0.05 s were sufficient for accurate results.

The flow rates of each combustible gas were defined (reactions 1-4 of Equation 6.13), but a momentum for these gases could not be specified. The mass addition of these gases produced a velocity (from volume expansion) that was an order of magnitude lower than the inlet velocity (2 m/s). Thus the flammable species tended to remain by the leaf surface, causing oxygen to diffuse to the leaf, and spiking the temperature (similar to char combustion) to values much higher than those observed experimentally. These cases

typically diverged. To give convergence and more accurate leaf temperatures, the flow rates of these flammable species were reduced to 1/5 of the original rates given in Equation 6.14. A surface temperature profile with these corrected rates is shown in Figure 6.8.

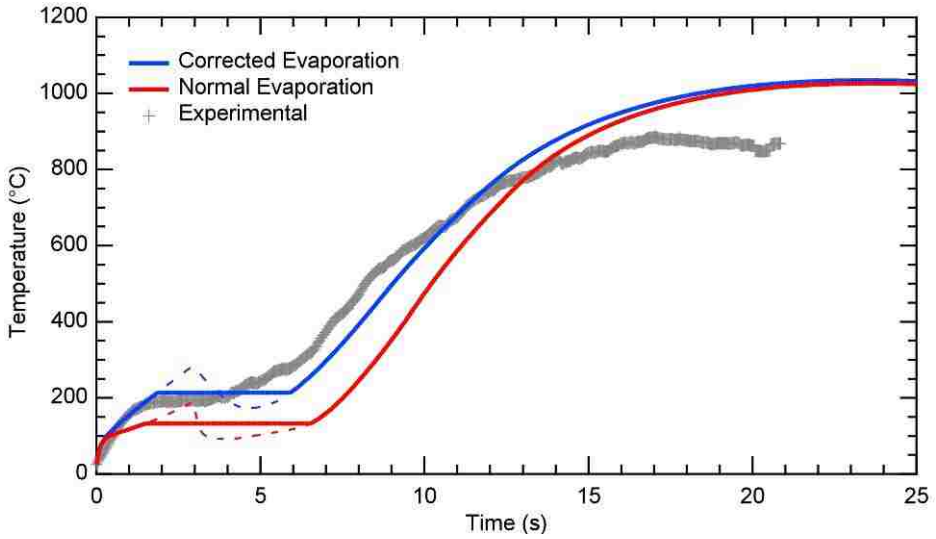

Figure 6.8. Temperature profiles showing corrected and normal evaporation as compared to an experimental profile. Dotted lines indicate discontinuity resulting from model inputs.

The discontinuity observed at the ignition time (3 s) is due to the different moisture flow rates before and after ignition (see Table 6.2). Since this discontinuity was a result of the input parameters and was not due to a physical phenomenom, the profile was smoothed to give a plateau at the temperature that equally intersects the area above and below the plateau line. All remaining profiles are shown in this plateau form. The profile shows a plateau at 130°C and a profile that is delayed from the experimental profile; this plateau is middle IR temperature profile shown in Figure 5.18. To improve the model profile, the sink term (moisture evaporation) was reduced to 3/5 of the original value, which gave a plateau at 210°C and a profile much closer to the experimental

profile at the perimeter. A video is also found in Appendix D. 'C. Model Video Files' which shows the discontinuity in leaf temperature following ignition as shown in Figure 6.8.

The temperatures at various axial distances in the leaf (bottom, top, middle) were recorded and are shown in Figure 6.9. It is interesting to note that the temperature varied by as much as 80°C between the surface (top and bottom) and the middle of the leaf during the region of heat-up, ignition, and moisture evaporation.

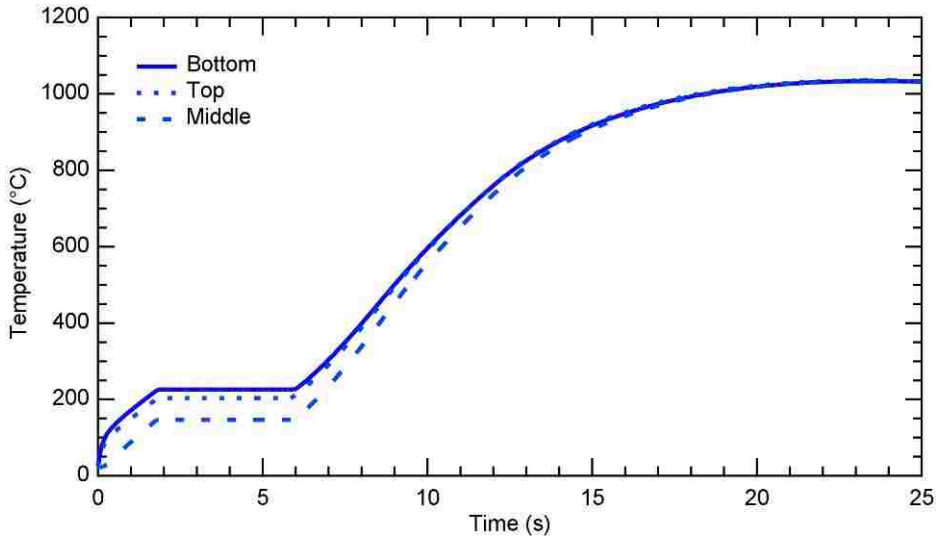

Figure 6.9. Model profiles showing temperatures at the bottom, top, and middle of the leaf.

This model can be improved by including a momentum boundary condition to the mass flow rate of the flammable species; this would give reactions more like devolatilization and not char combustion. This would possibly eliminate the need to alter the original flow rates and sink term, and thus give a more physical representation of the leaf combustion.

6.2 Two-Leaf Model

The Fluent model described in Section 6.1.2.2. Fluent Model (2D) was adapted to include a second leaf, similar to the experimental setup described in Section 5.2. Two-Leaf Experiments. UDF's created for this model assumed that all time-defined functions in the single-leaf model were shifted or delayed by t_{id}. This value was assumed to be 1.15 s which is consistent with experimental data for the two-leaf experiments. Configurations 2, 3, and 4 (described in Section 4.1.7. Fuel Sample Placement) were run and are reported below. Videos of temperature and oxygen concentration are shown in Appendix D. 'C. Model Video Files' for each configuration.

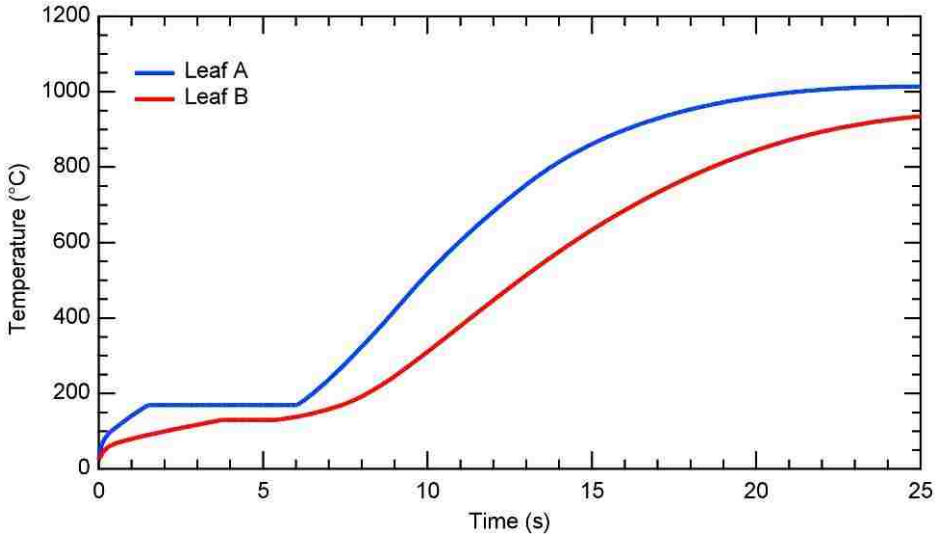

Figure 6.10. Fluent two-leaf model temperature profiles for leaves A and B of configuration 2.

Configuration 2 consists of two leaves, an upper leaf directly above a lower leaf. The surface temperatures (total surface area) for both the lower (A) and upper (B) leaves are shown in Figure 6.10. The temperature of the leaf A was much lower than leaf B, indicating that the presence of leaf A alters the combustion behavior of leaf B; this was

also observed experimentally. Also, the profile for leaf A was slightly different from the one-leaf model in the previous section. It appears that the presence of the leaf B can affect, though slightly, the burning of leaf A also. Configuration 3 consisted of a leaf in the upper position only. The profile was similar to that of the leaf A on configuration 2. This was not expected to vary significantly since energy was not lost from the system before it heats up (adiabatic side wall).

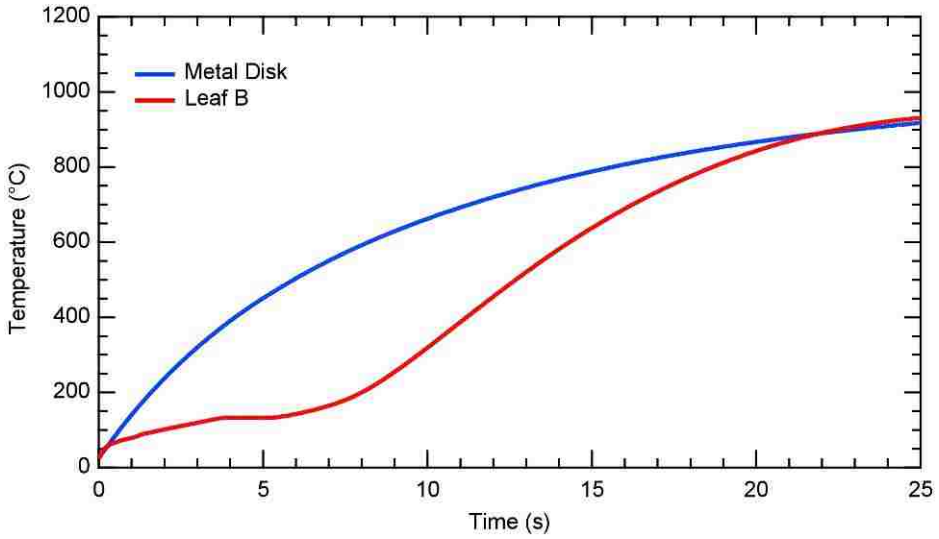

Figure 6.11. Fluent two-leaf model temperature profiles for the metal disk and leaf B of configuration 4.

Configuration 4 consisted of a metal disk in the lower position and a leaf in the upper position. The profiles for both disk and leaf are shown in Figure 6.11. The surface temperature for leaf B for this configuration is similar to that of configuration 2 (leaf/leaf). Since the flammable species from the lower leaf are stagnant once they enter the gas phase, they do not significantly interact with the upper leaf, which would be expected during normal devolatilization. Again, this is one of the main setbacks of the model.

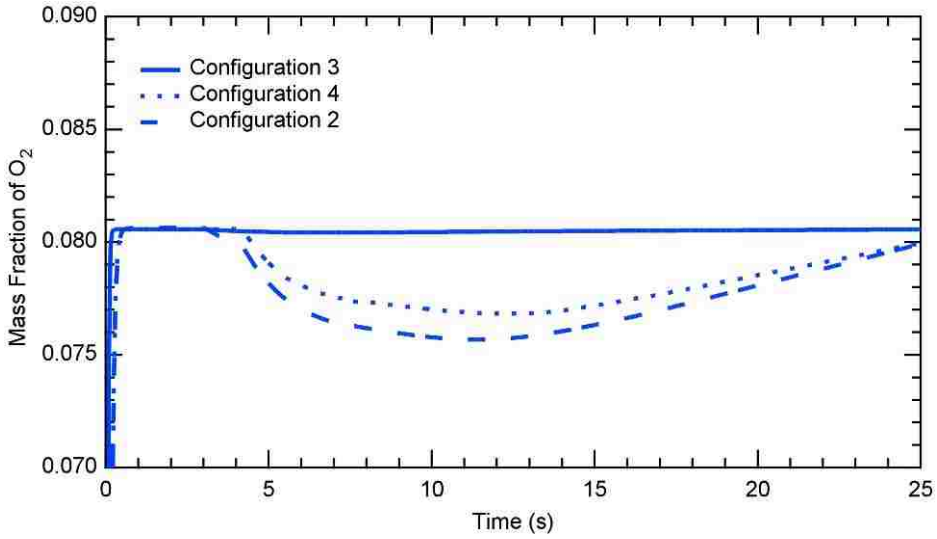

Figure 6.12. Oxygen mass fraction at location midway between positions A and B for various configurations.

Since O_2 concentration was found to be an important parameter that can affect the burning rate of the upper leaf, O_2 was monitored similarly to configurations 6 and 7 (see Section 4.1.7. Fuel Sample Placement) where the O_2 was measured in between positions A and B. The monitor was used for each modeled configuration (2, 3, and 4). The mass fraction of O_2 is shown Figure 6.12 through the burn time for each configuration.

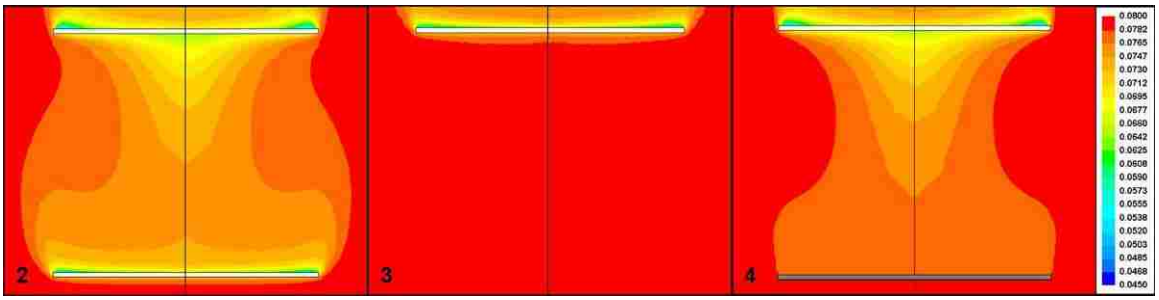

Figure 6.13. Contour plots of oxygen mass fraction for various configurations (2-4).

The O_2 content remained the same with no obstruction (configuration 3) throughout the burn time, while the obstructions (configurations 2 and 4) showed a

minimum in O_2 content. The configuration with a leaf at position A (2) had a minimum that was 6.0% lower than configuration 3, while the configuration with the disk (3) had a minimum 4.5% lower than configuration 3. This shows that the combustion of leaf A does lower the O_2 concentration, but the obstruction itself, due to wake effects, can cause a significant decrease in O_2 content. A steady-state solution of the two-disk configurations (2 and 4) showed a recirculation zone in the wake region of position A. The experimental results showed about a 20% decrease in O_2 concentration from configurations 3 to 2. If the flow rate of flammable species had not been reduced, the 6.0% decrease would be much larger. A contour plot of the mass fraction of O_2 for all configurations (2-4) is shown in Figure 6.13 at 10 s into the burn time; this gives a visual representation of the O_2 content between positions A and B.

6.3 Bush Model

Because of the large amount of scatter in the data and the numerous variations from leaf-to-leaf, a physical model may fall short in predicting overall fire behavior when propagating through a porous fuel medium. For this reason, a statistical model that incorporates physical phenomena may be useful to describe fire spread. A statistical model was developed to describe the burning of a bush. No experimental work was done to validate this model, but the ideas brought forth may be useful in heterogeneous fire spread.

The bush was confined to a 2D domain, though a 3D domain could be easily adapted. Random number generation was used to specify the location and also radius of a specified number of leaves in the domain. Fuel loading (*FL*) was defined as the number of leaves divided by the area of the domain. Each leaf had an ignition zone (or area)

which has the possibility to ignite nearby leaves. Initially, the ignition zone area was set to zero, but once the leaf ignited, the ignition zone grew, reached a maximum area, diminished, and extinguished, setting the area back to zero. This sequence is shown in Figure 6.14.

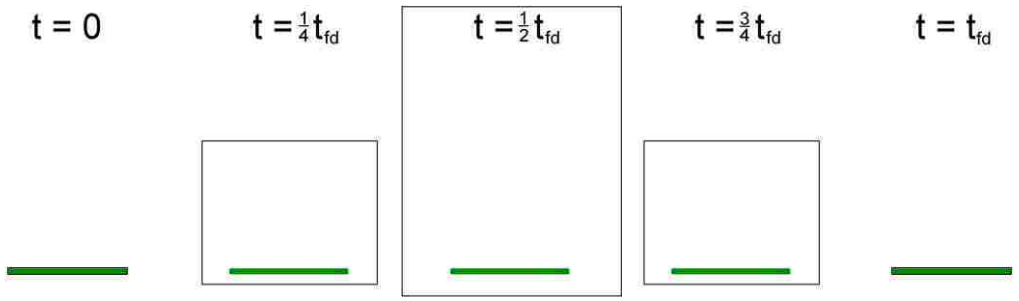

Figure 6.14. Sequence of growing and shrinking ignition zone used in bush model. Distances are not to scale.

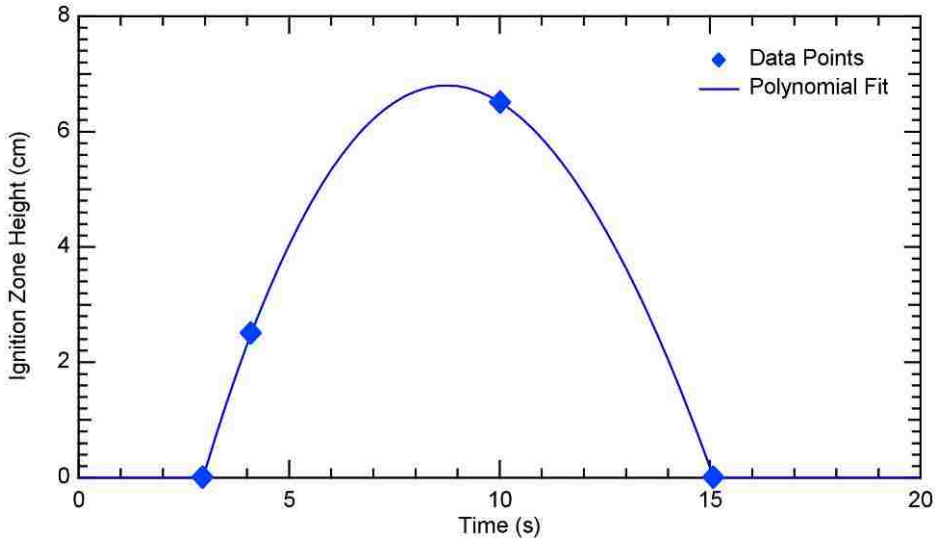

Figure 6.15. Data points from experimental apparatus to determine a polynomial ignition zone height.

For simplicity, the ignition zone was defined as a growing/shrinking rectangle (or cylinder in 3D). To determine the rate at which the ignition zone grew above the leaf, 4 times with corresponding heights were used from the experimental data: (1) average time

to ignition (t_{ig} = 2.953, IZ = 0), (2) average time of ignition delay of a leaf 2.5 cm above the previously ignited leaf ($t_{id} + t_{ig}$ = 4.102, IZ = 2.5), (3) average maximum flame height and time assuming that the ignition zone required at least 1.0 cm of flame to be sufficient to ignite the upper leaf ($t_{FH} + t_{ig}$ = 10.024, IZ = 7.5 – 1.0), and (4) the average flame duration time ($t_{fd} + t_{ig}$ = 15.088, IZ = 0). These 4 points were fit to a cubic polynomial and used in the bush model for the ignition zone of each leaf (see Figure 6.15). Ignition zone growth below the leaf and in the radial direction (to the sides of the leaf) was assumed to be fractions (0.05 and 0.1, respectively) of the growth above the leaf.

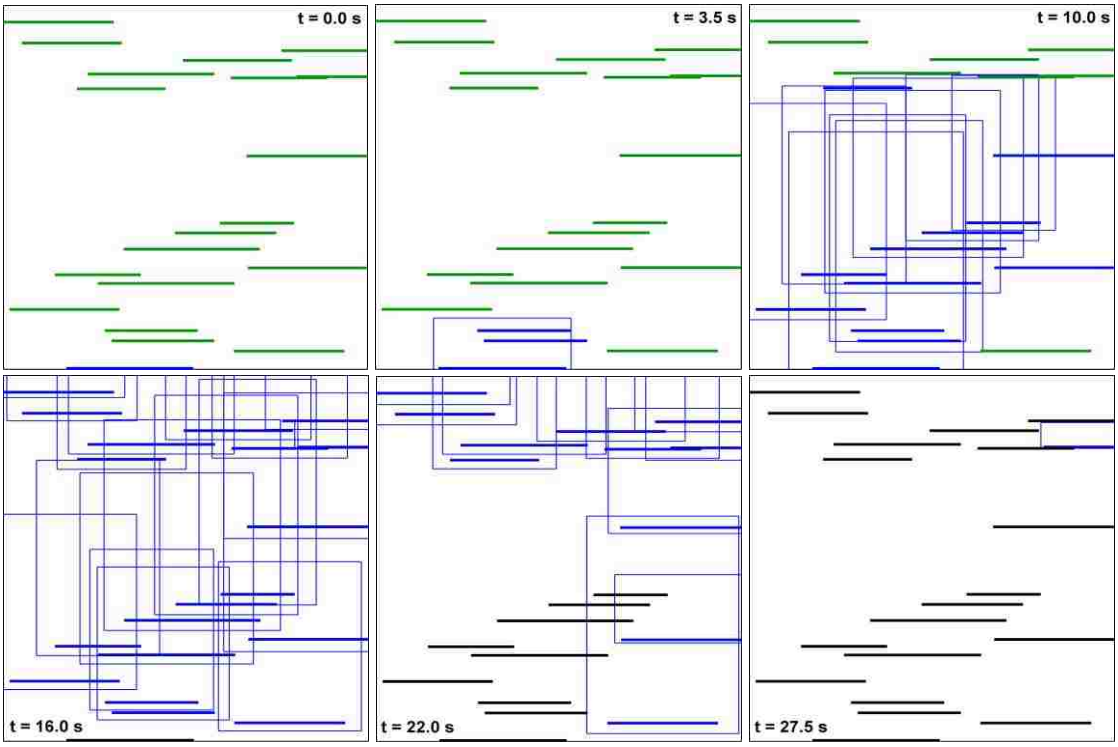

Figure 6.16. Sequence showing the propagation of ignition zones in a bush model. Video in Appendix D.

Once the location and size of the leaves were determined, the lowest vertical leaf in the domain started the ignition zone growth process, similar to having a heat source

applied to the leaf. A simple algorithm (Appendix A. 'E. Bush Burning Model') was developed that tracts the ignition zone area of each leaf within the domain, and if a leaf were within the ignition zone of a previously ignited leaf, that leaf would begin its own ignition zone sequence (e.g. a flame from an ignited leaf contacts a neighboring leaf that subsequently ignites the neighboring leaf). This continued until all leaves (if ignited) within the domain finished an ignition zone sequence. A sequence of this process is shown in Figure 6.16 with 20 leaves and a domain of 10 cm × 10 cm (FL = 0.2 leaves/cm^2). Horizontal green lines indicate leaves that have not started an ignition zone sequence (un-ignited). Horizontal blue lines indicate leaves that have started the ignition sequence with blue rectangles showing the ignition zone. Horizontal black lines indicate leaves that have finished an ignition zone sequence (extinguished).

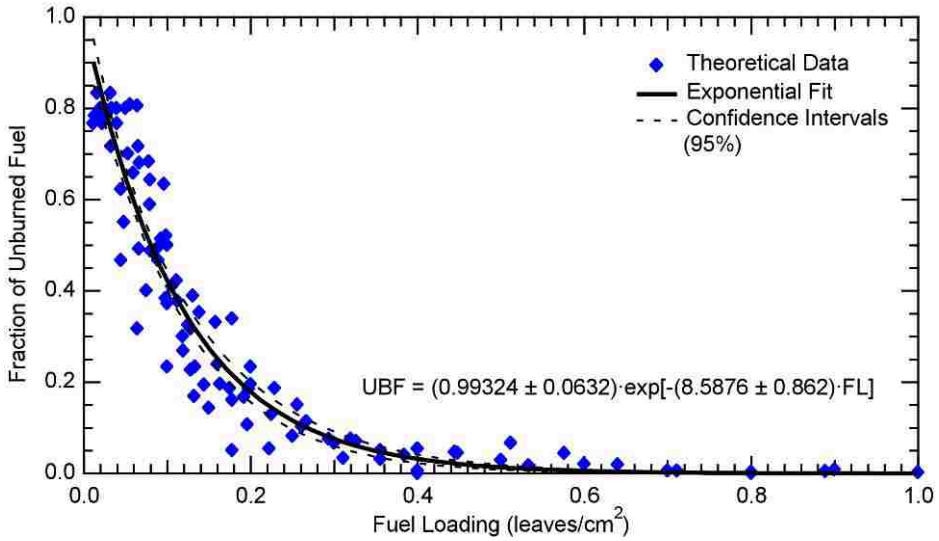

Figure 6.17. Fraction of unburned fuel versus the fuel loading for the theoretical bush model. Exponential regression with confidence bands (95%) included.

Figure 6.16 shows that all leaves within the domain ignited and burned. However, this did not always occur because the location and size of the leaves changed. The

random selection of position and leaf radius allowed for leaves to remain unburned. This model predicted the fraction of unburned fuel (*UBF*) after combustion as well as the overall flame duration of the bush (t_{fd_b}). The bush model was run at various leaf numbers and domain sizes and computed the *UBF* as well as the t_{fd_b}. Since statistical models vary naturally, multiple replicates (6) of the model were performed at each leaf number and domain size, and the average data are presented here. Figure 6.17 shows how *UBF* decreased exponentially with *FL*.

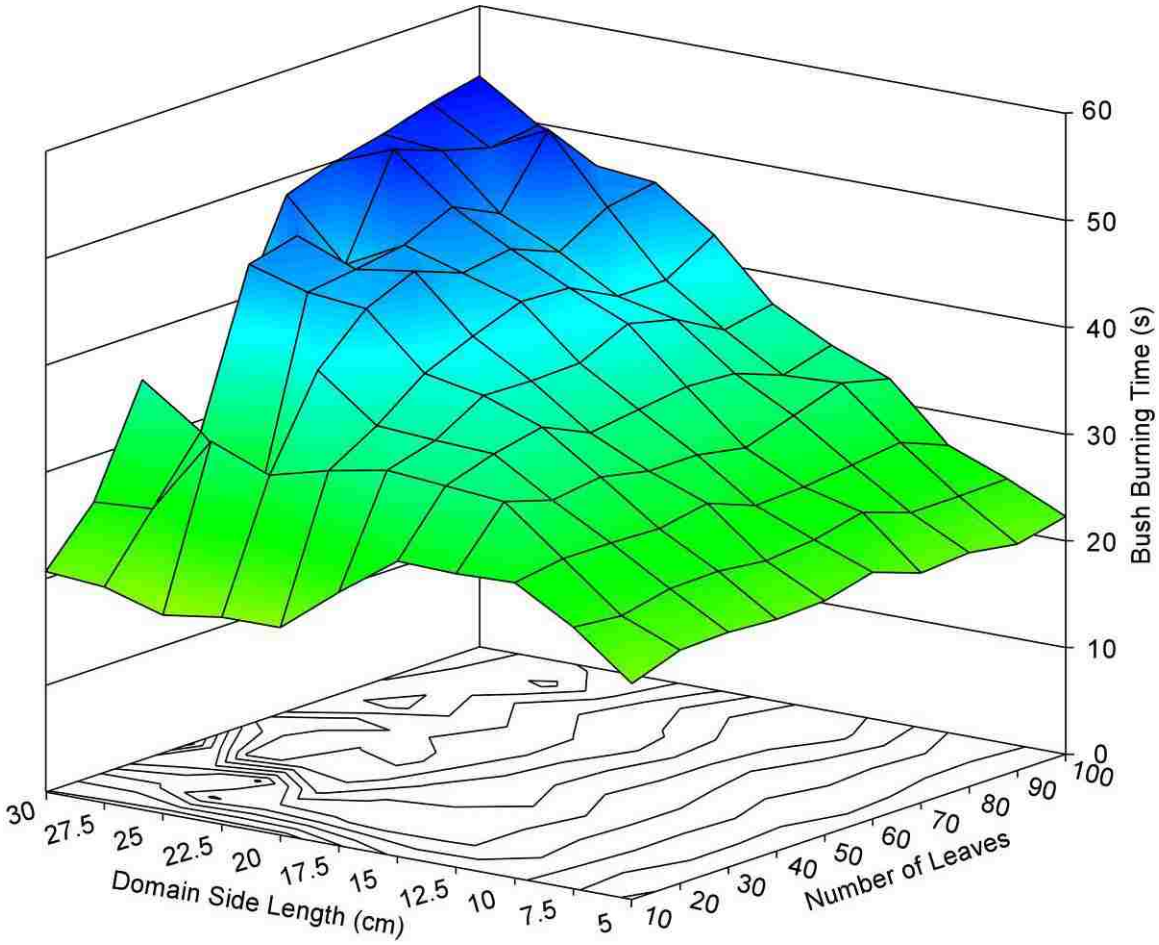

Figure 6.18. Surface plot of the bush flame duration as it varied with the number of leaves and the domain size.

The t_{fd_b} was found to vary with both the number of leaves and the domain size, but not necessarily with the *FL* only. Because of the placement and diameter of the randomly assigned leaves, the t_{fd_b} is shorter if only one or two leaves ignite. A surface plot showing t_{fd_b} vs. the number of leaves and the domain side length (square domain area) is shown in Figure 6.18. The general trend shows that the burning time increases the number of leaves as well as the size of the domain. Some of the variability can be reduced by increasing the number of replicates to give a more accurate average.

Some improvements to the model could be to include a mass release function for each leaf that corresponds to the ignition zone function. This would allow for an overall mass release rate to be estimated during the combustion of the bush. Also, parameters could be included in the ignition zone function that allow for wake effects or O_2 consumption (as with the two-leaf experiments). These parameters may inhibit combustion for leaves above a burning leaf. Another factor that could be included is to account for overlapping flames by increasing the size of the ignition zone. If multiple sources (ignition zones) are within a boundary of a leaf, this would result is a larger heat flux to that leaf, which would affect its own ignition zone.

This model can be used to describe combustion on individual samples, though relating the overall combustion to an entire system. With improvement of the code, this model can run in real-time and may be applied to operational field models where bushes or other fuel beds are involved. The idea of an ignition zone, given certain input parameters (e.g. wind speed and slope), might also be applied to other heterogeneous systems, such as individual trees or bushes that ignite other nearby trees or bushes.

6.4 Summary of Modeling

Semi-physical models were developed to better describe evaporation and attempt to show a delayed moisture plateau at 200-300°C. Two models were developed that described only heat transfer to and from the leaf. The first was a lumped capacitance model which gave preliminary results, but no evaporation plateau. The second was a 2D analytical model that assumed constant physical properties, but allowed changing boundary conditions with time and also a source/sink function with time. This model showed an initial difference in temperature during heat-up between the top and bottom surfaces of the leaf. Improvements to this model could be the better definition of the source/sink function and boundary conditions. The assumption of constant properties was a major fallback in the model.

A Fluent model was developed that included both heat and mass transfer to and from the leaf. This model described the flow dynamics of gases around a 2D leaf as well as heat transfer to the leaf. Mass transfer and a source/sink were defined as combustible gases determined from the elemental composition and moisture content of the leaf. This model showed a profile comparable to the observed experimental profile with a plateau at approximately 200°C. Temperature on the surface of the leaf was substantially higher than the temperature in the middle of the leaf during heat-up, ignition, and moisture evaporation. One main setback of this model was the need to include momentum to the flammable species for them to behave like devolatilization combustion, not char combustion. This one-leaf model was adapted to include two leaves which showed that obstructions caused the upper leaf to burn at a lower temperature. Oxygen content was

also observed to decrease due to both the combustion of the lower leaf and to the wake effects of the obstruction. This was consistent with the experimental results.

A statistical bush model was developed to describe fire propagation through a heterogeneous system. Each individual leaf with a specified domain had its own ignition zone which possibly ignited surrounding leaves within the domain. This model could estimate the overall burning time as well the amount of unburned fuel of the bush. The overall burning time of the bush was found to increase with the number of leaves in the domain as well as the domain size. Also, the fraction of unburned fuel was found to exponentially decrease with fuel loading.

7. Conclusions and Recommendations

To better understand the effects of moisture on combustion of live wildland fuels, experiments were performed on individual samples over a flat-flame burner which simulated an oncoming fire front to a stationary sample. Experimental data were analyzed and qualitative and quantitative results were found. Fourteen lives species, along with dry excelsior samples, were studied. Also, physical and statistical models were developed that characterized combustion through one-leaf, two-leaf, and bush systems. Specific conclusions from this research as well as suggestions for future work are presented below.

7.1 Conclusions

Numerous experiments were performed on live fuel samples over a FFB. Qualitative and quantitative results were determined after analysis of the data. Qualitative data included various phenomena that were observed from video images of the experiments. These phenomena occurred at different leaf conditions such as species, level of *MC*, heating rate, thickness, and the amount of cuticle on the leaf surface. These qualitative phenomena include:

- Jetting – high mass transfer rates from the leaf surface at various angles and directions in the forms of moisture and volatiles. Non-broadleaf species typically experienced this phenomenon.

- Color change – a melting of the waxy layer, most likely the cuticle on the outer leaf surface. The original dusty green color changed to a wet green color as the FFB was first brought under the sample. This was observed in nearly all broadleaf species.
- Bubbling (occurred in two forms):
    - Liquid bubbling – a melting of the waxy layer, though the waxes pooled or congregated on the surface to form liquid bubbles; this was indicative of large amounts of cuticle. The waxes resolidified on removal from the FFB. This was observed in manzanita samples.
    - Interior bubbling – moisture escaping from the leaf interior through the outer epidermal walls in the form of tiny bubbles that were observed on the leaf surface. This typically occurred in on broadleaf samples at moderate *MC*.
- Bursting – moisture escaping from the sample which typically left craters or pockmarks on the surface. This typically occurred in thicker broadleaf samples at high *MC* and high heat flux.
- Brand formation – the ejection of some or the entire sample that was detached from the main body or stem of the sample. The main type (though numerous forms existed) occurred when the stem prematurely burned and could not sustain the weight of the sample.
- Bending – the breaking down or swelling of the lower epidermal layer causing the broadleaf to bend or curl toward the convective gases of the

FFB. This was observed in all broadleaf species, though more prominent in thinner leaves with large surface area.

Quantitative results obtained from the experiments showed ignition values (time to ignition, ignition temperature, normalized mass at ignition) varied significantly by species. Linear correlations were determined between these ignition values (e.g. time to ignition correlated with ignition temperature, time to ignition correlated with normalized mass at ignition). Other linear correlations were determined to relate leaf characteristics (such as thickness, moisture content, initial mass of moisture, surface area, perimeter) to recorded combustion characteristics of ignition (time to ignition, ignition temperature, normalized mass at ignition).

A significant amount of moisture remained within the leaf sample at the time of ignition for all species studied. This is not consistent with the classical model of evaporation in combustion where all evaporation occurs first before devolatilization. It was also observed that the temperature history profile for a leaf typically showed a plateau at 200-300°C, not at the generally accepted 100°C. This plateau was due to delayed moisture evaporation.

Mass release rates at ignition and maximum flame height also varied with species, though non-broadleaf species typically had higher mass release rates at both ignition and maximum flame height. Excelsior had normalized mass release rates that were significantly higher than live species. The flame height and flame duration were found to have a linear relationship with the amount of fuel available (volatile matter) from the sample. Also, these live individual samples did not follow the generally accepted two-fifths power-law, but followed a power-law correlation where the where data were

significantly lower then the two-fifths power-law. Both leaf and combustion characteristics were studied for samples burned at different seasons of the year to study variations by seasons. Though some species showed differences by season, no overriding parameter was found to show significantly seasonal variations for all species.

Experiments were performed in two-leaf configurations to determine combustion interactions between leaves. A second leaf was placed directly above the normally tested leaf. The main difference found during combustion was the the flame duration of the upper leaf was significantly longer when the lower leaf was present. This prolonged burning could be due to the flow dynamics that divert the energy from the FFB away from the upper leaf and/or the consumption of O_2 from the lower leaf which is needed to burn the upper leaf.

The cuticle was removed from some broadleaf species by a solvent (i.e. treated samples), burned over the FFB, and compared to results of experiments performed on untreated samples. No significant differences in combustion parameters were found between the treated and untreated leaves. However, the time of color change was observed to be significantly longer for untreated leaves. This helped show validation that at least some of the cuticle was removed from the leaf surface by solvent treatment.

Semi-physical models were developed to better describe evaporation and attempt to show a delayed moisture plateau at 200-300°C. Two models were developed that described only heat transfer to and from the leaf. The first was a lumped capacitance model which gave preliminary results, but no evaporation plateau. The second was a 2D analytical model that assumed constant physical properties, but allowed changing boundary conditions with time and also a source/sink function with time. This model

showed an initial difference in temperature during heat-up between the top and bottom surfaces of the leaf. Improvements to this model could be the better definition of the source/sink function and boundary conditions. The assumption of constant properties was a major fallback in the model.

A Fluent model was developed that included both heat and mass transfer to and from the leaf. This model described the flow dynamics of gases around a 2D leaf as well as heat transfer to the leaf. Mass transfer and a source/sink were defined as combustible gases determined from the elemental composition and moisture content of the leaf. This model showed a profile comparable to the observed experimental profile with a plateau at approximately 200°C. Temperature on the surface of the leaf was substantially higher than the temperature in the middle of the leaf during heat-up, ignition, and moisture evaporation. One main setback of this model was the need to include momentum to the flammable species for them to behave like devolatilization combustion, not char combustion. This one-leaf model was adapted to include two leaves which showed that obstructions caused the upper leaf to burn at a lower temperature. Oxygen content was also observed to decrease due to both the combustion of the lower leaf and to the wake effects of the obstruction. This was consistent with the experimental results.

A statistical bush model was developed to describe fire propagation through a heterogeneous system. Each individual leaf with a specified domain had its own ignition zone which possibly ignited surrounding leaves within the domain. This model could estimate the overall burning time as well the amount of unburned fuel of the bush. The overall burning time of the bush was found to increase with the number of leaves in the

domain as well as the domain size. Also, the fraction of unburned fuel was found to exponentially decrease with fuel loading.

7.2 Recommendations

Many new questions arose as research was performed for this project. Answers to these questions would be helpful to better determine the influence of moisture on ignition in wildland fires. Some of the important recommendations for future work are listed here.

- Determine the composition of the waxes from the liquid bubbling manzanita samples. This could be done by gas chromatography, mass spectrometry, etc. or a combination of these techniques.
- Use the radiant panel to better characterize the influence of both radiation and convection on the leaf sample. These heat transfer phenomena play a significant role in wildland fires, but the defining roles have yet to be completely understood.
- Vary the heat flux of the flat-flame burner (and also radiant panel) by changing the flow rates of fuels, inert, and oxidizer. This could improve understanding of fire behavior at various heating rates which are experienced during wildland fires.
- Modify the two-leaf configurations to include the effects of angle. The upper leaf could be positioned slightly to the side of the present location. This would allow the upper leaf to not experience the full brunt of the flat-flame burner and allow for more characterization of the interactions between leaves.

- Remove leaves from the flat-flame burner at a specified time and perform the proximate and ultimate analyses on the partially burned sample. This could better characterize the mass release curve of the combustible gases used for the Fluent model (Section 6.1.2.2. Fluent Model (2D)).
- Scale-up to a bush and attempt to validate and/or improve the statistical bush model.
- Improve the source/sink terms used in the analytical model (Section 6.1.1.2. Analytical Model (2D)) and the Fluent model (Section 6.1.2.2. Fluent Model (2D)).
- Include momentum to the flow rates of the Fluent model (Section 6.1.2.2. Fluent Model (2D)) so that the flammable species behave like flaming (devolatilization) combustion.
- Use the idea of ignition zone as used in the bush model (Section 6.3. Bush Model) for other heterogeneous fuel beds. Instead of a 2D vertical domain, it could be a 2D horizontal domain that describes individual trees on a specified terrain.

8. References

Albini, F. A., "Computer-Based Models of Wildland Fire Behavior: A User's Manual," U. F. Service, Ogden, UT, USDA Forest Service**:** 68 (1975).

Albini, F. A., "Estimating Wildfire Behavior and Effects," General Technical Report INT-30, USDA Forest Service (1976).

Albini, F. A., "Thermochemical Properties of Flame Gases from Fine Wildland Fuels," Research Paper INT-243, USDA Forest Service (1980).

Albini, F. A., "A Model for the Wind-Blown Flame from a Line Fire," *Combustion and Flame,* **43**, 155-174 (1981).

Andrews, P. L., "BEHAVE: Fire Behavior Prediction and Fuel Modeling System- BURN Subsystem, Part 1," General Technical Report INT-194, USDA Forest Service (1986).

Babrauskas, V., "Ignition of Wood: A Review of the State of the Art," *Interflam*, 71-88 (2001).

Babrauskas, V., Ignition Handbook, Issaquah, WA, Fire Science Publishers (2003).

Brousseau, A., "Ceanothus Image - Photo ID: 5205-1622-0665-0038 - Accessed 1/30/2008," Br. Alfred Brousseau Collection, Saint Mary's College, http://calphotos.berkeley.edu, Olowin, R. P. (2008).

Brown, A. L., B. R. Hames, J. W. Daily and D. C. Dayton, "Chemical Analysis of Solids and Pyrolytic Vapors from Wildland Trees," *Energy & Fuels,* **17**, 1022-1027 (2003).

Burrows, N. D., "Flame Residence Times and Rates of Weight Loss of Eucalypt Forest Fuel Particles," *International Journal of Wildland Fire,* **10**, 137-143 (2001).

Butler, B. W., J. Cohen, D. J. Latham, R. D. Schuette, P. Sopko, K. S. Shannon, D. Jimenez and L. S. Bradshaw, "Measurements of Radiant Emissive Power and Temperatures in Crown Fires," *Canadian Journal of Forest Research,* **34**, 1577-1587 (2004a).

Butler, B. W., M. A. Finney, P. L. Andrews and F. A. Albini, "A Radiation-Driven Model for Crown Fire Spread," *Canadian Journal of Forest Research,* **34**(8), 1588-1599 (2004b).

Byram, G. M., "Chapter 3: Combustion of Forest Fuels," Forest Fire: Control and Use, K. P. Davis, McGraw-Hill**:** 61-89 (1959).

Campbell, C. S. and K. J. McInnes, "Response of In Situ Leaf Psychrometer to Cuticle Removal by Abrasion," *Agronomy Journal,* **91**, 859-862 (1999).

Catchpole, W. R., E. A. Catchpole, A. G. Tate, B. W. Butler and R. C. Rothermel, A Model for the Steady Spread of Fire through a Homogeneous Fuel Bed, Rotterdam, Millpress (2002).

Clark, T. L., M. A. Jenkins, J. L. Coen and D. Packham, "A Coupled Atmospheric-Fire Model: Convective Feedback on Fire Line Dynamics," *Journal of Applied Meteorology,* **35**, 875-901 (1996a).

Clark, T. L., M. A. Jenkins, J. L. Coen and D. Packham, "A Coupled Atmospheric-Fire Model: Convective Froude Number and Dynamic Fingering," *International Journal of Wildland Fire,* **6**, 177-190 (1996b).

Cohen, J., M. A. Finney and B. W. Butler, "Personal Communication," B. M. Pickett and T. H. Fletcher, Missoula, MT**:** Experimental results given during presentation in June 2006. (2006).

Debnath, L., Integral Transformations and Their Applications, CRC Press (1995).

Dimitrakopoulos, A. P. and K. K. Papaioannou, "Flammability Assessment of Mediterranean Forest Fuels," *Fire Technology,* **37**(2), 143-152 (2001).

DIPPR, "Chemical Database of Physical and Thermodynamica Properties," Brigham Young University Thermophysical Properties Laboratory (2008).

Dittmann, L., "Chamise Image - Photo ID: 0000-0000-1200-0151 - Accessed 1/30/2008," http://calphotos.berkeley.edu (2008).

Drysdale, D., An Introduction to Fire Dynamics, Chichester, England, John Wiley & Sons (1999).

Dunlap, F., "The Specific Heat of Wood," *US Forest Service Bull.,* **110**, 28 (1912).

Dupuy, J. L. and M. Larini, "Fire Spread through a Porous Forest Fuel Bed: A Radiative and Convective Model Including Fire-Induced Flow Effects," *International Journal of Wildland Fire,* **9**, 155-172 (1999).

Dupuy, J. L., J. Marechal and D. Morvan, "Fires from a Cylindrical Forest Fuel Burner: Combustion Dynamics and Flame Properties," *Combustion and Flame,* **135**(1-2), 65-76 (2003).

Engstrom, J. D., J. K. Butler, S. G. Smith, L. L. Baxter, T. H. Fletcher and D. R. Weise, "Ignition Behavior of Live California Chaparral Leaves," *Combustion Science and Technology,* **176**, 1577-1591 (2004).

Finney, M. A., "FARSITE: Fire Area Simulator-Model Development and Evaluation," Research Paper RMRS-RP-4, USDA Forest Service (1998).

Fletcher, T. H., B. M. Pickett, S. G. Smith, G. S. Spittle, M. M. Woodhouse, E. Haake and D. R. Weise, "Effects of Moisture on Ignition Behavior of Moist California Chaparral and Utah Leaves," *Combustion Science and Technology,* **179**, 1183-1203 (2007).

Fons, W. L., H. B. Clements and P. M. George, "Scale Effects on Propagation Rate of Laboratory Crib Fires," Ninth Symposium (International) on Combustion (1963).

Fosberg, M. A. and J. E. Deeming, "Derivation of the 1- and 10-Hour Timelag Fuel Moisture Calculations for Fire Danger Rating.," Fort Collins, CO, USDA Forest Service, Rocky Mountain Forest and Range Experiment Station (1971).

Fralish, J. S. and S. B. Franklin, Taxonomy and Ecology of Woody Plants in North American Forests, New York, NY, John Wiley & Sons, Inc. (2002).

Frandsen, W. H., "Fire Spread through Porous Fuels from the Conservation of Energy," *Combustion and Flame,* **16**(1), 9-16 (1971).

Gonzalez, R. C., R. E. Woods and S. L. Eddins, Digital Image Processing using Matlab, Upper Saddle River, NJ, Pearson Prentice Hall (2004).

Haberman, R., Applied Partial Differential Equations with Fourier Series and Boundary Value Problems - Fourth Edition, Upper Saddle River, NJ, Pearson Education Inc., Pearson Prentice Hall (2004).

Hilpert, R., "Warmeabgabe von geheizten Drahten und Rohren im Luftstrom," *Forschung im Ingenieurwesen,* **4**, 215-224 (1933).

Howitt, B. F., "Manzanita Image - Photo ID: 8253-3202-4137-0079 - Accessed 1/30/2008," California Academy of Sciences, http://calphotos.berkeley.edu (2008).

Incropera, F. P. and D. P. DeWitt, Fundamentals of Heat and Mass Transfer - Fifth Edition, New York, John Wiley & Sons, Inc. (2002).

Karr, C., Jr., Ed. Analytical Methods for Coal and Coal Products, New York, Academic Press, Inc. (1978).

Kramer, N., "Scrub Oak Image - Photo ID: 0000-0000-1207-0515 - Accessed 1/30/2008," http://calphotos.berkeley.edu (2008).

Landry, L.-M., "White Fir Image - Photo ID: 0000-0000-0506-1031 - Accessed 1/30/2008," http://calphotos.berkeley.edu (2008).

Lee, L., "Southeastern Species Images - Accessed 1/30/2008," University of South Carolina Herbarium, http://cricket.biol.sc.edu/herb (2008).

Li, Y. and D. Drysdale, "Measurement of the Ignition Temperature of Wood," Fire Science and Technology - First Asian Conference, Beijing, Intl. Academic Publishers(1992).

Linn, R. R., "A Transport Model for Prediction of Wildfire Behavior," Ph.D. Dissertation, Mechanical Engineering, New Mexico State (1997).

Linn, R. R., J. Reisner, J. J. Colman and J. Winterkamp, "Studying Wildfire Behavior using FIRETEC," *International Journal of Wildland Fire,* **11**, 233-246 (2002).

Linn, R. R., J. Winterkamp, J. J. Colman, C. Edminster and J. D. Bailey, "Modeling Interactions Between Fire and Atmosphere in Discrete Element Fuel Beds," *International Journal of Wildland Fire,* **14**(1), 37-48 (2005).

Lu, H., "Experimental and Modeling Investigations of Biomass Particle Combustion," Ph. D. Dissertation, Chemical Engineering, Brigham Young University (2006).

Mardini, J. and A. S. Lavine, "Heat and Mass Transfer in Green Wood During Fires," ASME Heat Transfer Division, ASME (1995).

Martin, J. T. and B. E. Juniper, The Cuticles of Plants, Edinburgh, Edward Arnold Ltd (1970).

McClellan, J. E. and B. McClellan, "Utah Juniper Image - Photo ID: 1351-3163-4289-0027 - Accessed 1/30/2008," California Academy of Sciences, http://calphotos.berkeley.edu (2008).

Miller, J. H. and K. V. Miller, Forest Plants of the Southeast and their Wildlife Uses, Athens, GA, University of Georgia Press (1999).

Moghtaderi, B., V. Novozhilov, D. F. Fletcher and J. H. Kent, "A New Correlation for Bench-Scale Piloted Ignition Data of Wood," *Fire Safety Journal,* **29**, 41-59 (1997).

Montgomery, K. R. and P. C. Cheo, "Moisture and Salt Effects on Fire Retardance in Plants," *American Journal of Botany,* **56**(9), 1028-1032 (1969).

Montgomery, K. R. and P. C. Cheo, "Effect of Leaf Thickness on Ignitability," *Forest Science,* **17**(4), 475-478 (1971).

Nelson, R. M., Jr., "Flame Characteristics for Fires in Southern Fuels," Research Report SE-205, Asheville, N. C., USDA Forest Service (1980).

Ornduff, R., Introduction to California Plant Life, Berkeley, CA, University of California Press (2003).

Patankar, S. V., Numerical Heat Transfer and Fluid Flow, Taylor & Francis (1980).

Petrides, G. A., A Field Guide to Western Trees, Boston, MA, Houghton Mifflin Company (1998).

Philpot, C. W., "Seasonal Changes in Heat Content and Ether Extractive Content of Chamise," Research Paper INT-92, U. F. Service**:** 10 (1969).

Philpot, C. W., "Influence of Mineral Content on the Pyrolysis of Plant Material," *Forest Science,* **16**(4), 461-471 (1970).

Philpot, C. W., "The Pyrolysis Products and Thermal Characteristics of Cottonwood and its Components," Research Paper INT-107, USDA Forest Service (1971).

Philpot, C. W. and R. W. Mutch, "The Seasonal Trends in Moisture Content, Ether Extractives, and Energy of Ponderosa Pine and Douglas-Fir Needles," Research Paper INT-102, USDA Forest Service (1971).

Pompe, A. and R. G. Vines, "The Influence of Moisture on the Combustion of Leaves," *Australian Forestry,* **30**, 231-241 (1966).

Putnam, A. A., "A Model Study of Wind-Blown Free-Burning Fires," 10th Symposium (International) on Combustion, Pittsburg, PA (1965).

Reisner, J., S. Wynne, L. Margolin and R. R. Linn, "Coupled Atmospheric-Fire Modeling Employing the Method of Averages," *Monthly Weather Review,* **128**, 3683-3691 (2000).

Rogers, J. M., R. A. Susott and R. G. Kelsey, "Chemical Composition of Forest Fuels Affecting their Thermal Behavior," *Canadian Journal of Forest Research,* **16**, 721-726 (1986).

Rothermel, R. C., "A Mathematical Model for Predicting Fire Spread in Wildland Fuels," Research Paper INT-115, USDA Forest Service (1972).

Sadava, D., H. C. Heller, G. H. Orians, W. K. Purves and D. M. Hillis, Life: The Science of Biology - Eighth Edition, Sinauer Associates, Inc. and W.H. Freeman and Company (2008).

Shafizadeh, F., "Pyrolysis and Combustion of Cellulosic Materials," *Advanced Carbohydrate Chemistry,* **23**, 419-474 (1968).

Shafizadeh, F. and G. D. McGinnis, "Chemical Composition and Thermal Analysis of Cottonwood," *Carbohydrate Research,* **16**, 273-277 (1971).

Shafizadeh, F., P. P. S. Chin and W. F. DeGroot, "Effective Heat Content of Green Forest Fuels," *Forest Science,* **23**(1), 81-89 (1977).

Simpson, W. and A. TenWolde, "Physical Properties and Moisture Relationships of Wood - Chapter 3," Wood Handbook: Wood as an Engineering Material, FPL-GTR-113, Madison, WI, USDA Forest Service, Forest Products Laboratory**:** 463 (1999).

Sivinski, R., "Gambel Oak and Canyon Maple Images - Photo ID's: 0000-0000-0705-1119 and 0000-0000-1005-1228 - Accessed 1/30/2008," http://calphotos.berkeley.edu (2008).

Smith, S. G., "Effects of Moisture on Combustion Characteristics of Live California Chaparral and Utah Foliage," M.S. Thesis, Chemical Engineering, Brigham Young University (2005).

Solovjov, V., "Intermediate Heat Transfer - Class Notes," Mechanical Engineering 540, Provo, UT, Brigham Young University (2007).

Stubbendieck, J., S. L. Hatch and L. M. Landholt, North American Wildland Plants. A Field Guide, Lincoln, NE, University of Nebraska Press (2003).

Sun, L., X. Zhou, S. Mahalingam and D. R. Weise, "Comparison of Burning Characteristics of Live and Dead Chaparral Fuels," *Combustion and Flame,* **144**(1-2), 349-359 (2006).

Susott, R. A., "Thermal Behavior of Conifer Needle Extractives," *Forest Science,* **26**(3), 347-360 (1980).

Susott, R. A., "Characterization of the Thermal Properties of Forest Fuels by Combustible Gas Analysis," *Forest Science,* **28**(2), 404-420 (1982).

Tang, W., "Effect of Inorganic Salts on Pyrolysis of Wood, Alpha-Cellulose, and Lignin, Determined by Dynamic Thermogravimetry," Research Paper FPL-82, Madison, WI, USDA Forest Service**:** 30 (1967).

Thomas, P. H., "The Size of Flames from Natural Fires," Ninth Symposium (International) on Combustion (1963).

Trujillo, D. P., "Chemical Properties of Chaparral Fuels Change During Preheating Before Flaming," Research Note RM-320, USDA Forest Service (1976).

Van Wagner, C. E., "Height of Crown Scorch in Forest Fires," *Canadian Journal of Forest Research,* **3**, 373-378 (1973).

Weast, R. C. and M. J. Astle, Eds., Handbook of Chemistry and Physics 62nd Edition, Boca Raton, FL, CRC Press. Inc (1982).

Webber, C., "Douglas-Fir Image - Photo ID: 8253-3202-3491-0038 - Accessed 1/30/2008," California Academy of Sciences, http://calphotos.berkeley.edu (2008).

Weber, R. O., "Modelling fire spread through fuel beds," *Progress in Energy and Combustion Science,* **17**(1), 67-82 (1991).

Weise, D. R., T. H. Fletcher, S. G. Smith, S. Mahalingam, X. Zhou and L. Sun, "Correlation of Mass Loss Rate and Flame Height for Live Fuels," Sixth Symposium on Fire and Forest Meteorology, Canmore, AB, Canada (2005a).

Weise, D. R., R. H. White, F. C. Beall and M. Etlinger, "Use of the Cone Calorimeter to Detect Seasonal Differences in Selected Combustion Characteristics of Ornamental Vegetation," *International Journal of Wildland Fire,* **14**, 321-338 (2005b).

Weise, D. R., X. Zhou, L. Sun and S. Mahalingam, "Fire Spread in Chaparral - "Go or No-Go?"" *International Journal of Wildland Fire,* **14**(1), 99-106 (2005c).

Willand, J. E., "Big Sagebrush Image - Photo ID: 0000-0000-0507-1849 - Accessed 1/30/2008," http://calphotos.berkeley.edu (2008).

Willmer, C. and M. Fricker, Stomata - Second Edition, London, Chapman & Hall (1996).

Wylie, C. R. and L. C. Barrett, Advanced Engineering Mathematics - Sixth Edition, McGraw-Hill, Inc. (1995).

Xanthopoulos, G. and R. H. Wakimoto, "A Time to Ignition - Temperature - Moisture Relationship for Branches of Three Western Conifers," *Canadian Journal of Forest Research,* **23**, 253-258 (1993).

Zhou, X., S. Mahalingam and D. Weise, "Modeling of Marginal Burning State of Fire Spread in Live Chaparral Shrub Fuel Bed," *Combustion and Flame,* **143**(3), 183-198 (2005).

Appendix A. Computer Codes

A. Analysis Macros for BYU Forest Fire Research (VB Applications)

```
Option Explicit 'Dimmed variables
Public rwlast As Long, timign As Double, timbrn As Double, timstp As Double
Public rwign As Long, rwbrn As Long, rwstp As Long, rwinit As Long, t1 As Long, tl As
                            Long
Public emis As Double, ten As Long, rwirlast As Long, irstp As Double, rwirstp As Long
Public rwirignlo As Long, rwirignhi As Long, ntign As Double, b1 As Double, bl As Double
Public rwb1 As Long, rwbl As Long, massinit As Double, tifh As Double, rwfh As Long,
                            rwbl20 As Long
Public rwign1 As Long, rwignl As Long, rwfh1 As Long, rwfhl As Long, rwbrn1 As Long
Public rwbrnl As Long, igntext As String, fhtext As String, brntext As String, dt As
                            Date, rwrun As Long
Public species As String, run As Long, endrow As Long, switchrow As Long, switchrow2 As
                            Long, endrow1 As Long
Public FFBtemp As Double, i As Long, cc As Long, mm As Double, mint As Long, ntbrn As
                            Double
Public ntfh As Double, rwirbrnlo As Long, rwirbrnhi As Long, rwirfhlo As Long, rwirfhhi
                            As Long, rwcopy As Long

Public Sub Macro_Part1()
'Created by Brent M. Pickett - modified by Carl Isackson
'First macro that combines temperature profiles from LabView and the IR Camera
'Must have Labview output file already opened (e.g. Cham 3.xls), the two IR temp profile
                            files (AR0*Max.irp),
'and Reference Sheet - Final.xls.
   species = InputBox("Enter Species (Manz, Oak, Cean, Cham, Maple, etc.).")
   run = InputBox("Enter Run Number.")
   mint = InputBox("Enter number of cells for combined IR temperature profile.")
                            'Number of time frames for small area
   Windows("" & species & " " & run & ".xls").Activate   'Reading input worksheet to
                            collect previously defined values
   ActiveSheet.Select                                          'e.g. time of ignition, time of
                            burnout etc.
   ActiveSheet.Name = "mass"
   dt = Range("A1").Value   'Date of run
   Windows("Reference Sheet - Final.xls").Activate
   Sheets("Macros").Select
   Range("A3").Select
   Do While ActiveCell.Value <> dt Or ActiveCell.Offset(0, 1).Value <> species Or
                            ActiveCell.Offset(0, 2).Value <> run
      ActiveCell.Offset(1, 0).Select  'Finding row of needed data
   Loop
   rwrun = ActiveCell.Row      'Determining row of run (input worksheet "Macros") with
                            corresponding species, date, and run #
   timign = Range("I" & rwrun & "").Value   'Values for analysis (on input worksheet)
   timbrn = Range("K" & rwrun & "").Value
   timstp = Range("H" & rwrun & "").Value
   emis = Range("E" & rwrun & "").Value
   ten = Range("D" & rwrun & "").Value
   irstp = Range("F" & rwrun & "").Value
   FFBtemp = Range("G" & rwrun & "").Value
   Windows("" & species & " " & run & ".xls").Activate  'Going to LabView output file
   Sheets("mass").Range("1:1").Insert
   Range("A1").Value = "Date"     'Setup sheet
   Range("B1").Value = "Time"
   Range("C1").Value = "Labview Time"
   Range("D1").Value = "Labview Temp"
```

```
Range("E1").Value = "Labview Mass"
Range("C2").Select     'Correcting for minute loops - finding final row (rwlast)
Do While ActiveCell.Offset(1, 0).Value <> Empty Or ActiveCell.Offset(2, 0).Value <>
                        Empty
   If ActiveCell.Offset(1, 0).Value < ActiveCell.Value Then
      ActiveCell.Offset(1, 0).Value = ActiveCell.Offset(1, 0).Value + 60
   End If
   ActiveCell.Offset(1, 0).Select
Loop
rwlast = ActiveCell.Row
Range("C2").Select    'Finding Initial, Ignition, Burnout, Stop Times
Do While ActiveCell.Offset(0, 1).Value < 30   'Initial time
   ActiveCell.Offset(1, 0).Select
Loop
rwinit = ActiveCell.Row
Range("C2").Select
Do While ActiveCell.Row <> rwlast
   If ActiveCell.Value > (timign - 0.00001) And ActiveCell.Value < (timign + 0.00001)
                        Then
      rwign = ActiveCell.Row   'Ignition Time
   ElseIf ActiveCell.Value > (timbrn - 0.00001) And ActiveCell.Value < (timbrn +
                        0.00001) Then
      rwbrn = ActiveCell.Row   'Burnout Time
   End If
   ActiveCell.Offset(1, 0).Select
Loop
Range("C2").Select
Do While ActiveCell.Value <> timstp    'Time of burner stop
   ActiveCell.Offset(1, 0).Select
Loop
rwstp = ActiveCell.Row
ActiveCell.Font.ColorIndex = 5
Range("F1").Value = "Mass Fraction"  'Calculating Mass Fraction and Mass Release Rate
Range("G1").Value = "Mass Release Rate"   'This mass release rate is not used - better
                        calculated later
Range("F2").Select
For i = 2 To rwlast
   ActiveCell.FormulaR1C1 = "=RC[-1]/R2C5"
   ActiveCell.Offset(0, 1).FormulaR1C1 = "=(R[1]C[-2]-RC[-2])/(RC[-4]-R[1]C[-4])"
   ActiveCell.Offset(1, 0).Select
Next i
ActiveCell.Offset(-1, 1).Clear
Range("A" & rwinit & ":G" & rwinit & "").Interior.ColorIndex = 10   'Coloring initial,
                        ignition, burnout rows
Range("A" & rwign & ":G" & rwign & "").Interior.ColorIndex = 3
Range("A" & rwbrn & ":G" & rwbrn & "").Interior.ColorIndex = 49
Range("J3:L5").Interior.ColorIndex = 37  'Getting ignition time, temp, burnout
Range("J3").Value = "Time to Ignition"
Range("J4").Value = "Ignition Temperature"
Range("J5").Value = "Flame Duration"
Range("L3").Value = "sec"
Range("L4").Value = "oC"
Range("L5").Value = "sec"
Range("K3").FormulaR1C1 = "=R" & rwign & "C3-R" & rwinit & "C3"   'Putting values for
                        tig, Tig, tfd
Range("K4").FormulaR1C1 = "=R" & rwign & "C4"
Range("K5").FormulaR1C1 = "=R" & rwbrn & "C3-R" & rwign & "C3"
Range("D:D").Insert  'Preparing to normalize time according to burner stopping time
Range("D2").Select
For i = 2 To rwlast
   ActiveCell.FormulaR1C1 = "=RC[-1]-R" & rwstp & "C3"
   ActiveCell.Offset(1, 0).Select
Next i
Range("1:1").Font.Bold = True                         'Formating
Range("1:1").HorizontalAlignment = xlCenter
Range("1:1").VerticalAlignment = xlCenter
Range("1:1").WrapText = True
Range("C:G").ColumnWidth = 8.15
Range("H:H").ColumnWidth = 12
Range("I:I").ColumnWidth = 11.3
Range("K:K").ColumnWidth = 17.3
```

```
t1 = Range("C2").Value                                    'Creating Mass Graph
tl = Range("C" & rwlast & "").Value
Charts.Add
ActiveChart.ChartType = xlXYScatter
ActiveChart.SeriesCollection.NewSeries
ActiveChart.SeriesCollection.NewSeries
ActiveChart.SeriesCollection.NewSeries
ActiveChart.SeriesCollection.NewSeries
ActiveChart.SeriesCollection.NewSeries
ActiveChart.SeriesCollection(1).XValues = "=mass!R2C3:R" & rwlast & "C3"
ActiveChart.SeriesCollection(1).Values = "=mass!R2C6:R" & rwlast & "C6"
ActiveChart.SeriesCollection(1).Name = "=""Mass (g)"""
ActiveChart.SeriesCollection(2).XValues = "=mass!R2C3:R" & rwlast & "C3"
ActiveChart.SeriesCollection(2).Values = "=mass!R2C7:R" & rwlast & "C7"
ActiveChart.SeriesCollection(2).Name = "=""Mass Fraction"""
ActiveChart.SeriesCollection(3).XValues = "=mass!R2C3:R" & rwlast & "C3"
ActiveChart.SeriesCollection(3).Values = "=mass!R2C8:R" & rwlast & "C8"
ActiveChart.SeriesCollection(3).Name = "=""Mass Release (g/s)"""
ActiveChart.SeriesCollection(4).XValues = "=mass!R" & rwign & "C3"
ActiveChart.SeriesCollection(4).Values = "=mass!R" & rwign & "C6"
ActiveChart.SeriesCollection(4).Name = "=""Ignition"""
ActiveChart.SeriesCollection(5).XValues = "=mass!R" & rwbrn & "C3"
ActiveChart.SeriesCollection(5).Values = "=mass!R" & rwbrn & "C6"
ActiveChart.SeriesCollection(5).Name = "=""Burnout"""
ActiveChart.Location Where:=xlLocationAsNewSheet, Name:="Mass Graph"
ActiveChart.ChartArea.Select
ActiveChart.Axes(xlValue).MajorGridlines.Select
Selection.Delete
ActiveChart.PlotArea.Select
Selection.ClearFormats
ActiveChart.SeriesCollection(3).Select
With Selection.Border
   .ColorIndex = 10
   .Weight = xlHairline
   .LineStyle = xlContinuous
End With
With Selection
   .MarkerStyle = xlNone
End With
ActiveChart.SeriesCollection(4).Select
With Selection
   .MarkerBackgroundColorIndex = 3
   .MarkerForegroundColorIndex = 3
   .MarkerStyle = xlDiamond
   .Smooth = False
   .MarkerSize = 10
   .Shadow = False
End With
ActiveChart.SeriesCollection(5).Select
With Selection
   .MarkerBackgroundColorIndex = 4
   .MarkerForegroundColorIndex = 4
   .MarkerStyle = xlDiamond
   .Smooth = False
   .MarkerSize = 10
   .Shadow = False
End With
ActiveChart.Axes(xlCategory).Select
With ActiveChart.Axes(xlCategory)
   .MinimumScale = t1
   .MaximumScaleIsAuto = tl
   .MinorUnitIsAuto = 0.5
   .MajorUnitIsAuto = 2
End With                                                  'Obtaining temperature profile
                          from IR camera
Windows("AR01Max.irp").Activate       'Smaller Area on Sample (must be AR01Max.irp)
Rows("1:1").Delete Shift:=xlUp
Windows("AR02Max.irp").Activate       'Larger Area on Sample (must be AR02Max.irp)
Rows("1:1").Delete Shift:=xlUp
Columns("A:A").Copy                     'Copying, AR01Max is the smaller area and will
                          be the main sheet'
```

```
Windows("AR01Max.irp").Activate
Range("O1").Select
ActiveSheet.Paste
Do While ActiveCell.Offset(1, 0).Value <> Empty Or ActiveCell.Offset(2, 0).Value <>
                          Empty
   ActiveCell.Offset(1, 0).Select
Loop
endrow = ActiveCell.Row
Range("P1").Select
ActiveCell.FormulaR1C1 = "=RC[-1]-273.15"    'Converting to oC
Selection.AutoFill Destination:=Range("P1:P" & endrow & "")
Range("C:C,E:E,F:F").Delete Shift:=xlToLeft
Range("F1").FormulaR1C1 = "=ROUNDDOWN(RC[-4],-1)"
Range("F1").Offset(0, 1).Value = ten     'Needed to convert AR*.irp output to actual
                          time
Range("E1").Select
ActiveCell.FormulaR1C1 = "=RC[-4]-273.15"   'Converting to oC
Selection.AutoFill Destination:=Range("E1:E" & endrow & "")
Range("D1").Select
ActiveCell.FormulaR1C1 = "=RC[-2]-R1C6+R1C7"
Selection.AutoFill Destination:=Range("D1:D" & endrow & "")
Range("M1").Select
Do While ActiveCell.Value < FFBtemp   'FFBtemp is defined from input worksheet
   ActiveCell.Offset(1, 0).Select     'Defined as the temperature of the FFB initially
                          from the IR camera
Loop
switchrow = ActiveCell.Row            'This is where the two AR profiles will switch.
Range("R1").Select                       'Initially it will start on the smaller area,
                          then transition to the larger area.
mm = 0
Do While ActiveCell.Row <> endrow + 1        'Transitioning between small area profile
                          to large area profile
   If ActiveCell.Row < switchrow Then
      ActiveCell.FormulaR1C1 = "=RC[-13]"
   ElseIf ActiveCell.Row >= switchrow And ActiveCell.Row < (switchrow + mint) Then
      mm = mm + (1 / mint)
      ActiveCell.FormulaR1C1 = "=(1-" & mm & ")*RC[-13]+" & mm & "*RC[-5]"
   ElseIf ActiveCell.Row >= switchrow + mint Then
      ActiveCell.FormulaR1C1 = "=RC[-5]"
   End If
   ActiveCell.Offset(1, 0).Select
Loop
Range("A:R").Select                                    'Formatting
Selection.Copy
Selection.PasteSpecial Paste:=xlPasteValues, Operation:=xlNone, SkipBlanks _
   :=False, Transpose:=False
Rows("1:1").Insert Shift:=xlDown
Range("D1").Value = "IR Time"
Range("E1").Value = "Small Area IR Temp"
Range("M1").Value = "Large Area Temp"
Range("R1").Value = "IR Temp Emis=" & emis
Columns("A:B").Delete Shift:=xlToLeft
Columns("A:A").NumberFormat = "m/d/yy h:mm;@"
Range("B1,P1").Font.Bold = True
Range("B1,P1").HorizontalAlignment = xlCenter
Range("B1,P1").VerticalAlignment = xlCenter
Range("B1,P1").WrapText = True
Range("B:B").ColumnWidth = 6.6
Range("P:P").ColumnWidth = 9.35
Range("B:B,P:P").Copy
Windows("" & species & " " & run & ".xls").Activate
Sheets("mass").Select
Range("I1").Select
Selection.PasteSpecial Paste:=xlPasteValues, Operation:=xlNone, SkipBlanks _
   :=False, Transpose:=False               'Pasting IR time and Temp to LabView File
Range("I:I").ColumnWidth = 6.6
Range("J:J").ColumnWidth = 9.35
rwirlast = endrow + 1                                  'Combine Labview output with IR
                          temperature profile
Range("I2").Select
Do While ActiveCell.Value < (irstp - 0.00001) Or ActiveCell.Value > (irstp + 0.00001)
```

```
   ActiveCell.Offset(1, 0).Select   'IR burner stopping time
Loop
rwirstp = ActiveCell.Row
Selection.Font.ColorIndex = 5
Range("J:J").Insert
Range("J2").Select
Selection.FormulaR1C1 = "=RC[-1]-R" & rwirstp & "C9"      'Normalizing IR time to
                        stopping point
Selection.AutoFill Destination:=Range("J2:J" & rwirlast & "")
Range("E:E,K:K").Insert
Range("E2").Select
Selection.FormulaR1C1 = "=RC[-1]-min(R2C4,R2C11)"     'Normalizing time for Labview
Selection.AutoFill Destination:=Range("E2:E" & rwlast & "")
Range("L2").Select
Selection.FormulaR1C1 = "=RC[-1]-min(R2C4,R2C11)"     'Normalizing time for IR
Selection.AutoFill Destination:=Range("L2:L" & rwirlast & "")
Range("E1").Value = "Lab NTime"                    'Format
Range("L1").Value = "IR NTime"
Range("E:E,L:L").ColumnWidth = 6.6
Range("1:1").RowHeight = 27.75
Range("D:D,K:K").EntireColumn.Hidden = True
Range("N7").Value = "Initial Time"
Range("N7").Interior.ColorIndex = 10
Range("N8").Value = "Ignition Time"
Range("N8").Interior.ColorIndex = 3
Range("N9").Value = "Flame Height Time"
Range("N9").Interior.ColorIndex = 26
Range("N10").Value = "Burnout Time"
Range("N10").Interior.ColorIndex = 49
Charts.Add                        'Creates a Temperature graph with the normalized time
                        with the IR and Labview Profiles
ActiveChart.ChartType = xlXYScatter
ActiveChart.SeriesCollection.NewSeries
ActiveChart.SeriesCollection.NewSeries
ActiveChart.SeriesCollection(1).Name = "=mass!R1C13"
ActiveChart.SeriesCollection(1).XValues = "=mass!R2C12:R" & rwirlast & "C12"
ActiveChart.SeriesCollection(1).Values = "=mass!R2C13:R" & rwirlast & "C13"
ActiveChart.SeriesCollection(2).Name = "=mass!R1C6"
ActiveChart.SeriesCollection(2).XValues = "=mass!R2C5:R" & rwlast & "C5"
ActiveChart.SeriesCollection(2).Values = "=mass!R2C6:R" & rwlast & "C6"
ActiveChart.SeriesCollection(3).Name = "Ignition"
ActiveChart.SeriesCollection(3).XValues = "=mass!R" & rwign & "C5"
ActiveChart.SeriesCollection(3).Values = "=mass!R" & rwign & "C6"
ActiveChart.Location Where:=xlLocationAsNewSheet, Name:="Temp Combo"
With ActiveChart
   .HasTitle = True
   .ChartTitle.Characters.Text = "Temperature Profiles"
   .Axes(xlCategory, xlPrimary).HasTitle = True
   .Axes(xlCategory, xlPrimary).AxisTitle.Characters.Text = "Time (s)"
   .Axes(xlValue, xlPrimary).HasTitle = True
   .Axes(xlValue, xlPrimary).AxisTitle.Characters.Text = "Temperature (ºC)"
   With ActiveChart.Axes(xlCategory)
      .HasMajorGridlines = False
      .HasMinorGridlines = False
   End With
   With ActiveChart.Axes(xlValue)
      .HasMajorGridlines = False
      .HasMinorGridlines = False
   End With
   ActiveChart.PlotArea.Select
   With Selection.Border
      .ColorIndex = 16
      .Weight = xlThin
      .LineStyle = xlContinuous
   End With
   Selection.Interior.ColorIndex = xlNone
   ActiveChart.SeriesCollection(3).Select
   With Selection
      .MarkerBackgroundColorIndex = 3
      .MarkerForegroundColorIndex = 3
      .MarkerStyle = xlDiamond
```

```
         .Smooth = False
         .MarkerSize = 10
         .Shadow = False
      End With
   End With
   Sheets("mass").Select          'Calculates the average ignition temperature from both
                              the Labview and IR profiles
   Range("L2").Select
   ntign = Sheets("mass").Cells(rwign, 5).Value
   Do While ActiveCell.Offset(1, 0).Value <= ntign
      ActiveCell.Offset(1, 0).Select
   Loop
   rwirignlo = ActiveCell.Row
   rwirignhi = rwirignlo + 1
   ActiveCell.Interior.ColorIndex = 3
   ActiveCell.Offset(1, 0).Interior.ColorIndex = 3
   ActiveCell.Offset(0, 1).Interior.ColorIndex = 3
   ActiveCell.Offset(1, 1).Interior.ColorIndex = 3
   ntbrn = Sheets("mass").Cells(rwbrn, 5).Value
   Do While ActiveCell.Offset(1, 0).Value <= ntbrn
      ActiveCell.Offset(1, 0).Select
   Loop
   rwirbrnlo = ActiveCell.Row
   rwirbrnhi = rwirbrnlo + 1
   ActiveCell.Interior.ColorIndex = 49
   ActiveCell.Offset(1, 0).Interior.ColorIndex = 49
   ActiveCell.Offset(0, 1).Interior.ColorIndex = 49
   ActiveCell.Offset(1,             1).Interior.ColorIndex             =             49
                              'Interpolates for IR Temp at ignition
   Range("Q6").FormulaR1C1  =  "=R"  &  rwirignlo  &  "C13+(R"  &  rwirignhi  &  "C13-R"  &
                              rwirignlo  &  "C13)  *  (R"  &  rwign  &  "C5-R"  &  rwirignlo  &
                              "C12)/(R" & rwirignhi & "C12-R" & rwirignlo & "C12)"
   Range("Q5").Value = "Ign Temp IR"
   Range("Q4").FormulaR1C1 = "=average(R6C17,R4C15)"
   Range("Q3").Value = "Ave Temp IR_Lab"                          'After mass graph is
                              created, need to obtain buoyancy values
   MsgBox ("Check buoyancy effects and enter into reference sheet.")     'and enter them
                              into the input values worksheet.
End Sub

Public Sub Macro_Part2()
'Created by Brent M. Pickett - modified by Carl Isackson
'Second part of macros - compensate for buoyancy and determines release rates (mass, TTC,
                              TIR)
   Windows("Reference Sheet - Final.xls").Activate
   Sheets("Macros").Select             'Reading values from input worksheet
   b1 = Range("N" & rwrun & "").Value      'Buoyancy values (times)
   bl = Range("O" & rwrun & "").Value
   massinit = Range("L" & rwrun & "").Value
   tifh  =  Range("J"  &  rwrun  &  "").Value      'Flame  Height  Time  -  can  be  easier  to
                              determine after first macro is run
   Windows("" & species & " " & run & ".xls").Activate                          'not
                              essential though
   Sheets("mass").Select
   Range("C2").Select
   Do While ActiveCell.Row <> rwlast
      If ActiveCell.Value = b1 Then
         If b1 = bl Then
            rwb1  =  ActiveCell.Row:  rwbl  =  rwb1:  ActiveCell.Font.Bold  =  True     'First
                              buoyancy frame
            rwbl20 = rwbl + 20
         Else
            rwb1 = ActiveCell.Row: ActiveCell.Font.Bold = True    'Last buoyancy frame
         End If
      ElseIf ActiveCell.Value = bl Then
         rwbl = ActiveCell.Row: ActiveCell.Font.Bold = True
         rwbl20 = rwbl + 20       'About 1 second after buoyancy is observed (20 frames)
      ElseIf ActiveCell.Value = tifh Then
         rwfh = ActiveCell.Row: ActiveCell.Interior.ColorIndex = 26
      End If
      ActiveCell.Offset(1, 0).Select
```

```
Loop
ntfh = Sheets("mass").Cells(rwfh, 5).Value     'Indicating Flame Height on normalized
                          IR Time
Range("L2").Select
Do While ActiveCell.Offset(1, 0).Value <= ntfh
   ActiveCell.Offset(1, 0).Select
Loop
rwirfhlo = ActiveCell.Row
rwirfhhi = rwirfhlo + 1
ActiveCell.Interior.ColorIndex = 26
ActiveCell.Offset(1, 0).Interior.ColorIndex = 26
ActiveCell.Offset(0, 1).Interior.ColorIndex = 26
ActiveCell.Offset(1, 1).Interior.ColorIndex = 26
Range("H:H").Insert                                    'Normalizing mass - adjusting for
                          buoyancy
Range("H1").Value = "Norm Mass"
Range("P8").Value = "Buoy Slope"      'Linear slope of "downstream" mass - 20 frames
                          after last buoyancy
Range("P9").FormulaR1C1 = "=slope(R" & rwbl & "C7:R" & rwbl20 & "C7,R" & rwbl & "C5:R"
                          & rwbl20 & "C5)"
Range("H2").Select
If b1 = bl Then
   For i = 2 To rwlast
      ActiveCell.FormulaR1C1 = "=RC[-1]"
      ActiveCell.Offset(1, 0).Select
   Next i
Else
   For i = 2 To rwb1
      ActiveCell.FormulaR1C1 = "=RC[-1]"
      ActiveCell.Offset(1, 0).Select
   Next i
   For i = rwb1 + 1 To rwbl   'During buoyancy region - uses slope of "downstream"
      ActiveCell.FormulaR1C1 = "=R" & rwb1 & "C8+(R9C16*(RC[-3]-R" & rwb1 & "C5))"
      ActiveCell.Offset(1, 0).Select
   Next i
   For i = rwbl + 1 To rwlast    'Adjusting the "downstream" mass
      ActiveCell.FormulaR1C1 = "=RC[-1]+(R" & rwb1 & "C7-R" & rwbl & "C7)-(R" & rwb1 &
                          "C8-R" & rwbl & "C8)"
      ActiveCell.Offset(1, 0).Select
   Next i
End If
Range("O11").Value = "Initial Mass"
Range("O12").Value = massinit
Range("O13").Value = "Lab_Init Error"
Range("O14").FormulaR1C1 = "=(R12C15-R2C8)/R12C15"    'Difference in LabView mass to
                          Initial measured mass
Range("P13").Value = "Rel Ign"
Range("Q13").Value = "Rel Burn"
Range("R13").Value = "Rel FH"
Range("P14").FormulaR1C1 = "=(R2C8-R" & rwign & "C8)/R2C8"     'Percent released at
                          ignition
Range("Q14").FormulaR1C1 = "=(R2C8-R" & rwbrn & "C8)/R2C8"     'Percent released at
                          burnout
Range("R14").FormulaR1C1 = "=(R2C8-R" & rwfh & "C8)/R2C8"      'Percent released at
                          flame height
Range("O14:R14").NumberFormat = "0.00%"
Sheets("Mass Graph").Select                             'Adding corrected mass to mass
                          graph
ActiveChart.PlotArea.Select
ActiveChart.SeriesCollection.NewSeries
ActiveChart.SeriesCollection.NewSeries
ActiveChart.SeriesCollection(6).XValues = "=mass!R2C3:R" & rwlast & "C3"
ActiveChart.SeriesCollection(6).Values = "=mass!R2C8:R" & rwlast & "C8"
ActiveChart.SeriesCollection(6).Name = "=""Norm Mass (g)"""
ActiveChart.SeriesCollection(7).XValues = "=mass!R" & rwfh & "C3"
ActiveChart.SeriesCollection(7).Values = "=mass!R" & rwfh & "C7"
ActiveChart.SeriesCollection(7).Name = "=""Flame Height"""
ActiveChart.SeriesCollection(7).Select
With Selection
   .MarkerBackgroundColorIndex = 6
   .MarkerForegroundColorIndex = 6
```

```
   .MarkerStyle = xlDiamond
   .Smooth = False
   .MarkerSize = 10
   .Shadow = False
End With
Sheets.Add.Name = "MassRelease"              'Determining Mass Release Rate (dm/dt)
Sheets("mass").Select                        'uses cubic regression function "cubic()"
Range("C:C,E:E,H:H").Select
Selection.Copy                         'Copying needed values to new sheet
Sheets("MassRelease").Select
Range("A1").Select
ActiveSheet.Paste
Range("D2").Select                     'Raw dm/dt data
Selection.FormulaR1C1 = "=(RC[-1]-R[1]C[-1])/(RC[-2]-R[1]C[-2])"
Selection.AutoFill Destination:=Range("D2:D" & rwlast - 1 & "")
Range("E2").Select
For i = 2 To 26   'Available frames                  'Moving Cubic fit for dm/dt
   ActiveCell.FormulaR1C1 = "=PERSONAL.XLS!cubic(R2C2:R" & i + 25 & "C2,R2C3:R" & i +
                            25 & "C3,3)"  '3rd order
   ActiveCell.Offset(0,  1).FormulaR1C1  =  "=PERSONAL.XLS!cubic(R2C2:R"  &  i  +  25  &
                            "C2,R2C3:R" & i + 25 & "C3,2)" '2nd order
   ActiveCell.Offset(0,  2).FormulaR1C1  =  "=PERSONAL.XLS!cubic(R2C2:R"  &  i  +  25  &
                            "C2,R2C3:R" & i + 25 & "C3,1)" '1st order
   ActiveCell.Offset(0,  3).FormulaR1C1  =  "=3*RC[-3]*RC[-6]^2+2*RC[-2]*RC[-6]+RC[-1]"
                            'dm/dt
   ActiveCell.Offset(1, 0).Select
Next i
For i = 27 To rwlast - 25
   ActiveCell.FormulaR1C1  =  "=PERSONAL.XLS!cubic(R" & i - 25 & "C2:R" & i + 25 &
                            "C2,R" & i - 25 & "C3:R" & i + 25 & "C3,3)"
   ActiveCell.Offset(0, 1).FormulaR1C1 = "=PERSONAL.XLS!cubic(R" & i - 25 & "C2:R" & i
                            + 25 & "C2,R" & i - 25 & "C3:R" & i + 25 & "C3,2)"
   ActiveCell.Offset(0, 2).FormulaR1C1 = "=PERSONAL.XLS!cubic(R" & i - 25 & "C2:R" & i
                            + 25 & "C2,R" & i - 25 & "C3:R" & i + 25 & "C3,1)"
   ActiveCell.Offset(0, 3).FormulaR1C1 = "=3*RC[-3]*RC[-6]^2+2*RC[-2]*RC[-6]+RC[-1]"
   ActiveCell.Offset(1, 0).Select
Next i
For i = rwlast - 24 To rwlast
   ActiveCell.FormulaR1C1  =  "=PERSONAL.XLS!cubic(R"  &  i  -  25  &  "C2:R"  &  rwlast  &
                            "C2,R" & i - 25 & "C3:R" & rwlast & "C3,3)"
   ActiveCell.Offset(0,  1).FormulaR1C1 = "=PERSONAL.XLS!cubic(R" & i - 25 & "C2:R" &
                            rwlast & "C2,R" & i - 25 & "C3:R" & rwlast & "C3,2)"
   ActiveCell.Offset(0,  2).FormulaR1C1 = "=PERSONAL.XLS!cubic(R" & i - 25 & "C2:R" &
                            rwlast & "C2,R" & i - 25 & "C3:R" & rwlast & "C3,1)"
   ActiveCell.Offset(0, 3).FormulaR1C1 = "=3*RC[-3]*RC[-6]^2+2*RC[-2]*RC[-6]+RC[-1]"
   ActiveCell.Offset(1, 0).Select
Next i
Range("D1").Value = "Raw dm/dt"    'Formatting
Range("E1").Value = "a3"
Range("F1").Value = "a2"
Range("G1").Value = "a1"
Range("H1").Value = "Fit dm/dt"
Range("J1").Value = "Ignition"
Range("K1").Value = "Flame Height"
Range("L1").Value = "Burnout"
Range("1:1").Select
Selection.Font.Bold = True
Selection.HorizontalAlignment = xlCenter
Selection.VerticalAlignment = xlCenter
Selection.WrapText = True
Range("J2").FormulaR1C1 = "=R" & rwign & "C8"
Range("K2").FormulaR1C1 = "=R" & rwfh & "C8"
Range("L2").FormulaR1C1 = "=R" & rwbrn & "C8"
Charts.Add                        'Creating graph for mass release rate and moving cubic
                            regression fit.
ActiveChart.ChartType = xlXYScatter
ActiveChart.SeriesCollection.NewSeries
ActiveChart.SeriesCollection.NewSeries
ActiveChart.SeriesCollection.NewSeries
ActiveChart.SeriesCollection(1).XValues = "=MassRelease!R2C2:R" & rwlast - 1 & "C2"
ActiveChart.SeriesCollection(1).Values = "=MassRelease!R2C4:R" & rwlast - 1 & "C4"
```

```
ActiveChart.SeriesCollection(1).Name = "Raw dm/dt"
ActiveChart.SeriesCollection(2).XValues = "=MassRelease!R2C2:R" & rwlast & "C2"
ActiveChart.SeriesCollection(2).Values = "=MassRelease!R2C8:R" & rwlast & "C8"
ActiveChart.SeriesCollection(2).Name = "Fit dm/dt"
ActiveChart.SeriesCollection(3).XValues     =     "=MassRelease!R"     &     rwign     &
                          "C2,MassRelease!R"  &  rwfh  &  "C2,MassRelease!R"  &  rwbrn  &
                          "C2"
ActiveChart.SeriesCollection(3).Values = "=MassRelease!R" & rwign & "C8,MassRelease!R"
                          & rwfh & "C8,MassRelease!R" & rwbrn & "C8"
ActiveChart.SeriesCollection(3).Name = "Ign,FH,Burn"
ActiveChart.Location Where:=xlLocationAsObject, Name:="MassRelease"
ActiveChart.PlotArea.Select
Selection.ClearFormats
ActiveChart.Axes(xlValue).MajorGridlines.Select
Selection.Delete
ActiveChart.SeriesCollection(2).Border.LineStyle = xlContinuous
ActiveChart.SeriesCollection(2).MarkerStyle = xlNone
ActiveChart.SeriesCollection(3).MarkerBackgroundColorIndex = 10
ActiveChart.SeriesCollection(3).MarkerForegroundColorIndex = 10
ActiveChart.SeriesCollection(3).MarkerSize = 8
ActiveChart.Axes(xlValue).Select
With ActiveChart
   .Axes(xlCategory, xlPrimary).HasTitle = True
   .Axes(xlCategory, xlPrimary).AxisTitle.Characters.Text = "time (s)"
   .Axes(xlValue, xlPrimary).HasTitle = True
   .Axes(xlValue, xlPrimary).AxisTitle.Characters.Text = "mass release rate (g/s)"
End With
Sheets.Add.Name  =  "HR_TC"                                  'HeatRelease  for  Thermocouple
                          Temperature
Sheets("mass").Select
Range("C:C,E:E,F:F").Select
Selection.Copy
Sheets("HR_TC").Select
Range("A1").Select
ActiveSheet.Paste
Range("D2").Select                'Raw dT/dt data
Selection.FormulaR1C1 = "=(RC[-1]-R[1]C[-1])/(RC[-2]-R[1]C[-2])"
Selection.AutoFill Destination:=Range("D2:D" & rwlast - 1 & "")
Range("E2").Select
For i = 2 To 26 'Available frames              'Moving Cubic fit for dT/dt
   ActiveCell.FormulaR1C1 = "=PERSONAL.XLS!cubic(R2C2:R" & i + 25 & "C2,R2C3:R" & i +
                          25 & "C3,3)" '3rd order
   ActiveCell.Offset(0,  1).FormulaR1C1  =  "=PERSONAL.XLS!cubic(R2C2:R"  &  i  +  25  &
                          "C2,R2C3:R" & i + 25 & "C3,2)" '2nd order
   ActiveCell.Offset(0,  2).FormulaR1C1  =  "=PERSONAL.XLS!cubic(R2C2:R"  &  i  +  25  &
                          "C2,R2C3:R" & i + 25 & "C3,1)" '1st order
   ActiveCell.Offset(0,  3).FormulaR1C1  =  "=3*RC[-3]*RC[-6]^2+2*RC[-2]*RC[-6]+RC[-1]"
                          'dT/dt
   ActiveCell.Offset(1, 0).Select
Next i
For i = 27 To rwlast - 25
   ActiveCell.FormulaR1C1  =  "=PERSONAL.XLS!cubic(R"  &  i  -  25  &  "C2:R"  &  i  +  25  &
                          "C2,R" & i - 25 & "C3:R" & i + 25 & "C3,3)"
   ActiveCell.Offset(0, 1).FormulaR1C1 = "=PERSONAL.XLS!cubic(R" & i - 25 & "C2:R" & i
                          + 25 & "C2,R" & i - 25 & "C3:R" & i + 25 & "C3,2)"
   ActiveCell.Offset(0, 2).FormulaR1C1 = "=PERSONAL.XLS!cubic(R" & i - 25 & "C2:R" & i
                          + 25 & "C2,R" & i - 25 & "C3:R" & i + 25 & "C3,1)"
   ActiveCell.Offset(0, 3).FormulaR1C1 = "=3*RC[-3]*RC[-6]^2+2*RC[-2]*RC[-6]+RC[-1]"
   ActiveCell.Offset(1, 0).Select
Next i
For i = rwlast - 24 To rwlast
   ActiveCell.FormulaR1C1  =  "=PERSONAL.XLS!cubic(R"  &  i  -  25  &  "C2:R"  &  rwlast  &
                          "C2,R" & i - 25 & "C3:R" & rwlast & "C3,3)"
   ActiveCell.Offset(0,  1).FormulaR1C1 = "=PERSONAL.XLS!cubic(R" & i - 25 & "C2:R" &
                          rwlast & "C2,R" & i - 25 & "C3:R" & rwlast & "C3,2)"
   ActiveCell.Offset(0,  2).FormulaR1C1 = "=PERSONAL.XLS!cubic(R" & i - 25 & "C2:R" &
                          rwlast & "C2,R" & i - 25 & "C3:R" & rwlast & "C3,1)"
   ActiveCell.Offset(0, 3).FormulaR1C1 = "=3*RC[-3]*RC[-6]^2+2*RC[-2]*RC[-6]+RC[-1]"
   ActiveCell.Offset(1, 0).Select
Next i
Range("D1").Value = "Raw dT/dt"    'Formatting
```

```
Range("E1").Value = "a3"
Range("F1").Value = "a2"
Range("G1").Value = "a1"
Range("H1").Value = "Fit dT/dt"
Range("J1").Value = "Ignition"
Range("K1").Value = "Flame Height"
Range("L1").Value = "Burnout"
Range("1:1").Select
Selection.Font.Bold = True
Selection.HorizontalAlignment = xlCenter
Selection.VerticalAlignment = xlCenter
Selection.WrapText = True
Range("J2").FormulaR1C1 = "=R" & rwign & "C8"
Range("K2").FormulaR1C1 = "=R" & rwfh & "C8"
Range("L2").FormulaR1C1 = "=R" & rwbrn & "C8"
Charts.Add                    'Creating graph for heating rate from thermocouple and
                              moving cubic regression fit.
ActiveChart.ChartType = xlXYScatter
ActiveChart.SeriesCollection.NewSeries
ActiveChart.SeriesCollection.NewSeries
ActiveChart.SeriesCollection.NewSeries
ActiveChart.SeriesCollection(1).XValues = "=HR_TC!R2C2:R" & rwlast - 1 & "C2"
ActiveChart.SeriesCollection(1).Values = "=HR_TC!R2C4:R" & rwlast - 1 & "C4"
ActiveChart.SeriesCollection(1).Name = "Raw dT/dt"
ActiveChart.SeriesCollection(2).XValues = "=HR_TC!R2C2:R" & rwlast & "C2"
ActiveChart.SeriesCollection(2).Values = "=HR_TC!R2C8:R" & rwlast & "C8"
ActiveChart.SeriesCollection(2).Name = "Fit dT/dt"
ActiveChart.SeriesCollection(3).XValues = "=HR_TC!R" & rwign & "C2,HR_TC!R" & rwfh &
                              "C2,HR_TC!R" & rwbrn & "C2"
ActiveChart.SeriesCollection(3).Values = "=HR_TC!R" & rwign & "C8,HR_TC!R" & rwfh &
                              "C8,HR_TC!R" & rwbrn & "C8"
ActiveChart.SeriesCollection(3).Name = "Ign,FH,Burn"
ActiveChart.Location Where:=xlLocationAsObject, Name:="HR_TC"
ActiveChart.PlotArea.Select
Selection.ClearFormats
ActiveChart.Axes(xlValue).MajorGridlines.Select
Selection.Delete
ActiveChart.SeriesCollection(2).Border.LineStyle = xlContinuous
ActiveChart.SeriesCollection(2).MarkerStyle = xlNone
ActiveChart.SeriesCollection(3).MarkerBackgroundColorIndex = 10
ActiveChart.SeriesCollection(3).MarkerForegroundColorIndex = 10
ActiveChart.SeriesCollection(3).MarkerSize = 8
ActiveChart.Axes(xlValue).Select
With ActiveChart
   .Axes(xlCategory, xlPrimary).HasTitle = True
   .Axes(xlCategory, xlPrimary).AxisTitle.Characters.Text = "time (s)"
   .Axes(xlValue, xlPrimary).HasTitle = True
   .Axes(xlValue, xlPrimary).AxisTitle.Characters.Text = "heat release rate (K/s)"
End With
Sheets.Add.Name = "HR_IR"               'Heat Release for IR Temperature Profile
Sheets("mass").Select
Range("K:K,M:M,N:N").Select
Selection.Copy
Sheets("HR_IR").Select
Range("A1").Select
ActiveSheet.Paste
Range("D2").Select                'Raw dT/dt data
Selection.FormulaR1C1 = "=(RC[-1]-R[1]C[-1])/(RC[-2]-R[1]C[-2])"
Selection.AutoFill Destination:=Range("D2:D" & rwirlast - 1 & "")
Range("E2").Select
For i = 2 To 26 'Available frames              'Moving Cubic fit for dT/dt
   ActiveCell.FormulaR1C1 = "=PERSONAL.XLS!cubic(R2C2:R" & i + 25 & "C2,R2C3:R" & i +
                              25 & "C3,3)" '3rd order
   ActiveCell.Offset(0,  1).FormulaR1C1  =  "=PERSONAL.XLS!cubic(R2C2:R"  &  i  +  25  &
                              "C2,R2C3:R" & i + 25 & "C3,2)" '2nd order
   ActiveCell.Offset(0,  2).FormulaR1C1  =  "=PERSONAL.XLS!cubic(R2C2:R"  &  i  +  25  &
                              "C2,R2C3:R" & i + 25 & "C3,1)" '1st order
   ActiveCell.Offset(0,  3).FormulaR1C1  =  "=3*RC[-3]*RC[-6]^2+2*RC[-2]*RC[-6]+RC[-1]"
                              'dT/dt
   ActiveCell.Offset(1, 0).Select
Next i
```

```
For i = 27 To rwirlast - 25
   ActiveCell.FormulaR1C1 = "=PERSONAL.XLS!cubic(R" & i - 25 & "C2:R" & i + 25 &
                            "C2,R" & i - 25 & "C3:R" & i + 25 & "C3,3)"
   ActiveCell.Offset(0, 1).FormulaR1C1 = "=PERSONAL.XLS!cubic(R" & i - 25 & "C2:R" & i
                            + 25 & "C2,R" & i - 25 & "C3:R" & i + 25 & "C3,2)"
   ActiveCell.Offset(0, 2).FormulaR1C1 = "=PERSONAL.XLS!cubic(R" & i - 25 & "C2:R" & i
                            + 25 & "C2,R" & i - 25 & "C3:R" & i + 25 & "C3,1)"
   ActiveCell.Offset(0, 3).FormulaR1C1 = "=3*RC[-3]*RC[-6]^2+2*RC[-2]*RC[-6]+RC[-1]"
   ActiveCell.Offset(1, 0).Select
Next i
For i = rwirlast - 24 To rwirlast
   ActiveCell.FormulaR1C1 = "=PERSONAL.XLS!cubic(R" & i - 25 & "C2:R" & rwirlast &
                            "C2,R" & i - 25 & "C3:R" & rwirlast & "C3,3)"
   ActiveCell.Offset(0, 1).FormulaR1C1 = "=PERSONAL.XLS!cubic(R" & i - 25 & "C2:R" &
                            rwirlast & "C2,R" & i - 25 & "C3:R" & rwirlast & "C3,2)"
   ActiveCell.Offset(0, 2).FormulaR1C1 = "=PERSONAL.XLS!cubic(R" & i - 25 & "C2:R" &
                            rwirlast & "C2,R" & i - 25 & "C3:R" & rwirlast & "C3,1)"
   ActiveCell.Offset(0, 3).FormulaR1C1 = "=3*RC[-3]*RC[-6]^2+2*RC[-2]*RC[-6]+RC[-1]"
   ActiveCell.Offset(1, 0).Select
Next i
Range("D1").Value = "Raw dT/dt"   'Formatting
Range("E1").Value = "a3"
Range("F1").Value = "a2"
Range("G1").Value = "a1"
Range("H1").Value = "Fit dT/dt"
Range("J1").Value = "Ignition"
Range("K1").Value = "Flame Height"
Range("L1").Value = "Burnout"
Range("1:1").Select
Selection.Font.Bold = True
Selection.HorizontalAlignment = xlCenter
Selection.VerticalAlignment = xlCenter
Selection.WrapText = True
Range("J2").FormulaR1C1 = "=R" & rwirignlo & "C8+((" & ntign & "-R" & rwirignlo &
                          "C2)/(R" & rwirignhi & "C2-R" & rwirignlo & "C2))*(R" &
                          rwirignhi & "C8-R" & rwirignlo & "C8)"
Range("K2").FormulaR1C1 = "=R" & rwirfhlo & "C8+((" & ntfh & "-R" & rwirfhlo &
                          "C2)/(R" & rwirfhhi & "C2-R" & rwirfhlo & "C2))*(R" &
                          rwirfhhi & "C8-R" & rwirfhlo & "C8)"
Range("L2").FormulaR1C1 = "=R" & rwirbrnlo & "C8+((" & ntbrn & "-R" & rwirbrnlo &
                          "C2)/(R" & rwirbrnhi & "C2-R" & rwirbrnlo & "C2))*(R" &
                          rwirbrnhi & "C8-R" & rwirbrnlo & "C8)"
Charts.Add     'Creating graph for heating rate from IR camera and moving cubic
                          regression fit.
ActiveChart.ChartType = xlXYScatter
ActiveChart.SeriesCollection.NewSeries
ActiveChart.SeriesCollection.NewSeries
ActiveChart.SeriesCollection.NewSeries
ActiveChart.SeriesCollection(1).XValues = "=HR_IR!R2C2:R" & rwirlast - 1 & "C2"
ActiveChart.SeriesCollection(1).Values = "=HR_IR!R2C4:R" & rwirlast - 1 & "C4"
ActiveChart.SeriesCollection(1).Name = "Raw dT/dt"
ActiveChart.SeriesCollection(2).XValues = "=HR_IR!R2C2:R" & rwirlast & "C2"
ActiveChart.SeriesCollection(2).Values = "=HR_IR!R2C8:R" & rwirlast & "C8"
ActiveChart.SeriesCollection(2).Name = "Fit dT/dt"
ActiveChart.SeriesCollection(3).XValues = "=HR_IR!R" & rwirignlo & "C2,HR_IR!R" &
                          rwirfhlo & "C2,HR_IR!R" & rwirbrnlo & "C2"
ActiveChart.SeriesCollection(3).Values = "=HR_IR!R" & rwirignlo & "C8,HR_IR!R" &
                          rwirfhlo & "C8,HR_IR!R" & rwirbrnlo & "C8"
ActiveChart.SeriesCollection(3).Name = "Ign,FH,Burn"
ActiveChart.Location Where:=xlLocationAsObject, Name:="HR_IR"
ActiveChart.PlotArea.Select
Selection.ClearFormats
ActiveChart.Axes(xlValue).MajorGridlines.Select
Selection.Delete
ActiveChart.SeriesCollection(2).Border.LineStyle = xlContinuous
ActiveChart.SeriesCollection(2).MarkerStyle = xlNone
ActiveChart.SeriesCollection(3).MarkerBackgroundColorIndex = 10
ActiveChart.SeriesCollection(3).MarkerForegroundColorIndex = 10
ActiveChart.SeriesCollection(3).MarkerSize = 8
ActiveChart.Axes(xlValue).Select
With ActiveChart
```

```
   .Axes(xlCategory, xlPrimary).HasTitle = True
   .Axes(xlCategory, xlPrimary).AxisTitle.Characters.Text = "time (s)"
   .Axes(xlValue, xlPrimary).HasTitle = True
   .Axes(xlValue, xlPrimary).AxisTitle.Characters.Text = "heat release rate (K/s)"
End With
Sheets("mass").Select      'Getting temperature values (ig, FH, brn) for thermocouple
                           and IR Camera
Range("P19").Value = "Tig_TC"
Range("Q19").Value = "Tig_IR"
Range("R19").Value = "Tfh_TC"
Range("S19").Value = "Tfh_IR"
Range("T19").Value = "Tbrn_TC"
Range("U19").Value = "Tbrn_IR"
Range("P20").FormulaR1C1 = "=R" & rwign & "C6"
Range("R20").FormulaR1C1 = "=R" & rwfh & "C6"
Range("T20").FormulaR1C1 = "=R" & rwbrn & "C6"
Range("Q20").FormulaR1C1 = "=R" & rwirignlo & "C14+((R" & rwign & "C5-R" & rwirignlo &
                           "C13)/(R" & rwirignhi & "C13-R" & rwirignlo & "C13))*(R" &
                           rwirignhi & "C14-R" & rwirignlo & "C14)"
Range("S20").FormulaR1C1 = "=R" & rwirfhlo & "C14+((R" & rwfh & "C5-R" & rwirfhlo &
                           "C13)/(R" & rwirfhhi & "C13-R" & rwirfhlo & "C13))*(R" &
                           rwirfhhi & "C14-R" & rwirfhlo & "C14)"
Range("U20").FormulaR1C1 = "=R" & rwirbrnlo & "C14+((R" & rwbrn & "C5-R" & rwirbrnlo &
                           "C13)/(R" & rwirbrnhi & "C13-R" & rwirbrnlo & "C13))*(R" &
                           rwirbrnhi & "C14-R" & rwirbrnlo & "C14)"
Range("P22").Value = "Tig_ave"    'Averaging Temp
Range("Q22").Value = "Ig_diff"    'Temp Diff
Range("R22").Value = "Tfh_ave"
Range("S22").Value = "FH_diff"
Range("T22").Value = "Tbrn_ave"
Range("U22").Value = "Brn_diff"
Range("P23").FormulaR1C1 = "=average(R20C16:R20C17)"
Range("R23").FormulaR1C1 = "=average(R20C18:R20C19)"
Range("T23").FormulaR1C1 = "=average(R20C20:R20C21)"
Range("Q23").FormulaR1C1 = "=abs(R20C16-R20C17)"
Range("S23").FormulaR1C1 = "=abs(R20C18-R20C19)"
Range("U23").FormulaR1C1 = "=abs(R20C20-R20C21)"
Range("A1").Select
Windows("Reference Sheet - Final.xls").Activate   'Copying values into reference sheet
Sheets("All Runs").Select
Range("B2").Select
Do  While  ActiveCell.Value  <>  dt  Or  ActiveCell.Offset(0,  2).Value  <>  species  Or
                           ActiveCell.Offset(0, 3).Value <> run
   ActiveCell.Offset(1, 0).Select                 'Finding location on reference sheet
                           "All Species"
Loop
rwcopy = ActiveCell.Row
Windows("" & species & " " & run & ".xls").Activate
Sheets("mass").Range("O14:R14").Copy            'Release %
Windows("Reference Sheet - Final.xls").Activate
Sheets("All Runs").Range("Z" & rwcopy & "").PasteSpecial xlPasteValues
Windows("" & species & " " & run & ".xls").Activate
Sheets("MassRelease").Range("J2:L2").Copy       'Mass release rates
Windows("Reference Sheet - Final.xls").Activate
Sheets("All Runs").Range("AJ" & rwcopy & "").PasteSpecial xlPasteValues
Windows("" & species & " " & run & ".xls").Activate
Sheets("HR_TC").Range("J2:L2").Copy             'Heating rates_TC
Windows("Reference Sheet - Final.xls").Activate
Sheets("All Runs").Range("AM" & rwcopy & "").PasteSpecial xlPasteValues
Windows("" & species & " " & run & ".xls").Activate
Sheets("HR_IR").Range("J2:L2").Copy             'Heating rates_IR
Windows("Reference Sheet - Final.xls").Activate
Sheets("All Runs").Range("AP" & rwcopy & "").PasteSpecial xlPasteValues
Windows("" & species & " " & run & ".xls").Activate
Sheets("mass").Range("P3").Copy                 'tig
Windows("Reference Sheet - Final.xls").Activate
Sheets("All Runs").Range("AS" & rwcopy & "").PasteSpecial xlPasteValues
Sheets("Macros").Range("M" & rwrun & "").Copy   'tFH
Sheets("All Runs").Range("AT" & rwcopy & "").PasteSpecial xlPasteValues
Windows("" & species & " " & run & ".xls").Activate
Sheets("mass").Range("P20:U20").Copy            'Temperatures - TC & IR
```

```
   Windows("Reference Sheet - Final.xls").Activate
   Sheets("All Runs").Range("AU" & rwcopy & "").PasteSpecial xlPasteValues
   Windows("" & species & " " & run & ".xls").Activate
   Sheets("mass").Range("P5").Copy                'tbrn
   Windows("Reference Sheet - Final.xls").Activate
   Sheets("All Runs").Range("BB" & rwcopy & "").PasteSpecial xlPasteValues
End Sub
```

B. Cubic Function and Gauss Elimination Technique (VB Applications)

```
Option Explicit
Dim i As Long, j As Long, k As Long, n As Long, er As Long, nn As Long
Dim a() As Double, b() As Double, x() As Double, val As Double
Dim S(1 To 800) As Double, tol As Double, div As Double, sum As Double
Dim x1 As Double, x2 As Double, x3 As Double, x4 As Double, x5 As Double, x6 As Double
Dim y1 As Double, x1y1 As Double, x2y1 As Double, x3y1 As Double
Dim y() As Double, ord As Long

Public Function cubic(xs As Range, ys As Range, ord As Long) As Double
'Created by Brent M. Pickett
'Function that returns the cubic coefficient (0,1,2,3) according to input x's, y's, and
                            order level desired
   tol = 0.0000000000001: er = 0   'Initializing values - if solution does not occur,
                            lower tolerance (tol)
   nn = xs.Cells.Count: n = 4   'Number of cells in element
   ReDim a(1 To n, 1 To n) As Double, b(1 To n) As Double, x(1 To n) As Double
   For i = 1 To n     'Defining storage arrays a, b
      b(i) = 0
      For j = 1 To n
         a(i, j) = 0
      Next j
   Next i
   x1 = 0: x2 = 0: x3 = 0: x4 = 0: x5 = 0: x6 = 0: y1 = 0: x1y1 = 0: x2y1 = 0: x3y1 = 0
                            'Initialize
   For i = 1 To nn
      x1 = x1 + xs.Cells(i, 1).Value           'Getting values for a matrix
      x2 = x2 + xs.Cells(i, 1).Value ^ 2
      x3 = x3 + xs.Cells(i, 1).Value ^ 3
      x4 = x4 + xs.Cells(i, 1).Value ^ 4
      x5 = x5 + xs.Cells(i, 1).Value ^ 5
      x6 = x6 + xs.Cells(i, 1).Value ^ 6
      y1 = y1 + ys.Cells(i, 1).Value           'b array
      x1y1 = x1y1 + (xs.Cells(i, 1).Value * ys.Cells(i, 1).Value)
      x2y1 = x2y1 + ((xs.Cells(i, 1).Value ^ 2) * ys.Cells(i, 1).Value)
      x3y1 = x3y1 + ((xs.Cells(i, 1).Value ^ 3) * ys.Cells(i, 1).Value)
   Next i
   a(1, 1) = nn: a(4, 4) = x6: a(1, 2) = x1: a(2, 1) = x1: a(3, 4) = x5: a(4, 3) = x5
   a(3, 1) = x2: a(2, 2) = x2: a(1, 3) = x2: a(4, 2) = x4: a(3, 3) = x4: a(2, 4) = x4
   a(4, 1) = x3: a(3, 2) = x3: a(2, 3) = x3: a(1, 4) = x3
   b(1) = y1: b(2) = x1y1: b(3) = x2y1: b(4) = x3y1    'Assigning a matrix and b array
   Call Gauss(a, b, x, n, tol, er)  'Solving by Gaussian elimination
   cubic = x(ord + 1)
End Function

Public Sub Gauss(a, b, x, n, tol, er)
'Created by Brent M. Pickett
'More advanced Guass Elimination Method. Able to pivot
   For i = 1 To n
      S(i) = Abs(a(i, 1))           'Setting largest magnitude value of system of eqs to
                            S(i)
      For j = 2 To n
         If Abs(a(i, j)) > S(i) Then    'Used in pivoting and tolerance analysis
            S(i) = Abs(a(i, j))
         End If
      Next j
   Next i
   Call Eliminate(a, b, S, n, tol, er)  'Calling Forward Elimination subroutine
   If er <> -1 Then
```

```
      Call Substitute(a, b, x, n)  'Calling Back Substitution subroutine
   ElseIf er = -1 Then         'If discrepancy with tolerance, gives "No Solution" output
                              in cells.
      For i = 1 To n
         x(i) = "No Sol"
      Next i
   End If
End Sub

Public Sub Eliminate(a, b, S, n, tol, er)
'Created by Brent M. Pickett
'Forward Elimination subroutine
   For k = 1 To n - 1
      Call Pivot(a, b, S, n, k)     'Calling Pivoting subroutine
      If Abs(a(k, k) / S(k)) < tol Then  'Checking tolerance level
         er = -1
         Exit For
      End If
      For i = k + 1 To n
         div = a(i, k) / a(k, k)
         For j = k + 1 To n
            a(i, j) = a(i, j) - div * a(k, j)  'Obtaining a`'s from Gauss Elimination
         Next j
         b(i) = b(i) - div * b(k)   'Obtaining b`'s from Gauss Elimination
      Next i
   Next k
   If Abs(a(k, k) / S(k)) < tol Then  'Checking tolerance level
      er = -1
   End If
End Sub

Public Sub Pivot(a, b, S, n, k)
'Created by Brent M. Pickett
'Pivoting Subroutine
   Dim p As Long, big As Double, ii As Long, dummy As Double, jj As Long
   p = k
   big = Abs(a(k, k) / S(k))
   For ii = k + 1 To n
      dummy = Abs(a(ii, k) / S(ii))     'Determines if switching is needed
      If dummy > big Then
         big = dummy
         p = ii
      End If
   Next ii
   If p <> k Then              'Switches rows of a if needed
      For jj = k To n
         dummy = a(p, jj)
         a(p, jj) = a(k, jj)
         a(k, jj) = dummy
      Next jj
      dummy = b(p)
      b(p) = b(k)
      b(k) = dummy
      dummy = S(p)
      S(p) = S(k)
      S(k) = dummy
   End If
End Sub

Public Sub Substitute(a, b, x, n)
'Created by Brent M. Pickett
'Back Substitution subroutine - obtains final solution vector (x)
   x(n) = b(n) / a(n, n)    'x(n) solution
   For i = n - 1 To 1 Step -1
      sum = 0
      For j = 1 + 1 To n
         sum = sum + a(i, j) * x(j)
      Next j
      x(i) = (b(i) - sum) / a(i, i)   'x(n-1), x(n-2, etc. solutions
   Next i
End Sub
```

C. Surface Area and Perimeter Code (Matlab)

```
%Created by Brent M. Pickett
%Determines the time frame when the maximum flame height occurs according
%to the largest area of "white" space.
clear all;
f=ls('*.tif');   %Reading all TIFF files (should be B&W) in working directory
[row,col]=size(f);
for j= 1:col-4
   fi(j)=cat(2,f(1,j));  %Getting name of first file
end
AA=imread(fi,'tiff');   %Getting 1st raw image
figure(1);    %Displaying first image
imshow (AA);
title('Raw Image')
figure(1);
hold on;       %Cropping image to reasonable area
fprintf('Select top left corner of rect region by mouse-click in image:\n')
[xul,yul]=ginput(1);
fprintf('Upper left coord are x = %.0f & y = %.0f \n',xul,yul);
fprintf('Select bottom right corner of rect region by mouse-click in image:\n')
[xbr,ybr]=ginput(1);
fprintf('Bottom right coord are x = %.0f & y = %.0f \n',xbr,ybr);
hold off;
nxul=round(xul);
nxbr=round(xbr);
nyul=round(yul);
nybr=round(ybr);
AAsub=AA(nyul:nybr,nxul:nxbr);  %New area of cropped image
figure(2);   %Displaying cropped image
imshow (AAsub);
title('Subset of Image');
ansa='y';     % Set a threshold and color dark regions black
while ansa=='y';
    threshold = []; %Initialize threshold
    threshold=input('Enter threshold, 0=black, 255=white <100> : ');
    if isempty(threshold)  %Default value
        threshold=100;
    end
    AAfilt=255*ones(size(AAsub));  %Completely White array
    cntr=0;    %If value < threshold - defines as 0
    AAfilt(find(double(AAsub)<threshold))=0;
    cntr=length(find(double(AAfilt)==0));  %Counting # of 0 pixels
    figure(3);  %Display Filtered image
    imshow(AAfilt);
    title('Area');
    ansa=[];
    ansa=input('Do you want to try another threshold? <n>:','s');
    if isempty(ansa)    %Repeat if desired
        ansa='n';
    end
end
zz=1;              %Looping through all frames of experimental run.
while zz<=row
   for j= 1:col-4
       fi(j)=cat(2,f(zz,j));  %Getting name for zz (counter) file
   end
   AA=imread(fi,'tiff');
   AAsub=AA(nyul:nybr,nxul:nxbr);   %Cropping
   [nrow,ncol]=size(AAsub);
   maxval=double(max(max(AAsub(:,:,1))));
   meanval=mean(mean(AAsub(:,:,1)));
   minval=double(min(min(AAsub(:,:,1))));
   AAfilt=255*ones(size(AAsub));   %Filtering
   cntr=0;
   AAfilt(find(double(AAsub)<threshold))=0;
   cntr=length(find(double(AAfilt)==0));  %Counting Pixels
   maxx(zz)=maxval;
   minn(zz)=minval;
   meann(zz)=meanval;
```

```
   ar(zz)=1-(cntr/(nrow*ncol));  %Determing area
   zz=zz+1;   %Loop
end
maxx=transpose(maxx);  %Arranging Table
minn=transpose(minn);
meann=transpose(meann);
ar=transpose(ar);
for i=1:row
   tab(i,1)=maxx(i);
   tab(i,2)=minn(i);
   tab(i,3)=meann(i);
   tab(i,4)=ar(i);
end     %Eliminating area (frames) prior to stopping of FFB
stp=input('Enter number of frames from the first to the stopping burner frame : ');
for i=1:stp-1
    fhmod(i)=0;
end
for i=stp:row
    fhmod(i)=tab(i,4);
end
fhmod=transpose(fhmod);
armin=max(fhmod);
qq=1;
while qq<=row
    dum=fhmod(qq);
    if dum==armin
        fhrw=qq;
    end
    qq=qq+1;
end
for j= 1:col-4     %Looking at burner stopping time frame
   fistp(j)=cat(2,f(stp,j));
end
AAstp=imread(fistp,'tiff');
AAsubstp=AAstp(nyul:nybr,nxul:nxbr);
ansa='y';
while ansa=='y';  %Obtaining possible area for stopping frame
    threshold = [];                 %Threshold for stopping
    threshold=input('Enter threshold for stopping frame, 0=black, 255=white <100> : ');
    if isempty(threshold)
        threshold=100;
    end
    AAfiltstp=255*ones(size(AAsubstp));
    cntr=0;                 %Filtering
    AAfiltstp(find(double(AAsubstp)<threshold))=0;
    cntr=length(find(double(AAfiltstp)==0));
    fprintf('White   area   fraction   (burner   stop)   above   threshold   is   %g.\n',1-
                              (cntr/(nrow*ncol)));
    ar_stp=1-(cntr/(nrow*ncol));
    figure(4);   %Displaying stopping frame
    imshow(AAsubstp);
    title('Burner stopping frame');
    figure(5);   %Displaying filtered stopping frame
    imshow(AAfiltstp);
    title('Burner stopping frame - Dark Area');
    ansa=[];
    ansa=input('Do you want to try another threshold? <n>:','s');
    if isempty(ansa)   %Repeat if desired
        ansa='n';
    end
end
for j= 1:col-4     %Looking at flame height time frame
   fifh(j)=cat(2,f(fhrw,j));
end
AAfh=imread(fifh,'tiff');
AAsubfh=AAfh(nyul:nybr,nxul:nxbr);
ansa='y';
while ansa=='y';   %Obtaining possible area for maximum flame height
    threshold = [];                         %Threshold for FH
    threshold=input('Enter  threshold  for  flame  height  frame,  0=black,  255=white  <100>  :
                              ');
```

```
    if isempty(threshold)
        threshold=100;
    end
    AAfiltfh=255*ones(size(AAsubfh));
    cntr=0;                          %Filtering
    AAfiltfh(find(double(AAsubfh)<threshold))=0;
    cntr=length(find(double(AAfiltfh)==0));
    fprintf('White    area    fraction    (flame    height)    above    threshold    is
                          %g.\n',(cntr/(nrow*ncol)));
    ar_fh=1-(cntr/(nrow*ncol));
    figure(6);              %Displaying FH Frame
    imshow(AAsubfh);
    title('Flame height frame');
    figure(7);              %Displaying filtered FH Frame
    imshow(AAfiltfh);
    title('Flame height frame - Dark Area');
    ansa=[];
    ansa=input('Do you want to try another threshold? <n>:','s');
    if isempty(ansa)        %Repeat if desired
        ansa='n';
    end
end
for j= 1:col-4
   fifh(j)=cat(2,f(fhrw,j));
end           %Printing
fifh      %Flame Height Frame
ar_stp    %Area of stopping frame
ar_fh     %Area of FH frame
area=ar_fh-ar_stp;
area      %Supposed area of the flame - not used for analysis
```

D. Flame Height Time Code (Matlab)

```
%Created by Brent M. Pickett
%Determines the time frame when the maximum flame height occurs according
%to the largest area of "white" space.
clear all;
f=ls('*.tif');   %Reading all TIFF files (should be B&W) in working directory
[row,col]=size(f);
for j= 1:col-4
   fi(j)=cat(2,f(1,j));  %Getting name of first file
end
AA=imread(fi,'tiff');   %Getting 1st raw image
figure(1);    %Displaying first image
imshow (AA);
title('Raw Image')
figure(1);
hold on;       %Cropping image to reasonable area
fprintf('Select top left corner of rect region by mouse-click in image:\n')
[xul,yul]=ginput(1);
fprintf('Upper left coord are x = %.0f & y = %.0f \n',xul,yul);
fprintf('Select bottom right corner of rect region by mouse-click in image:\n')
[xbr,ybr]=ginput(1);
fprintf('Bottom right coord are x = %.0f & y = %.0f \n',xbr,ybr);
hold off;
nxul=round(xul);
nxbr=round(xbr);
nyul=round(yul);
nybr=round(ybr);
AAsub=AA(nyul:nybr,nxul:nxbr);  %New area of cropped image
figure(2);   %Displaying cropped image
imshow (AAsub);
title('Subset of Image');
ansa='y';     % Set a threshold and color dark regions black
while ansa=='y';
    threshold = []; %Initialize threshold
    threshold=input('Enter threshold, 0=black, 255=white <100> : ');
    if isempty(threshold)  %Default value
```

```
        threshold=100;
    end
    AAfilt=255*ones(size(AAsub));  %Completely White array
    cntr=0;    %If value < threshold - defines as 0
    AAfilt(find(double(AAsub)<threshold))=0;
    cntr=length(find(double(AAfilt)==0));  %Counting # of 0 pixels
    figure(3);  %Display Filtered image
    imshow(AAfilt);
    title('Area');
    ansa=[];
    ansa=input('Do you want to try another threshold? <n>:','s');
    if isempty(ansa)    %Repeat if desired
        ansa='n';
    end
end
zz=1;              %Looping through all frames of experimental run.
while zz<=row
   for j= 1:col-4
       fi(j)=cat(2,f(zz,j));  %Getting name for zz (counter) file
   end
   AA=imread(fi,'tiff');
   AAsub=AA(nyul:nybr,nxul:nxbr);   %Cropping
   [nrow,ncol]=size(AAsub);
   maxval=double(max(max(AAsub(:,:,1))));
   meanval=mean(mean(AAsub(:,:,1)));
   minval=double(min(min(AAsub(:,:,1))));
   AAfilt=255*ones(size(AAsub));   %Filtering
   cntr=0;
   AAfilt(find(double(AAsub)<threshold))=0;
   cntr=length(find(double(AAfilt)==0));  %Counting Pixels
   maxx(zz)=maxval;
   minn(zz)=minval;
   meann(zz)=meanval;
   ar(zz)=1-(cntr/(nrow*ncol));  %Determing area
   zz=zz+1;   %Loop
end
maxx=transpose(maxx);  %Arranging Table
minn=transpose(minn);
meann=transpose(meann);
ar=transpose(ar);
for i=1:row
   tab(i,1)=maxx(i);
   tab(i,2)=minn(i);
   tab(i,3)=meann(i);
   tab(i,4)=ar(i);
end     %Eliminating area (frames) prior to stopping of FFB
stp=input('Enter number of frames from the first to the stopping burner frame : ');
for i=1:stp-1
    fhmod(i)=0;
end
for i=stp:row
    fhmod(i)=tab(i,4);
end
fhmod=transpose(fhmod);
armin=max(fhmod);
qq=1;
while qq<=row
    dum=fhmod(qq);
    if dum==armin
        fhrw=qq;
    end
    qq=qq+1;
end
for j= 1:col-4     %Looking at burner stopping time frame
   fistp(j)=cat(2,f(stp,j));
end
AAstp=imread(fistp,'tiff');
AAsubstp=AAstp(nyul:nybr,nxul:nxbr);
ansa='y';
while ansa=='y';  %Obtaining possible area for stopping frame
    threshold = [];                %Threshold for stopping
```

```
    threshold=input('Enter threshold for stopping frame, 0=black, 255=white <100> : ');
    if isempty(threshold)
        threshold=100;
    end
    AAfiltstp=255*ones(size(AAsubstp));
    cntr=0;                %Filtering
    AAfiltstp(find(double(AAsubstp)<threshold))=0;
    cntr=length(find(double(AAfiltstp)==0));
    fprintf('White   area   fraction   (burner   stop)   above   threshold   is   %g.\n',1-
                            (cntr/(nrow*ncol)));
    ar_stp=1-(cntr/(nrow*ncol));
    figure(4);   %Displaying stopping frame
    imshow(AAsubstp);
    title('Burner stopping frame');
    figure(5);   %Displaying filtered stopping frame
    imshow(AAfiltstp);
    title('Burner stopping frame - Dark Area');
    ansa=[];
    ansa=input('Do you want to try another threshold? <n>:','s');
    if isempty(ansa)   %Repeat if desired
        ansa='n';
    end
end
for j= 1:col-4     %Looking at flame height time frame
   fifh(j)=cat(2,f(fhrw,j));
end
AAfh=imread(fifh,'tiff');
AAsubfh=AAfh(nyul:nybr,nxul:nxbr);
ansa='y';
while ansa=='y';   %Obtaining possible area for maximum flame height
    threshold = [];                        %Threshold for FH
    threshold=input('Enter  threshold  for  flame height  frame,  0=black,  255=white  <100>  :
                            ');
    if isempty(threshold)
        threshold=100;
    end
    AAfiltfh=255*ones(size(AAsubfh));
    cntr=0;                              %Filtering
    AAfiltfh(find(double(AAsubfh)<threshold))=0;
    cntr=length(find(double(AAfiltfh)==0));
    fprintf('White    area    fraction    (flame    height)    above    threshold    is
                            %g.\n',(cntr/(nrow*ncol)));
    ar_fh=1-(cntr/(nrow*ncol));
    figure(6);               %Displaying FH Frame
    imshow(AAsubfh);
    title('Flame height frame');
    figure(7);               %Displaying filtered FH Frame
    imshow(AAfiltfh);
    title('Flame height frame - Dark Area');
    ansa=[];
    ansa=input('Do you want to try another threshold? <n>:','s');
    if isempty(ansa)         %Repeat if desired
        ansa='n';
    end
end
for j= 1:col-4
   fifh(j)=cat(2,f(fhrw,j));
end           %Printing
fifh      %Flame Height Frame
ar_stp    %Area of stopping frame
ar_fh     %Area of FH frame
area=ar_fh-ar_stp;
area      %Supposed area of the flame - not used for analysis
```

E. Bush Burning Model (VB Applications)

```
Option Explicit
Dim i As Long, j As Long, m As Long, n As Long, cc As Long, rmin As Double, rmax As
                              Double
Dim Dt As Double, t_tot As Double, t_c As Double, IgCLS() As Long, tl() As Double, rr()
                              As Double
Dim ex As Boolean, xx() As Double, yy() As Double, nmb As Long, dm1 As Double, mrk1 As
                              Long
Dim xdist As Double, ydist As Double, tfd As Double, tig As Double

Public Sub BUSHBURN()
   'Bush model - describes burning of individual leaves within a burning bush
   'Created by Brent M. Pickett
   Range("A2:E52").Clear
   rmin = 1: rmax = 2  'Range of leaf radius [cm]
   Dt = 0.05    'Time Step [s]
   t_tot = 1000  'Total time to burn the bush [s]
   t_c = 0     'Current time - Should be 0 initially
   nmb = 20   'Number of leaves inside control volume
   xdist = 10: ydist = 10   'Control volume [cm]
   tig = 2.953        '2.953 is the average ignition time for manzanita
   tfd = 12.135 + tig     '12.135 is the average flame duration time for manzanita
   ReDim xx(1 To nmb), yy(1 To nmb), IgCLS(1 To nmb), tl(1 To nmb), rr(1 To nmb)
   For i = 1 To nmb
      xx(i) = 0
      yy(i) = 0
      rr(i) = 0
   Next i
   For i = 1 To nmb
      xx(i) = xdist * Rnd    'Location for leaf
      yy(i) = ydist * Rnd
      rr(i) = rmin + (rmax - rmin) * Rnd    'Radius of leaf
   Next i
   dm1 = ydist + 1: mrk1 = 1
   For i = 1 To nmb
      If yy(i) < dm1 Then
         dm1 = yy(i): mrk1 = i   'Lowest leaf location
      End If
   Next i
   For i = 1 To nmb
      If i = mrk1 Then
         IgCLS(i) = 2    'Igniting lowest leaf
      Else
         IgCLS(i) = 1
      End If
   Next i
   Sheets("Bush").Cells(1, 1).Value = "x"   'Printing headers
   Sheets("Bush").Cells(1, 2).Value = "y"
   Sheets("Bush").Cells(1, 3).Value = "r"
   Sheets("Bush").Cells(1, 4).Value = "Ig"
   Sheets("Bush").Cells(1, 5).Value = "tl"
   Sheets("Bush").Cells(2, 7).Value = Dt    'Printing some values
   Sheets("Bush").Cells(5, 6).Value = nmb
   Sheets("Bush").Cells(5, 7).Value = xdist * ydist
   For i = 1 To nmb
      Sheets("Bush").Cells(i + 1, 1).Value = xx(i)   'Printing location and radius
      Sheets("Bush").Cells(i + 1, 2).Value = yy(i)
      Sheets("Bush").Cells(i + 1, 3).Value = rr(i)
      Sheets("Bush").Cells(i + 1, 4).Value = IgCLS(i)   'Printing if leaf is ignited
   Next i
   Do While t_c <= t_tot
      For i = 1 To nmb
         If IgCLS(i) = 2 Then
            For m = 1 To nmb
               If  InIZ(tl(i),  rr(i),  xx(i),  yy(i),  rr(m),  xx(m),  yy(m))  =  True  And
                              IgCLS(m) = 1 Then
                  IgCLS(m) = 2     'Igniting nearby unignited leaves if they are inside
                              ignition zone
               End If
```

```
            Next m
            tl(i) = tl(i) + Dt
            If tl(i) > tfd Then
               IgCLS(i) = 3: tl(i) = 0
            End If
         End If
      Next i
      For i = 1 To nmb
         Sheets("Bush").Cells(i + 1, 4).Value = IgCLS(i)  'Printing
         Sheets("Bush").Cells(i + 1, 5).Value = tl(i)
      Next i
      Sheets("Bush").Cells(2, 6).Value = t_c
      ex = False      'Exits if any leaf is still ignited
      For i = 1 To nmb
          If IgCLS(i) = 2 Then
             ex = True
          End If
      Next i
      If ex = False Then
         GoTo Line2
      End If
      t_c = t_c + Dt
      Calculate
   Loop
Line2:
   cc = 0
   For i = 1 To nmb
      If IgCLS(i) = 1 Then
         cc = cc + 1
      End If
   Next i
   Sheets("Bush").Cells(8, 7) = cc
   End Sub

Public Function IZ(t As Double, r As Double, x_c As Double, y_c As Double, corn As
                              String, xy As String) As Double
   'Ignition Zone Function - Determines how large the zone is at a given time.
   'Created by Brent M. Pickett
   Dim Dx As Double, Dyup As Double, Dydwn As Double, func As Double
   If t > tfd Or t < tig Then
      Dx = 0: Dyup = 0: Dydwn = 0
   Else         'Polynomial fit for vertical growth above the leaf
      func = 0.002790701 * t ^ 3 - 0.259847021 * t ^ 2 + 3.903928483 * t - 9.334243201
      Dx = 0.1 * func: Dyup = func: Dydwn = 0.05 * func
   End If
   If xy = "x" Then
      If corn = "ll" Or corn = "ul" Then
         IZ = x_c - r - Dx
      ElseIf corn = "lr" Or corn = "ur" Then
         IZ = x_c + r + Dx
      End If
   ElseIf xy = "y" Then
      If corn = "ll" Or corn = "lr" Then
         IZ = y_c - Dydwn
      ElseIf corn = "ul" Or corn = "ur" Then
         IZ = y_c + Dyup
      End If
   End If
End Function

Public Function InIZ(t As Double, r As Double, x_c As Double, y_c As Double, r_s As
                              Double x_s As Double, y_s As Double) As Boolean
   'Determines if a specified leaf is within an ignition zone.
   'Created by Brent M. Pickett
   Dim xll As Double, xlr As Double, xul As Double, xur As Double
   Dim yll As Double, ylr As Double, yul As Double, yur As Double
   xll = IZ(t, r, x_c, y_c, "ll", "x"): yll = IZ(t, r, x_c, y_c, "ll", "y")
   xlr = IZ(t, r, x_c, y_c, "lr", "x"): ylr = IZ(t, r, x_c, y_c, "lr", "y")
   xul = IZ(t, r, x_c, y_c, "ul", "x"): yul = IZ(t, r, x_c, y_c, "ul", "y")
   xur = IZ(t, r, x_c, y_c, "ur", "x"): yur = IZ(t, r, x_c, y_c, "ur", "y")
   If xll <= (x_s + r_s) And (x_s + r_s) <= xur And yll <= y_s And y_s <= yur Then
```

```
      InIZ = True
   ElseIf xll <= (x_s - r_s) And (x_s - r_s) <= xur And yll <= y_s And y_s <= yur Then
      InIZ = True
   ElseIf xll <= x_s And x_s <= xur And yll <= y_s And y_s <= yur Then
      InIZ = True
   Else
      InIZ = False
   End If
End Function
```

Appendix B. Extra Tables

A. Average Values with Seasonal Variation

The following are tables that list the average values with 95% confidence intervals (±) for leaf and combustion variables. Individual seasons are also tabulated. The variable is noted in the upper left-hand corner of each table.

***MC* (%)**	**All**	**Spring**	**Summer**	**Fall**	**Winter**
Manzanita	50 ± 3	46 ± 6	57 ± 4	29 ± 3	56 ± 2
Ceanothus	68 ± 3	69 ± 7	71 ± 3	49	46
Scrub Oak	58 ± 3	54 ± 6	64 ± 4	44 ± 8	53 ± 7
Chamise	72 ± 4	83 ± 1	77 ± 3	18	48
Gambel Oak	68 ± 5	96	65 ± 6	80	-
Canyon Maple	96 ± 4	159	91 ± 4	-	-
Big Sagebrush	143 ± 5	192	141 ± 5	-	-
Utah Juniper	63 ± 3	99	67 ± 2	-	45 ± 2
Douglas-Fir	116 ± 9	121 ± 9	-	78	-
White Fir	92 ± 2	93 ± 2	-	91 ± 7	-
Fetterbush	80	80	-	-	-
Gallberry	96	96	-	-	-
Wax Myrtle	103	103	-	-	-
Saw Palmetto	71	71	-	-	-
Excelsior	18 ± 3	23 ± 1	-	-	4 ± 0
All	71 ± 2	70 ± 4	79 ± 2	45 ± 4	47 ± 3

Δx (mm)	**All**	**Spring**	**Summer**	**Fall**	**Winter**
Manzanita	0.50 ± 0.01	0.49 ± 0.04	0.48 ± 0.01	0.44 ± 0.02	0.64 ± 0.02
Ceanothus	0.54 ± 0.02	0.46 ± 0.04	0.60 ± 0.02	0.57 ± 0.05	0.48 ± 0.03
Scrub Oak	0.35 ± 0.01	0.32 ± 0.03	0.38 ± 0.02	0.37 ± 0.07	0.31 ± 0.02
Chamise	0.62 ± 0.07	-	0.62 ± 0.11	-	0.63 ± 0.05
Gambel Oak	0.21 ± 0.01	0.17 ± 0.02	0.20 ± 0.01	0.28 ± 0.01	-
Canyon Maple	0.21 ± 0.01	0.27 ± 0.03	0.21 ± 0.02	-	-
Big Sagebrush	0.26 ± 0.01	0.40 ± 0.07	0.26 ± 0.01	-	-
Utah Juniper	1.41 ± 0.03	-	1.41 ± 0.03	-	-
Douglas-Fir	0.47 ± 0.03	0.47 ± 0.03	-	-	-
White Fir	0.63 ± 0.05	0.63 ± 0.05	-	-	-
Fetterbush	0.40 ± 0.05	0.40 ± 0.05	-	-	-
Gallberry	0.34 ± 0.02	0.34 ± 0.02	-	-	-
Wax Myrtle	0.38 ± 0.04	0.38 ± 0.04	-	-	-
Saw Palmetto	0.26 ± 0.03	0.26 ± 0.03	-	-	-
Excelsior	0.79 ± 0.15	-	-	-	0.79 ± 0.15
All	0.41 ± 0.01	0.42 ± 0.02	0.38 ± 0.01	0.40 ± 0.02	0.53 ± 0.03

***SA* (cm^2)**	**All**	**Spring**	**Summer**	**Fall**	**Winter**
Manzanita	5.1 ± 0.2	-	4.9 ± 0.3	4.7 ± 0.3	5.9 ± 0.4
Ceanothus	1.4 ± 0.1	-	1.4 ± 0.1	-	1.2 ± 0.2
Scrub Oak	3.8 ± 0.3	-	4.2 ± 0.3	-	2.7 ± 0.2
Chamise	-	-	-	-	-
Gambel Oak	11.3 ± 1.7	7.9 ± 1.2	12.4 ± 2.1	7.9 ± 1.2	-
Canyon Maple	12.1 ± 1.0	15.7 ± 3.7	11.7 ± 1.0	-	-
Big Sagebrush	1.0 ± 0.1	1.3 ± 0.3	0.9 ± 0.1	-	-
Utah Juniper	-	-	-	-	-
Douglas-Fir	-	-	-	-	-
White Fir	-	-	-	-	-
Fetterbush	6.2 ± 1.1	6.2 ± 1.1	-	-	-
Gallberry	2.5 ± 0.4	2.5 ± 0.4	-	-	-
Wax Myrtle	5.7 ± 1.0	5.7 ± 1.0	-	-	-
Saw Palmetto	3.4 ± 0.7	3.4 ± 0.7	-	-	-
Excelsior	-	-	-	-	-
All	5.9 ± 0.4	6.0 ± 1.0	6.2 ± 0.5	6.0 ± 0.8	4.0 ± 0.4

***P* (cm)**	**All**	**Spring**	**Summer**	**Fall**	**Winter**
Manzanita	8.9 ± 0.2	-	8.7 ± 0.2	9.0 ± 0.3	9.5 ± 0.3
Ceanothus	4.8 ± 0.2	-	4.9 ± 0.2	-	4.4 ± 0.3
Scrub Oak	8.6 ± 0.3	-	9.1 ± 0.4	-	7.1 ± 0.4
Chamise	-	-	-	-	-
Gambel Oak	21.5 ± 1.3	18.7 ± 1.3	22.4 ± 1.7	19.1 ± 1.7	-
Canyon Maple	29.8 ± 1.3	34.5 ± 4.3	29.3 ± 1.4	-	-
Big Sagebrush	6.8 ± 0.3	8.6 ± 0.7	6.6 ± 0.3	-	-
Utah Juniper	-	-	-	-	-
Douglas-Fir	-	-	-	-	-
White Fir	-	-	-	-	-
Fetterbush	11.0 ± 1.1	11.0 ± 1.1	-	-	-
Gallberry	7.3 ± 0.5	7.3 ± 0.5	-	-	-
Wax Myrtle	13.4 ± 1.2	13.4 ± 1.2	-	-	-
Saw Palmetto	14.9 ± 1.4	14.9 ± 1.4	-	-	-
Excelsior	-	-	-	-	-
All	13.0 ± 0.6	14.8 ± 1.8	13.6 ± 0.8	13.3 ± 1.9	7.7 ± 0.4

m_0 **(g)**	**All**	**Spring**	**Summer**	**Fall**	**Winter**
Manzanita	0.23 ± 0.01	0.22 ± 0.02	0.21 ± 0.01	0.20 ± 0.02	0.33 ± 0.03
Ceanothus	0.09 ± 0.01	0.09 ± 0.01	0.08 ± 0.01	0.10 ± 0.02	0.07 ± 0.01
Scrub Oak	0.17 ± 0.02	0.29 ± 0.03	0.11 ± 0.01	0.21 ± 0.08	0.16 ± 0.04
Chamise	0.80 ± 0.54	-	0.20 ± 0.08	6.64 ± 3.07	0.32 ± 0.14
Gambel Oak	0.19 ± 0.02	0.12 ± 0.02	0.20 ± 0.02	0.11 ± 0.02	-
Canyon Maple	0.17 ± 0.01	0.13 ± 0.03	0.17 ± 0.02	-	-
Big Sagebrush	0.03 ± 0.00	0.03 ± 0.00	0.03 ± 0.00	-	-
Utah Juniper	0.81 ± 0.16	0.53 ± 0.15	0.97 ± 0.24	-	0.58 ± 0.17
Douglas-Fir	0.68 ± 0.10	0.69 ± 0.12	-	0.61 ± 0.16	-
White Fir	0.61 ± 0.08	0.66 ± 0.06	-	0.50 ± 0.23	-
Fetterbush	0.26 ± 0.04	0.26 ± 0.04	-	-	-
Gallberry	0.12 ± 0.02	0.12 ± 0.02	-	-	-
Wax Myrtle	0.13 ± 0.04	0.13 ± 0.04	-	-	-
Saw Palmetto	0.15 ± 0.02	0.15 ± 0.02	-	-	-
Excelsior	0.02 ± 0.00	0.02 ± 0.00	-	-	0.02 ± 0.00
All	0.24 ± 0.02	0.25 ± 0.02	0.20 ± 0.02	0.46 ± 0.22	0.27 ± 0.04

m_{iq}/m_0	All	Spring	Summer	Fall	Winter
Manzanita	0.12 ± 0.01	-	0.12 ± 0.02	0.12 ± 0.04	0.14 ± 0.03
Ceanothus	0.33 ± 0.03	-	0.34 ± 0.04	-	0.29 ± 0.07
Scrub Oak	0.18 ± 0.03	-	0.15 ± 0.04	-	0.34 ± 0.06
Chamise	0.11 ± 0.05	-	0.13 ± 0.05	-	0.01 ± 0.04
Gambel Oak	0.14 ± 0.03	0.17 ± 0.07	0.18 ± 0.04	0.05 ± 0.02	-
Canyon Maple	0.21 ± 0.03	0.16 ± 0.02	0.22 ± 0.04	-	-
Big Sagebrush	0.28 ± 0.09	0.26 ± 0.49	0.28 ± 0.10	-	-
Utah Juniper	0.11 ± 0.03	0.04 ± 0.02	0.12 ± 0.03	-	0.13 ± 0.06
Douglas-Fir	0.04 ± 0.04	0.01 ± 0.01	-	0.29 ± 0.26	0.00 ± 0.00
White Fir	0.06 ± 0.04	0.03 ± 0.02	-	0.17 ± 0.19	-
Fetterbush	0.28 ± 0.11	0.28 ± 0.11	-	-	-
Gallberry	0.31	0.31	-	-	-
Wax Myrtle	0.08 ± 0.04	0.08 ± 0.04	-	-	-
Saw Palmetto	0.08 ± 0.05	0.08 ± 0.05	-	-	-
Excelsior	0.08 ± 0.03	0.08 ± 0.04	-	-	0.05 ± 0.06
All	0.16 ± 0.01	0.09 ± 0.02	0.18 ± 0.01	0.12 ± 0.04	0.17 ± 0.03

m_{FH}/m_0	All	Spring	Summer	Fall	Winter
Manzanita	0.56 ± 0.01	-	0.55 ± 0.02	0.46 ± 0.02	0.62 ± 0.02
Ceanothus	0.75 ± 0.02	-	0.75 ± 0.03	-	0.73 ± 0.04
Scrub Oak	0.67 ± 0.03	-	0.67 ± 0.03	-	0.63 ± 0.07
Chamise	0.58 ± 0.07	-	0.58 ± 0.08	-	0.58 ± 0.25
Gambel Oak	0.63 ± 0.04	0.65 ± 0.08	0.67 ± 0.04	0.50 ± 0.06	-
Canyon Maple	0.66 ± 0.05	0.51 ± 0.10	0.68 ± 0.05	-	-
Big Sagebrush	0.69 ± 0.08	0.83 ± 0.31	0.66 ± 0.08	-	-
Utah Juniper	0.67 ± 0.03	0.68 ± 0.09	0.70 ± 0.05	-	0.62 ± 0.06
Douglas-Fir	0.73 ± 0.04	0.71 ± 0.05	-	0.82 ± 0.11	-
White Fir	0.76 ± 0.05	0.76 ± 0.06	-	0.76 ± 0.13	-
Fetterbush	0.67 ± 0.05	0.67 ± 0.05	-	-	-
Gallberry	0.82 ± 0.07	0.82 ± 0.07	-	-	-
Wax Myrtle	0.52 ± 0.06	0.52 ± 0.06	-	-	-
Saw Palmetto	0.57 ± 0.07	0.57 ± 0.07	-	-	-
Excelsior	0.77 ± 0.04	0.78 ± 0.04	-	-	0.64 ± 0.20
All	0.66 ± 0.01	0.71 ± 0.02	0.64 ± 0.01	0.57 ± 0.06	0.64 ± 0.02

m_{Brn}/m_0	All	Spring	Summer	Fall	Winter
Manzanita	0.80 ± 0.01	-	0.80 ± 0.01	0.76 ± 0.02	0.83 ± 0.02
Ceanothus	0.88 ± 0.02	-	0.88 ± 0.02	-	0.88 ± 0.02
Scrub Oak	0.81 ± 0.02	-	0.81 ± 0.02	-	0.81 ± 0.07
Chamise	0.67 ± 0.06	-	0.68 ± 0.08	-	0.65 ± 0.08
Gambel Oak	0.68 ± 0.04	0.65 ± 0.09	0.74 ± 0.04	0.55 ± 0.05	-
Canyon Maple	0.73 ± 0.05	0.50 ± 0.01	0.76 ± 0.04	-	-
Big Sagebrush	0.86 ± 0.08	0.90 ± 0.25	0.85 ± 0.10	-	-
Utah Juniper	0.92 ± 0.02	0.93 ± 0.05	0.92 ± 0.02	-	0.92 ± 0.03
Douglas-Fir	0.90 ± 0.03	0.89 ± 0.04	-	0.94 ± 0.07	-
White Fir	0.96 ± 0.04	0.96 ± 0.05	-	0.96 ± 0.09	-
Fetterbush	0.77 ± 0.05	0.77 ± 0.05	-	-	-
Gallberry	0.91 ± 0.07	0.91 ± 0.07	-	-	-
Wax Myrtle	0.60 ± 0.06	0.60 ± 0.06	-	-	-
Saw Palmetto	0.74 ± 0.05	0.74 ± 0.05	-	-	-
Excelsior	0.88 ± 0.08	0.88 ± 0.08	-	-	-
All	0.82 ± 0.01	0.83 ± 0.03	0.81 ± 0.01	0.77 ± 0.05	0.84 ± 0.02

MR_{iq} (g/s)	All	Spring	Summer	Fall	Winter
Manzanita	0.012 ± 0.001	-	0.011 ± 0.001	0.009 ± 0.002	0.015 ± 0.002
Ceanothus	0.009 ± 0.002	-	0.009 ± 0.002	-	0.008 ± 0.002
Scrub Oak	0.014 ± 0.002	-	0.015 ± 0.002	-	0.012 ± 0.003
Chamise	0.023 ± 0.013	-	0.026 ± 0.016	-	0.009 ± 0.011
Gambel Oak	0.022 ± 0.004	0.033 ± 0.009	0.024 ± 0.005	0.008 ± 0.002	-
Canyon Maple	0.028 ± 0.005	0.046 ± 0.014	0.024 ± 0.005	-	-
Big Sagebrush	0.008 ± 0.001	0.007 ± 0.003	0.008 ± 0.002	-	-
Utah Juniper	0.042 ± 0.009	0.044 ± 0.016	0.027 ± 0.009	-	0.057 ± 0.018
Douglas-Fir	0.093 ± 0.025	0.098 ± 0.027	-	0.045 ± 0.054	-
White Fir	0.168 ± 0.034	0.177 ± 0.032	-	0.135 ± 0.130	-
Fetterbush	0.026 ± 0.015	0.026 ± 0.015	-	-	-
Gallberry	0.042 ± 0.026	0.042 ± 0.026	-	-	-
Wax Myrtle	0.024 ± 0.015	0.024 ± 0.015	-	-	-
Saw Palmetto	0.013 ± 0.004	0.013 ± 0.004	-	-	-
Excelsior	0.019 ± 0.007	0.013 ± 0.001	-	-	0.041 ± 0.029
All	0.028 ± 0.003	0.056 ± 0.010	0.015 ± 0.001	0.032 ± 0.022	0.023 ± 0.005

MR_{FH} (g/s)	All	Spring	Summer	Fall	Winter
Manzanita	0.018 ± 0.001	-	0.017 ± 0.001	0.021 ± 0.002	0.020 ± 0.002
Ceanothus	0.008 ± 0.001	-	0.008 ± 0.001	-	0.008 ± 0.005
Scrub Oak	0.012 ± 0.001	-	0.012 ± 0.001	-	0.011 ± 0.002
Chamise	0.018 ± 0.006	-	0.015 ± 0.007	-	0.029 ± 0.017
Gambel Oak	0.010 ± 0.002	0.006 ± 0.003	-	0.010 ± 0.003	-
Canyon Maple	0.015 ± 0.003	0.014 ± 0.025	0.016 ± 0.003	-	-
Big Sagebrush	0.012 ± 0.014	0.008 ± 0.005	0.012 ± 0.015	-	-
Utah Juniper	0.029 ± 0.006	0.035 ± 0.009	0.024 ± 0.007	-	0.032 ± 0.014
Douglas-Fir	0.061 ± 0.015	0.060 ± 0.017	-	0.066 ± 0.030	-
White Fir	0.040 ± 0.014	0.038 ± 0.013	-	0.044 ± 0.038	-
Fetterbush	0.008 ± 0.007	0.008 ± 0.007	-	-	-
Gallberry	0.008 ± 0.002	0.008 ± 0.002	-	-	-
Wax Myrtle	0.023 ± 0.015	0.023 ± 0.015	-	-	-
Saw Palmetto	0.021 ± 0.005	0.021 ± 0.005	-	-	-
Excelsior	0.021 ± 0.006	0.013 ± 0.001	-	-	0.049 ± 0.026
All	0.019 ± 0.002	0.026 ± 0.005	0.014 ± 0.001	0.028 ± 0.009	0.022 ± 0.004

t_{iq} (s)	All	Spring	Summer	Fall	Winter
Manzanita	2.95 ± 0.22	2.70 ± 0.47	2.72 ± 0.26	2.62 ± 0.45	4.60 ± 0.77
Ceanothus	5.14 ± 0.33	5.27 ± 0.63	5.29 ± 0.42	5.16 ± 0.92	3.69 ± 0.92
Scrub Oak	1.24 ± 0.25	0.49 ± 0.11	1.40 ± 0.39	1.74 ± 1.12	2.21 ± 0.47
Chamise	1.14 ± 0.20	-	1.19 ± 0.22	-	0.97 ± 0.49
Gambel Oak	0.71 ± 0.07	0.84 ± 0.17	0.71 ± 0.08	0.63 ± 0.15	-
Canyon Maple	0.64 ± 0.10	0.50 ± 0.13	0.66 ± 0.11	-	-
Big Sagebrush	1.57 ± 0.13	1.41 ± 0.52	1.58 ± 0.14	-	-
Utah Juniper	1.45 ± 0.24	0.38 ± 0.08	1.82 ± 0.30	-	0.89 ± 0.38
Douglas-Fir	0.30 ± 0.15	0.13 ± 0.03	-	1.51 ± 0.46	-
White Fir	0.68 ± 0.38	0.34 ± 0.15	-	1.50 ± 1.23	-
Fetterbush	2.50 ± 0.37	2.50 ± 0.37	-	-	-
Gallberry	2.79 ± 0.57	2.79 ± 0.57	-	-	-
Wax Myrtle	0.90 ± 0.56	0.90 ± 0.56	-	-	-
Saw Palmetto	0.90 ± 0.62	0.90 ± 0.62	-	-	-
Excelsior	0.29 ± 0.05	0.32 ± 0.06	-	-	0.18 ± 0.07
All	1.98 ± 0.11	1.83 ± 0.22	1.92 ± 0.13	2.10 ± 0.37	2.77 ± 0.44

t_{FH} (s)	All	Spring	Summer	Fall	Winter
Manzanita	7.07 ± 0.32	6.53 ± 0.79	6.67 ± 0.36	5.15 ± 0.59	9.69 ± 0.64
Ceanothus	6.65 ± 0.40	7.13 ± 0.71	6.74 ± 0.58	-	5.22 ± 0.58
Scrub Oak	4.90 ± 0.37	6.16 ± 0.76	4.55 ± 0.45	-	3.45 ± 0.35
Chamise	5.44 ± 0.72	-	5.45 ± 0.69	-	5.43 ± 2.48
Gambel Oak	3.01 ± 0.26	3.65 ± 0.62	2.95 ± 0.34	2.86 ± 0.19	-
Canyon Maple	3.82 ± 0.27	3.23 ± 0.52	3.88 ± 0.29	-	-
Big Sagebrush	2.70 ± 0.26	3.19 ± 0.79	2.66 ± 0.28	-	-
Utah Juniper	8.06 ± 0.68	9.58 ± 2.21	8.02 ± 0.95	-	7.41 ± 1.04
Douglas-Fir	6.62 ± 0.91	6.68 ± 1.04	-	6.15 ± 1.57	-
White Fir	7.70 ± 1.02	7.13 ± 0.80	-	9.12 ± 3.22	-
Fetterbush	5.53 ± 0.65	5.53 ± 0.65	-	-	-
Gallberry	3.74 ± 0.36	3.74 ± 0.36	-	-	-
Wax Myrtle	2.50 ± 0.38	2.50 ± 0.38	-	-	-
Saw Palmetto	4.46 ± 1.26	4.46 ± 1.26	-	-	-
Excelsior	0.84 ± 0.08	0.92 ± 0.09	-	-	0.53 ± 0.07
All	5.32 ± 0.17	5.34 ± 0.32	5.05 ± 0.21	5.41 ± 0.88	6.30 ± 0.60

t_{fd} (s)	All	Spring	Summer	Fall	Winter
Manzanita	12.13 ± 0.42	10.73 ± 1.07	11.81 ± 0.44	10.91 ± 0.82	15.57 ± 0.85
Ceanothus	9.53 ± 0.37	10.18 ± 0.65	9.42 ± 0.51	-	7.80 ± 0.58
Scrub Oak	8.63 ± 0.55	11.77 ± 1.01	7.23 ± 0.56	-	6.43 ± 0.66
Chamise	16.33 ± 2.31	27.90 ± 4.19	11.08 ± 1.51	-	14.84 ± 3.89
Gambel Oak	6.32 ± 0.27	6.77 ± 0.71	6.37 ± 0.31	5.61 ± 0.59	-
Canyon Maple	5.77 ± 0.27	4.89 ± 0.51	5.85 ± 0.29	-	-
Big Sagebrush	3.49 ± 0.16	4.05 ± 0.57	3.48 ± 0.17	-	-
Utah Juniper	21.08 ± 1.91	23.98 ± 6.86	21.72 ± 2.65	-	18.01 ± 1.94
Douglas-Fir	17.14 ± 2.33	17.45 ± 2.64	-	15.02 ± 3.45	-
White Fir	18.43 ± 2.68	16.16 ± 1.31	-	24.12 ± 8.84	-
Fetterbush	9.86 ± 0.74	9.86 ± 0.74	-	-	-
Gallberry	6.49 ± 0.55	6.49 ± 0.55	-	-	-
Wax Myrtle	8.17 ± 1.89	8.17 ± 1.89	-	-	-
Saw Palmetto	7.14 ± 1.38	7.14 ± 1.38	-	-	-
Excelsior	1.94 ± 0.16	2.02 ± 0.16	-	-	1.65 ± 0.40
All	9.71 ± 0.34	11.07 ± 0.7	8.50 ± 0.39	12.51 ± 2.48	11.67 ± 1.02

T_{ig} (°C)	All	Spring	Summer	Fall	Winter
Manzanita	359 ± 12	374 ± 24	332 ± 16	396 ± 37	401 ± 25
Ceanothus	408 ± 20	445 ± 27	378 ± 29	526 ± 75	416 ± 71
Scrub Oak	312 ± 18	276 ± 41	306 ± 22	347 ± 75	373 ± 41
Chamise	266 ± 20	-	260 ± 24	-	291 ± 27
Gambel Oak	240 ± 16	215 ± 20	242 ± 19	238 ± 41	-
Canyon Maple	252 ± 17	198 ± 24	257 ± 18	-	-
Big Sagebrush	331 ± 23	239 ± 47	334 ± 24	-	-
Utah Juniper	274 ± 23	188 ± 22	299 ± 30	-	276 ± 37
Douglas-Fir	189 ± 22	198 ± 23	-	127 ± 20	-
White Fir	190 ± 16	196 ± 16	-	177 ± 45	-
Fetterbush	262 ± 29	262 ± 29	-	-	-
Gallberry	323 ± 46	323 ± 46	-	-	-
Wax Myrtle	270 ± 42	270 ± 42	-	-	-
Saw Palmetto	274 ± 43	274 ± 43	-	-	-
Excelsior	262 ± 14	266 ± 18	-	-	249 ± 25
All	313 ± 7	306 ± 13	306 ± 8	335 ± 30	364 ± 19

T_{FH} (°C)	All	Spring	Summer	Fall	Winter
Manzanita	814 ± 16	-	795 ± 18	764 ± 35	882 ± 34
Ceanothus	736 ± 24	-	704 ± 21	-	842 ± 54
Scrub Oak	791 ± 21	-	807 ± 21	-	740 ± 61
Chamise	764 ± 42	-	787 ± 41	-	684 ± 134
Gambel Oak	858 ± 28	867 ± 29	838 ± 43	903 ± 34	-
Canyon Maple	823 ± 27	810 ± 40	825 ± 32	-	-
Big Sagebrush	712 ± 38	598 ± 110	722 ± 40	-	-
Utah Juniper	859 ± 38	805 ± 81	879 ± 43	-	-
Douglas-Fir	942 ± 27	955 ± 27	-	853 ± 88	-
White Fir	873 ± 41	903 ± 25	-	796 ± 133	-
Fetterbush	872 ± 45	872 ± 45	-	-	-
Gallberry	876 ± 52	876 ± 52	-	-	-
Wax Myrtle	862 ± 83	862 ± 83	-	-	-
Saw Palmetto	877 ± 89	877 ± 89	-	-	-
Excelsior	496 ± 27	506 ± 33	-	-	463 ± 50
All	799 ± 10	823 ± 25	790 ± 11	821 ± 34	788 ± 33

T_{Brn} (°C)	All	Spring	Summer	Fall	Winter
Manzanita	943 ± 10	-	936 ± 13	957 ± 25	956 ± 19
Ceanothus	861 ± 12	-	847 ± 11	-	905 ± 24
Scrub Oak	902 ± 11	-	909 ± 13	-	879 ± 22
Chamise	926 ± 34	-	908 ± 42	-	986 ± 30
Gambel Oak	894 ± 19	899 ± 27	871 ± 28	949 ± 14	-
Canyon Maple	823 ± 18	837 ± 43	819 ± 20	-	-
Big Sagebrush	813 ± 57	-	813 ± 57	-	-
Utah Juniper	1014 ± 24	967 ± 74	1026 ± 24	-	-
Douglas-Fir	1028 ± 20	1038 ± 20	-	959 ± 52	-
White Fir	965 ± 35	997 ± 26	-	887 ± 98	-
Fetterbush	911 ± 17	911 ± 17	-	-	-
Gallberry	937 ± 27	937 ± 27	-	-	-
Wax Myrtle	875 ± 61	875 ± 61	-	-	-
Saw Palmetto	981 ± 41	981 ± 41	-	-	-
Excelsior	629 ± 42	599 ± 37	-	-	691 ± 106
All	903 ± 8	910 ± 23	897 ± 9	941 ± 22	902 ± 21

FH (cm)	All	Spring	Summer	Fall	Winter
Manzanita	7.5 ± 0.2	6.2 ± 0.2	8.1 ± 0.3	7.4 ± 0.3	7.2 ± 0.6
Ceanothus	5.5 ± 0.2	4.7 ± 0.3	6.2 ± 0.4	-	5.7 ± 0.4
Scrub Oak	6.4 ± 0.2	6.3 ± 0.3	6.6 ± 0.3	-	5.8 ± 0.5
Chamise	5.4 ± 0.7	-	4.4 ± 0.6	-	8.7 ± 0.7
Gambel Oak	6.7 ± 0.4	4.0 ± 0.6	6.9 ± 0.4	7.4 ± 1.0	-
Canyon Maple	5.3 ± 0.3	5.8 ± 1.2	5.3 ± 0.3	-	-
Big Sagebrush	4.1 ± 0.5	2.8 ± 2.1	4.3 ± 0.5	-	-
Utah Juniper	8.0 ± 0.5	7.7 ± 1.1	7.4 ± 0.7	-	8.8 ± 1.0
Douglas-Fir	10.7 ± 0.7	10.2 ± 0.7	-	14.0 ± 1.0	-
White Fir	8.5 ± 0.8	8.0 ± 0.7	-	9.9 ± 2.1	-
Fetterbush	11.1 ± 0.9	11.1 ± 0.9	-	-	-
Gallberry	8.4 ± 0.8	8.4 ± 0.8	-	-	-
Wax Myrtle	7.5 ± 1.7	7.5 ± 1.7	-	-	-
Saw Palmetto	11.7 ± 1.1	11.7 ± 1.1	-	-	-
Excelsior	6.5 ± 0.5	6.2 ± 0.6	-	-	7.3 ± 1.5
All	6.8 ± 0.1	7.0 ± 0.3	6.5 ± 0.2	8.5 ± 0.8	7.1 ± 0.3

t_{FH}/t_{fd}	All	Spring	Summer	Fall	Winter
Manzanita	0.58 ± 0.01	0.62 ± 0.04	0.56 ± 0.02	0.47 ± 0.03	0.62 ± 0.02
Ceanothus	0.69 ± 0.02	0.71 ± 0.03	0.69 ± 0.02	-	0.66 ± 0.04
Scrub Oak	0.58 ± 0.02	0.53 ± 0.04	0.62 ± 0.02	-	0.56 ± 0.03
Chamise	0.50 ± 0.05	-	0.54 ± 0.05	-	0.37 ± 0.14
Gambel Oak	0.49 ± 0.03	0.54 ± 0.09	0.47 ± 0.04	0.53 ± 0.07	-
Canyon Maple	0.66 ± 0.03	0.67 ± 0.11	0.66 ± 0.03	-	-
Big Sagebrush	0.77 ± 0.04	0.87 ± 0.30	0.76 ± 0.04	-	-
Utah Juniper	0.45 ± 0.03	0.44 ± 0.10	0.49 ± 0.04	-	0.42 ± 0.05
Douglas-Fir	0.40 ± 0.04	0.40 ± 0.04	-	0.41 ± 0.06	-
White Fir	0.45 ± 0.05	0.45 ± 0.05	-	0.45 ± 0.15	-
Fetterbush	0.56 ± 0.04	0.56 ± 0.04	-	-	-
Gallberry	0.58 ± 0.03	0.58 ± 0.03	-	-	-
Wax Myrtle	0.34 ± 0.09	0.34 ± 0.09	-	-	-
Saw Palmetto	0.60 ± 0.09	0.60 ± 0.09	-	-	-
Excelsior	0.44 ± 0.03	0.46 ± 0.03	-	-	0.35 ± 0.04
All	0.57 ± 0.01	0.54 ± 0.02	0.60 ± 0.01	0.48 ± 0.04	0.54 ± 0.03

B. Linear Correlations

The following are tables that list the linear correlations (slope = α, intercept = β) for various dependent and independent variables with 95% confidence intervals (±). Fewer species were significant in these correlations and are not presented in the text. The correlation with dependent and independent variables is noted in the top box of the table.

Species	t_{iq} (s) vs. *MC* (%)			
	α	β	r^2	Significant ?
Manzanita	2.334 ± 0.769	1.760 ± 0.444	0.0873	+
Ceanothus	6.227 ± 1.265	0.987 ± 0.883	0.3518	+
Scrub Oak	0.887 ± 1.007	0.703 ± 0.679	0.0125	
Chamise	1.871 ± 1.239	-0.194 ± 0.903	0.1738	+
Gambel Oak	0.742 ± 0.162	0.179 ± 0.122	0.3531	+
Canyon Maple	0.504 ± 0.364	0.169 ± 0.360	0.0568	+
Big Sagebrush	0.454 ± 0.418	0.929 ± 0.609	0.0308	+
Utah Juniper	-0.057 ± 1.521	1.486 ± 1.022	0.0001	
Douglas-Fir	-0.006 ± 0.110	0.150 ± 0.134	0.0005	
White Fir	-8.197 ± 4.928	8.247 ± 4.560	0.2640	-
Fetterbush	-	2.502 ± 0.374	-	
Gallberry	-	2.785 ± 0.568	-	
Wax Myrtle	-	0.900 ± 0.555	-	
Saw Palmetto	-	0.903 ± 0.618	-	
Excelsior	0.575 ± 0.569	0.217 ± 0.119	0.0775	+
All	-0.021 ± 0.284	2.021 ± 0.233	0.0000	

Species	t_{iq} (s) vs. SA (cm^2)			
	α	β	r^2	Significant ?
Manzanita	0.335 ± 0.171	1.508 ± 0.917	0.0656	+
Ceanothus	2.644 ± 1.087	1.370 ± 1.543	0.2435	+
Scrub Oak	0.527 ± 0.317	-0.576 ± 1.374	0.1010	+
Gambel Oak	-0.016 ± 0.009	0.798 ± 0.129	0.1172	-
Canyon Maple	-0.010 ± 0.025	0.763 ± 0.326	0.0066	
Big Sagebrush	0.391 ± 0.675	1.311 ± 0.687	0.0235	
Fetterbush	0.083 ± 0.162	1.987 ± 1.073	0.0605	
Gallberry	0.957 ± 0.683	0.379 ± 1.777	0.4133	+
Wax Myrtle	0.282 ± 0.327	-0.705 ± 1.924	0.2707	
Saw Palmetto	-0.313 ± 0.481	1.946 ± 1.710	0.1437	
All	-0.114 ± 0.030	2.899 ± 0.241	0.0749	-

Species	t_{iq} (s) vs. P (cm)			
	α	β	r^2	Significant ?
Manzanita	0.285 ± 0.211	0.686 ± 1.899	0.0322	+
Ceanothus	1.299 ± 0.510	-1.240 ± 2.476	0.2606	+
Scrub Oak	0.342 ± 0.275	-1.472 ± 2.489	0.0590	+
Gambel Oak	-0.018 ± 0.011	1.016 ± 0.259	0.1010	-
Canyon Maple	-0.006 ± 0.018	0.835 ± 0.549	0.0053	
Big Sagebrush	0.240 ± 0.170	0.074 ± 1.165	0.1246	+
Fetterbush	0.101 ± 0.154	1.385 ± 1.737	0.0961	
Gallberry	0.239 ± 0.740	1.044 ± 5.435	0.0360	
Wax Myrtle	0.094 ± 0.318	-0.360 ± 4.321	0.0412	
Saw Palmetto	-0.028 ± 0.255	1.319 ± 3.872	0.0047	
All	-0.101 ± 0.017	3.541 ± 0.269	0.1658	-

Species	T_{iq} (°C) vs. Δx (mm)			
	α	β	r^2	Significant ?
Manzanita	84.061 ± 100.466	317.569 ± 51.758	0.0081	
Ceanothus	-33.581 ± 145.327	426.353 ± 80.742	0.0013	
Scrub Oak	346.768 ± 144.154	193.761 ± 52.964	0.0976	+
Chamise	-27.816 ± 128.670	260.427 ± 83.004	0.0113	
Gambel Oak	-154.172 ± 273.804	271.528 ± 58.668	0.0090	
Canyon Maple	344.354 ± 188.061	177.026 ± 43.930	0.0995	+
Big Sagebrush	-386.033 ± 299.404	432.639 ± 81.878	0.0460	-
Utah Juniper	-338.042 ± 510.457	802.760 ± 720.644	0.1788	
Douglas-Fir	164.258 ± 260.733	122.288 ± 121.733	0.0583	
White Fir	-92.814 ± 142.807	254.183 ± 90.641	0.0800	
Fetterbush	128.619 ± 291.744	210.092 ± 120.392	0.0455	
Gallberry	-938.489 ± 1733.368	643.469 ± 593.443	0.0952	
Wax Myrtle	182.819 ± 725.619	201.499 ± 276.768	0.0306	
Saw Palmetto	-336.787 ± 828.871	361.088 ± 219.902	0.0613	
Excelsior	-18.687 ± 100.870	263.857 ± 84.450	0.0134	
All	130.778 ± 34.029	265.159 ± 15.323	0.0432	+

Species	T_{iq} (°C) vs. m_{H2O} (g)			
	α	β	r^2	Significant ?
Manzanita	434.790 ± 231.691	325.313 ± 21.534	0.0378	+
Ceanothus	-746.099 ± 957.856	433.486 ± 37.856	0.0147	
Scrub Oak	-150.721 ± 293.142	322.236 ± 26.414	0.0047	
Chamise	-96.380 ± 163.222	275.191 ± 25.480	0.0372	
Gambel Oak	109.336 ± 326.782	231.962 ± 29.035	0.0033	
Canyon Maple	-4.7530 ± 409.072	252.032 ± 37.380	0.0000	
Big Sagebrush	55.524 ± 2957.310	330.278 ± 54.214	0.0000	
Utah Juniper	-138.459 ± 160.238	305.365 ± 42.669	0.0617	
Douglas-Fir	50.244 ± 112.032	171.846 ± 44.259	0.0263	
White Fir	124.378 ± 149.400	154.195 ± 46.364	0.0851	
Fetterbush	-181.017 ± 732.424	282.398 ± 89.589	0.0148	
Gallberry	-1501.299 ± 3565.853	409.299 ± 209.971	0.0598	
Wax Myrtle	180.759 ± 1398.525	258.320 ± 103.059	0.0082	
Saw Palmetto	-359.203 ± 2562.991	295.863 ± 165.619	0.0077	
Excelsior	11589.310 ± 7679.737	241.423 ± 24.492	0.1887	+
All	-242.628 ± 70.884	333.244 ± 8.613	0.0318	-

Species	T_{iq} (°C) vs. *MC* (%)			
	α	β	r^2	Significant ?
Manzanita	104.777 ± 43.466	306.611 ± 24.701	0.0608	+
Ceanothus	-9.239 ± 95.459	414.475 ± 67.157	0.0002	
Scrub Oak	38.966 ± 76.344	286.756 ± 52.997	0.0047	
Chamise	-194.303 ± 128.197	407.416 ± 95.193	0.2031	-
Gambel Oak	113.363 ± 53.474	157.757 ± 41.737	0.1184	+
Canyon Maple	-10.112 ± 64.438	261.316 ± 63.992	0.0008	
Big Sagebrush	-32.043 ± 75.251	376.209 ± 108.213	0.0052	
Utah Juniper	-165.867 ± 143.175	391.672 ± 103.808	0.1057	-
Douglas-Fir	46.618 ± 78.348	136.917 ± 90.342	0.0454	
White Fir	-131.498 ± 245.768	311.467 ± 226.854	0.0370	
Fetterbush	-	261.540 ± 29.373	-	
Gallberry	-	323.131 ± 46.285	-	
Wax Myrtle	-	270.361 ± 41.678	-	
Saw Palmetto	-	273.524 ± 43.015	-	
Excelsior	211.422 ± 166.883	240.286 ± 28.844	0.1408	+
All	-13.209 ± 17.717	323.699 ± 14.707	0.0016	

Species	T_{iq} (°C) vs. *SA* (cm^2)			
	α	β	r^2	Significant ?
Manzanita	7.331 ± 8.223	292.578 ± 44.167	0.0149	
Ceanothus	1.901 ± 52.474	323.447 ± 74.375	0.0001	
Scrub Oak	-4.144 ± 13.317	304.037 ± 56.818	0.0039	
Gambel Oak	-2.748 ± 2.898	249.991 ± 31.181	0.0437	
Canyon Maple	-1.697 ± 2.840	242.682 ± 37.301	0.0152	
Big Sagebrush	-18.035 ± 44.804	271.448 ± 43.827	0.0117	
Fetterbush	-8.845 ± 12.394	316.410 ± 82.019	0.1110	
Gallberry	-30.181 ± 70.479	399.024 ± 183.316	0.0618	
Wax Myrtle	-4.509 ± 28.531	295.993 ± 168.065	0.0122	
Saw Palmetto	-13.477 ± 35.181	318.395 ± 125.085	0.0549	
All	-5.537 ± 1.582	315.809 ± 11.409	0.0660	-

Species	T_{iq} (°C) vs. P (cm)			
	α	β	r^2	Significant ?
Manzanita	6.182 ± 10.083	275.047 ± 90.728	0.0071	
Ceanothus	7.774 ± 25.097	288.909 ± 121.870	0.0053	
Scrub Oak	-4.958 ± 11.180	330.644 ± 99.254	0.0078	
Gambel Oak	-2.907 ± 3.077	282.391 ± 63.436	0.0434	
Canyon Maple	-1.458 ± 2.048	265.635 ± 62.795	0.0215	
Big Sagebrush	-0.556 ± 11.199	258.349 ± 75.535	0.0002	
Fetterbush	-6.981 ± 12.267	338.428 ± 138.214	0.0736	
Gallberry	-33.636 ± 58.072	568.748 ± 426.515	0.1075	
Wax Myrtle	-12.487 ± 22.769	438.308 ± 309.017	0.1299	
Saw Palmetto	-0.183 ± 17.831	276.262 ± 270.272	0.0000	
All	-3.933 ± 0.797	334.721 ± 12.275	0.1234	-

Species	m_{iq}/m_0 vs. Δx (mm)			
	α	β	r^2	Significant ?
Manzanita	-0.109 ± 0.148	0.182 ± 0.081	0.0116	
Ceanothus	-0.128 ± 0.322	0.400 ± 0.186	0.0089	
Scrub Oak	-0.090 ± 0.469	0.232 ± 0.154	0.0019	
Chamise	-0.156 ± 0.198	0.179 ± 0.127	0.1824	
Gambel Oak	-0.227 ± 0.472	0.200 ± 0.119	0.0172	
Canyon Maple	0.214 ± 0.435	0.165 ± 0.096	0.0177	
Big Sagebrush	0.282 ± 1.464	0.194 ± 0.452	0.0076	
Utah Juniper	0.729 ± 1.348	-0.821 ± 1.899	0.1143	
Douglas-Fir	-0.034 ± 0.095	0.026 ± 0.047	0.0275	
White Fir	-0.0280 ± 0.151	0.047 ± 0.095	0.0074	
Fetterbush	-0.910 ± 1.006	0.652 ± 0.423	0.2271	
Gallberry	-	-	-	
Wax Myrtle	0.355 ± 0.880	-0.053 ± 0.322	0.1395	
Saw Palmetto	-1.230 ± 0.912	0.395 ± 0.231	0.5086	-
Excelsior	-0.073 ± 0.252	0.116 ± 0.210	0.0637	
All	-0.052 ± 0.053	0.195 ± 0.027	0.0064	

Species	m_{iq}/m_0 vs. m_{H2O} (g)			
	α	β	r^2	Significant ?
Manzanita	0.559 ± 0.282	0.077 ± 0.027	0.0787	+
Ceanothus	0.219 ± 1.818	0.320 ± 0.077	0.0008	
Scrub Oak	0.983 ± 1.670	0.153 ± 0.093	0.0175	
Chamise	-0.127 ± 0.324	0.136 ± 0.060	0.0292	
Gambel Oak	-0.046 ± 1.176	0.145 ± 0.070	0.0001	
Canyon Maple	0.567 ± 0.893	0.169 ± 0.073	0.0292	
Big Sagebrush	-5.618 ± 8.798	0.357 ± 0.149	0.0775	
Utah Juniper	-0.137 ± 0.079	0.156 ± 0.034	0.1492	-
Douglas-Fir	-0.170 ± 0.222	0.123 ± 0.103	0.0942	
White Fir	0.163 ± 0.455	0.010 ± 0.147	0.0204	
Fetterbush	-3.545 ± 2.275	0.693 ± 0.278	0.4658	-
Gallberry	-	-	1.0000	
Wax Myrtle	0.851 ± 1.957	0.028 ± 0.117	0.1589	
Saw Palmetto	-1.762 ± 3.687	0.199 ± 0.237	0.1149	
Excelsior	11.981 ± 19.500	0.067 ± 0.079	0.0467	
All	-0.227 ± 0.067	0.189 ± 0.013	0.0608	-

Species	m_{iq}/m_0 vs. *MC* (%)			
	α	β	r^2	Significant ?
Manzanita	0.265 ± 0.067	0.000 ± 0.034	0.2521	+
Ceanothus	0.067 ± 0.204	0.282 ± 0.144	0.0060	
Scrub Oak	0.306 ± 0.225	-0.037 ± 0.181	0.0867	+
Chamise	0.167 ± 0.344	-0.004 ± 0.265	0.0441	
Gambel Oak	-0.129 ± 0.158	0.241 ± 0.124	0.0530	
Canyon Maple	0.056 ± 0.089	0.151 ± 0.099	0.0287	
Big Sagebrush	-0.083 ± 0.286	0.378 ± 0.353	0.0171	
Utah Juniper	-0.096 ± 0.152	0.179 ± 0.102	0.0231	
Douglas-Fir	-0.211 ± 0.148	0.297 ± 0.177	0.2646	-
White Fir	-0.868 ± 0.531	0.865 ± 0.493	0.3028	-
Fetterbush	-	0.280 ± 0.110	-	
Gallberry	-	-	-	
Wax Myrtle	-	0.075 ± 0.045	-	
Saw Palmetto	-	0.090 ± 0.062	-	
Excelsior	0.116 ± 0.420	0.088 ± 0.087	0.0098	
All	0.070 ± 0.035	0.115 ± 0.027	0.0228	+

Species	m_{iq}/m_0 vs. *SA* (cm^2)			
	α	β	r^2	Significant ?
Manzanita	0.008 ± 0.008	0.081 ± 0.046	0.0204	
Ceanothus	0.023 ± 0.080	0.297 ± 0.115	0.0046	
Scrub Oak	-0.012 ± 0.023	0.253 ± 0.105	0.0127	
Gambel Oak	-0.006 ± 0.012	0.192 ± 0.099	0.0186	
Canyon Maple	-0.002 ± 0.007	0.234 ± 0.092	0.0056	
Big Sagebrush	-0.070 ± 0.191	0.354 ± 0.222	0.0270	
Fetterbush	-0.056 ± 0.042	0.630 ± 0.280	0.3859	-
Gallberry	-	-	-	
Wax Myrtle	0.005 ± 0.064	0.049 ± 0.325	0.0065	
Saw Palmetto	-0.040 ± 0.046	0.223 ± 0.162	0.3031	
All	-0.006 ± 0.003	0.222 ± 0.022	0.0277	-

Species	m_{iq}/m_0 vs. *P* (cm)			
	α	β	r^2	Significant ?
Manzanita	0.007 ± 0.011	0.065 ± 0.096	0.0083	
Ceanothus	0.004 ± 0.038	0.308 ± 0.186	0.0007	
Scrub Oak	-0.021 ± 0.021	0.398 ± 0.194	0.0505	-
Gambel Oak	-0.003 ± 0.009	0.192 ± 0.176	0.0057	
Canyon Maple	-0.002 ± 0.005	0.276 ± 0.159	0.0132	
Big Sagebrush	-0.023 ± 0.059	0.436 ± 0.408	0.0311	
Fetterbush	-0.058 ± 0.051	0.937 ± 0.586	0.3164	-
Gallberry	-	-	-	
Wax Myrtle	-0.002 ± 0.067	0.102 ± 0.862	0.0009	
Saw Palmetto	0.000 ± 0.027	0.091 ± 0.421	0.0000	
All	-0.002 ± 0.002	0.211 ± 0.023	0.0108	-

C. Common and Scientific Names

Since not all species in the dissertation text indicated a scientific name (only common names), particularly in Section 2. Literature Review, all species are here listed with both common and scientific names.

Common Name	Scientific Name
White fir	*Abies concolor* (Gord. & Glend.) Lindl. ex Hildebr.
Canyon maple	*Acer grandidentatum* Nutt.
Chamise	*Adenostoma fasciculatum Hook. & Am*
Mananita	*Arctostaphylos glandulosa*
Pointleaf manzanita	*Arctostaphylos pungens* H.B.K.
Big sagebrush	*Artemisia tridentata* Nutt.
Incense cedar	*Calocedrus decurrens*
Ceanothus	*Ceanothus crassifolius*
Mountail mahogany	*Cercocarpus montanus*
Gum rock rose	*Cistus ladaniferus* L.
Hairy yerba santa	*Eriodictyon trichocalyx* Heller
River redgum	*Eucalyptus camaldulensis* Dehnh.
Gallberry	*Ilex glabra* (L.) Gray
Utah juniper	*Juniperus osteosperma* (Torr.) Little
Sweet bay	*Laurus nobilis* L.
Fetterbush	*Lyonia lucida* (Lam.) K. Koch
Obeche	*Margaranthus colanaceus*
Wax myrtle	*Myrica cerifera*
White pine	*Pinus monticola*
Ponderosa pine	*Pinus ponderosa*
Quaking aspen	*Populus tremuloides Michx.*
Douglas-fir	*Pseudotsuga menziesii* (Mirbel) Franco
Scrub oak	*Quercus berberidifolia*
Scrub oak	*Quercus dumosa* Nutt.
Gambel oak	*Quercus gambelii* Nutt.
Shrub live oak	*Quercus turbinella* Greene
Laurel sumac	*Rhus laurina* Nutt.
Black sage	*Salvia mellifera* Greene
Saw palmetto	*Serenoa repens* (Bartr.) Small
Mahogany	*Swietenia Jacq.*
Western red cedar	*Thuja plicata*

Appendix C. Analytical Models

A. Thermocouple Conduction through Leads

Because the leads of the thermocouple were exposed to the convective gases of the FFB, the leads can transfer heat to the bead of the thermocouple via conduction, which can increase the overall temperature measurement. To determine the effects of conduction through the thermocouple leads, a heat transfer model was developed. This model first solved a steady-state energy balance including conduction, convection, and radiation (similar to a fin model) with temperature specified boundary conditions on the lead as shown in Equation C.1. This model assumes no radial temperature gradient, only in the axial (x) direction, as well as gray-body emission from the wire ($\varepsilon = 0.57$ for oxidized nickel (Incropera and DeWitt, 2002)).

$$\frac{d^2T}{dx^2} - \frac{4}{k_w d_w}\left[h\left(T - T_\infty\right) + \varepsilon\sigma\left(T^4 - T_{surr}^4\right)\right] = 0 \tag{C.1a}$$

$$T(x = 0) = T_0 \tag{C.1b}$$

$$T(x = b) = T_b \tag{C.1c}$$

where $x = b$ is at bead connection and $x = 0$ is an arbitrary length away from the bead where the temperature is at room temperature (not in the FFB gases). T_∞ is the temperature of the FFB gases (1010°C), while T_{surr} is the temperature of the surroundings (300°C). The convective heat transfer coefficient determined from empirical correlations for a cylinder (Hilpert, 1933).

$$h = 0.989\frac{k_a}{d_w}\mathrm{Re}_w^{0.330}\,\mathrm{Pr}^{1/3} \tag{C.2}$$

By using an initial guess for T_b, the differential equation was solved giving a temperature profile along the lead. The temperature profile in the axial direction (along the wire) showed a maximum plateau, indicating that the length chosen (b) was sufficient to determine the heat flux at the bead boundary (q_b), which was done by taking the derivative of the temperature profile as shown in Equation 5.3.

$$q_b = -k_w d_w^2 \frac{\pi}{4}\left.\frac{dT}{dx}\right|_b \tag{C.3}$$

Assuming that the temperature remains constant through the bead, an energy balance was performed on the bead itself by conduction through the two wires and conduction to the leaf (Equation C.4).

$$2q_b = q_l\left(T_b, T_l, \Delta r\right) = -k_l d_b^2 \pi \frac{T_l - T_b}{\Delta r} \tag{C.4}$$

Heat transfer by conduction to the leaf from the spherical bead was linearly estimated with the primary unknowns being the leaf temperature (T_l) and the distance from the bead in the radial dirction (Δr). The bead temperature (T_b), and thus the temperature difference (T_b-T_l), was determined by numerically solving Equations C.3 and C.4 at varying values of T_l and Δr . This is shown in Figure C.1.

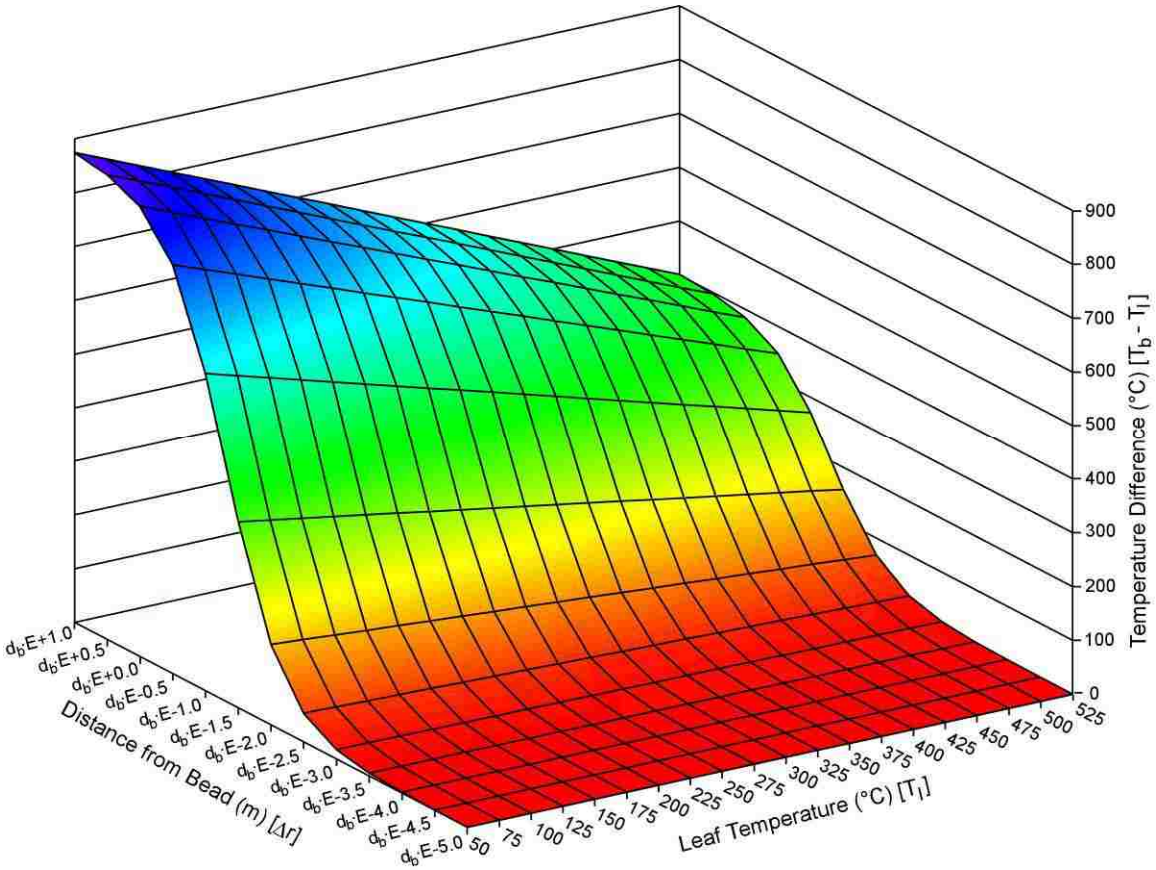

Figure C.1. Temperature correction on thermocouple bead due to conduction as leaf temperature and distance from the bead varies.

Figure C.1 shows that as the distance from the bead (Δr) increases, the temperature difference between bead and leaf increases dramatically. A value of $0.01 \cdot d_b$ has a temperature difference about 150°C; this temperature difference decreases linearly with increasing leaf temperature (T_l). A smaller distance (e.g. $0.001 \cdot d_b$) shows only a 18°C temperature difference at the lowest leaf temperature (T_l = 50°C). Since the distance from the bead is largely unknown, the temperature difference is also unknown. This model assumes a perfect connection (no resistance) between the bead and lead. An imperfect connection would yield a lower temperature difference than what is here reported.

Because of the large dependence of Δr in the temperature difference, a more sophisticated model may be needed that solves the spatial gradients of temperature in the leaf (e.g. 2D or 3D heat transfer leaf model).

B. Analytical Heat Transfer Model Derivation

Equation 6.4 describes the energy transfer for a leaf sample with boundary and initial conditions. The normalized equations are repeated here for reference.

Norm. Eq. $$\frac{1}{r}\frac{\partial}{\partial r}\left(r\frac{\partial u}{\partial r}\right)+\frac{\partial^2 u}{\partial x^2}+\frac{g(t)}{k}=\frac{1}{\alpha}\frac{\partial u}{\partial t} \tag{6.4b}$$

BC: $x = 0$ $$\left[-k\frac{\partial u}{\partial x}+h_0 u\right]_{x=0}=f_0(t)-h_0 T_0 \tag{6.4c}$$

BC: $x = \Delta x$ $$\left[k\frac{\partial u}{\partial x}+h_X u\right]_{x=\Delta x}=f_X(t)-h_X T_0 \tag{6.4d}$$

BC: $r = R$ $$\left[k\frac{\partial u}{\partial r}+h_R u\right]_{r=R}=f_R(t)-h_R T_0 \tag{6.4e}$$

BC: $r = 0$ $$u\big|_{r=0}<\infty \tag{6.4f}$$

IC: $t = 0$ $$u(r,x,0)=0 \tag{6.4g}$$

Each term in Equation 6.4b is applied to both a finite Fourier and Hankel integral transform. Definitions of these transformations are found in Equation C.5, respectively.

$$\bar{u}_n(r,t)=\int_0^{\Delta x} u(x,r,t)K_n(x)dx=F_x\{u(x,r,t)\} \tag{C.5a}$$

$$\bar{u}_m(x,t)=\int_0^{R} u(x,r,t)rJ_0(\omega_m r)dr=H_r\{u(x,r,t)\} \tag{C.5b}$$

where $K_n(x)$ is the kernel from Robin-Robin boundary conditions in the axial direction as defined in Equation 6.9, and $J_0(r)$ is the zero-order Bessel function in the radial direction. F_x and H_r are operators that perform the the finite Fourier and Hankel transforms, respectively, for each term in Equation 6.4b, and are shown in Equation C.6.

$$K_n(x)=\frac{\lambda_n\cos(\lambda_n x)+H_0\sin(\lambda_n x)}{\sqrt{\frac{\lambda_n^2+H_0^2}{2}\left(\Delta x+\frac{H_X}{\lambda_n^2+H_X^2}\right)+\frac{H_0}{2}}} \tag{6.9}$$

$$F_x H_r\left\{\frac{1}{r}\frac{\partial}{\partial r}\left(r\frac{\partial u}{\partial r}\right)\right\}+H_r F_x\left\{\frac{\partial^2 u}{\partial x^2}\right\}+H_r F_x\left\{\frac{g(t)}{k}\right\}=H_r F_x\left\{\frac{1}{\alpha}\frac{\partial u}{\partial t}\right\} \tag{C.6}$$

With the specified Robin and symmetrical boundary conditions in the radial direction, an operational property of the first term of Equation 6.4b ($1/r\partial/\partial r(r\partial u/\partial r)$) applied to the Hankel transform is shown in Equation C.7. With the specified Robin-Robin boundary conditions in the axial direction, an operational property of the second term of Equation 6.4b ($\partial^2 u/\partial x^2$) applied to the Fourier transform is shown in Equation C.8.

$$\int_0^R \frac{r}{r}\frac{\partial}{\partial r}\left(r\frac{\partial u}{\partial r}\right)J_0(\omega_m r)dr = RJ_0(\omega_m R)\frac{f_R(t)-h_R T_0}{k} - \omega_m^2 \bar{u}_m \tag{C.7}$$

$$\int_0^{\Delta x} \frac{\partial^2 u}{\partial x^2}K_n(x)dx = \frac{f_0(t)-h_0 T_0}{k}K_n(0) + \frac{f_X(t)-h_X T_0}{k}K_n(\Delta x) - \lambda_n^2 \bar{u}_n \tag{C.8}$$

Transformations are performed on Equation C.6 and reduced to obtain the transformed ODE (Equation 6.6) with *Q(t)* (Equation 6.8). These steps are shown in Equation C.9 below.

$$\begin{aligned}
&F_x\left\{RJ_0(\omega_m R)\frac{f_R(t)-h_R T_0}{k} - \omega_m^2 \bar{u}_m(x,t)\right\} + \\
&\quad H_r\left\{\frac{f_0(t)-h_0 T_0}{k}K_n(0) + \frac{f_X(t)-h_X T_0}{k}K_n(\Delta x) - \lambda_n^2 \bar{u}_n(r,t)\right\} + \\
&\quad H_r\left\{\int_0^{\Delta x}\frac{g(t)}{k}K_n(x)dx\right\} = H_r\left\{\frac{1}{\alpha}\frac{\partial \bar{u}_n(r,t)}{\partial t}\right\}
\end{aligned} \tag{C.9a}$$

$$\begin{aligned}
&RJ_0(\omega_m R)\frac{f_R(t)-h_R T_0}{k}\int_0^{\Delta x}K_n(x)dx - \omega_m^2 \bar{\bar{u}}_{n,m}(t) + \\
&\quad \frac{f_0(t)-h_0 T_0}{k}K_n(0)\int_0^R rJ_0(\omega_m r)dr + \frac{f_X(t)-h_X T_0}{k}K_n(\Delta x)\int_0^R rJ_0(\omega_m r)dr - \\
&\quad \lambda_n^2 \bar{\bar{u}}_{n,m}(t) + \frac{g(t)}{k}\int_0^{\Delta x}K_n(x)dx\int_0^R rJ_0(\omega_m r)dr = \frac{1}{\alpha}\frac{\partial \bar{\bar{u}}_{n,m}(t)}{\partial t}
\end{aligned} \tag{C.9b}$$

$$\frac{\partial \bar{\bar{u}}_{n,m}}{\partial t} + \alpha(\lambda_n^2 + \omega_m^2)\bar{\bar{u}}_{n,m} = \frac{\alpha}{k}Q(t) \tag{6.6}$$

$$\begin{aligned}
Q(t) &= RJ_0(\omega_m R)[f_R(t)-h_R T_0]\int_0^{\Delta x}K_n(x)dx + [f_0(t)-h_0 T_0]K_n(0)\int_0^R J_0(\omega_m r)rdr \\
&\quad + [f_X(t)-h_X T_0]K_n(\Delta x)\int_0^R J_0(\omega_m r)rdr + g(t)\int_0^{\Delta x}K_n(x)dx\int_0^R J_0(\omega_m r)rdr
\end{aligned} \tag{6.8}$$

The solution for the transformed ODE is obtained with variation of parameters and is shown in Equation 6.10. The inverse Fourier and Hankel transforms are defined in Equation C.10, respectively, with the overall inverse transformations shown in Equation 6.11.

$$\overline{\overline{u}}_{n,m}(t) = \alpha \cdot e^{-\alpha\cdot\left(\lambda_n^2+\omega_m^2\right)t}\int_0^t Q(t)e^{\alpha\cdot\left(\lambda_n^2+\omega_m^2\right)\tau}d\tau \tag{6.10}$$

$$u(x,t) = \sum_{n=1}^{\infty}\overline{u}_n(t)K_n(x) \tag{C.10a}$$

$$u(r,t) = \sum_{m=1}^{\infty}\overline{u}_m(t)\frac{J_0(\omega_m r)}{\left\|J_0(\omega_m r)\right\|^2} = \sum_{m=1}^{\infty}\overline{u}_m(t)\frac{J_0(\omega_m r)}{\int_0^R\left[J_0(\omega_m r)r\right]^2 dr} \tag{C.10b}$$

$$u(r,x,t) = \sum_{n=1}^{\infty}\sum_{m=1}^{\infty}\overline{\overline{u}}_{n,m}(t)K_n(x)\frac{J_0(\omega_m r)}{\int_0^R\left[J_0(\omega_m r)r\right]^2 dr} \tag{6.11}$$

The heterogeneous forcing function, $f_i(t)$, was assumed to decrease exponentially and was assumed to be essentially 0 at the time of burnout (16 s) (see Figure C.2). Each boundary conditions at the tip ($r = R$) and on the top of the leaf ($x = \Delta x$) were assumed to be ¼ of the value of the bottom ($x = 0$) because the wake effects would yield lower effective heat transfer on those areas.

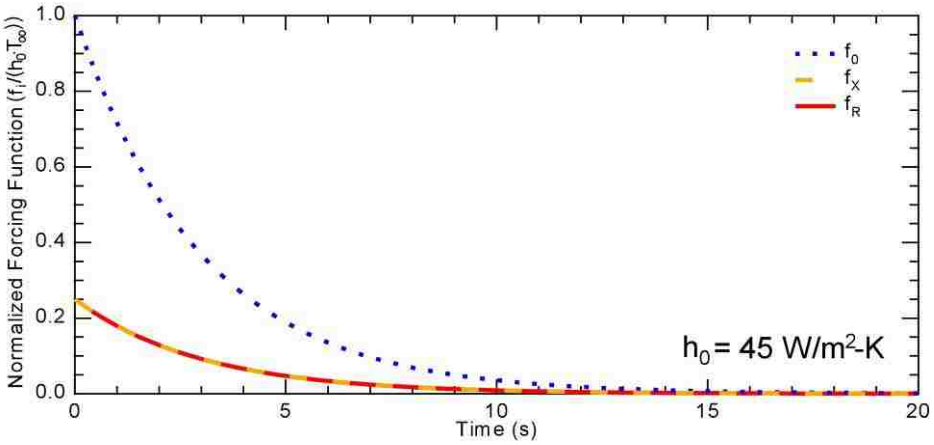

Figure C.2. Exponential decrease of forcing function for boundary conditions used in analytical model.

The source/sink function, $g(t)$, was determined from the heats of evaporation, pyrolysis, and combustion and were assumed to be constant through the specific time applied to each phenomena. Heats of evaporation, pyrolysis and combustion were determined from the time applied, the mass, and volume of the leaf (giving consistent units of W/m^3). The overall function with time is shown in Figure C.3.

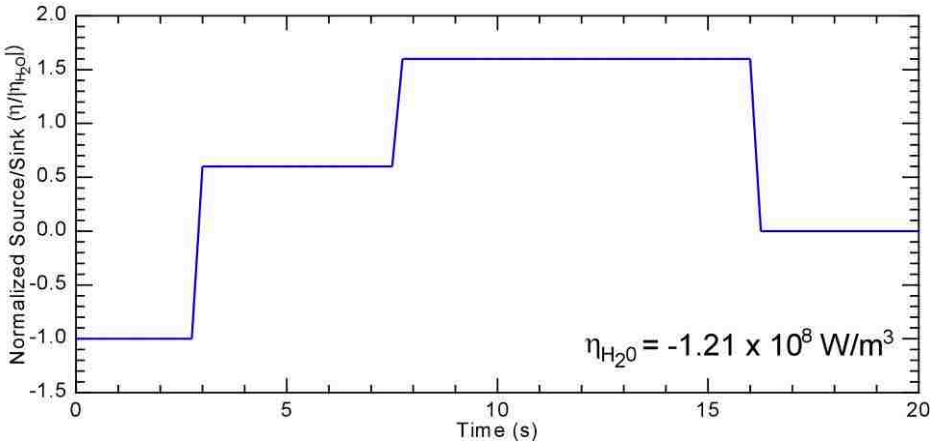

Figure C.3. Source/sink function used in analytical model.

Appendix D. Data and Video Files (CD)

A. Raw Data

Over 2500 experimental runs were performed using the FFB. The leaf and combustion characteristics were recorded on a spreadsheet; these data are found on the CD under the file entitled 'Reference Sheet - Dissertation.xls'. Both individual samples as well as two-leaf experiments are included. From this spreadsheet, the data were analyzed and correlations were determined.

B. Phenomena Video Files

The table below lists a variety of video files that describe certain qualitative phenomena observed during the course of the experiments. These video files are intended to compliment the images found in the body of this dissertation.

Phenomenon	File Name	Date	Species / Run #	Corresponding Figure
Jetting	Jetting_Dfir.wmv	10/26/2006	Douglas-Fir 1	Figure 5.2
Color Change	Color_Change.wmv	2/4/2005	Manzanita 1	Figure 5.3
Liquid Bubbling	Liquid_Bubbling.wmv	1/20/2004	Manzanita 3	Figure 5.4
Interior Bubbling	Interior_Bubbling.wmv	6/29/2005	Gambel Oak 10	Figure 5.6
Bursting	Burst_Manz.wmv	7/31/2003	Manzanita 4	Figure 5.7a
Bursting	Burst_IR_Labview_1.wmv	7/14/2005	Manzanita 4	Figure 5.8
Bursting	Burst_IR_Labview_2.wmv	8/9/2007	Scrub Oak 1	-
Brand Formation	Brand_Sage.wmv	6/28/2006	Big Sagebrush 7	Figure 5.12
Brand Formation	Brand_Chamise.wmv	5/21/2003	Chamise 11	Figure 5.13
Brand Formation	Brand_Berry.wmv	5/9/2006	Utah Juniper 9	Figure 5.14
Bending	Bending_Maple.wmv	6/28/2005	Canyon Maple 1	Figure 5.15
Disk Turbulence	Disk_Flame_Turb.wmv	10/24/2007	Manzanita 19	Figure 5.26

C. Model Video Files

The table below lists video files derived from the Fluent and bush models with various configurations. These video files are intended to compliment the images and figures found in the body of the dissertation.

Model	File Name	Configuration	Variable	Corresponding Figure
Fluent one-leaf	Config_1_Temp.mpeg	1	Temperature	Figure 6.8
Fluent two-leaf	Config_2_Temp.mpeg	2	Temperature	Figure 6.10
Fluent two-leaf	Config_2_O2.mpeg	2	Oxygen	Figure 6.12 Figure 6.13
Fluent two-leaf	Config_3_Temp.mpeg	3	Temperature	-
Fluent two-leaf	Config_3_O2.mpeg	3	Oxygen	Figure 6.12 Figure 6.13
Fluent two-leaf	Config_4_Temp.mpeg	4	Temperature	Figure 6.11
Fluent two-leaf	Config_4_O2.mpeg	4	Oxygen	Figure 6.12 Figure 6.13
Burning bush	Bush_Model.wmv	-	Ignition zone	Figure 6.16